



## **2018 STIC Incentive Project (BFRP-RC Standardization) - 18 Month Report**

**Fed Project No: STIC-0004-00A; FPID 443377-1**

This is the third report for the Basalt Fiber-Reinforced Polymer (BFRP) Bar Standardization for Reinforced Concrete (RC) with the FHWA allocation memorandum dated March 1, 2018. This report covers a period from May 2019 until October 2019. Underlined text is additional to previous reports.

### **Description of the proposed work**

Develop standard (guide) design specification, and standard material and construction specifications for basalt fiber-reinforced polymer (BFRP) bars for the internal reinforcement of structural concrete. Tasks involve (*highlighted tasks are completed or partially completed*):

- i. Establishing design and durability parameters using current state-of-the-art BFRP test data with *ACI 440.1R* as a design model framework, supplemented with *AASHTO's LRF Bridge Design Guide Specification for GFRP Reinforced Concrete - 2<sup>nd</sup> Edition (BDGS-2)* published December 2018; *BDV30 986-01 Final Report* provided recommendations for design and future refinement (see *Appendix A*).
- ii. Develop FDOT design modifications to *BDGS-2* for inclusion of BFRP reinforcing - see *BDV30 986-01 Final Report – Chapter 6* (previously received as *Deliverable #3*) recommendations which have been incorporated into the draft *2020 Structures Manual for January 2020 publication*. No increase in BFRP design parameters above those currently established for GFRP are proposed at this time, until additional testing is performed to refine the environmental reduction factors for different limit states. Some of the necessary work for this effort is ongoing under FDOT research project *BE694 - Improving Testing Protocol and Material Specifications for BFRP Bars*.
- iii. Develop FDOT material specification for acceptance based on the 2017 *ASTM D7957: Standard Specification for Solid Round Glass Fiber Reinforced Polymer Bars for Concrete Reinforcement* - see *BDV30 986-01 Final Report – Chapter 6* (previously received as *Deliverable #4*), and FDOT *Materials Manual – Section 12.1* (see *Appendix B*).
- iv. Develop FDOT Construction Specifications based on *BDGS-2* and *FDOT Specification Section 415 & 932* GFRP reinforcing specifications – *Specification Section 932* updates (416 had no updates required) where submitted for *FHWA final approval August 23, 2019* (see *Appendix C*).
- v. Develop BFRP Reinforcing Database for collection of current and future test results based on FDOT GFRP reinforcing test library developed under *BDV30 977-18* and new research project *BE694 “Testing Protocol and Material Specification for BFRP Rebars”*

established under [BE694-Deliverable 2](#). Test data from **BDV30 986-01** published in [Chapter 3/Appendix A](#);

- vi. Deliver a designer focus live workshop at the end of the STIC project in central Florida (and national event if funding permits). Post the delivered training material on [FDOT FRP Innovation](#) website for broader access and future updating.
  - (a) BFRP-RC Designer Training schedule for 3 sessions at the FDOT Transportation Symposium (FTS2019) on June 4<sup>th</sup> (see [FDOT Transportation Symposium FRP-RC Design - Part 1, Part 2, & Part 3](#));
  - (b) [BEI-2019 FRP Composites II \(Session B-9\)](#) on BFRP-RC for coastal and marine structures was provide as the Bridge Engineering Institute conference July 23-25. Additionally, several papers on BFRP-RC were presented and published in the [Conference Proceedings](#), pp 514-523, 527-531, & 551-562; see [Appendix D](#))
  - (c) Peer Exchange BFRP-RC Designer Training was provided to Hawaii DOT Bridge Office on July 22, 2019 (see [BFRP-RC Design - Part 1, Part 2, Part 3, & Part 4](#));
- vii. Demonstration Project - Plans developed and contract awarded for BFRP-RC link-slab on pedestrian bridge in Port Charlotte, FL (along US 41). Construction delayed until September 2019 due to utility coordination issues. Monitoring contract executed with University of North Florida under **BDV29 986-02**, to instrument link-slab and BFRP rebar to monitor initial and longer-term response. [Deliverable #1](#) for literature review, and [Deliverable #2](#) (see [Appendix E](#)) for revised instrumentation plan.

## Project Breakdown and Schedule

The project is broken into several phases with distinct tasks some of which were not completely scoped, pending progress and findings in the early Phases. **Table 1** shows a summary of the project Phases. There will be at least two services contracts with Florida Universities for the various tasks of: Existing information collection and curation (Phase 1a); Development of model specifications and standards (Phase 1b); Provision of supplemental test data and analysis (Phase 2a); Development of Materials Database (Phase 2b); Technology Transfer (Phase 3).

PROJECT PHASE	1	2	3
<b>PROJECT WORK TASKS</b>	Develop Standards: <b><i>(BDV30 986-01)</i></b> <ul style="list-style-type: none"> <li>Design Spec.</li> <li>Materials Qualification and Verification Test Procedures</li> <li>Construction Spec.</li> </ul>	<ul style="list-style-type: none"> <li>Full-scale <u>Link-Slab Demo and Monitoring</u> <b><i>(BDV34 986-02)</i></b></li> <li>Supplemental Bar Testing</li> <li>BFRP Database Completion <b><i>(BDV30 986-01)</i></b></li> </ul>	<ul style="list-style-type: none"> <li>Technology Transfer <b><i>(FTS-2019 &amp; BEI-2019)</i></b></li> <li>Final Report</li> </ul>
<b>PROJECT DELIVERABLES</b>	<ul style="list-style-type: none"> <li>LRFD Guide Design Spec. <i>(in AASHTO format)</i></li> <li>Testing Spec. <i>(in ASTM format)</i></li> <li>Construction Spec. <i>(in FDOT format)</i></li> </ul>	<ul style="list-style-type: none"> <li>Test Reports</li> <li>Electronic Database of physical and mechanical properties</li> </ul>	T <sup>2</sup> Workshop in central Florida for information dissemination and training
	•	•	
<b>PROJECT TIMELINE</b>	Month 1-11	Month 7- <del>15</del> <u>23</u>	Month <u>15-17</u> & <u>24</u>

Table 1- Project Summary (***update 3/28/19 & 10/24/19***)

#### Activities March-September 2018:

- 04/05/2018 - Funding authorization from Division FHWA approved under 2018 STIC Incentive Proposal: STIC-004-00A / FPID 443377-1;
- 05/21/2018 - Procurement completed for Principle Investigator of Phase 1 & 2b: Technology Review, Specifications & Database Development. Research Task Work Order (TWO) issued under FDOT research project ***BDV30-986-01***;
- 05/30/2018 - Kickoff meeting held for ***BDV30-986-01***;
- 09/11/2018 - ***BDV30-986-01***, Task 1 completed and Deliverable 1 (BFRP Technology Review Report) approved;
- 09/14/2018 - Collaboration meeting on design of Full-Scale demonstration of BFRP-RC element for testing and monitoring.

#### Activities October-May 2019:

- 12/7/2018 - ***BDV30-986-01***, Task Work Order Amendment#1 executed for time extension due to manufacturer delays in providing BFRP rebar samples for testing.
- 1/11/2019 - Procurement completed for Principle Investigator of Phase 2a BFRP-FRC Link-Slab Demonstration Project. Research Task Work Order issued under FDOT research project ***BDV34-986-02***.
- 2/6/2019 - ***BDV34-986-02***, (BFRP-FRC Link-Slab Demonstration Project) Kickoff Meeting held.
- 2/4/2019 - ***BDV30-986-01***, Draft Deliverable 2 (BFRP Testing Procedure and Results) submitted. Revisions requested by PM.

5. 2/28/2019 - **BDV30-986-01**, Task 2 completed and Deliverable 2 (BFRP Testing Procedure and Results) approved.
6. 2/28/2019 - **BDV30-986-01**, Draft Deliverable 3 (BFRP Material Specification Recommendation Report) submitted. Revisions requested by PM.
7. 3/26/2019 - **BDV30-986-01**, Task 3 completed and Deliverable 3 (BFRP Material Specification Recommendations) approved.
8. 3/4/2019 - **BDV34-986-02**, Draft Deliverable 1 (BFRP-FRC Link-Slab Demonstration Project - Literature Review) submitted. Revisions requested by PM.
9. 3/24/2019 - **BDV34-986-02**, Task 1 completed and Deliverable 1 (BFRP-FRC Link-Slab Literature Review) approved.
10. 5/4/2019 - **BDV30-986-01**, Draft Deliverable 4 (BFRP Design Specification Recommendations) submitted. Revisions requested by PM.
11. 5/13/2019 - **BDV34-986-02**, Draft Deliverable 2 (BFRP-FRC Link-Slab Demonstration Project: Instrumentation and Monitoring Plan) submitted and under review.
12. **BEI-2019** Mini-Symposium/Session organization with Prof. Jimmy Kim (TRB co-sponsored event June 22-25: <http://www.beibridge.org/BEI2019.html> ). Three Abstracts accepted for presentation.

#### Activities May-October 2019:

1. 5/24/2019 - **BDV30-986-01**, Revised Deliverable 4 (BFRP Design Specification Recommendations) accepted by PM (see Final Report).
2. 5/31/2019 - **BDV30-986-01**, Deliverable 5 (Draft Final Report) received, then revised and accepted by PM (see Final Report).
3. 5/31/2019 - **BDV30-986-01**, Deliverable 6 (Closeout Video Conference) held. See **Appendix F** presentation.
4. 6/4/2019 – **Technology Transfer 1: FDOT Transportation Symposium FRP-RC Designer Training - Part 1, Part 2, & Part 3.**
5. 6/30/2019 - **BDV30-986-01**, Deliverable 7 (Final Report – “Performance Evaluation, Material and Specification Development for Basalt FRP Reinforcing Bars Embedded in Concrete”) submitted and accepted 7/17/2019. See **Appendix A.**
6. 7/22/2019 – **Technology Transfer 2: HDOT Peer Exchange BFRP Designer Training - Part 1, Part 2, Part 3, & Part 4).**
7. 7/24/2019 - **Technology Transfer 3: BEI-2019 FRP Composites II Session -**. Three papers presented See **Appendix D:**
  - a. *Basalt FRP-RC Standardization for Florida DOT Structures;*
  - b. *Effect of the Fiber Content on the Tensile Strength Properties of Basalt Fiber Reinforced Polymer Rebars;*
  - c. *Bond-to-Concrete Characteristic of Basalt Fiber-Reinforced Polymer Rebars for Design Code Implementation*
8. 8/23/2019 – Material Specification Section 932-3 updates for BFRP rebar completed Industry Review and submitted as Supplemental Specification to FHWA for approval in 2020 Workbook
9. 8/30/2019 - **BDV34-986-02**, Revised Deliverable 2 (BFRP-FRC Link-Slab Demonstration Project: Instrumentation and Monitoring Plan) re-submitted and under review. See **Appendix E.**

10. 10/11/2019 – Test pile driving began for link-slab demonstration bridge under FPID 435390-1-52-01: US 41 from Midway Blvd to Enterprise project.

### **Planned Activities for November 2019-May 2020**

*Phase 1:*

1. Complete

*Phase 2:*

2. Continued coordination with District 1 EOR on final design, instrumentation, and monitoring for full-scale FRP-RC Link-Slab under FPID 435390-1-52-01: US 41 from Midway Blvd to Enterprise project. Link-Slab construction activity anticipated in mid-January 2020.
3. Complete initial database for BFRP characterization (*BDV30-986-01*, Task 2 results)

*Phase 3:*

4. Completed initial proposed T<sup>2</sup> activities.
5. Additional T<sup>2</sup> opportunities will be explored with Principal Investigators while STIC project is ongoing.
6. Final Report

### **Budget**

Project Line Item	FHWA STIC Contribution	FDOT In-Kind Match (20%)	Total Budget
<b>Phase 1</b> <i>(100% BDV30 986-01)</i>	\$48,000	\$12,000	\$60,000
<b>Phase 2</b> <i>(50% BDV30 986-01; 50% BDV34 986-02 &amp; Demonstration Project Monitoring)</i>	\$36,000	\$9,000	\$45,000
<b>Phase 3</b>	\$16,000	\$4,000	\$20,000
<b>Total Project</b>	<b>\$100,000</b>	<b>\$25,000</b>	<b>\$125,000</b>

*Table 2- Project Phase Funding Distribution (update 5/21/18)*

## Project Schedule

Work Phase	Month																								
	1	2	3	4	5	6	7	8	9	10	11	12	13	14	15	16	17	18	19	20	21	22	23	24	
1. Develop Design, Materials and Construction Specifications	[Grey shaded]																								
2a. Mockup testing at SRC and/or Full-scale slab instrumentation and monitoring																									
2b. BFRP Supplemental bar testing and Database																									
3. Technology Transfer Workshop and Final Report																									

Table 3- Project Timeline: Month 1 = April 2018 (updated 10/17/19)

### Appendices include:

- [Appendix A - BDV30 986-01 Final Report BDV30 986-02 Kickoff Meeting](#)
- [Appendix B - FDOT Materials Manual, Section 12.1 – BFRP Rebar Producer updates](#)
- [Appendix C - FDOT Materials Specification - Section 932-3 BFRP Rebar updates](#)
- [Appendix D - Bridge Engineering Institute – 2019 Conference Papers](#)
- [Appendix E - BDV30 986-02 Draft Deliverable 2: BFRP-FRC Link Slab – Instrumentation & Monitoring Plan](#)
- [Appendix F - BDV30 986-02 Deliverable 6: Closeout Presentation](#)



## **Appendix A**

### **BDV30 986-01 Final Report BDV30 986-02 Kickoff Meeting**

(170 pages)

Final Report

**Performance Evaluation, Material and Specification Development for  
Basalt Fiber Reinforced Polymer (BFRP) Reinforcing Bars  
Embedded in Concrete**

Contract Number BDV30 TWO 986-01  
FSU Project ID: 042088

---

*Submitted to:*

**Florida Department of Transportation**  
Research Center  
605 Suwannee Street  
Tallahassee, Florida 32399-0450

**Steven Nolan, Ph.D.**  
Project Manager  
FDOT State Materials Office



---

*Prepared by:*

**Raphael Kampmann, Ph.D.**

Principal Investigator

**Michelle Rambo-Roddenberry, Ph.D., P.E.**

Co-Principal Investigator

**Srichand Telikapalli, M.E.**

Graduate Research Assistant



**FAMU-FSU  
Engineering**

FAMU-FSU College of Engineering  
Department of Civil and Environmental Engineering  
2525 Pottsdamer Street  
Tallahassee, FL 32310

---

06/30/2019

# Disclaimer

The opinions, findings, and conclusions expressed in this report are those of the author(s) and not necessarily those of the Florida Department of Transportation or the U.S. Department of Transportation.

# Acknowledgements

The authors would like to thank the Florida Department of Transportation (FDOT) for financial support for this study and for a progressive approach toward an implementation of FRP rebars in concrete construction. Special thanks go to Steven Nolan and Chase Knight for technical and engineering support. Likewise, engineering advice and technical know-how was provide by Francisco De Caso from the University of Miami, who effectively acted as a co-PI. His FRP rebar knowledge and advices were indispensable for this report. In addition, many people have contributed to the successful completion of this research project, and this study would have not been possible without their assistance and help. Andre Schmidt and Tim Schneider worked tirelessly on numerous test setups, experiments, and other research tasks to obtain important data and to conducted the relevant analysis procedures. Susanna Becker and Jessica Frahling supported many tasks and were always available and helpful when called upon. Steven Squillacote provided exceptional hands-on support for all preparation tasks and for any laboratory efforts. In addition, the authors would like to thank the High Performance Material Institute (HPMI) for providing test equipment; specifically Marquese Pollard provided a lot of help for all tensile and shear tests that were conducted for this research.

# Executive Summary

Florida is a coastal state with bridge infrastructure exposed to aggressive environments through direct and indirect contact with saline solutions. Due to this exposure, conventional black steel reinforcement that is traditionally used for bridges is corroding prematurely, resulting in early structural deterioration which in-turn may cause huge financial and personal losses. In a successful effort to overcome such corrosion and deteriorating effects, reinforcing bars (rebars) made from fiber reinforced polymers (FRP) were developed. FRP rebars are composite materials, in which fibers, resin, and sizing (interface material between fibers and resin) are the main constituent materials. Different fiber types are used to produce such rebars, and the most common type in the US is glass fiber. In the former Soviet Bloc, continuous fibers made from basalt rock were favored and since the collapse of the Union of Soviet Socialist Republics (USSR), previously proprietary/military technologies have been made public and continuous basalt fibers (CBF) have entered the world market as a viable alternative to glass fibers. CBF are now used to produce basalt fiber reinforced polymers (BFRP) in rebar applications and these rebars are now imported or produced in the North America. Various types of BFRP rebars with dissimilar sizes, physical and strength properties, are currently produced to be used for civil engineering construction. In this project, representative and commonly available BFRP rebars were tested to evaluate various physical properties (cross-sectional properties, fiber content, and moisture absorption properties) and different strength characteristics (horizontal and transverse shear, tensile strength, elastic modulus, and bond-to-concrete properties) according to ASTM standards, in an effort to develop basalt specific acceptance criteria for FDOT Specifications Section 932, which governs the use of non-metallic auxiliary materials for civil engineering construction.

BFRP rebars from three different manufacturers, two different production lots, and two most commonly used rebar sizes (# 3 and # 5) were included in this study. The obtained results were

used to evaluate the performance of each rebar type in a relativistic comparison to existing benchmark values for glass FRP (GFRP) rebars. The fiber content test proved that all tested samples had consistent and nearly identical results with acceptable performance. Moisture absorption property of the rebars varied significantly based on the manufacturers, type of raw materials used, and the production techniques. Transverse shear strength of the tested BFRP rebars proved to be 116% stronger than GFRP bars. Tensile strength measurements and horizontal shear strength measurements were consistent for all rebar types and the recorded values surpassed the strengths generally reported for GFRP rebars. The bond-to-concrete strength of the tested BFRP rebars were not significantly different from bond-to-concrete strength commonly reported for GFRP rebars because similar surface enhancement techniques are used for either rebar type. Based on the obtained results it was noted that the tested BFRP rebars surpassed the strength related acceptance criteria for GFRP rebars. While the manufacturer reported properties varied and each rebar type performed different, the tested BFRP rebars were generally stronger (higher performance) than GFRP rebars. Ultimately, it was found that BFRP rebars are a suitable and viable alternative for construction in Florida and that those materials should be considered for FDOT Specification 932.

# Table of Contents

List of Figures . . . . .	x
List of Tables . . . . .	xiv
<b>1 Introduction</b>	<b>1</b>
1.1 Introduction . . . . .	1
1.2 Problem Statement . . . . .	4
1.3 Project Objectives . . . . .	5
1.4 Project Scope . . . . .	6
1.5 Report Organization . . . . .	6
<b>2 Background</b>	<b>8</b>
2.1 Igneous Rocks . . . . .	9
2.2 Fiber Types and Production . . . . .	10
2.2.1 Basalt Fiber . . . . .	10
2.2.2 Glass Fiber . . . . .	11
2.2.3 Carbon Fiber . . . . .	12
2.2.4 Aramid Fiber . . . . .	13
2.2.5 Fiber Types Summary . . . . .	13
2.2.6 Properties of Basalt Fibers . . . . .	14
2.3 Sizing . . . . .	14
2.4 Resin Types and Properties . . . . .	14
2.4.1 Epoxy . . . . .	16
2.4.2 Polyester . . . . .	16
2.4.3 Vinylester . . . . .	17

2.5	BFRP Rebar Production . . . . .	17
2.5.1	Pultrusion . . . . .	18
2.5.2	Wet Lay-Up . . . . .	20
2.6	BFRP Rebar Properties . . . . .	21
2.7	Test Procedures for FRP Rebar . . . . .	23
2.7.1	Physical Characteristics . . . . .	23
2.7.2	Strength Characteristics . . . . .	25
2.8	Failure Characteristics of FRP Rebars . . . . .	30
2.9	Durability of FRP Rebars . . . . .	31
2.10	Concrete Elements Reinforced with BFRP . . . . .	35
<b>3</b>	<b>BFRP Building Compliance and Market</b>	<b>38</b>
3.1	Regulations for FRP Rebars . . . . .	38
3.2	Acceptance Criteria for FRP Rebars . . . . .	41
3.3	Global BFRP Rebar Manufacturer Analysis . . . . .	43
3.4	BFRP Products Database . . . . .	48
<b>4</b>	<b>Experimental Program</b>	<b>50</b>
4.1	Introduction . . . . .	50
4.2	Experimental Concept . . . . .	50
4.2.1	Acceptance Criteria . . . . .	52
4.3	Equipment and Test Devices . . . . .	54
4.3.1	Cutting Saw . . . . .	54
4.3.2	Precision Saw . . . . .	55
4.3.3	Caliper . . . . .	55
4.3.4	Precision Balance . . . . .	56
4.3.5	Support Frame for Specimen Alignment . . . . .	56
4.3.6	Test Fixture for Transverse Shear Tests . . . . .	57
4.3.7	Test Fixture for Apparent Horizontal Shear Tests . . . . .	60
4.3.8	Test Fixture for Tensile Strength Tests . . . . .	61
4.3.9	Test Fixture for Bond-to-Concrete Test . . . . .	62

4.3.10	Load Frame . . . . .	65
4.3.11	Extensometer . . . . .	66
4.4	Test Procedures . . . . .	67
4.4.1	Cross-Sectional Area Test — Specific Gravity (Relative Density) . . . . .	67
4.4.2	Fiber Content Test — Ignition Loss . . . . .	68
4.4.3	Moisture Absorption Test . . . . .	69
4.4.4	Transverse Shear Strength Test . . . . .	70
4.4.5	Apparent Horizontal Shear Test . . . . .	70
4.4.6	Tensile Strength and Modulus Test . . . . .	71
4.4.7	Bond-to-Concrete Strength Test . . . . .	72
4.5	Data Acquisition and Data Analysis . . . . .	72
<b>5</b>	<b>Results</b>	<b>74</b>
5.1	Introduction . . . . .	74
5.2	Cross-Sectional Properties . . . . .	74
5.3	Fiber Content . . . . .	75
5.4	Moisture Absorption . . . . .	78
5.5	Transverse Shear Test . . . . .	78
5.5.1	Load vs. Displacement . . . . .	79
5.5.2	Stress vs. Displacement . . . . .	81
5.6	Modes of Failure . . . . .	84
5.7	Summary of Transverse Shear Properties . . . . .	86
5.8	Apparent Horizontal Shear Test . . . . .	87
5.8.1	Load vs. Displacement . . . . .	87
5.8.2	Stress vs. Displacement . . . . .	88
5.9	Modes of Failure . . . . .	92
5.10	Summary of Horizontal Shear Strength Properties . . . . .	93
5.11	Tensile Test . . . . .	94
5.11.1	Load vs. Displacement Behavior . . . . .	94
5.11.2	Stress vs. Strain Behavior . . . . .	96
5.12	Modes of Failure . . . . .	99

5.13	Summary of Tensile Properties . . . . .	101
5.14	Bond-to-Concrete Strength . . . . .	102
5.15	Bond Stress vs. Slip at Free End . . . . .	102
5.16	Modes of Failure . . . . .	108
5.17	Summary of Bond-to-Concrete Strength . . . . .	111
5.18	BFRP Rebar Performance . . . . .	111
<b>6</b>	<b>Discussion</b>	<b>115</b>
6.1	Research Significance . . . . .	115
6.2	Critical Analysis of Major Findings . . . . .	116
6.2.1	Cross-Sectional property . . . . .	116
6.2.2	Fiber Content . . . . .	117
6.2.3	Moisture Absorption of BFRP rebar . . . . .	118
6.2.4	Transverse Shear Strength . . . . .	118
6.2.5	Apparent Horizontal Shear Strength . . . . .	119
6.2.6	Tensile Properties . . . . .	120
6.2.7	Bond-to-Concrete Strength . . . . .	121
6.3	Supplementary Findings . . . . .	121
6.4	BFRP Design Specifications . . . . .	122
6.4.1	Design Guide Considerations . . . . .	126
6.5	Research Limitations . . . . .	127
6.6	Future and Further Directions . . . . .	128
<b>7</b>	<b>Conclusions</b>	<b>131</b>
7.1	Summary . . . . .	131
7.2	Conclusions . . . . .	132
7.3	Further Recommendations . . . . .	134
	<b>Appendices</b>	<b>144</b>
<b>A</b>	<b>Individual Specimen Results</b>	<b>145</b>
A.1	Density and Cross-Sectional Dimension Test . . . . .	145

A.2	Fiber Content Test . . . . .	147
A.3	Transverse Shear Test . . . . .	148
A.4	Horizontal Shear Test . . . . .	149
A.5	Tensile Test . . . . .	151
A.6	Bond-to-Concrete Test . . . . .	152

# List of Figures

2.1	Continuous basalt fiber production process (Ipbüker et al., 2014)	10
2.2	Thermoset polymeric resin used in FRP rebars	15
2.3	Schematic diagram of FRP rebar pultrusion (Borges et al., 2015)	18
2.4	Obtain position of exothermic peak (Borges et al., 2015)	19
2.5	Basalt FRP rebar production steps	21
2.6	Tensile stress and strain of different types of FRP according to Busel (2016)	22
2.7	Transverse shear fixture — Main body of fixture disassembled	25
2.8	Transverse shear fixture	26
2.9	Tensile strength test load transfer (Schesser et al., 2014)	27
2.10	FRP rebar tensile failure mechanism (Ehrenstein, 2006)	31
3.1	Chronology of documents related to the use of FRP rebar for concrete reinforcement	39
3.2	BFRP manufacturer locations	45
3.3	Production and storage strategies chosen by BFRP manufacturers	47
3.4	BFRP production rates (as reported by manufacturers)	48
4.1	Sample pictures of tested BFRP # 3 Rebars	52
4.2	Sample pictures of tested BFRP # 5 Rebars	52
4.3	Saw and diamond blade for BFRP rebar cutting	54
4.4	Precision saw	55
4.5	Electronic caliper	56
4.6	Precision scale, used to meet ASTM D 792 requirements	57
4.7	Tensile test preparation alignment frame	58
4.8	Transverse shear test concept	58

4.9	Transverse shear test — methodology . . . . .	59
4.10	Transverse shear box — parts . . . . .	59
4.11	Horizontal shear test concept . . . . .	60
4.12	Horizontal shear test — methodology . . . . .	60
4.13	Horizontal shear test fixture . . . . .	61
4.14	Bottom unit connected to actuator . . . . .	62
4.15	Tensile fixture installed in load frame . . . . .	62
4.16	Bond-to-concrete experimental setup . . . . .	63
4.17	Schematic of the mold . . . . .	64
4.18	Fixing the rebar and the plastic tube . . . . .	64
4.19	Laboratory setup in the HPMI . . . . .	65
4.20	MTS control panel . . . . .	66
4.21	MTS extensometer . . . . .	67
5.1	Fiber content percentage of rebars from all manufacturers . . . . .	76
5.2	Fiber content specimen of rebar type C #3, 5 after test . . . . .	77
5.3	Fiber content specimen of rebar #3 after test . . . . .	77
5.4	Moisture absorption results of rebars from all manufacturers . . . . .	78
5.5	Extension vs. transverse shear load behavior of type A rebars Lot 1 size 3 and 5 . . . . .	79
5.6	Extension vs. transverse shear load behavior of type B rebars Lot 1 size 3 and 5 . . . . .	80
5.7	Extension vs. transverse shear load behavior of type C rebars Lot 1 size 3 and 5 . . . . .	80
5.8	Extension vs. transverse shear load behavior of type C rebars Lot 2 size 3 and 5 . . . . .	81
5.9	Transverse shear stress vs. extension behavior of rebar type A Lot 1 size 3 and 5 . . . . .	82
5.10	Transverse shear stress vs. extension results of rebar type B Lot 1 size 3 and 5 . . . . .	82
5.11	Transverse shear stress vs. extension behavior of type C Lot 1 size 3 and 5 . . . . .	83
5.12	Transverse shear stress vs. extension behavior of type C Lot 2 size 3 and 5 . . . . .	83
5.13	Failure pattern for tested rebar after transverse shear test . . . . .	85
5.14	Extension vs. horizontal shear load behavior of rebar type A Lot 1 size 3 and 5 . . . . .	87
5.15	Extension vs. horizontal shear load behavior of rebar type B Lot 1 size 3 and 5 . . . . .	88
5.16	Extension vs. horizontal shear load behavior of type C Lot 1 size 3 and 5 . . . . .	89
5.17	Extension vs. horizontal shear load behavior of type C Lot 2 size 3 and 5 . . . . .	89

5.18	Horizontal shear stress vs. extension behavior of rebar type A Lot 1 size 3 and 5 . . .	90
5.19	Horizontal shear stress vs. extension behavior of rebar type B Lot 1 size 3 and 5 . . .	90
5.20	Horizontal shear stress vs. extension behavior of rebar type C Lot 1 size 3 and 5 . . .	91
5.21	Horizontal shear stress vs. extension behavior of rebar type C Lot 2 size 3 and 5 . . .	91
5.22	Failure pattern for tested rebar after horizontal shear test . . . . .	92
5.23	Tensile strength vs. displacement behavior of rebar type A Lot 1 size 3 and 5 . . . . .	94
5.24	Tensile strength vs. displacement behavior of rebar type B Lot 1 size 3 and 5 . . . . .	95
5.25	Tensile strength vs. displacement behavior of rebar type C Lot 1 size 3 and 5 . . . . .	95
5.26	Tensile strength vs. displacement behavior of rebar type C Lot 2 size 3 and 5 . . . . .	96
5.27	Tensile stress vs. strain behavior of rebar type A Lot 1 rebar size 3 and 5 . . . . .	97
5.28	Tensile stress vs. strain behavior of rebar type B Lot 1 rebar size 3 and 5 . . . . .	97
5.29	Tensile stress vs. strain behavior of rebar type C Lot 1 rebar size 3 and 5 . . . . .	98
5.30	Tensile stress vs. strain behavior of rebar type C Lot 2 rebar size 3 and 5 . . . . .	98
5.31	# 3 rebar final failure pattern after tensile test . . . . .	100
5.32	# 5 rebar final failure pattern after tensile test . . . . .	100
5.33	Free end slip behavior of the tested rebar type A Lot 1 # 3 . . . . .	103
5.34	Free end slip behavior of the tested rebar type A Lot 1 # 5 . . . . .	104
5.35	Free end slip behavior of the tested rebar type A Lot 1 # 3 and # 5 . . . . .	104
5.36	Free end slip behavior of the tested rebars type B Lot 1 # 3 . . . . .	105
5.37	Free end slip behavior of the tested rebars type B Lot 1 # 5 . . . . .	105
5.38	Free end slip behavior of the tested rebars type B Lot 1 # 3 and # 5 . . . . .	106
5.39	Free end slip behavior of the tested rebar type C Lot 1 # 3 . . . . .	106
5.40	Free end slip behavior of the tested rebar type C Lot 1 # 5 . . . . .	107
5.41	Free end slip behavior of the tested rebar type C Lot 1 # 3 and # 5 . . . . .	107
5.42	Overview rebar surface after bond strength test on type A Lot 1 rebar # 3 . . . . .	108
5.43	Overview rebar surface after bond strength test on type A Lot 1 rebar # 5 . . . . .	108
5.44	Overview rebar surface after bond strength test on type B Lot 1 rebar # 3 . . . . .	109
5.45	Overview rebar surface after bond strength test on type B Lot 1 rebar # 5 . . . . .	109
5.46	Overview rebar surface after bond strength test on type C Lot 1 rebar # 3 . . . . .	109
5.47	Overview rebar surface after bond strength test on type C Lot 1 rebar # 5 . . . . .	110

6.1	Gaussian distribution for tensile strength of # 3 rebars . . . . .	125
6.2	Gaussian distribution for tensile strength of # 5 rebars . . . . .	125

# List of Tables

- 2.1 Average chemical composition of basaltic rocks based on 3594 analyzed rock samples 9
- 2.2 Typical properties of resin matrices . . . . . 16
- 2.3 Environmental reduction factor for various fibers and exposure conditions . . . . . 32
  
- 3.1 Required test procedures and specimen quantities per acceptance test and production lot . . . . . 42
- 3.2 Required sizes and tensile loads of FRP reinforcing bars . . . . . 43
- 3.3 Production logistics and rates per manufacturer . . . . . 46
- 3.4 BFRP rebars produced by manufacturer . . . . . 49
  
- 4.1 Physical and mechanical tests on BFRP rebars . . . . . 51
- 4.2 Physical characteristics of tested BFRP rebars . . . . . 52
- 4.3 Acceptance criteria for GFRP rebar # 3 . . . . . 53
- 4.4 Acceptance criteria for GFRP rebar # 5 . . . . . 53
  
- 5.1 Statistical evaluation of diameter measurements for rebar size # 3 and # 5 . . . . . 75
- 5.2 Transverse Shear test statistical values for each sample group (US Customary Units) 86
- 5.3 Horizontal Shear test statistical values for each sample group (US Customary Units) 93
- 5.4 Tensile strength test statistical values for each sample group (US Customary Units) 102
- 5.5 Bond-to-concrete strength test statistical values for each sample . . . . . 111
- 5.6 Acceptance criteria for rebar type A # 3 . . . . . 112
- 5.7 Acceptance criteria for rebar type A # 5 . . . . . 112
- 5.8 Acceptance criteria for rebar type B # 3 . . . . . 113
- 5.9 Acceptance criteria for rebar type B # 5 . . . . . 113
- 5.10 Acceptance criteria for rebar type C # 3 . . . . . 114

5.11	Acceptance criteria for rebar type C # 5 . . . . .	114
6.1	Guaranteed shear and bond-to-concrete strength of rebars . . . . .	123
6.2	Guaranteed strength and elastic modulus of rebars . . . . .	124
6.3	Reduction factors . . . . .	127
A.1	Diameter measurements for each individual specimen . . . . .	146
A.2	Fiber content test results for each individual specimen . . . . .	147
A.2	Fiber content test results for each individual specimen . . . . .	148
A.3	Transverse shear test results (ultimate values) for each individual specimen . . . . .	148
A.3	Transverse shear test results (ultimate values) for each individual specimen . . . . .	149
A.4	Horizontal shear test results (ultimate values) for each individual specimen . . . . .	150
A.5	Tensile strength test results (ultimate values) for each individual specimen . . . . .	151
A.5	Tensile strength test results (ultimate values) for each individual specimen . . . . .	152
A.6	Bond-to-Concrete strength test results for each individual specimen (Imperial Units)	152
A.6	Bond-to-Concrete strength test results for each individual specimen (Imperial Units)	153
A.7	Bond-to-Concrete strength test results for each individual specimen (Metric Units) .	153
A.7	Bond-to-Concrete strength test results for each individual specimen (Metric Units) .	154

# Chapter 1

## Introduction

### 1.1 Introduction

The Florida Department of Transportation (FDOT) continues to implement innovative materials to enhance the sustainability and durability of the infrastructure. Because Florida is a coastal state with many structures exposed to saltwater (e.g., the splash zone for bridge piers), the FDOT currently works progressively on research and applications of non-corrosive materials, such as fiber reinforced polymers (FRP) reinforcement bars (rebars), in an effort to replace or substitute traditional steel rebars. Over the last two decades, technological advancements have facilitated the use of glass fiber reinforced polymer (GFRP) and basalt fiber reinforced polymer (BFRP) composites as internal rebars for concrete structures. These emerging materials are a modern, viable alternative to traditional steel reinforcement due to significant advantages (e.g., magnetic transparency, lightness, and — most importantly — corrosion resistance) that can lead to more durable concrete members and extended structural life. Hence, a key initiative for the Florida Department of Transportation is the progressive implementation of FRP technology for concrete reinforcement in infrastructure projects.

In a recently completed FDOT research project, GFRP rebars were evaluated for physio-mechanical and bond-to-concrete properties to properly implement GFRP rebars in concrete for the use in aggressive environments (FDOT research project BDV 30 977-18). The project showed that the material properties of FRP rebars are beneficial for the use in concrete, and that the technology has the potential for standardized use in publicly funded construction projects via im-

plementations in design specifications (FDOT's Standard Specifications for Road and Bridge Construction — Section 932-3). However, the past projects have mostly focused on glass FRP rebars, because glass fibers are more dominant in the US market and Basalt FRP rebars have not yet been thoroughly investigated for public agencies. The activities performed for this project followed similar efforts as conducted for BDV 30 977-18, but target the virgin material characteristics and bond-to-concrete properties of basalt fiber reinforced polymer reinforcement bars (BFRP Rebars) to evaluate a second/additional alternative that can replace traditional rebars.

Basalt is a volcanic rock which can be formed into continuous fibers through melting raw basalt at approximately 1500 °C and using technologies similar to those used for the production of E-Glass and AR-Glass fibers. Only raw basalt rock is necessary to produce the fibers, and the purity of the basalt depends on the source rock only. Because no additional chemical components are needed to produce basalt fibers, they are considered a “greener product” (relative to glass fibers). Basalt filaments are formed by platinum-rhodium bushings (similar as for glass filaments), and a sizing agent is applied during the cooling process, before the fibers are spooled. Due to the inherent properties of basalt and the different chemistry from glass fibers, basalt fibers are more chemically resistant, have a higher tensile strength, and have a modulus of elasticity that exceeds the elasticity of E-glass fibers by about 15 % to 30 % (Rarnalaishnan and Tolmare, 1998). In addition, basalt fibers are more UV-resistant, have a higher fire resistance, and better retain physical characteristics in cold temperatures. Finally, the production of basalt fibers are more environmentally friendly than the production of glass fibers because toxic ingredients can be omitted.

For the production of BFRP reinforcing bars, the basalt fibers are embedded in a polymeric resin matrix, similar to GFRP rebars. In a high quality produced basalt fiber reinforced polymer rebar, the basalt fibers carry the load (primarily in tension), while the resin matrix protects the fibers, binds them, and also transfers the load between them. Matrices are typically thermosetting resins; epoxy resins seem to be preferred for BFRP because of the high mechanical toughness and excellent corrosion resistance; coupled with ease of manufacturing, epoxy resins are ideal for FRP pultruded systems. Drawbacks of epoxy resins include low modulus of elasticity, sensitivity to abrasion, relatively low fatigue resistance, and high cost. The main factors affecting the characteristics of an FRP rebar include fiber volume, dimensional effects, rate of curing, manufacturing process, and quality control measures during manufacturing. The unit weight of BFRP rebars is about one-third

of steel, which reduces transportation costs and makes the rebars easy to handle at the job site, yielding additional benefits to its implementation (Rarnalaishnan and Tolmare, 1998). To ensure proper bond between the the pultruded BFRP rebar and the concrete, a surface treatment is applied to increase the friction at the bond interface or to improve the interlocking effect. Manufacturers have developed different BFRP rebar types, where the surface enhancement varies (sand-coated, helical wrapping, lugs, etc.). Accordingly, various different BFRP rebars exist and their properties are highly dependent on the used raw and the proprietary production techniques.

The American Concrete Institute Committee 440 (ACI440) has led the effort to address the technical implementation for GFRP rebars by developing and publishing test methods, specifications, and design guidelines (ACI Committee 440, 2006, 2012, 2008b, 2013). Previous versions of ACI440 (ACI Committee 440, 2008a) and the 2010 version of the Canadian-CSA Specifications for Fiber Reinforced Polymers (Canadian Standard Association, 2010) were developed to standardize glass, carbon, and aramid FRP bars. The Canadian Standards Association (CSA) has led the western effort for developing specifications and design guidelines for BFRP, and the new CSA S807 (Benmokrane, 2018) standard includes FRP bars made with basalt fibers that emphasize the current importance of this material and the confidence of a commercialized usage in the field (Vincent et al., 2013). Similarly, ASTM Committees D30 and D20 have addressed the emergence of this technology by developing a number of test methods (ASTM-International, 2015a) intended to characterize GFRP rebars. In addition, the FDOT has developed documents to aid the implementation and design of GFRP rebar technology for the built infrastructure, specifically Section 932 for nonmetallic accessory materials for concrete pavement and concrete structures (Ruelke, 2014), and more recently the fiber reinforced polymer guidelines (FRPG) (Florida Department of Transportation, 2015) are important documents in this context. At the national level, AASHTO has also developed guides for the use of FRP technology (AASHTO, 2012) for externally bonded systems. AASHTO (2018) describes the unique material properties of GFRP composite materials and lists provisions for the design and construction of concrete bridge elements reinforced with GFRP reinforcing bars. It is desired to add BFRP specific criteria to these specifications and guidelines as soon as practical to provide redundant supply chains and potentially improved performance expectations. Moreover, the International Code Council Evaluation Service (ICC-ES), which is the industry leader in performing technical evaluations for code compliance as part of the International

Code Council (ICC) that develops model codes and standards, published the Acceptance Criteria for the use of GFRP and BFRP rebars for concrete reinforcement, known as AC454 (International Code Council Evaluation Services, 2017). Hence, today any structure that is to be built according to the requirements of the Florida Building Code, which is based on the model code (International Building Code, IBC), can be realized with BFRP rebar technology.

Unlike carbon and glass fiber reinforced materials, basalt fibers have not been widely used, which results from a lack of research and required testing to establish this material as a serious competitor. The increasing demand on the infrastructure, as well as environmental challenges due to the unique climate and location of the State of Florida, resulting in accelerated degradation of infrastructure, need to be addressed by making progress toward safe and long-term infrastructure solutions.

## 1.2 Problem Statement

In recent years, the number of reinforced concrete (RC) structures specifying FRP rebars has increased significantly due to a more pronounced need for more resilient structures. In response to these structural trends, the number of BFRP rebar manufacturers has grown quickly. However, compared to other construction materials (and specifically compared to traditional steel rebar manufacturing), the production of BFRP rebars has not been standardized yet. Consequently, different products have been developed by various manufacturers, and these products differ notably in characteristics — dependent on the raw materials, material proportions, production processes, and final geometric features. Accordingly, the most suitable products are yet to be identified and the present state-of-production-practice has to be studied to identify the currently available products and the market trends in an effort to centralize the most important strength and material properties that engineers will need throughout the structural design process. This is important because inferior rebar products are available in the current market, and if these products remain indistinguishable from high-quality BFRP rebars, they may lead to misuse and potential failure. To consistently and safely use or implement BFRP rebar technology for infrastructure projects, the material properties of high-quality rebar products from different manufacturers have to be characterized and evaluated to develop robust acceptance criteria for basalt based FRP rebars in FDOT Specifications Section 932. A strategic approach is needed to better use and improve this technology such that the different products can be categorized and the effect of individual BFRP rebar attributes can be determined.

Minimum criteria specific to Basalt FRP rebars are desirable because such benchmark values will help manufacturers most efficiently target defined quality parameters that FDOT, and ultimately other state DOTs, can rely on. Likewise, threshold values are needed, under the mandatory low-bid procurement system, to guarantee safe and reliable designs of future concrete structures, which are internally reinforced with BFRP rebars.

### **1.3 Project Objectives**

The project objective was to complement existing FRP rebar specifications and to identify non-corrosive BFRP rebar technologies for concrete reinforcement with suitable surface enhancements for the construction of durable, resilient, and potentially more sustainable infrastructure in Florida. It was the goal to provide test data and recommendations to inform the currently ongoing efforts toward a full implementation of this emerging technology by the FDOT, such that special project specific approvals for BFRP rebars may not be necessary in the future. To embrace BFRP rebar technology, a comprehensive literature review and a worldwide state-of-the art summary of currently manufactured BFRP rebars was necessary to provide relevant information for the selection of representative BFRP rebars for the subsequent experimental program. It was the intention of the experimental program to target physical, mechanical, and bond-to-concrete characteristics of BFRP rebars to evaluate the most essential material properties of virgin (or unaged) BFRP rebars in an effort to classify the material performance. These tasks aimed to identify suitable BFRP rebar technologies for use in Florida. Because potential future research projects will focus on refining durability modeling of BFRP rebars, it was an additional goal to obtain benchmark values for subsequent studies — in which BFRP rebars may be exposed to harsh environments for extended times, before they are tested for property retention characteristics. While material characterization was an important objective for this research project, the ultimate goal was to provide experimentation-based recommendations and relevant updates to existing FDOT guidelines and specifications for the use of BFRP rebar in concrete structures. Likewise, recommendations and relevant updates for future updates of the 2<sup>nd</sup> edition of the AASHTO LRFD Bridge Design Guide Specifications for the GFRP Reinforced Concrete was an additional goal of this research.

## 1.4 Project Scope

In this research project, the physical characteristics and material properties of three representative but distinct BFRP rebars were evaluated. These three rebar types were produced by different manufacturers (Galen Panamerica, RockRebar<sup>®</sup>, Pultrall), and each rebar type had various distinctive features (dissimilar fiber types, various resin types, different surface enhancement properties, etc.). Representative samples (specimen groups) of two commonly used rebar sizes (# 3 and # 5) were exposed to a multitude of experiments in their virgin material state. First, the physical properties of each rebar type and size were studied before the mechanical strength properties were evaluated. Physical tests on rebars included density measurements or measurement of cross-sectional dimensions, percentage of fiber contents, and moisture absorption characteristics. Mechanical tests were conducted to determine the transverse shear strength, horizontal shear strength, tensile strength including elastic modulus properties, as well as the bond-to-concrete characteristics. All test data were statistically reduced and compared to the prevailing material specifications or acceptance criteria for FRP rebars (AC454, ASTM D7957, etc.). Because ASTM acceptance criteria for BFRP rebars in the US are yet to be established, the performance of the tested BFRP rebars was evaluated based on the available acceptance criteria for glass FRP rebars according to FDOT Specification Section 932. Based on the experimental findings, theoretical analysis of the results, and literature reflections, recommendations were provided to supplement FDOT Specifications Section 932 for the implementation of acceptance criteria for BFRP rebars and to develop AASHTO design guide recommendations for BFRP reinforced concrete structures.

## 1.5 Report Organization

To provide a structured overview of the completed research, this report was divided into seven chapters, which are briefly described here. After the introduction presented in this chapter, the following Chapter 2 presents background information about BFRP rebar technology, historical developments in the basalt fiber and BFRP rebar industry, as well as information about raw constituent materials, and the production processes. In addition, existing literature with a focus on physical and mechanical properties of BFRP rebars are presented. Chapter 3 describes the development of BFRP rebar specifications and the current state-of-the-market (industry profile). A detailed description of

the experimental methodology, the conducted test procedures, and the experimental concepts are detailed in Chapter 4. The relevant test protocols (ASTM, ACI, etc.) that were followed for each individual experiment are described to ensure the repeatability and accuracy of the experimental approach. Likewise, all equipment and test devices are listed and described in detail along with the materials that were needed to prepare the specimens for testing. While Appendix A lists all individual test results for each tested specimen, Chapter 5 concisely presents the obtained test group results for all conducted experiments in the form of graphs and tables; it also documents the typical failure patterns for each conducted test procedure and for each evaluated rebar type. A detailed discussion addressing recommendations for BFRP strength and material properties along with design specifications for FDOT Specifications Section 932 and propose AASHTO design guidance for BFRP reinforced concrete structures is presented in Chapter 6. Finally, in Chapter 7, a summary of this project is followed by a concise list of conclusions that were drawn based on the entirety of this research project.

## Chapter 2

# Background

After a brief introduction of the research, this chapter provides a detailed description of Basalt Fiber Reinforced Polymer (BFRP) reinforcement bars (rebars) from the production of the fiber over the properties of the composition material of the rebar and its usage. Fibers and composite materials have gained a lot of attention in the recent decades because of their wide availability and special properties like the high strength-to-weight ratio. The first attempts to produce basalt fibers go back to Paul Dhé (from Paris, France), who invented a basalt fiber furnace in the United States in 1923 (Dhé, 1923; Colombo et al., 2012). The technology did not gain a lot of traction in the US due to initial production difficulties and more profitable opportunities with glass fibers. After the manufacturing process for glass fibers was successfully industrialized in Toledo, Ohio, by Games Slayter in 1933 (Slayter, 1938), the major fiber producers in the US abandoned basalt fiber research in favor of their main glass products (Faruk et al., 2017). However, extensive research on basalt fibers was conducted in the former Soviet Union, during the Cold War (Jamshaid and Mishra, 2016), for military purposes in a search for ballistic resistant textiles. After the Soviet Union collapse in 1991, the research projects were declassified (in 1995) and released for civilian applications. In consequence, basalt fibers are a recent development in the construction industry and most basalt fiber producing companies are now located in countries that used to be associated with the Eastern Bloc (Zych and Wojciech, 2012). Nowadays, basalt fibers gain attention from different industry fields all over the world. Before the fibers can be used for composite products, the fiber itself is produced from raw basalt. Therefore, the next section 2.1 introduces the origin of continuous basalt fibers.

## 2.1 Igneous Rocks

The source material is an important factor in the characterization process for basalt fibers. Igneous rocks are one of the three main classes of rocks, besides sedimentary and metamorphic rocks. Igneous rocks are formed from molten material, mostly classified on the basis of their composition (either mineralogical or chemical) and according to their silica content. Molten rock material below the surface is called magma and then described as lava as soon as it reaches the earth surface. Igneous rocks have to be separated into plutonic rocks (coarse-grained igneous rocks that solidified within the crust), which are usually classified according to their mineralogical composition, or volcanic lava rocks (fine-grained and solidified at or very near the earth crust surface with a faster cooling process), which are classified according to their chemical composition (Best, 2003).

Basalt is the most common volcanic rock on Earth and basaltic rocks (including gabbro, diabase, and their metamorphosed equivalents) are the most common rocks in the Earth's crust. Gabbro is a coarse-grained plutonic equivalent of basalt that solidified within the Earth's crust. Diabase is compositionally equivalent to gabbro and basalt but in its physical structure (grain structure) between them. It forms into basalt when it solidifies rapidly and to gabbro when more time is given for the crystals to grow (Maitre, 2002). Besides the structural differences, the chemical structure is defined for all three types of raw basalt similar to that shown in Table 2.1. Basalt has a strict

Table 2.1: Average chemical composition of basaltic rocks based on 3594 analyzed rock samples

Rock Type	$SiO_2$	$TiO_2$	$Al_2O_3$	$Fe_2O_3$	$FeO$	$MnO$	$MgO$	$CaO$	$Na_2O$	$K_2O$	$P_2O_5$
Basalt	50	1.8	16	3.9	7.2	0.2	6.8	9.7	3.0	1.1	0.3

chemical definition that contains more than 45 percent and less than 52% of  $SiO_2$  and less than five percent of total alkalis ( $K_2O + Na_2O$ ). High silica and low iron contents ensure the production of fibers with high strength properties. When meeting the requirements of the chemical composition, any of the described raw materials can be used for the basalt fiber production, which is regulated by different national documents. Russian specifications for basalt fiber are defined as melted basalt or gabbro-diabase (ISC, 2014). After the clarification of the proper source for the fiber production, the next section 2.2 shows the manufacturing process of fibers.

## 2.2 Fiber Types and Production

The section below summarizes the main fiber types that are in use for structural engineering applications. Additionally, the two production methods for basalt and glass fibers are explained to have a comparison to the most used fiber types.

Fibers commonly used to produce FRP rebars are glass, carbon, and aramid because of their higher tensile strength in comparison to traditional steel. As a drawback compared to steel, tensile failure of FRP rebars show linear-elastic response with sudden breakage. Basalt fibers show better mechanical properties than glass fibers, and they are more widely available and cheaper than carbon fibers (Zych and Wojciech, 2012). Continuous basalt fibers have become commercially available as an alternative to glass fibers. Glass has been the predominant fiber for many civil engineering applications because of an economical balance of cost and specific strength properties. In addition, they were (in exactly the same way becoming available to the international market offering different kinds of fibers (ACI Committee 440, 2007). The following subsections detail the production of different fiber types, starting with basalt based fibers.

### 2.2.1 Basalt Fiber

According to the Russian specifications for fiber reinforced polymer bars, basalt fibers for polymer composites reinforcement are made from melted basalt or gabbro-diabase (ISC, 2014) as described in Section 2.1. The schematic process of the basalt fiber production is shown in Figure 2.1. Starting

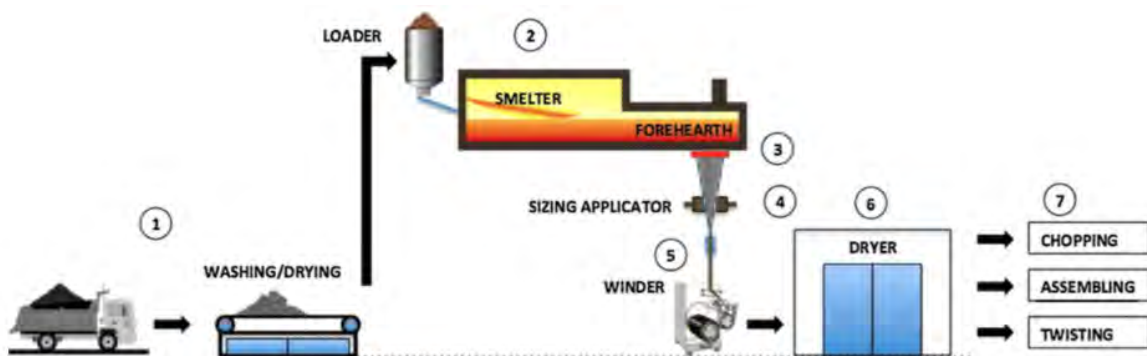


Figure 2.1: Continuous basalt fiber production process (Ipbüker et al., 2014)

on the left side of the figure, the raw basaltic rock is first crushed, washed, and then transported to a furnace. The melting process requires a minimum melting temperature of approximately 1450°C

(2640°F). Unlike glass, infrared energy is absorbed by the opaque basalt, and therefore, it is more difficult to uniformly heat the entire basalt mixture. Molten basalt must be held in the smelter for extended periods of time to ensure a homogeneous temperature. When melting occurs and uniformity is reached by removal of gases, the molten basalt flows into the fore hearth (Ipbüker et al., 2014). The molten material is forced through a platinum/rhodium crucible bushing with 9 to 24 micrometer nozzles to extrude continuous fibers. Basalt fibers are sized during the manufacturing process (in the same way as glass) to protect the fiber and to impart the resin compatibility needed for optimum performance. Sizing such as silences, starch, gelatin, oil, or wax is applied to improve the bond and to minimize degradation of filament strength that would otherwise be caused by filament-to-filament abrasion (Bagherpour, 2012; Zych and Wojciech, 2012). The fibers can be made in the form of chopped fibers (cheaper and lower mechanical properties) or continuous fibers rovings (spinneret method) (Fiore et al., 2015). After the basalt fibers are produced, they are converted (packaged or spooled) into a suitable form for each particular application (Pavlovski et al., 2007).

Only raw basalt is necessary to produce the fibers, and the purity of the raw material for the fibers depends only on the rock source. As a consequence of specific kinds of original rock sources, more than one category of basalt fibers with different chemical compositions may be obtained. Due to these factors, basalt fibers may take on different mechanical or physical properties (Zych and Wojciech, 2012). During the production process no additional chemical components are needed to produce basalt fibers. Toxic ingredients, typically used in glass formulation, can be omitted, therefore, they are considered as a “greener product” (relative to glass fibers) (Zych and Wojciech, 2012). The production of glass fibers requires the addition of several ingredients and a tedious mixing process. The properties and production process are listed in the upcoming subsection 2.2.2.

### **2.2.2 Glass Fiber**

This subsection describes glass fibers and their production for comparison to basalt. The most common types of glass fibers are electrical (E-glass), high strength (S-glass), and alkali-resistance (AR-glass). E-glass is the most common reinforcement material used in civil and industrial structures. Those fibers are named E-Glass because they offer high electrical insulating properties. In addition, they are known for low susceptibility to moisture, and high mechanical strength. It is

produced from lime-alumina-borosilicate, which can be easily obtained from an abundance of raw materials like sand (Bagherpour, 2012). S-glass provides higher tensile strength and modulus of elasticity but is more cost prohibitive and so less preferable than E-glass. AR-glass is resistant in high alkali environments such as in concrete, but at the moment, no compatible sizing is available to use it in the FRP production where the fibers are combined with a thermoplastic resin (Nanni et al., 2014).

The main difference to basalt fibers is that glass is made from a complex batch of materials, whereas basalt filament is made from melting basalt rock with no other additives, which reduces the environmental impact. Major glass ingredients of the batch of materials are silica sand, lime stone, and soda ash. Silica sand is the glass former, while lime stone and soda ash is added for lowering the melting temperature. Additional materials can be mixed in for manipulating certain properties like adding borax for more chemical resistance (Aubourg et al., 1991). Fiberglass furnaces are generally divided into three distinct sections. First, the batch is delivered into the furnace section for melting. Then, the molten glass flows into the refiner section, where the temperature of the glass is lowered from 1370°C (2500°F) to about 1260°C (2300°F). In the last step, the molten glass is transferred into the end section located directly above the fiber-forming stations. The molten mass is rapidly cooled to prevent crystallization and formed into glass fibers by a process also known as fiberization. Nearly all continuous glass fibers are made by a direct draw process and formed by extruding molten glass through a platinum alloy bushing that may contain up to several thousand individual orifices (Wallenberger et al., 2001). Typical glass fiber diameters range from 3 to 20 micrometers. Individual filaments are combined into multifilament strands, which are pulled by mechanical winders at velocities of up to 61 m/s (200 ft/s) and wound onto tubes or forming packages (Wallenberger et al., 2001). After describing the production of glass fibers, carbon fibers are presented in the next subsection.

### **2.2.3 Carbon Fiber**

Primarily, carbon fibers are used for pre-stressed strands (and not as much for regular rebar purposes) in civil structures because of their high tensile strength, high modulus of elasticity, and most importantly, because of its creep resistance, which is significantly higher when compared to glass or basalt fibers. Carbon fibers made from polyacrylonitrile (PAN) are typically classified as

high-modulus carbon fiber. Fibers made from carbon typically have a high fatigue strength, high resistance to alkali or acid attacks, a low coefficient of thermal expansion (CTE), and high electrical conductivity. However, it also has a relatively low impact resistance, can cause galvanic corrosion in contact with metals, and has a significantly higher unit cost. Accordingly, proper sizing must be applied before these fibers can be embedded in resin similar to other fibers on the market. Moreover, carbon fibers have the highest tensile strength (three times the strength of glass fibers) , but they are also the most expensive (about ten times more than glass fibers) (Nanni et al., 2014). Another fiber type used for engineering purposes are aramid fibers (see subsection 2.2.4).

#### **2.2.4 Aramid Fiber**

Aramid fibers are organic aromatic polyamide based with high fatigue and creep resistance. In addition, these fibers are good isolators for electricity or heat. However, they are sensitive to ultraviolet (UV) light, high temperature, and moisture, and a good chemical or mechanical bond between the aramid fibers and resin is difficult to achieve (Bagherpour, 2012). Within the wide availability of different grades, Kevlar 29, 49, and 149 are the most common fibers in structural applications. Compared to glass fibers, aramid fibers have a higher tensile strength and also a 50 % higher modulus of elasticity. Nevertheless, the use of these fibers is limited by the high material costs in the production of FRP bars (Nanni et al., 2014).

#### **2.2.5 Fiber Types Summary**

Compared to the other fibers, basalt has the highest density and a considerably high ultimate strain. The lowest strain combined with the highest tensile modulus is generally found for carbon fibers (Low- and high-modulus). Glass fibers measure the lowest tensile strength and modulus. Aramid fibers, in addition to carbon fibers, are not suitable for the commercial use of composite rebars because of economical aspects. Therefore, the focus for FRP rebars is on glass and basalt fibers because of a wide availability and cost efficiency. While the most important fiber types are shown in the subsections above, the next section 2.2.6 focuses on the properties of basalt and its comparison to glass fibers.

## 2.2.6 Properties of Basalt Fibers

The paragraph below is summarizing properties with their advantages and disadvantages of basalt fibers. Basalt is a volcanic rock that can be formed into continuous fibers through melting pure raw basalt and using technologies similar to those used for the production of glass fibers. Due to the inherent properties of basalt, the fibers are more chemically resistant, have a higher tensile strength, and a modulus of elasticity that exceeds the elasticity of glass fibers by about 15% to 30% (Rarnalaishnan and Tolmare, 1998). In addition, basalt fibers are more UV-resistant, have a higher fire resistance, and they better maintain their physical characteristics in cold temperatures. Basalt fibers are reported to withstand temperatures from  $-260^{\circ}\text{C}$  to  $750^{\circ}\text{C}$  (Bagherpour, 2012). The variety of advantages is combined in a stiff rod used as reinforcement by adding a resin matrix. The composite system of fibers and resin is combining advantages of two materials to eliminated disadvantages of the individual parts. Therefore, the following section 2.4 details the different resin types, their individual properties, and how the resin is used in the FRP rebar production.

## 2.3 Sizing

Sizing is a protective coating applied in the fiber manufacturing process. The sizing not only plays a key role in improving rebar properties (due to the load transfer between fiber/matrix inter-phase) but also crucial role in enhancing the durability properties of rebar. Sizing is typically selected and paired based on the type of fiber-resin matrix. Although sizing is an important process, it was observed that no specification or standards exist. Due to the proprietary nature of sizing material and application, it is considered that specifying sizing is not feasible, and durability aging tests must be used to identify adequate sizing, that are compatible with the fiber and matrix.

## 2.4 Resin Types and Properties

Next to the fibers, the resin is the other important material to produce a high quality FRP rebar. It is used to bond the fibers together a two-component system. The main functions of the resin matrix are to protect the fibers from mechanical and environmental attacks, to maintain the alignment of fibers, and to guarantee proper load transfer between individual fibers. Resins have proven their suitability for use in FRP reinforcing bars by maintaining chemical stability under

harsh environmental conditions and by protecting the fibers from aggressive chemicals that would otherwise damage the filaments (Benmokrane et al., 2002).

Two major groups of resins exist: the thermoset (once cured, they cannot be converted back to their liquid state) and thermoplastic (soft when heated) resins. Thermoplastic resins are typically not used for civil engineering purposes because they melt when heated and solidify when cooled. Thermoset resins cure permanently and irreversibly at elevated temperatures (Bagherpour, 2012). The most common thermosetting resins used in the composites industry are epoxies, unsaturated polyesters, and vinyl esters (ACI Committee 440, 2007). Currently, vinyl esters are predominantly used for the production of FRP rebars followed by epoxy, with polyesters typically excluded from permanent applications due to durability concerns. Initially, in their virgin state, thermoset polymeric resins are usually liquid at room temperature or solid with a low melting point as shown in Figure 2.2. The figure shows an example of a thermoset polymeric resin which is liquid at room



Figure 2.2: Thermoset polymeric resin used in FRP rebars

temperature, poured into a vessel. It can be used in the FRP rebar production process in a heated resin bath. Heat treatment and catalysts (hardeners) are used in the curing process to solidify the resin. After the curing process is completed, the material is permanently solidified through polymerization/cross linking of polymer chains, as it cannot be converted back to its initial liquid stage. The properties of typical resin matrices for FRP composites are listed in Table 2.2. Vinyl ester has the highest minimum tensile strength compared to epoxy and polyester, while polyester has the lowest moisture content and epoxy resin has the highest minimum glass transition temperature in the listed ranges. The density, the Poisson's ratio (transverse strain to axial strain), and the

Table 2.2: Typical properties of resin matrices

Resin Type	Density	Tensile Strength	Longitudinal Modulus	Poissons's Ratio	CTE	Moisture Content	Glass Transition Temperature
	$lb/yd^2$	$ksi$	$ksi$		$10^{-6}/^{\circ}F$	%	$^{\circ}F$
Epoxy	2000–2400	5–15	300–500	0.35–0.39	1.6–3.0	0.15–0.60	203–347
Polyester	2000–2400	7–19	400–600	0.38–0.40	1.3–1.9	0.08–0.15	158–212
Vinyl-ester	1900–2300	10–11	435–500	0.36–0.39	1.5–2.2	0.14–0.30	158–329

*Notes* :  $1lb/yd^3 = 0.593kg/m^3$ ;  $1ksi = 6.89N/mm^2$ ;  $^{\circ}F = (9/5^{\circ}C + 32)$

Coefficient of linear thermal expansion (CTE) are similar for all three types.

The following subsections describe suitable resins for an FRP production, starting with subsection 2.4.1 describing the specific properties of epoxy resin.

### 2.4.1 Epoxy

Epoxyes are well-established in the civil engineering sector because of their lower shrinkage properties in direct comparison to vinyl ester. Epoxy resins are usually used for high-performance composites with superior mechanical properties, resistance to corrosive liquids and environments, superior electrical properties, good performance at elevated temperatures, and excellent adhesion to a substrate. However, they have a low ultraviolet (UV) resistance and require post-cure (longer time in the die under certain temperatures) because of a higher viscosity than other resins (polyester or vinyl ester) (ACI Committee 440, 2007). Although epoxyes can be more expensive than other resins, they are more suitable for high performance applications. Epoxy resins are compatible with most composite manufacturing processes and are also, at the moment, the predominant adhesive of choice for concrete repair with FRP products. (Bagherpour et al., 2009). The following subsection 2.4.2 provides necessary information about polyester resin.

### 2.4.2 Polyester

Polyester can be classified as saturated and unsaturated. Thermoset unsaturated polyester resins represent approximately 75% of the composites industry. To initiate curing, the resin is dissolved in a monomer (like styrene) solution so that it can react with the unsaturated ends on the polymer, which then converts to a solid thermoset structure. The advantage is the balance of properties,

which include dimensional stability, cost efficiency, and ease of handling during processing. Because of different required properties such as flexibility, electrical insulation, corrosion, or heat resistance, a wide range of specific performance polyester resins are available (ACI Committee 440, 2007; Bagherpour et al., 2009). The last resin type combines advantages of epoxy and polyester, which are listed in subsection 2.4.3.

### **2.4.3 Vinylester**

Vinyl esters were developed to combine the properties of epoxy resins with the fast curing of polyester resins. In fact, it can have higher physical performance and costs less than epoxies. Due to the combined properties, mechanical toughness, and high corrosion resistance (ACI Committee 440, 2007). These characteristic enhancements do not need complex processing or a special fabricating process like epoxy resins. Vinyl ester resins are most commonly coupled with glass fibers (Nanni et al., 2014). However, in the current market, BFRP rebars are usually a combination of basalt fibers with epoxy resin.

Consequently, the next section 2.5 provides common production methods for BFRP rebars, combining the fibers with the resin in an automated process for mass production.

## **2.5 BFRP Rebar Production**

Different processes have been developed to combine the fibers and the resin for the efficient production of fiber reinforced polymer rebars. Typical production methods for fiber reinforced composite materials are pultrusion, wet-laying, braiding, or weaving. According to the literature and manufacturers, production processes like braiding or weaving are not used for the FRP rebar production. The following section describes the currently common processes to produce basalt FRP rebars: pultrusion and wet lay-up process. Based on cost efficiency, production speed, and product quality, pultrusion is the dominant manufacturing method. However, the production method is not standardized, which may lead to different rebar products from one manufacturer to another, such that each rebar manufacturer may produce entirely different rebars. Different investigations were obtained to verify these processes, identify possible weaknesses, and to make recommendations for standardization requirements. Scanning electron microscope (SEM) analysis has shown that porosity and voids are present with BFRP rebars. Researchers recommend that improvement in the

manufacturing process should be implemented to reduce and/or eliminate these defects (ElSafy et al., 2014). The first process is described in Subsection 2.5.1.

### 2.5.1 Pultrusion

The pultrusion method is the dominant process to manufacture FRP rebars because of its cost efficient and fast production. A continuous molding process combines fiber reinforcement and thermosetting resin, which produces a constant cross-sectional rebar (Figure 2.3). The figure shows

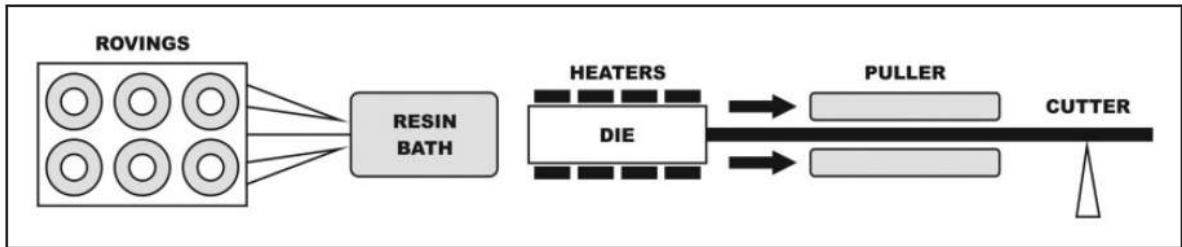


Figure 2.3: Schematic diagram of FRP rebar pultrusion (Borges et al., 2015)

from the left side on, that fibers are continuously pulled from rovings, to be wetted (impregnated) with the desired liquid resin in a resin bath. Borges et al. (2015), investigated the influence of resin bath temperature on the properties of pultruded GFRP rebars with polyester resin. It was shown that temperatures between 30 °C to 50 °C were suitable for the production process. Higher temperatures lead to a low viscosity and an insufficient wetting of the fibers before entering the heating die. The fibers are pulled through a heated metal die (with different heating zones) of the desired diameter, which defines the final shape. The recommended curing temperatures for resins is about 177 °C (Joshi et al., 2003). In the study of Borges et al. (2015) four heating zones were calculated ranging from 90 °C to 110 °C to 130 °C back to 110 °C again. The die was 900 mm long and the pulls speed was set at 0.46 m/min. Inside the pultrusion die, a controlled temperature lets the fibers and the resin harden while the heat activates the curing or polymerization of the thermoset resin until it changes its condition from liquid to solid. Inside the heating die the rebar reacts chemically and solidifies under an exothermic reaction forming from a liquid stage to a gel stage until the solid stage is reached. To set the rate of the manufacturing process, the gel time and the peak exothermic temperature of the thermoset resin need to be evaluated. The gel time is the moment where the mixed components start to solidify and the peak exothermic temperature is the maximum temperature the rebar itself reaches due to the reaction and therefore assigns the time of

the maximum reaction. Figure 2.4 shows a schematic of how the gel time and the position of the exothermic peak is evaluated (according to ASTM D 2471 - “Standard Test Method for Gel Time and Peak Exothermic Temperature of Reacting of Thermosetting Resins”). After the wet-out on the

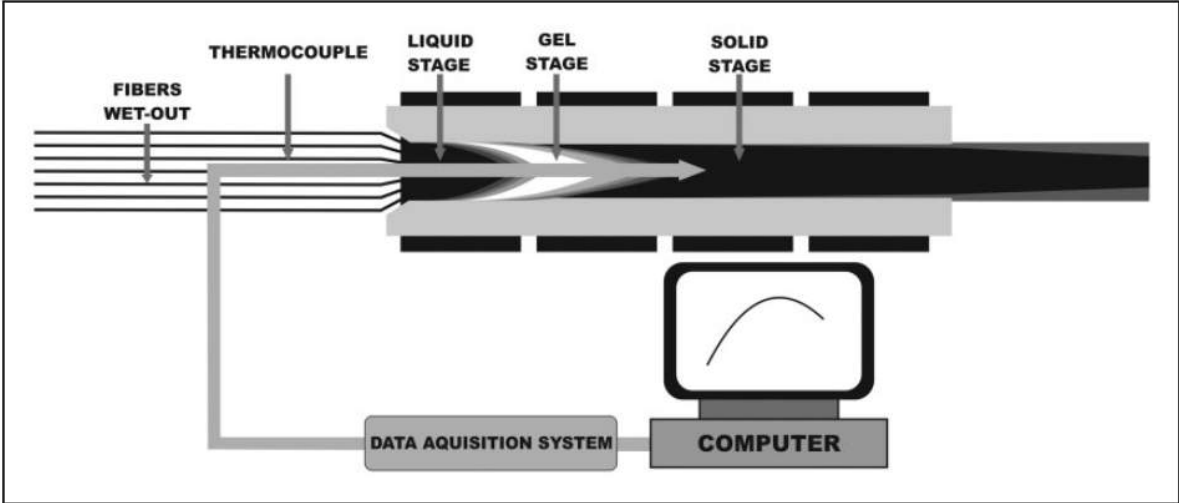


Figure 2.4: Obtain position of exothermic peak (Borges et al., 2015)

left side of the figure, the bundled fibers enter the heating die. A data acquisition system is collecting the data of the different hardening stages of the fibers to measure the exact point of the solid stage to determine the curing time in the die. Internal defects in the cured material, can lead to lower durability and mechanical properties, can be caused by estimating an incorrect rate. Therefore, the production rate is determined by the curing time of the resin. The composite solidifies when cooled and is cut to the desired length after pulling it through the pultrusion machine. Different processing variables can affect the quality and process efficiency such as die temperature, fiber content, pull speed, cure time, or resin viscosity. Accordingly, product availability and company logistics are constrained only by storage and transporting limitations. The pultrusion process has a significant influence on the final properties of FRP rebars, as it affects the rate of resin polymerization, the air void content, and thus, the fiber content. Moreover, to achieve a sufficient bond between concrete and the produced rebar in its final application, an additional process is required to apply the surface enhancement features. (You et al., 2015). These can come in the form of ribs, sand coating, , helical wrap, or combinations of both. Because of the fixed cross section of dies, a tight dimensional control of FRP rebars is assured. The pultrusion is considered to be a relatively simple process for the manufacturing of FRP bars, particularly for the production of straight rods. Coiling is also possible when smaller diameters are produced (ACI Committee 440, 2007; Patnaik, 2009). Because

of limitations of the method, small diameters are also produced with a different production process explained below (see Subsection 2.5.2)

### **2.5.2 Wet Lay-Up**

A newer automated FRP rebar production process is the wet lay-up process, developed by a Norwegian company (ReforceTech AS Norway). Because it is a recent development in the production of FRP rebars, products manufactured with this technique have not been researched widely. The production costs are believed to be reduced in comparison to the traditional pultrusion method because of a simple process with reduced working staff.

Wet lay-up is used to produce simple composites. A programmable arm with controlled movement in three orthogonal directions manufactures the rebars with the desired length and shape. Fibers impregnated with a polymeric resin are automatically laid to form an FRP rebar after curing. The fibers are guided through a funnel-like resin bath where thorough wetting and impregnation of the fiber take place. The wet fiber is then pulled to a working platform. Several layers are laid up one over the other to produce a one-dimensional FRP construct. This new production method is said to be less expensive, but contains several disadvantages such as inconsistent cross-sectional shapes or uneven surfaces due to non-uniform pull on the fiber threads, which leads to a wavy surface. However, this waviness attribute can be beneficial for bond-to-concrete behaviors but also leads to lower tensile strength. Bar diameters of 0.2 in. (5 mm) to 0.6 in. (16 mm) have been successfully produced using this process.

After the production process, tests of physical, mechanical, and durability properties are necessary for quality control and product verification processes. Mechanical testing is important for the specification and certification of FRP rebars. Therefore, the test procedures are described in Section 2.7, with a special focus on the tensile properties in Subsection 2.7.2, because they are the most important characteristic for the rebar classification and structural concrete design. Hence, the next section provides a general overview of the most important characteristics before detailing each test procedure individually.

## 2.6 BFRP Rebar Properties

This section focuses on the properties of the produced FRP rebar. These material characteristics of the final product are important for the application in civil structures. Figure 2.5 summarizes the process for the production of basalt fiber reinforced polymer (BFRP) reinforcing bars (rebar). Basalt fibers manufactured from molten basaltic rocks are embedded in a polymeric resin matrix,

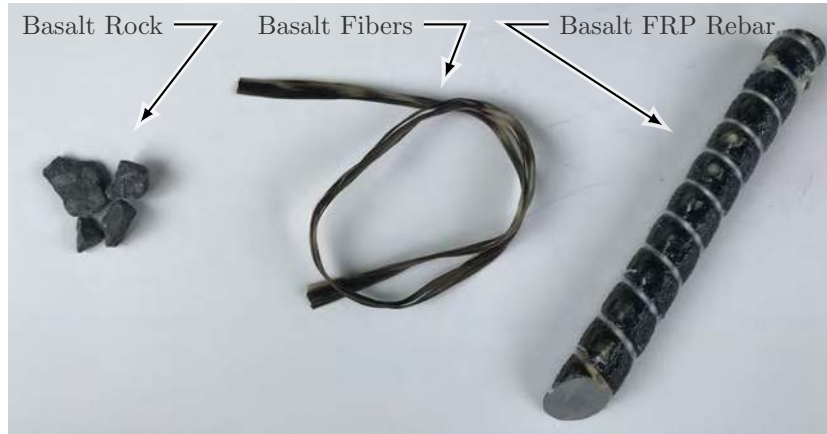


Figure 2.5: Basalt FRP rebar production steps

similar to GFRP rebars (from left to right). Mainly, fibers are known for their high tensile strength-to-weight ratio and — specifically when they form rebars — for corrosion resistance, as compared to carbon-steel (black) reinforcement. The fiber volume is mainly responsible for the tensile strength of the FRP rebar. According to the ASTM D 2584 “Standard Test Method for Ignition Loss of Cured Reinforced Resins,” the fiber content shall not be less than 55 % by volume or 70 % by mass and shall be reported by volume or by mass in accordance with the method used (ASTM-International, 2011). However, a volume fraction of about 80% is common for FRP rebars, and according to Bagherpour et al. (2009), a fiber content beyond that does not allow the fibers to be completely surrounded by the resin matrix. The tensile behavior of FRP rebars is characterized by a linear elastic stress-strain relationship up to failure as shown in Figure 2.6. The graph shows the stress-strain diagrams for different FRP composites compared to the stress-strain curve for steel (dot-dash line). The y-axis shows the tensile stress in MPa on the left and in ksi on the right side. The tensile strain in percent is provided on the x-axis. It can be seen that the incline of the FRP products are smaller than the one for steel (lower E-Modulus) but the point of maximum tensile stress is significantly higher for all FRP products. The biggest incline and highest tensile stress with the lowest strain

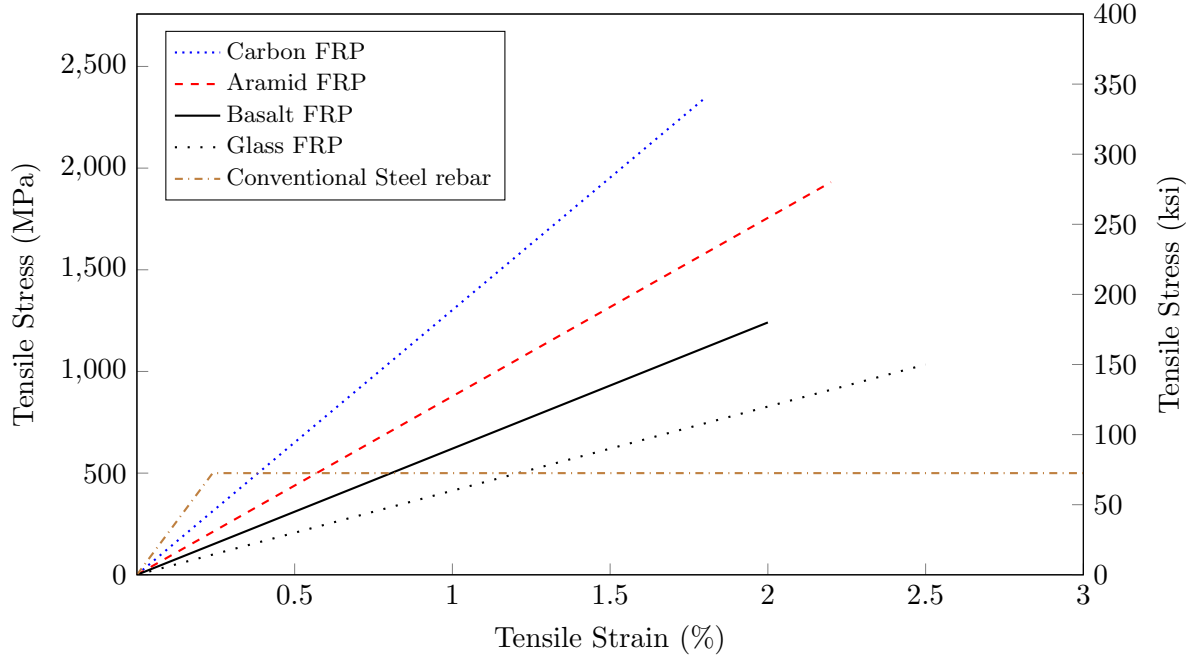


Figure 2.6: Tensile stress and strain of different types of FRP according to Busel (2016)

is reached by carbon FRP (tightly dotted line) followed by aramid FRP (dash line), which has a higher strain than basalt FRP (straight line). Glass FRP (wide dotted line) can be pointed out as the FPR product with the lowest tensile stress and lowest elastic modulus and basalt FRP is situated between aramid and glass. Compared to steel rebars, basalt FRP rebars offer higher tensile strength but lower ultimate tensile strain and lower tensile modulus of elasticity, which results in a more brittle failure for FRP products. Unlike steel, the tensile strength of an FRP rebar varies with its diameter, while the longitudinal modulus does not change appreciably. Based on the ongoing FDOT research project BDV 30 977-18, it is assumed that this phenomenon (known as shear lag) is due to the fact that the tensile force is usually introduced at the outer surface (via anchors) and the outer fibers have to transfer the load to the adjacent (inner) fibers through interface shear stresses in the resin matrix. Therefore, the shear lag effect becomes more significant as the bar diameter increases because the core of the bar is further distanced from the outer surface and more resin must be activated. This leads to lower strength measurements for larger diameter rebars because the inner core do not contribute completely to the load carrying mechanism before the outermost fibers start to fail. The tensile strain (or stretch) in the outermost fiber reaches its limit before the innermost fibers. The reason for the longitudinal modulus to remain almost constant (while the strength reduces with increasing bar diameter) is assumed to be a result of the measurement

technique, in which an extensometer is applied at the outermost surface — at the fiber that is activated to its full potential — independent of the rebar diameter.

## **2.7 Test Procedures for FRP Rebar**

To use any new FRP rebar product in publicly funded infrastructure projects, it has to meet or exceed specific test criteria and must be certified by an FDOT-approved laboratory. Numerous properties, such as the cross-sectional area, fiber content, moisture absorption, tensile strength, horizontal and transverse shear strength, bond strength, durability, etc., have to be evaluated for test groups that include multiple specimens from different production lots. The following subsections detail these tests to provide an overview of the general acceptance process and to provide context for the associated acceptance criteria listed in the next chapter.

### **2.7.1 Physical Characteristics**

#### **Density and Cross-Sectional Area**

To monitor physical changes in a sample while testing, and to indicate degree of uniformity in different specimens, the specific gravity of the product is determined through multiple specimens. A clean specimen is conditioned for at least 40 hours prior to testing in a temperature range from 21 °C to 25 °C at a moisture content between 40 % and 60 %, then it is cut to the desired length (while the minimum length is 10 mm and the maximum length is 50 mm) and the weight is recorded to the nearest 0.05 g. The recorded weight of the curtailed specimen should measure a minimum of 5 g and a maximum of 50 g. The density of test specimen is determined via the principle of buoyancy and the cross-sectional dimensions are calculated by dividing the determined volume by the measured specimen length. For the calculation of FRP rebar strength properties, the measured cross-sectional area is an important characteristic because strength values can differ significantly between strength values determined via nominal diameter dimensions and values determined from the experimentally measured area. It is the cross-sectional area per ASTM D 792 (ASTM-International, 2015b) that is used in many of the following test procedures to determine the strength characteristics.

## **Fiber Content**

To obtain the loss of resin in cured reinforced sample when exposed to constant high temperature, and to study the structure of the composite material via the relative material proportions (percentage of fibers vs. percentage of resin by weight), the FRP rebar specimens are tested for fiber content. A clean specimen is first conditioned for at least 40 hours prior to testing in temperature range from 21 °C to 25 °C at moisture content between 40 % and 60 %. Three samples (at minimum) with a known weight of at least 5 g and a maximum size of 25 mm × 25 mm in a crucible (of known mass) are exposed to a minimum of 565 °C in a muffle furnace until all resin is burnt and only the fibers remain. If the rebar product was made with sand on the surface for bond enhancement, this sand must be removed from the crucible before determining the fiber content. The percentage of fibers can be determined through the difference in weight before and after the burning process.

## **Absorption**

The moisture absorption properties of FRP rebars are determined according to ASTM D 5229 test standards. A total of 7 different methods are provided in ASTM D 5229 to find the moisture absorption in different environments. Procedure A is most commonly used, and is therefore, followed and described for this research project as well. At least three specimens per bar type are oven dried, if any moisture is present. Three diameter measurements are taken at 120° intervals perpendicular to the longitudinal axis of the FRP rebar, and those measurements are recorded to the nearest 0.001 mm. Then, each specimen is weighed with a precision of 0.05 g in its dry state. The specimens are then submerged in distilled water at a constant temperature. After two weeks in the water bath, the specimens are removed and the surface is toweled dry so that no free water remains on the surface of the rebar. Weight measurements are taken again with a precision of 0.05 g. This procedure is repeated and weight gains are monitored until three consecutive two-week measurements do not differ significantly from one another.



Figure 2.7: Transverse shear fixture — Main body of fixture disassembled

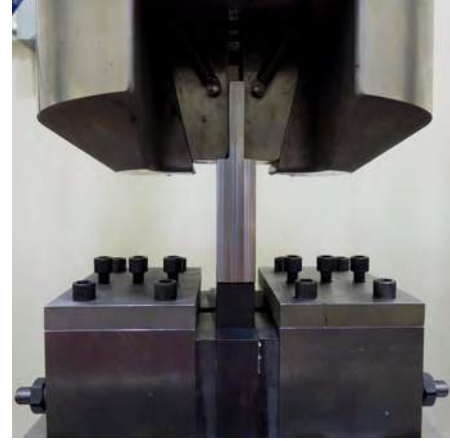
## 2.7.2 Strength Characteristics

### Transverse Shear Strength

The transverse shear strength is an important characteristic if the bars are used as dowels in concrete pavement, stirrups in concrete beams, or as general shear reinforcement elements. ASTM D 7617 (ASTM-International, 2012b) is used in the process of testing and analyzing the data. Before testing, the specimens are conditioned according to the ASTM D 5229 (ASTM, 2014). The conditioned specimen are then cut to length with a minimum length of 225 mm so that they fit in the shear fixture, which is a device that produces double shear on the FRP rebar specimen that is represented in Figure 2.8. This fixture has two bar seats, two lower plates, and two guides machined from steel, which are connected with two threaded rods using bolts and nuts. The conditioned and curtailed bars are placed inside the shear test fixture and tested with a displacement rate such that the test continuous for at least 1 minute and a maximum of 10 minutes until the force reaches 70% of the ultimate load. The transverse shear strength is determined using the ultimate load and the cross-sectional area of the specimen as measured per ASTM D 729 (see above).



(a) Assembled fixture in test frame



(b) Main body of fixture assembled

Figure 2.8: Transverse shear fixture

### Horizontal Shear Strength

Next, the FRP rebar product is tested for horizontal shear properties. The horizontal shear test is conducted according to the ASTM D 4475 (ASTM-International, 2012a) standards. This test alone does not suffice for design purposes, but the horizontal shear failure is an indicator for the strength of the resin, and therefore, is a well-suited quality control criteria and used for comparison among multiple specimens from the same manufacturer. First, the diameter at the center of the specimen is recorded and the specimens are conditioned at a temperature range from 21 °C to 25 °C and a moisture content between 40 % and 60 % before they are cut to a length of at least 5 times the diameter. A minimum of 5 specimen are tested per sample. The horizontal shear strength is assessed through a three-point load test over a span length that is short enough to prevent bending failure. The load is applied at the center of specimen with a displacement rate of  $1.3 \frac{\text{mm}}{\text{min}}$  until the shear failure is reached via horizontal delamination (failure of the resin). The ultimate load and the break type are recorded and analyzed.

### Tensile Properties

The test procedure to measure the tensile strength of FRP rebars is described in ASTM D 7205 (ASTM-International, 2015a). Because of the low shear strength of the FRP rebar, special preparations are required to properly test the rebars and to obtain proper results. A naked FRP rebar, gripped by the testing machine, would fail under high transverse stresses at the grip during the pulling process without reaching the ultimate tensile strength. Therefore, ASTM D 7205 describes

a method in which the FRP rebar has to be anchored on both ends with a steel pipe that is filled with an expansive grout or resin to transfer the loads from the testing machine into the rebar through friction. The grout or epoxy inside the anchor forms a cylindrical shell around the specimen. Because of the high stiffness of the steel tubes, the grout or epoxy exerts pressure on the specimen, which decreases the risk of premature failing in the grip region and clamps the rebar inside the steel tube. The basic idea of this system was to provide lateral pressure on the rebar in a sleeve to prevent slippage of the rebar. Further research work has shown that an internal pressure between 25 MPa (3.6 ksi) and 70 MPa (10 ksi) generated by the expansive cementitious material in the sleeve is enough to grip FRP tendons with different surface treatments (Schesser et al., 2014). The rebar with two anchors on the ends is then installed (after the grout cured one week) into the testing machine or into a fixture which is mounted into a test frame. Figure 2.9 illustrates one end of the prepared FRP sample with the applied anchor system. Normally, such grouts are poured

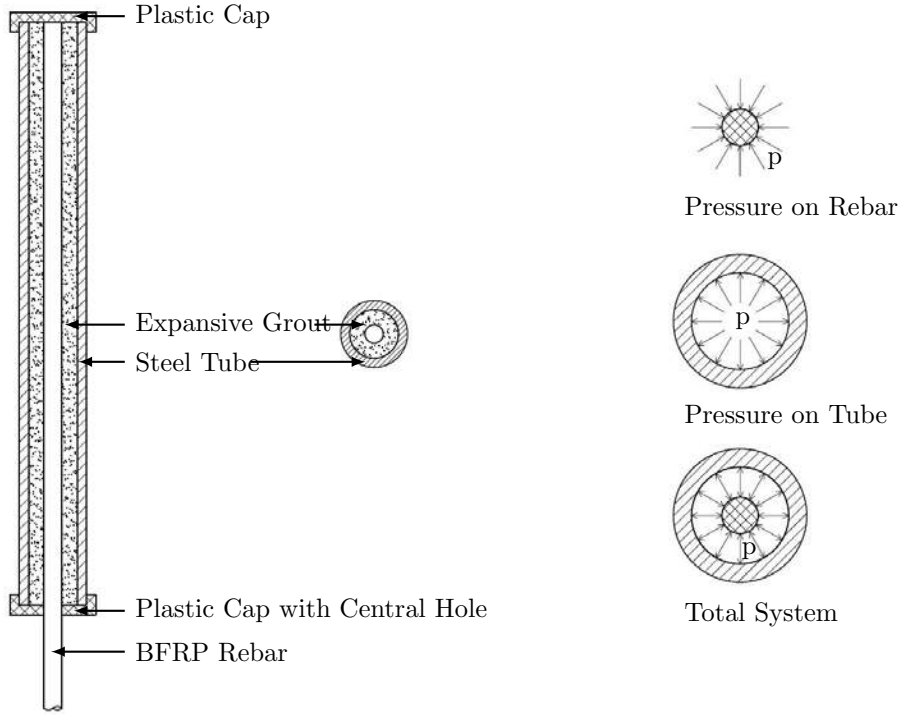


Figure 2.9: Tensile strength test load transfer (Schesser et al., 2014)

into holes drilled in rock or concrete as a non-explosive demolition agent. Because larger diameter rebars fail under higher loads, a longer anchor length (more friction) is required for longer rebars. The rebar diameter dependent anchor length is listed in ASTM for each rebar size.

According to the ASTM, the specimen length is dependent on the tested diameter of the rebar.

The total specimen length consists of two anchors of the both ends of the FRP rebar and the free specimen length in between the anchors. Because of shear lag effects, ASTM D 7205 prescribes the free specimen length with 40 times the diameter. Besides the effect of the gripped part of the FRP rebar test specimen, the free specimen length has not been fully evaluated yet, and only a few researchers have studied the behavior on GFRP rebars. The study of Castro and Carino (1998) dealt with tensile tests on five different GFRP rebar types (Diameter 9 mm to 15 mm) with a free specimen length from 40 to 70 times the diameter. The anchor length was set with 15 times the rebar diameter, which was evaluated in an expeditious approach and found to be the minimum anchorage length to avoid slippage of the FRP rebar. The intention was to evaluate the influence of the free-length-to-bar-diameter ratio on the measured tensile strength. The tested specimen from different manufacturers and different rebar diameters lead to no significant influences on the results. Different than Castro and Carino (1998) approach of longer specimen, the project of Gieben (2017) evaluated tensile tests on GFRP rebars from different sizes and manufacturers with a smaller free specimen length from 20 to 40 times the diameter. Three tensile tests per manufacturer (three in total) occurred. Tests showed no significant impacts on the final results compared to mechanical results according the ASTM D 7205 regardless of the free specimen length. Additionally according to (Gieben, 2017), the elastic modulus, calculated from the standard range between 0.1% and 0.3%, should be calculated between 0.2% and 0.3% for short specimens with a free length of 20 times the rebar diameter. The tensile tests of the short specimen length illustrated a non-linear behavior under reduced loads (low strain range). Instead, all specimens in this research, independent of the free specimen length, measured identical elastic moduli (within each test group) in the higher strain ranges. However, it should be noted that the free test length (between the grips of the test machine) of traditional steel reinforcement bars is merely 15 times the bar diameter (G. and D., 2011).

Aside from the dimensions, ASTM D 7205/ D 7205M-06 ASTM-International (2015a) also prescribes the procedure for determining the elastic modulus of the rebars. The tensile modulus of elasticity should be calculated from the strain range of the lower half of the stress-strain curve, with the starting point at a strain of 0.1% and the end point at a strain of 0.3%. Therefore, the elastic modulus is calculated from deformation measurements at relatively low stress levels. Strain measurements are obtained on the outer fiber of the rebar with an extensometer. The shear lag effect is not considered in this method, underlined by constant values for the modulus of elasticity (Gieben,

2017).

The tensile strength, however, is determined from the ultimate load divided by the cross-sectional area. As a consequence, the test results of the elastic modulus are generally showing a low variance, while the ultimate stress differs widely from one specimen to another. This is because structural effects like local air voids and residual stresses are affecting the tensile properties, while these factors do not have an influence on the material behavior under low stress and thus no influence on the elastic modulus. The ultimate stress, in turn, is not only determined by the properties of the raw materials, but also by their interaction with each other (Ehrenstein, 2006).

These interactions allow the rebar to develop additional properties, which make the product suitable for use as reinforcement in concrete dealing with harsh environments. Accordingly, the properties of the combined materials as a reinforcement bar are described in section 2.6 below.

### **Bond-to-Concrete Properties**

In actual engineering applications where FRP rebars are used for internal concrete reinforcement, the bond-to-concrete behavior is of utmost importance because it defines the uniformity or the composite action of the final concrete element. A surface treatment is applied to the rebars to increase the friction at the bond interface or to improve the interlocking effect and to ensure proper bond between the pultruded BFRP rebar and the concrete. Manufacturers have developed different BFRP rebar types, where the surface enhancement vary. For instance the surface may be sand-coated, ribbed, or helical-wrapped. Ribbed rebars resemble the conventional black steel reinforcement and offer a high bond interaction with the surrounded concrete but another production step is needed to add the surface texture, which complexes the production. Sand coating is a simpler and faster way to treat the surface of a rebar and also offers good bond quality. The main factors affecting the properties of an FRP rebar include fiber volume, dimensional effects, rate of curing, manufacturing process, and quality control measures during manufacturing (Nanni et al., 2014). Therefore the production is decisive for the later properties of the rebar. The nature of the FRP manufacturing pultrusion process requires a marginal investment to set up (compared to traditional steel mills), while strict control measures, which are necessary to assure quality and consistency of the produced BFRP rebar, may not always be fully implemented. Although their initial cost (raw material and manufacturing costs) and environmental impact ( $CO_2$  emission during the manufacturing process)

may be slightly higher than that of conventional steel, the use of FRP rebars in concrete structures subjected to harsh environments generates a significant potential for extending the service life of these structures and lowering their overall life cycle cost.

While the FRP rebar is reacting over the life-period to environmental influences, the durability of a rebar needs to be evaluated. The next Section 2.9 shows the most important aspects to consider when durability of an FRP rebar may be an issue.

## 2.8 Failure Characteristics of FRP Rebars

The mechanical behavior from FRP rebars differs from steel and has to be considered in the design of reinforced concrete because FRP rebars do not yield and fail suddenly. In addition, the fibers are anisotropic, which means that they have different properties in different directions, and the high tensile strength only exists along the fiber axis. The composite FRP rebar (due to its production) also is an anisotropic material and is significantly weaker in the transverse direction than in its longitudinal direction. This property affects the shear strength as well as the bond behavior (ACI Committee 440, 2015).

The failure mode of the FRP rebar itself is strongly dependent on the bond behavior of the fibers and the surrounded resin. Figure 2.10 shows two different failure modes of the matrix after fiber breakage (in tension). The right failure mechanism is not able to transfer the load to the next fiber due to an insufficient bond and results in fiber breakage with slippage. A composite with such a relative low bonding strength between the fibers shows a brush-like formed failure pattern, because the failed fibers delaminate immediately after breakage. The left failure mechanism shows a transfer of the force from the broken fiber to the next one available, which results out of sufficient bonding strength. Not all the fibers reach their rupture strength at the same time. Individual fibers on the outer side of the rebar break and induce additional tension in the fibers nearby until the brittle failure of the rebar occurs (Ehrenstein, 2006). However, too much bond strength could transfer too much force to the surrounding fibers, which can cause a zip-effect that expands through the whole matrix and leads to an abrupt failure of the composite material. Moreover, a composite with a moderate bond strength is the most advantageous for a high strength material. BFRP rebars are produced to reinforce concrete, especially in harsh environments, where its non-rusting properties compared to conventional black steel reinforcement are advantageous. Therefore, the knowledge of

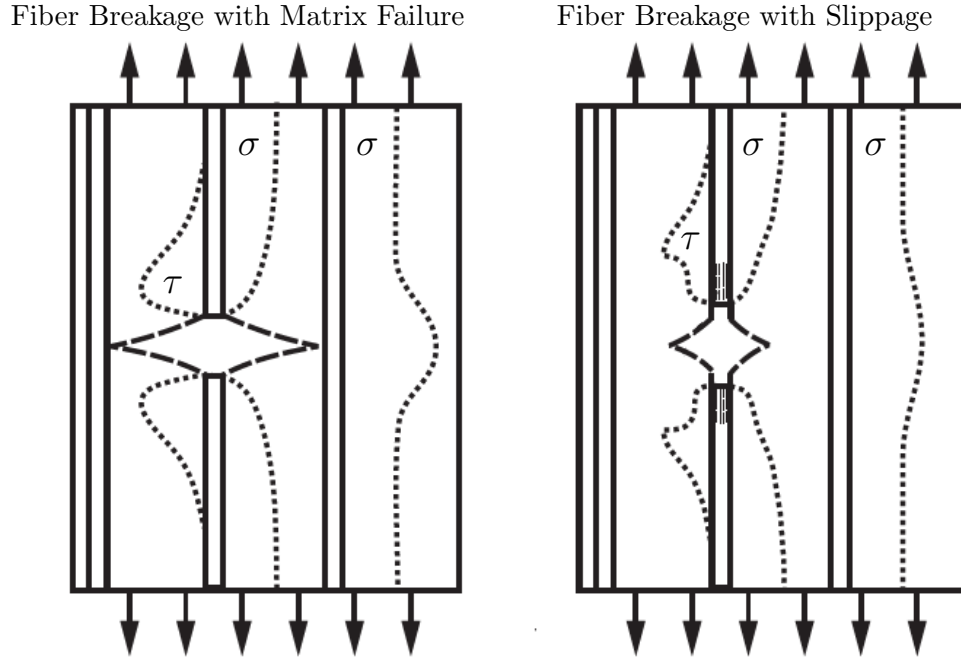


Figure 2.10: FRP rebar tensile failure mechanism (Ehrenstein, 2006)

the interactions of the rebars and concrete is essential. The following subsection 2.10 lists different failure mechanisms of concrete reinforced with FRP rebars.

## 2.9 Durability of FRP Rebars

Harsh environments have an influence on the properties of an FRP rebar. Because of its reaction to outer influences, the durability of FRP rebars is an important aspect and has to be considered in the designing process before failing suddenly and brittle due to influences occurring over the lifetime. FRP rebars are susceptible to varying amounts of strength and stiffness changes in the presence of environments before, during, and after construction. Environments can include water, ultraviolet exposure, elevated temperatures, or solutions (alkaline, acidic, or saline). Depending on the condition, the strength of the FRP may change (ACI Committee 440, 2015). To consider long-term exposure to the environment ACI 440 provides reduction factors for various fibers and exposure conditions listed in Table 2.3. Currently, the design code includes carbon, glass, and aramid fibers. The table provides two exposure conditions where fibers are exposed to earth and water or not. Due to outer influences, the tensile strength, creep rupture, and fatigue endurance can be reduced. Therefore, after the environmental situation is set, the tensile strength and strain has

Table 2.3: Environmental reduction factor for various fibers and exposure conditions

Exposure condition	Fiber type	Environmental reduction factor, $C_E$
Concrete not exposed to earth and water	Carbon	1.0
	Glass	0.8
	Aramid	0.9
Concrete exposed to earth and water	Carbon	0.9
	Glass	0.7
	Aramid	0.8

to be multiplied with the reduction factor  $C_E$  (last column in table), which reduces the design value or not in the case of carbon fibers in concrete not exposed to earth and water. Nevertheless, FRP composites are resistant in harsh environments; such environments, as well as acidic and alkali ones, could deteriorate the interface of fibers and matrix if they get in contact directly. For instance, acid diffuses into the macromolecule structure of the polymer and degrades the matrix. In addition, heat, moisture, and air pollution influence the mechanisms of degradation and the subsequent results of aging (Bagherpour, 2012). Serviceability criteria or fatigue and creep rupture can control the design of concrete members reinforced with FRP rebars in many cases. Aramid FRP (AFRP) and glass FRP (GFRP) are especially emphasized in the design code because of low stiffness characteristics.

Though FRP rebars made from basalt fibers are established as a promising replacement for CFRP and GFRP, the durability characteristics and their long-term behavior in concrete structures is not fully understood. For concrete elements exposed to harsh environmental conditions such as alkaline, saline, acidic, and de-iodized environments, FRP rebars appear to be the default alternative. But the durability of FRP materials (specifically basalt) in these harsh environments is one of the most important material-specific properties because it is often the primary reason for the use of this technology. While the high pH environment created by the cementitious matrix in concrete provides corrosion protection for conventional black steel rebars, the same high pH environment may attack FRP products and cause load capacity degradation. Accordingly, FRP rebars inside concrete elements situated in harsh environments are often exposed to multiple conditions or to a combination of chemically degrading elements simultaneously. The interaction of these combined conditions on FRP rebars are still not fully understood and research in this area is still needed.

However, initial efforts have been made and some of the completed projects are summarized below.

According to Wu et al. (2014), the durability of BFRP rebars exposed to alkaline solutions is less than the durability in saline, acidic, and de-iodized solutions when tested at 20 °C, 40 °C, and 55 °C. The degradation process of FRP rebars seems to be under control if the sustained load levels are kept below 20 % of ultimate tensile strength, but starts to accelerate beyond the 20 % threshold. According to Wu et al. (2014) findings, it takes 16.1 years for an alkaline solution to reduce the tensile strength of BFRP rebars by 50 %.

A study conducted by Lu et al. (2015) compared virgin to aged, pultruded BFRP plates and rebars to measure the effect of thermal aging (at 135 °C and 300 °C for four hours) on the longitudinal tensile strength and the interlaminar shear properties. At 300 °C, the resin decomposed thermally. As the immersion temperature and thermal aging was increased, the mechanical properties of BFRP plates notably decreased. The degradation process of aged rebars immersed in alkaline solution and distilled water accelerated due to thermal aging. While rebars aged at 135 °C and 300 °C degraded by 62.3 % and 74.1 % when exposed to high alkaline solution, the degradation process for un-aged BFRP bars exposed to high alkaline solution for three months at 60 °C was accelerated by 43.2 %.

Altamas et al. (2015) studied the bond-to-concrete durability properties of sand-coated basalt fiber reinforced polymer (BFRP) rebars and glass fiber reinforced polymer (GFRP) rebars via accelerated conditioning in acidic, saline, and alkaline solutions for 30 days, 60 days, and 90 days. The variations in slip of BFRP and GFRP bars after conditioning were negligible. The results showed that the bond strength of BFRP immersed in acid solution for 90 days was reduced by 14 % compared to bond strength of un-aged BFRP rebars, and the bond strength of rebars immersed in ocean water and alkaline solution for 90 days was reduced by 25 % in comparison with un-aged rebars. While the bond strength of GFRP rebars reduced by 25 % after acidic exposure, it reduced by 17 % after exposure to alkaline and saline environments in comparison with un-aged rebars. All specimens failed in interlaminar shear when tested for pullout strength.

Wang et al. (2017) tested tensile strength and Young's modulus properties of BFRP and GFRP rebars exposed to seawater and sea sand concrete (SWSSC). The rebars were exposed to normal SWSSC (N-SWSSC), and high-performance SWSSC (HP-SWSSC) at room temperature, 40 °C, 48 °C, and 50 °C for 21 days, 42 days, and 63 days. Damaging mechanisms were determined by using scanning electron microscopy (SEM), changes of microstructure were characterized via X-ray

computed tomography (CT), and energy dispersive X-ray spectroscopy (EDS) was used to compute chemical elements after exposure. Sodium Hydroxide ( $\text{NaOH}$ ,  $2.4 \frac{\text{g}}{\text{L}}$ ), potassium hydroxide ( $\text{KOH}$ ,  $19.4 \frac{\text{g}}{\text{L}}$ ), sodium chloride ( $\text{NaCl}$ ,  $35 \frac{\text{g}}{\text{L}}$ ), and calcium hydroxide ( $\text{Ca(OH)}_2$ ,  $2 \frac{\text{g}}{\text{L}}$ ) were mixed in 1 L of distilled water to prepare N-SWSSC with a pH level of 13.4. In addition, sodium hydroxide ( $\text{NaOH}$ ,  $0.6 \frac{\text{g}}{\text{L}}$ ), potassium hydroxide ( $\text{KOH}$ ,  $1.4 \frac{\text{g}}{\text{L}}$ ), sodium chloride ( $\text{NaCl}$ ,  $35 \frac{\text{g}}{\text{L}}$ ), and calcium hydroxide ( $\text{Ca(OH)}_2$ ,  $0.037 \frac{\text{g}}{\text{L}}$ ) were mixed in 1 L of distilled water to prepare N-SWSSC with a pH level of 12.7. Two BFRP rebar specimens and two GFRP rebar specimens per test group (conditioned vs. unconditioned), with a total length of 760 mm — including steel tube anchors with a length of 250 mm on both ends — were tested for ultimate tensile load. The rebars were embedded in the steel pipe anchors using an epoxy resin, and load rates for these experiments were set to  $2 \frac{\text{mm}}{\text{min}}$ . The ultimate tensile strength of BFRP specimen exposed to N-SWSSC in  $32^\circ\text{C}$  varied from 1317 MPa to 1253 MPa, whereas the ultimate tensile strength of BFRP specimen exposed to N-SWSSC in  $40^\circ\text{C}$  varied from 1273 MPa to 1103 MPa, while the ultimate tensile strength of BFRP specimen exposed to N-SWSSC in  $48^\circ\text{C}$  varied from 1257 MPa to 799 MPa, and the ultimate tensile strength of BFRP specimen exposed to N-SWSSC in  $55^\circ\text{C}$  varied from 908 MPa to 352 MPa. The ultimate tensile strength of BFRP specimen exposed to HP-SWSSC in  $32^\circ\text{C}$  varied from 1341 MPa to 1323 MPa, whereas the ultimate tensile strength of BFRP specimen exposed to HP-SWSSC in  $40^\circ\text{C}$  varied from 1288 MPa to 1219 MPa, and the ultimate tensile strength of BFRP specimen exposed to HP-SWSSC in  $55^\circ\text{C}$  varied from 1212 MPa to 1046 MPa. The ultimate tensile strength of GFRP specimen exposed to N-SWSSC in  $32^\circ\text{C}$  varied from 952 MPa to 925 MPa, whereas the ultimate tensile strength of GFRP specimen exposed to N-SWSSC in  $40^\circ\text{C}$  varied from 903 MPa to 961 MPa, and the ultimate tensile strength of GFRP specimen exposed to N-SWSSC in  $55^\circ\text{C}$  varied from 855 MPa to 848 MPa. The ultimate tensile strength of GFRP specimen exposed to HP-SWSSC in  $32^\circ\text{C}$  varied from 1031 MPa to 1036 MPa, whereas the ultimate tensile strength of GFRP specimen exposed to HP-SWSSC in  $40^\circ\text{C}$  varied from 959 MPa to 996 MPa, and the ultimate tensile strength of GFRP specimen exposed to HP-SWSSC in  $55^\circ\text{C}$  varied from 966 MPa to 948 MPa. Nearly no change was found in Young's Modulus for GFRP and BFRP bars after exposure to SWSSC solutions, mainly because this property depends on the Young's Modulus of the (basalt and glass) fibers, and because the modulus degradation for fibers in SWSSC solutions may not be significant. When compared to HP-SWSSC, N-SWSSC was more aggressive on both

BFRP and GFRP bars due to the high alkali ion concentration. In high-temperature environments, the GFRP rebars were more durable than the BFRP rebars because of the different resins. Based on the SEM, 3D X-ray, and CT-results, the resin properties of GFRP bars were more stable in SWSSC conditions than the resin used for the tested BFRP rebars.

Patnaik (2009) studied the mechanical properties of BFRP rebars and moment strength of concrete beams reinforced with BFRP rebars made by the wet lay-up process (see Section 2.5.2) and compared the results with beams reinforced by traditional pultruded BFRP rebars (see Section 2.5.1). The size of the rebars used in this study ranged from #1 rebars to #3 rebars. But more precisely, the rebar diameters for these tests included 4.3 mm, 7.1 mm, 9.8 mm. The average tensile strength of 4.3 mm rebars was 1110 MPa, the average tensile strength of 7.1 mm rebars was noted with 1084 MPa, and the average tensile strength of 9.8 mm rebar measured 1067 MPa. The average modulus of elasticity of 4.3 mm rebars was recorded with 41.1 GPa, while the average modulus of elasticity of 7.1 mm rebar was determined to be 41.4 GPa, and the average modulus of elasticity for 9.8 mm rebars was noted at 45.1 GPa. A total of 13 beams with a cross section of 203 mm  $\times$  203 mm, longitudinally reinforced with BFRP rebars, were tested. The beam measured a length of 2135 mm, while the span length was set to 1520 mm. All beams failed in a ductile manner, showing large mid-span deflections. The measured failure loads were greater than, or within the 3% range predicted by ACI 440.1R06 (ACI Committee 440, 2006). The results showed that the BFRP bars produced by wet lay-up were as strong as pultruded FRP rebars, but it was noted that the durability characteristics of the BFRP rebars via wet lay-up methods require additional research.

## **2.10 Concrete Elements Reinforced with BFRP**

Basalt FRP rebars are generally suitable alternatives to steel, epoxy-coated steel, or stainless steel bars in reinforced concrete structures, especially for durability or electromagnetic transparency purposes (Nanni et al., 2014). The occurring failure modes in FRP-reinforced structures are concrete crushing or FRP tensile rupture (Ehrenstein, 2006). In comparison to steel reinforced concrete with its three stages from the uncracked section, to the cracked section of linear-elastic yield up to the post-yield of reinforcement failure, FRP-reinforced concrete passes only through the first two stages without a post-yielding process (ACI Committee 440, 2007).

Due to the high alkalinity of the concrete (approximately pH 13), the steel is protected against

corrosion. For structures in aggressive environments, such as marine structures and bridges exposed to seawater or parking garages exposed to deicing salts, the alkalinity will be reduced. If the alkalinity reduces to a certain pH (approximately 9), the steel de-passivates and corrosion can initiate, which causes concrete deterioration and loss of serviceability (ACI Committee 440, 2015). Due to their advantages in durability aspects, FRP rebars are embedded in concrete for civil engineer applications such as highway barriers, offshore structures, and bridge decks, which are exposed to harsh environments where traditional black steel might corrode during the estimated service time (Brik, 2003). Mainly beams or flexural concrete members are reinforced by FRP rebars at this point. Concrete beams reinforced with BFRP bars achieved moment strengths that are consistent with the relevant properties of the constituent materials and are comparable to those predicted using ACI 440.1R-06 (Patnaik, 2009). However, a lack of experience exists in the use of FRP reinforcement in compression members (columns) and for moment frames or zones where moment redistribution is required (Nanni et al., 2014). Performed SEM analysis by ElSafty et al. (2014) of samples immersed in alkaline solution at elevated temperature for 1000 hours did not show significant signs of degradation. Only the outermost covering of the bar had been affected by the conditioning. Reductions of transverse and horizontal interlaminar shear strength due to conditioning in alkaline solution for 1000 and 3000 hours were detected. A reduction of flexure strength due to conditioning in alkaline solution was recorded after conditioning for 3000 hours with exposure to alkaline solution at 60 °C. Further tests should be required to gather sufficient information for a standardized usage to establish degradation factors for design purposes like they already exist in different codes for other FRP rebars.

Next to the durability factors, environmental impacts of the BFRP rebar production have to be considered to reduce pollution. Because of the high temperature required for production, steel reinforcement has a higher carbon footprint than FRP reinforcement. Recycling instead is not as easy as reproducing steel. Without corrosion, the life cycle costs associated with FRP-reinforced structures are likely lower where steel corrosion should be a concern. A comparison between FRP-reinforced pavement and steel-reinforced pavement over the lifetime determined that FRP reinforcement had a significantly smaller environmental impact than the version with steel (ACI Committee 440, 2015).

While the general properties and components of BFRP rebars are described above, the following chapter offers details about the certification process of FRP rebars and their implementation into

national and international codes. Moreover, an analysis of the current BFRP market was conducted to collect information about availability and production processes around the world. The gathered information about the available products shall help to provide recommendations for an implementation of BFRP rebars into the national design codes and for the use of these construction materials in public infrastructure projects. The next chapter deals with BFRP specifications and market.

## Chapter 3

# BFRP Building Compliance and Market

This chapter provides details about current regulations for FRP rebars with the focus on basalt fibers and the international BFRP market situation and the available products. The standardization progress in the FRP industry is described in Section 3.1. In addition, Section 3.2 provides a comparison of the different acceptance criteria for the mechanical properties on national and international levels followed by Section 3.3 and 3.4, which summarize the state of the art in the BFRP industry.

### 3.1 Regulations for FRP Rebars

This section describes the national and international regulations for FRP rebars and its historical development. Several global activities have been completed to implement FRP rebars into design codes and guidelines since the 1980s. In the United States, the initiatives and vision of the National Science Foundation and the Federal Highway Administration promoted the development of this technology to support research at different universities and research institutions.

In 1991, the American Concrete Institute (ACI) established Committee 440 — FRP Reinforcement. The objective of the committee was to provide the construction industry with science-based design guidelines, construction specifications, and inspection and quality control recommendations related to the use of FRP rebars for concrete structures. In 2001, Committee 440 published the first version of the document “Guide for the Design and Construction of Structural Concrete Rein-

forced with FRP Bars.” The availability of this document further expedited the adoption of FRP rebars (Nanni et al., 2014). Around the start of the millennium, research projects on fiber reinforced polymers were conducted in many countries (e.g., Japan, Europe, China, Canada, and America), which led to the development of standard documents and national design codes for the use and implementation of FRPs as illustrated in Figure 3.1. The first document that introduced test methods

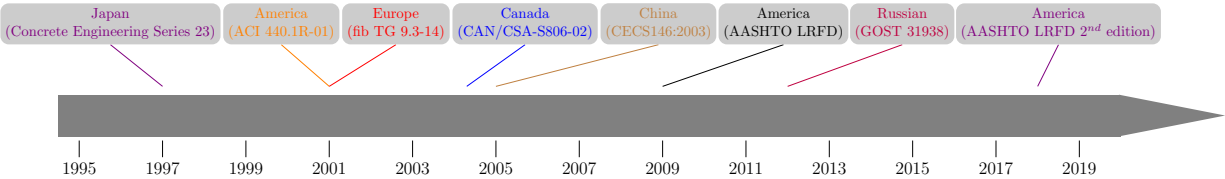


Figure 3.1: Chronology of documents related to the use of FRP rebar for concrete reinforcement

for FRP rebars was “Recommendation for Design and Construction of Concrete Structures Using Continuous Fiber Reinforcing Materials”, which was published in 1997 by the Japan Society for Civil Engineering (JSCE). ASTM International and the Organization for Standards (ISO) developed standardized test methods related to the use of FRP composites in structural engineering. Model test methods for FRP bars are recommended by the ACI document 440.3R, “Guide Test Methods for Fiber-Reinforced Polymers (FRPs) for Reinforcing or Strengthening Concrete and Masonry Structures,” effective since 2004, while earlier documents like ACI 440.2R introduced first design recommendations in 2002. Test procedures have also been developed by the Canadian Standards Association (CSA) or the European International Federation for Structural Concrete (fib) (Nanni et al., 2014).

The American Concrete Institute Committee 440 (ACI440) has led the effort to address the technical implementation for GFRP rebars by developing and publishing test methods, specifications, and design guidelines (ACI Committee 440, 2006, 2008a,b, 2012, 2013, 2015). The 2008 version of ACI440 (ACI Committee 440, 2008b) and the 2010 version of the Canadian-CSA Specifications for Fiber Reinforced Polymers (Canadian Standard Association, 2010) were developed to standardize glass, carbon, and aramid FRP bars. The Canadian Standards Association (CSA) has led the western effort for developing specifications and design guidelines for BFRP. The new CSA S807 (Benmokrane, 2018) standard includes FRP bars made from basalt fibers, which emphasize the current importance of this material and the confidence of a commercialized usage in the field (Vincent et al., 2013). Similarly, ASTM Committees D30 and D20 have addressed the

emergence of this technology by developing a number of test methods (ASTM-International, 2015a) intended to characterize GFRP rebars, while BFRP rebars do not have specifications in the US. Recently, in 2017, ASTM D 7957 specific guidelines for solid round glass fiber reinforced polymer bars for concrete reinforcement was adopted (ASTM-International, 2017). In addition, the FDOT has developed documents to aid the implementation and design of GFRP rebar technology in the built infrastructure, specifically the expanded Section 932 for nonmetallic accessory materials for concrete pavement and concrete structures (Ruelke, 2014), and more recently the fiber reinforced polymer guidelines (FRPG) (Florida Department of Transportation, 2015; Hurtado, 2018). At the national level, the American Association of State Highway and Transportation Officials (AASHTO) has also developed guides for the use of FRP technology (AASHTO, 2012) for externally bonded systems. It is desired to add BFRP-specific criteria to these specifications and guidelines as soon as practical to provide redundant supply chains and additional alternatives. Agencies are interested in BFRP composites because the technology has improved recently (as explained in Chapter 2). The variability of the raw source still presents uncertainty for its adoption in infrastructure applications, where fiber manufactures are working on providing solutions. Further reasons are properties such as a higher elastic modulus, higher tensile strength, and, for example, the consideration of a more environmentally friendly product.

In general, for a design guidelines to become official, it must be adopted by a model building code or by a regulatory agency. In the United States (and other parts of the world, including the United Nations), the International Building Code (IBC) part of the family of International Codes (I-Codes) is the predominant model code (adopted by all 50 states, Puerto Rico, and the US Virgin Islands) and covers the design and construction of new buildings. (Nanni et al., 2014) Moreover, the International Code Council Evaluation Service (ICC-ES), which is the industry leader in performing technical evaluations for code compliance as part of the International Code Council (ICC) that develops model codes and standards, published the “Acceptance Criteria for the use of GFRP and BFRP rebars for concrete reinforcement,” known as AC454 (International Code Council Evaluation Services, 2017). Hence, today any structure that is to be built according to the requirements of the Florida building code, which is based on the model code (International Building Code, IBC), can be realized with BFRP rebar technology.

For the implementation process of a product, the existence of a set of protocols and provi-

sions is necessary. Therefore, tests, analysis of the results, and the design have to be conducted. Moreover, ICC Evaluation Services (ICC-ES) develops in partnership with the proposers of new technology-specific documents called “acceptance criteria (AC)” for the purpose of issuing evaluation (research) reports. After it is demonstrated that the product is manufactured under an approved quality control program, the experimental program outlined in the AC is conducted by a certified independent laboratory, its outcomes are evaluated by ICC-ES, and, assuming compliance, a evaluation service report (ESR) is issued. Thus, the alternative material/technology now has official recognition (Nanni et al., 2014).

Through the development of standardized test procedures and available design documents, it became feasible to compare and evaluate standardized material performances, which lead to the development of acceptance criteria for different products. These acceptance criteria are described in Section 3.2 below.

### **3.2 Acceptance Criteria for FRP Rebars**

This section lists the acceptance criteria for the most important certification documents for FRP rebars. Acceptance criteria for FRP rebars include mechanical, physical, and durability requirements for implementation and usage in civil structures on a state, national, or international level. Physical requirements include testings of FRP properties such as the fiber content, glass transition temperature, measured cross-sectional, and durability tests that consider the moisture absorption, the resistance to alkaline environments, and the void content (International Code Council Evaluation Services, 2016). This section provides mechanical acceptance criteria for FRP rebars because this research project focuses on the mechanical tensile strength of BFRP rebars. Required criteria are listed in Table 3.1 for Section 932 in the State of Florida for FRP rebars, ASTM D 7957 on a national level for glass FRP rebars, and on the bottom for AC454 on an international level for glass or basalt FRP rebars. It can be seen that the table matches the required mechanical properties according to the official test procedure (ASTM and ACI) with the different available documents (FDOT Section 932 and AC454) that require these tests. The table details how many specimens per lot and how many lots have to be considered for each test and bar size. The different certification documents require testing of three to five to ten samples per production lot. In summary, each certification document requires a comparable amount of specimens and test repetitions per

Table 3.1: Required test procedures and specimen quantities per acceptance test and production lot

		Tensile		Shear		Bond
		Ultimate Load ASTM D7205	Elastic Modulus ASTM D7205	Transverse ASTM D7617	Apparent Horizontal ASTM D4475	Strength ACI 440.3R
FDOT 932-3	Bar Size	each	each	each	each	smallest (5), median (5), largest (5)
	Specimen per Lot	10	10	5	5	15
	Lots	3	3	3	3	3
ASTM D7957	Bar Size	each	each	each	each	each
	Specimen per Lot	8	8	8	8	8
	Lots	3	3	3	3	3
AC454	Bar Size	each	each	each	each	smallest (5), median (5), largest (5)
	Specimen per Lot	5	5	5	5	15
	Lots	5	5	5	5	1

specimens to gather sufficient data for a general use in the field.

According to the normal (Gaussian) distribution to estimate the mean strength with a 95% confidence level, within 5% margin of error, a sample size of at least five rebars are needed as stated in ACI 440.1R-01. To obtain a 99% level of confidence at the same margin of error, at least nine rebars are needed. To determine guaranteed values of strengths and strains at a 99.87% probability requires testing of 25 specimens (Kocaoza et al., 2004). The guaranteed strength or strain is to be derived based on statistical analysis if fewer test specimens are tested, or the distribution is not a normal distribution (ACI Committee 440, 2006). Additionally, to the required amount of test specimen, the certification documents (FDOT, ASTM, and AC454) present rebar size and tensile load requirements for FRP rebars. All three specifications define the minimum and maximum cross-sectional dimensions and the minimum guaranteed tensile strength values per rebar size as shown in Table 3.2. It can be seen that information for the rebar sizes and corresponding limits for the measured cross-sectional area and the minimum strength values for tensile capacities are listed. The span between the min. and max. cross section is included because of differences in surface enhancements and production processes. The last column lists minimum guaranteed tensile loads for each rebar size for GFRP and CFRP bars. The only difference between the FDOT Section 932,

Table 3.2: Required sizes and tensile loads of FRP reinforcing bars

Bar Size Designation	Nominal Bar Diameter	Nominal Cross-Sectional Area	Measured Cross Section		Minimum Guaranteed Tensile Load	
			Minimum	Maximum	GFRP Bars	CFRP Bars
#	in.	in. <sup>2</sup>	in. <sup>2</sup>	in. <sup>2</sup>	kip	kip
2	0.250	0.049	0.046	0.085	6.1	10.3
3	0.375	0.11	0.104	0.161	13.2	20.9
4	0.500	0.20	0.185	0.263	21.6	33.3
5	0.625	0.31	0.288	0.388	29.1	49.1
6	0.750	0.44	0.415	0.539	40.9	70.7
7	0.875	0.60	0.565	0.713	54.1	-
8	1.000	0.79	0.738	0.913	66.8	-
9	1.128	1.00	0.934	0.388	29.1	-
10	1.270	1.27	1.154	1.385	98.2	-

the ASTM D 7957, and the AC454 is that the AC454 provides additional minimum tensile loads for the measured diameters, which are a little higher than the minimum loads calculated by using the nominal diameter.

While different production techniques and processes exist in the FRP rebar market, these established acceptance criteria allow manufacturers to target specific properties. Nevertheless, BFRP rebars were produced before these acceptance criteria were available and manufacturers followed individual and proprietary production sequences. Accordingly, the market is diverse with various products, and new manufacturers enter the market quickly. However, an overview of the current BFRP rebar industry follows below.

### 3.3 Global BFRP Rebar Manufacturer Analysis

This section provides information about the BFRP rebar manufacturers, their production logistics, and the available products. The first FRP rebar became commercially available in the late 1980s, when the market demand for electromagnetic-transparent reinforcing systems increased. At that time, the technology was developed enough to provide a viable solution as internal reinforcement for concrete structures (Nanni et al., 2014). Afterwards, the technology gained traction and different BFRP rebar manufacturers were established around the world with a majority of the early companies

in Russia. European and Northern American companies followed the trend of manufacturing FRP rebars, while the basalt fiber was imported from areas with an easier access to basalt rock sources, such as Asia or parts of Europe. In the text below, the current BFRP rebar manufacturers are analyzed; first based on general data provided in the literature, and then based on market data gathered directly from manufacturers.

Markets and Markets (2016) conducted a study that projected the market growth up to \$91 million until 2021. This growth is fueled by the increasing demand for the renovation and strengthening of new and existing structurally deficient bridges, especially in harsh environments near the coast or connecting islands to the mainland. For instance, according to the National Bridge Inventory (NBI), more than 146,000 bridges are structurally deficient or functionally obsolete in the US as of 2010. From February 2003 to December 2013, FDOT District 7 conducted a study that evaluated the current status and the required repair costs of 54 (20 steel and 34 concrete) bridges. It concluded that 76% of all repair costs would be necessary to alleviate damages due to corrosion (Fallaha et al., 2017). Thus, the use of FRP rebars in these applications has the potential to reduce the life cycle costs, thereby enhancing service life and safety.

The Floodway Bridge (Canada) is one of the largest bridges constructed with FRP rebars. In addition, The Florida Keys Bridges (US) is one of the prominent examples for the use of CFRP rebars to strengthen structurally deficient bridges and bridge elements. Many similar projects, in which FRP rebars are used as internal concrete reinforcements, are executed in the US and Canada (Markets and Markets, 2016). Nevertheless, the lack of confidence in durability in aggressive environments (for 75 to 100 years of service life), limitations on strength due to low design resistance factors related to lack of ductility or due to degradation of properties over time, are challenges for the implementation. Moreover, creep-rupture mechanisms limit the service limit state design, and the comparatively low elastic modulus (relative to conventional black steel) leads to greater deflection and larger crack openings (Fallaha et al., 2017). Accordingly, a new challenge will be the development and implementation of new inspections and repair methods.

North America is one of the main leaders in the world market for FRP rebars and has the fastest-growing demand worldwide because of its high economic growth rate, numerous construction projects, and capacity expansion, although the basalt fibers are mostly produced in Russia and China and have to be imported. In 2018, the first basalt fiber production plant in North America

is being commissioned in North Carolina. Raw basalt rock is melted and shaped into basalt fibers. The produced fibers are combined with a resin in one process to produce the final FRP rebar shape. At this time, seven manufacturers produce BFRP rebars in the US either exclusively or in combination with other FRP rebar. Figure 3.2 provides a visualization of BFRP rebar manufacturer density worldwide, and it can be seen that (to this date and to the knowledge of the author) 23 manufacturers commercially produce BFRP rebar products year round. It is reported by Galen Panamerica that there are hundreds of “garage BFRP operations” that pultrude products in Russia and Ukraine during the warmer months. The circles on the map indicate number (per country)



Figure 3.2: BFRP manufacturer locations

and location of manufacturers. The highest density can be found in North America with nine manufacturers (seven in USA and two in Canada). A total of six BFRP rebar producers are located in Europe (two in Germany, one in Norway, one in Ukraine, one in Austria, and one in England), while eight Asian manufacturers exist (four in China, three in Russia, and one in India).

As part of this research project, 23 BFRP manufacturers from ten different countries were contacted to participate in a survey with the aim to collect manufacturer-specific data about production logistics, the produced BFRP rebar product types, their physical features, and the manufacturer guaranteed material properties. All manufacturers in these 23 countries were contacted via email, phone calls, or personal meetings. These initial conversations were followed by surveys with a BFRP rebar production-specific questionnaire. Details about the contacted BFRP rebar manufacturers and a copy of the survey that was shared with them can be found in Appendix A. Based

on the provided information, the state of the market was analyzed and the data is presented below to provide additional context for the technology, within a national and international framework. Table 3.3 lists the production and rates per manufacturer. The leftmost column in the table lists

Table 3.3: Production logistics and rates per manufacturer

Manufacturer	First BFRP bar Year	Production Logistic <sup>†</sup>	Production Rate	
			<i>m/d</i>	<i>ft/d</i>
No Rust Rebar Inc.	Before 1990	Stock in large quantities	4,600	15,000
Smarter Building System	2000	Stock in large quantities	6,000	19,700
Neuvokas Corp.	-	-	-	-
KODIAK Fiberglass Rebar	2014	Stock in large quantities	9,200	30,000
Advanced Filament Technologies	1998	Stock in large quantities	3,000	9,800
US Basalt	-	-	-	-
Proven Performance Chemicals	-	-	-	-
Pultrall Inc.	2010	Production on demand	8,800	28,800
Armkar Inc.	-	-	-	-
Incotology GmbH	-	-	-	-
Deutsche Basalt Faser GmbH	2017	Stock in small quantities	14,000	45,900
ASA.TEC GmbH	2012	Production on demand	960	3,150
Basalt Technologies UK Limited	-	-	-	-
ReforceTech AS	-	-	-	-
Technobasalt-Invest	2010	Stock in small quantities	16,000	52,500
Galen Panamerica	2001	Stock in large quantities	20,000	65,600
Rusnano (TBM)	-	-	-	-
Armastek	2007	Production on demand	50,000	164,000
GMV	-	-	-	-
Phoenix New Material Co., Ltd.	-	-	-	-
GBF Basalt Fiber Co., Ltd	-	-	-	-
Huabin General Machinery Co.,Ltd.	-	-	-	-
Flips India Engineering	-	-	-	-

<sup>†</sup> Small quantities below 500m (1640ft.); Large quantities over 500m (1640ft.)

the contacted manufacturers in this survey. Data about their first BFRP rebar production stocking quantities and the production rates are listed in the table (for those manufacturers who responded to the survey). Based on the received data from ten manufacturers, it can be inferred that just two manufacturers started their BFRP production before the year 2000. Furthermore, over 50% of the manufacturers started the production of BFRP rebars after 2007. The majority stock their products in large quantities and it can be seen that the production rates are significantly higher in the Asian and European countries compared to the United States. Kodiak Fiberglass Rebar is the company that (currently) provides the largest production capacity on the North American

continent for BFRP rebars with a production output of 4,600 m/d. In comparison the Russian company Armastek is able to produce 50,000 m/d, which is about 11 times more. Figure 3.3 shows a diagram that compares the different stocking options used by the various manufacturers in the industry. The part of the pie chart with solid diagonal lines identifies 50% of the companies that

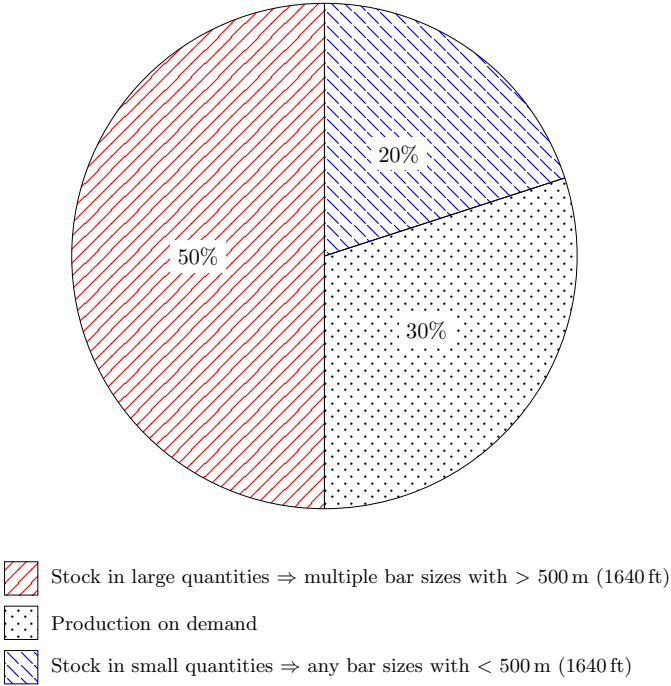


Figure 3.3: Production and storage strategies chosen by BFRP manufacturers

stock rebars in large quantities [ $> 500\text{ m}(1640\text{ ft})$ ], while the area with the dashed diagonal lines, signifies with 20% the stocking of small quantities [ $< 500\text{ m}(1640\text{ ft})$ ], and the dotted part represents manufacturers, who produce rebar on demand (30%). The next Figure visualizes the production rates of the manufacturers. The production rates are listed on the y-axis in ft/d (left axis) and m/d (right axis). Three character IDs (see Table reftab:BFRP rebars produced by manufacturer) for each manufacturer (which participated in the survey) are listed along the x-axis. The bars visualize the lowest production rate for ASA TEC GmbH (ASA) with 960 m/d (3150 ft/d) and the highest production rate for Armastek with 50 000 m/d (164 000 ft/d). The average production of all listed BFRP rebar producers is 13 000 m/d (42 650 ft/d).

17 questions about the chosen production logistics made up the first part of the BFRP rebar manufacturer survey; the second part was aimed at specific product properties and the following Section 3.4 summarizes the findings from part two.

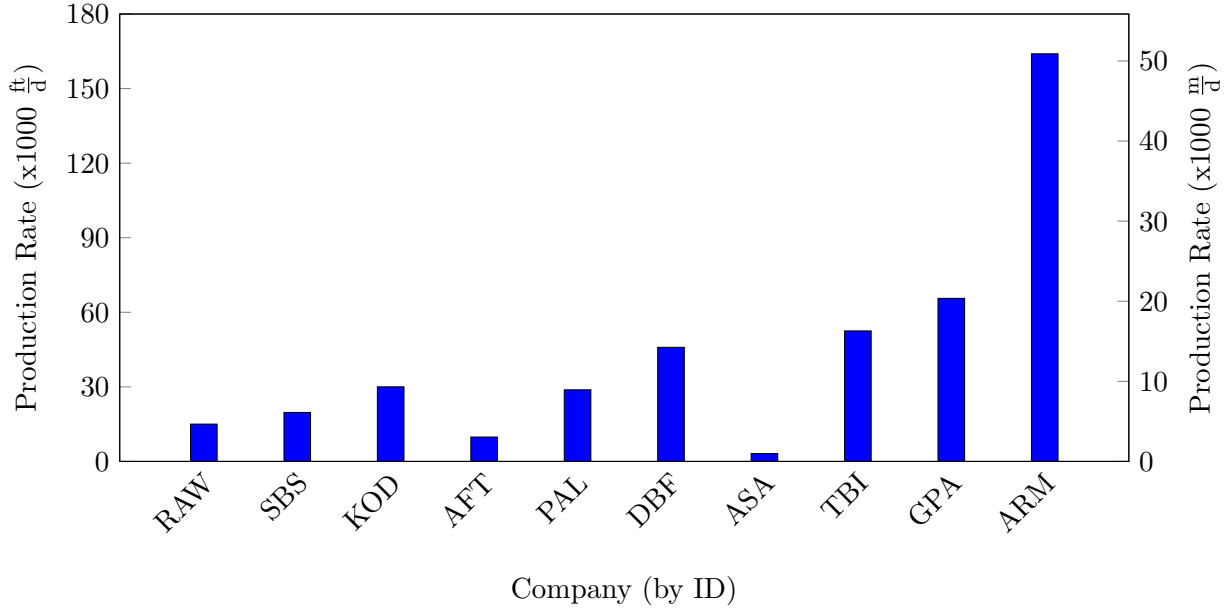


Figure 3.4: BFRP production rates (as reported by manufacturers)

### 3.4 BFRP Products Database

The data collected through the second part of the survey provides centralized information about parameters such as cross-sectional shape, resin type, surface enhancement, and produced diameters. The answers to all survey questions reflect the currently available products and the related parameters, cross-sectional shape, resin type, surface enhancement, and produced diameters. The acquired data are shown in Table 3.4. Based on the manufacturers who shared their company-specific data, the dominant cross-sectional shape is round and solid. The only exception is the German company Deutsche Basalt Faser GmbH, which produces round hollow rebars instead. In addition, the majority of the BFRP rebar producers focus exclusively on the production of basalt FRP rebars. However, four companies also produce rebars with other fiber types like glass or add basalt fibers afterward to their portfolio because the production sequences and processes for these rebars are similar. Besides vinyl ester, the most used resin type is epoxy: it is one of the more expensive types with a long curing time. The surface enhancement is the feature that varies the most between the listed manufacturers. The use of helical wrap, sand coat, or a combination of both is applied based on the manufacturer. The various produced rebar diameters differ in quantities/availability between manufacturers. Based on the preferred measurement system in the production country (metric vs. imperial), the available nominal rebar diameters differ. Some rebar producers only pro-

Table 3.4: BFRP rebars produced by manufacturer

Manufacturer	Cross-Sectional Shape	Fiber Type	Resin Type	Surface Enhancement	Produced Diameters
RAW	Round (solid)	Basalt	Epoxy	Helical wrap & Sand coat	#1, 2, 3, 4, 5, 6, 7, 8, 9, 10, 11
SBS	Round (solid)	Basalt	Epoxy / Vinyl Ester	Helical wrap	#1, 2, 3, 4, 5, 8
NVC	Round (solid)	Basalt	Epoxy	-	#3
KOD	Round (solid)	Basalt/Glass	Epoxy / Vinyl Ester	Helical wrap/rib & Sand coat	#2, 3, 4, 5, 6, 7,8
AFT	Round (solid)	Basalt	Epoxy	Helical wrap	#1, 2, 3, 4, 5, 6, 7, 8, 9, 10, 11
USB	-	Basalt	-	-	-
PPC	-	Basalt	-	-	-
PAL	Round (solid)	Basalt/Glass	Epoxy	Sand coat	#2, 3, 4, 5, 6, 7, 8, 9, 10, 11
AKI	-	Basalt	-	-	-
ICT	-	Basalt	-	-	-
DBF	Round (hollow)	Basalt	Thermoset	Sand coat	#1, 2, 3, 4, 5
ASA	Round (solid)	Basalt	Vinyl Ester	Helical rib	#2, 3, 4, 5, 6, 8
BTL	-	Basalt	-	-	-
RAS	-	Basalt	-	-	-
TBI	Round (solid)	Basalt	Epoxy	Helical rib	#1, 2, 3, 4
GPA	Round (solid)	Basalt/Glass	Epoxy	Sand coat	#1, 2, 3, 4, 5, 6, 7, 8, 9, 10, 11
RSN	-	Basalt	-	-	-
ARM	Round (solid)	Basalt/Glass	Epoxy	Helical wrap & Sand coat	#1, 2, 3, 4, 5, 6, 7, 8, 9, 10, 11
GMV	-	Basalt	-	-	-
PNM	-	Basalt	-	-	-
GBF	-	Basalt	-	-	-
HGM	-	Basalt	-	-	-
FIE	-	Basalt	-	-	-

duce a single size, while other producers have the capacity to supply a wide array of rebars (# 1 to # 12 or higher). Rebar # 3 with a diameter of 3/8 inch (10 mm) and rebar # 5 with a diameter of 5/8 inch (16mm) are the two most commonly available, and therefore, most used diameters in civil applications.

## Chapter 4

# Experimental Program

### 4.1 Introduction

The experimental program chapter details how the performance of three different BFRP rebar products was evaluated. The experimental concept and the general research approach as well as an overview of the different test procedures and a brief description of tested rebar material are described in the following Section 4.2. The equipment and test devices that were used to perform the experiments, including special test fixtures that were needed to test the strength properties of BFRP rebars, are described in Section 4.3. Finally, the test procedures based on the relevant and applicable ASTM standard documents are outlined in Section 4.4.

### 4.2 Experimental Concept

To properly evaluate a new material, such as BFRP rebars, for use in infrastructure projects, the physical and mechanical properties of the material must be evaluated and compared to acceptance criteria, if such criteria are available. Accordingly, the experimental approach aimed to fully characterize strategically chosen representative BFRP rebar samples for physical and strength characteristics. The relevant physical properties included the cross-sectional dimensions, fiber content, and moisture absorption characteristics, while the physical properties including the transverse shear strength, the apparent horizontal shear strength, the tensile properties, and the bond-to-concrete characteristics. Table 4.1 lists all these tests and references the applicable ASTM standards that were followed throughout the experimental program. In addition, the table shows how many speci-

Table 4.1: Physical and mechanical tests on BFRP rebars

		Test type	Test method	Specimen count	
				Per sample	Total
Physical		Cross-sectional area	ASTM D792	5	40
		Fiber content	ASTM D2584	5	40
		Moisture absorption	ASTM D570	5	40
Mechanical		Tensile strength	ASTM D7205	5	40
		Transverse shear strength	ASTM D7617	5	40
		Apparent horizontal shear strength	ASTM D4475	5	40
		Bond-to-concrete	ACI440.3R,B.3	5	30

mens (per sample group) were needed to reliably measure the materials' performance. Because # 3 rebar of lot 1 from manufacturer C had high moisture absorption property, manufacturers developed a new technology and provided a second lot. But two other producers were still developing the production line and could only provide prototype rebars (hence only one lot was tested).

In line with the previously described state-of-the-market situation (c.f. Section 3.1), and based on availability in the local market, representative rebar samples from three distinct BFRP rebar manufacturers were chosen. All materials that were tested for the purpose of this research project were provided by No Rust Rebar, Pultrall, and Galen Panamerica. These manufacturers provided specific products, which in the following will be referred to as Rebar Type A, Rebar Type B, and Rebar Type C (or simply Type A, Type B, and Type C), respectively. Because this research targeted the most commonly available and often used FRP rebar sizes, the manufacturer supplied # 3 and # 5 rebars, such that each Rebar Type had two sub-variants (e.g.; Type A # 3 and Type B # 3). All specimen types that were characterized throughout this research are shown in the following Figures 4.1 and 4.2. It can be seen that (at minimum) all rebar types featured a sand coat at the outer surface to improve the bond-to-concrete properties. In addition to surface sand, one product (Type A) also had helical fibers made from polyethylene terephthalate, produced by Dacron. The makeup and the surface enhancement properties of the tested rebars are described in Table 4.2. Because the precise material compositions are proprietary manufacturer information, no more data can be supplied here.

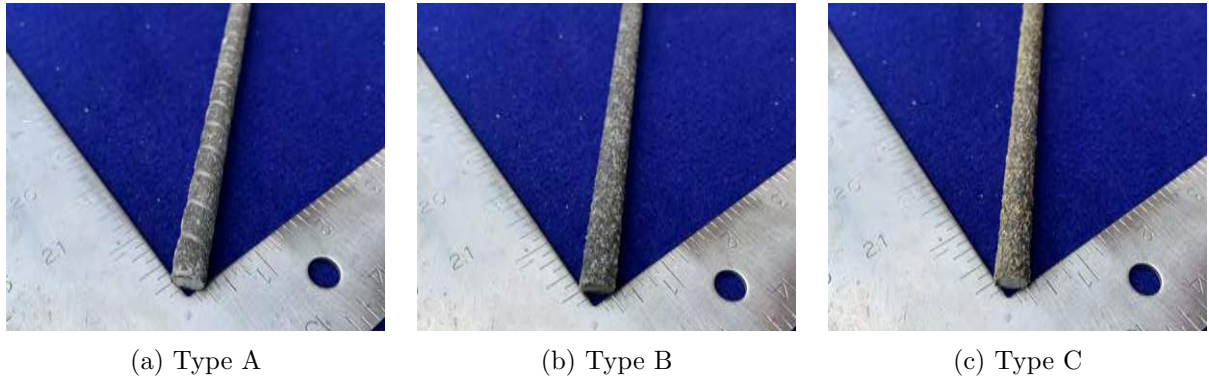


Figure 4.1: Sample pictures of tested BFRP # 3 Rebars

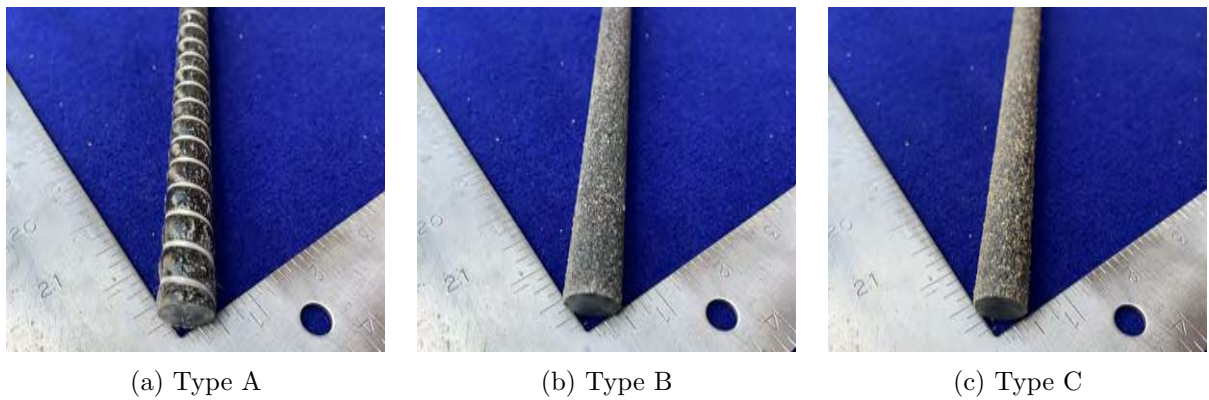


Figure 4.2: Sample pictures of tested BFRP # 5 Rebars

Table 4.2: Physical characteristics of tested BFRP rebars

Name	Cross Section	Surface Enhancement	Resin Type
A	Round (solid)	Sand coat and helical wrap	Epoxy
B	Round (solid)	Sand coat	Epoxy
C	Round (solid)	Sand coat	Vinyl-ester

#### 4.2.1 Acceptance Criteria

While acceptance criteria for basalt FRP rebars are not fully established yet, criteria for other fiber based rebars have been adopted. One of the most established composite rebar materials is the glass fiber reinforced polymer (GFRP) rebar, which is known to possess a lower ultimate tensile strength and a lower elastic modulus — compared to basalt FRP rebars. For reference, the data in the Tables 4.3 and 4.4 show common acceptance criteria for (GFRP) rebars. For the purpose of this research, the results obtained by testing BFRP rebars were compared to GFRP rebar acceptance

Table 4.3: Acceptance criteria for GFRP rebar # 3

Test Method	Test Description	Unit	FDOT 932-3/2017	AC454	ASTM D 7957
			Criteria	Criteria	Criteria
ASTM D 792	Measured Cross-Sectional Area	in. <sup>2</sup>	0.104 – 0.161	0.104 – 0.161	0.104 – 0.161
ASTM D 2584	Fiber Content	% wt.	≥ 70	≥ 70	≥ 70
ASTM D 570	Moist. Absorption short term @50 °C	%	≤ 0.25	≤ 0.25	≤ 0.25
ASTM D 570	Moist. Absorption long term @50 °C	%	≤ 1.0	n/a	≤ 1.0
ASTM D 7205	Min. Guaranteed Tensile Load	kip	≥ 13.2	≥ 13.2	≥ 13.2
ASTM D 7205	Min. Guaranteed Tensile Strength	ksi	n/a	n/a	n/a
ASTM D 7205	Tensile Modulus	ksi	≥ 6,500	≥ 6,500	≥ 6,500
ASTM D 7205	Max. Strain	%	n/a	n/a	n/a
ASTM D 7617	Min. Guaranteed Transverse Shear	ksi	≥ 22	≥ 22	≥ 19
ASTM D 4475	Horizontal Shear Stress	ksi	n/a	≥ 5.5	n/a
ACI440. 3R,B.3	Bond-to-concrete strength	ksi	≥ 1.1	≥ 1.1	≥ 1.1

Table 4.4: Acceptance criteria for GFRP rebar # 5

Test Method	Test Description	Unit	FDOT 932-3/2017	AC454	ASTM D 7957
			Criteria	Criteria	Criteria
ASTM D 792	Measured Cross-Sectional Area	in. <sup>2</sup>	0.288 – 0.388	0.288 – 0.388	0.288 – 0.388
ASTM D 2584	Fiber Content	% wt.	≥ 70	≥ 70	≥ 70
ASTM D 570	Moist. Absorption short term @50 °C	%	≤ 0.25	≤ 0.25	≤ 0.25
ASTM D 570	Moist. Absorption long term @50 °C	%	≤ 1.0	n/a	≤ 1.0
ASTM D 7205	Min. Guaranteed Tensile Load	kip	≥ 29.1	≥ 32.2	≥ 29.1
ASTM D 7205	Min. Guaranteed Tensile Strength	ksi	n/a	n/a	n/a
ASTM D 7205	Tensile Modulus	ksi	≥ 6,500	≥ 6,500	≥ 6,500
ASTM D 7205	Max. Strain	%	n/a	n/a	n/a
ASTM D 7617	Min. Guaranteed Transverse Shear	ksi	≥ 22	≥ 22	≥ 19
ASTM D 4475	Horizontal Shear Stress	ksi	n/a	≥ 5.5	n/a
ACI440. 3R,B.3	Bond-to-concrete strength	ksi	≥ 1.1	≥ 1.1	≥ 1.1

criteria because BFRP acceptance criteria in the US are yet to be established. Accordingly, the listed criteria (while established for glass) serve as reference points and are used for comparison and initial benchmark data only.

## 4.3 Equipment and Test Devices

All equipment and tools that were needed for sample preparation and to conduct the individual tests are listed in this section.

### 4.3.1 Cutting Saw

The BFRP rebar samples that were provided by the manufacturers had a length between 2.30 m (90 in.) and 2.50 m (98 in.). According to the ASTM, the tested samples have to be tested in a desired length according to their diameter. To cut the samples, a heavy-duty single-bevel compound miter saw with a diamond cutting wheel was used. It featured a machine-based frame to ensure a straight cut. The saw was placed on a stable and leveled working table for a safe working space. A wooden template was designed to ensure a fast workflow and a properly angled cut with 90° relative to the longitudinal axis of the rebar (Figure 4.3). The round blade that was used to cut the BFRP rebars



Figure 4.3: Saw and diamond blade for BFRP rebar cutting

was a Diamond Montage Y1-2 Series diamond disk, which was designed for general purpose cutting and to ensure a precise and clean cut of the sample. Because the saw dust caused by the cutting process can be dangerous for human health (especially when cutting fibers), protective equipment (respiratory masks, eye wear, and ear protection) was worn at any time the saw was used. While this kind of cut was sufficient to prepare the BFRP rebars for tensile strength testing, the specimens that were prepared for the evaluation of the cross-sectional properties had to be further cut with a

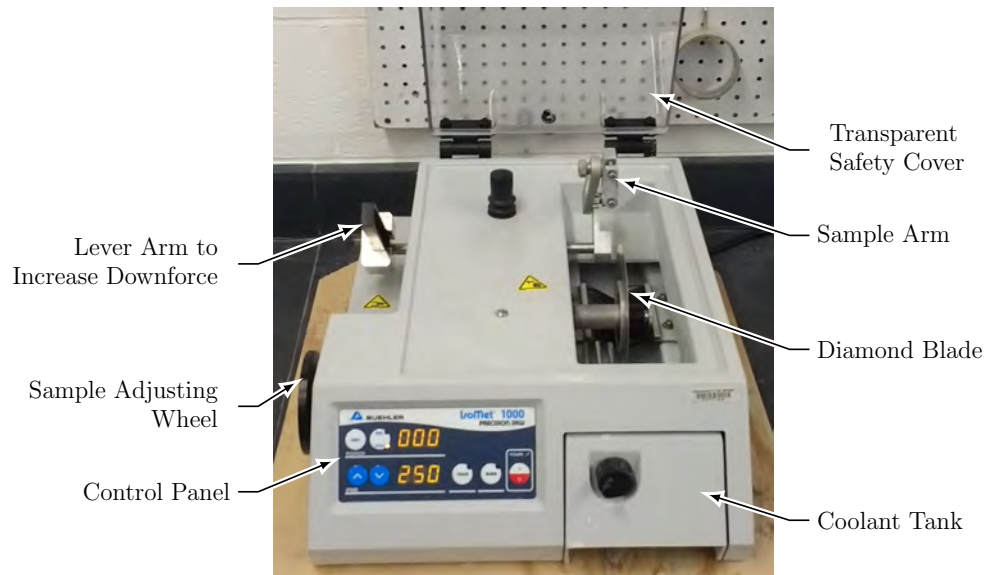


Figure 4.4: Precision saw

more precise instrument (cf. Subsection 4.3.2).

### 4.3.2 Precision Saw

According to ASTM D 792, a precision saw is necessary to cut the specimen for the determination of the cross-sectional area of the BFRP rebar via the water displacement method. For a proper cut of the BFRP material, the saw shown in Figure 4.4 was equipped with a 127 mm (5 in.) diameter diamond blade. The model used for this research was an IsoMet 1000 Precision Cutter<sup>1</sup> produced by Buehler. The machine was equipped with a Sample Arm to support the sample during the cutting process. The samples were guided over the blade — the specimen fell onto the blade, and not vice versa — through a gravity-fed system. Thereby, deformations throughout the cutting process were reduced. However, the contact pressure was adjustable and could be increased through the addition of load to the lever arm that was connected to the sample arm. After precision cuts, the exact specimen's length had to be recorded as explained next.

### 4.3.3 Caliper

A digital caliper was used to measure the exact length of each BFRP rebar specimen for the cross-sectional evaluation according to ASTM D 792 (ASTM-International, 2015b). The caliper had to fulfill the requirements of ASTM D 7205 (ASTM-International, 2015a) for the cross-sectional

<sup>1</sup> Information retrieved on June 13, 2018 from: [www.buehler.com](http://www.buehler.com)

area determination. Therefore, the electronic caliper shown in Figure 4.5 was used with a precision of 0.01 mm (0.001 in.). Before every use, the caliper was zeroed.



Figure 4.5: Electronic caliper

#### 4.3.4 Precision Balance

After the rebars were cut with the precision saw, different measurements for the water displacement method had to be obtained. The used precision balance, which was needed to determine the cross-sectional area, was a Nimbus Precision Balance NBL 623e<sup>2</sup> produced by Adam Equipment Inc (see Figure 4.6). Its readability of 0.001 g ( $2.205 \times 10^{-6}$  lbs.) and its operation with a repeatability of 0.002 g ( $4.409 \times 10^{-6}$  lbs.) matches the requirements for ASTM D 792 (ASTM-International, 2015b). For a balanced setup, the scale was equipped with a bubble level indicator for optimal results. Furthermore, this scale was equipped with a transparent and removable draft shield to reduce erroneous readings that may result from air flow. Because the included shield was not sufficient to accommodate the desired applications for this project, a customized extension was produced with 3D-printing technology.

#### 4.3.5 Support Frame for Specimen Alignment

For the installation of the steel tube anchors on specimens, a designated frame was provided to assure adequate alignment. As mentioned in Chapter 2, FRP rebars are anisotropic and have to be anchored according to the ASTM 7205 before their tensile properties can be evaluated. Therefore, an adjustable alignment frame made from aluminum was used, as shown in Figure 4.7. Two vertical supports were installed to hold the three horizontal supports, to which the rebars were fixed via movable pipe clamps. The frame was constructed with extruded aluminum profiles to guarantee a

---

<sup>2</sup> Information retrieved on June 14, 2018 from: [www.adamequipment.com/nbl-623e](http://www.adamequipment.com/nbl-623e)



Figure 4.6: Precision scale, used to meet ASTM D 792 requirements

high stiffness while maintaining its adjustability to adapt to different rebar sizes and lengths. The rebars were fixed in the plastic plug, which fitted precisely into one end of the steel tube. The rebar specimens were placed on the melamine-coated particleboard on the bottom and positioned along the horizontal supports to ensure a 90° angle before potting the anchors. After the grout was poured into the bottom-plugged steel tube, the upper end was sealed with a red plastic cup. The other end of the rebar was potted after a curing time of 24 hours, and after seven days — when the expansive grout reached its peak pressure — the specimens were ready to be tested and move to the test site.

#### 4.3.6 Test Fixture for Transverse Shear Tests

The fixture for the transverse shear test was built at the FAMU-FSU College of Engineering Machine Shop according to ASTM D7617 (ASTM-International, 2012b). The concept of the transverse shear test and the mechanics of the test can be seen in the Figure 4.8 and Figure 4.9. It can be seen that the top pusher was able to pass through the gap in the middle of the fixture, to cut the rebar — producing a localized shear force. The force was increased until the rebar failed in shear, in both the



Figure 4.7: Tensile test preparation alignment frame

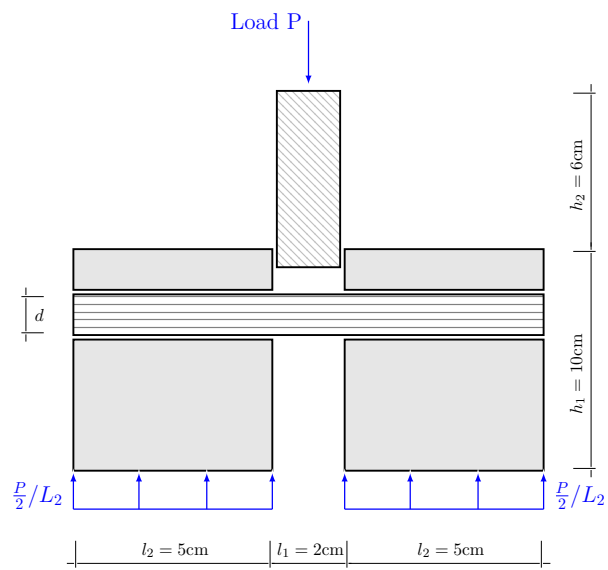


Figure 4.8: Transverse shear test concept

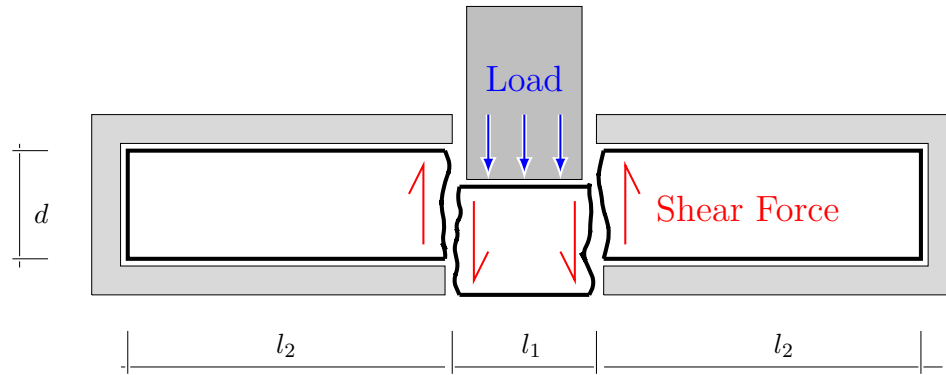


Figure 4.9: Transverse shear test — methodology

cutting planes (between both the surfaces of the top pusher and the fixture). Figure 4.10 shows the built transverse shear fixture that was used to conduct all transverse shear tests. The test fixture consisted of two V-form bar seats, two straps, two lower blades, an upper blade, and two guides machined from steel. The bar seats, the two lower blades, and the two guides were transversely bolted together with two threaded rods and nuts with washers. Between the lower blades and the



Figure 4.10: Transverse shear box — parts

guides, thin shims were placed to ensure that the upper blade fitted properly between the two lower blades (Kampmann et al., 2018).

### 4.3.7 Test Fixture for Apparent Horizontal Shear Tests

The apparent horizontal shear test fixture was built according to ASTM D4475 (ASTM-International, 2012a). The concept of this test is similar to a typical three-point bending test but with a short span to diameter ratio (5 to 1) (c.f. 4.11) which produces a inter-laminar shear force along the longitudinal axis of the bar leading it to failure in shear (c.f. 4.12) rather than in flexure. Accordingly,

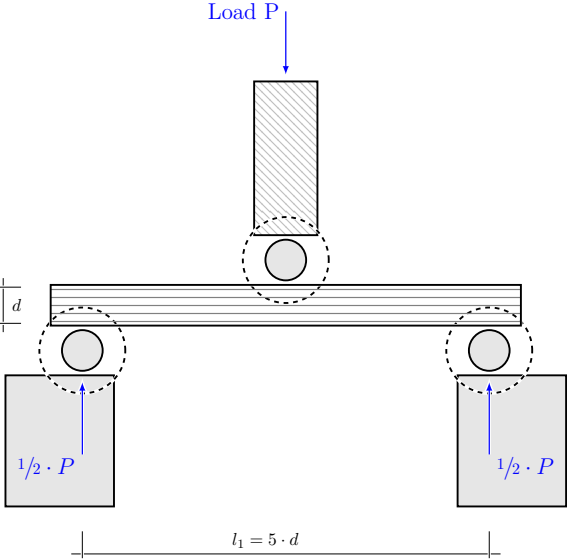


Figure 4.11: Horizontal shear test concept

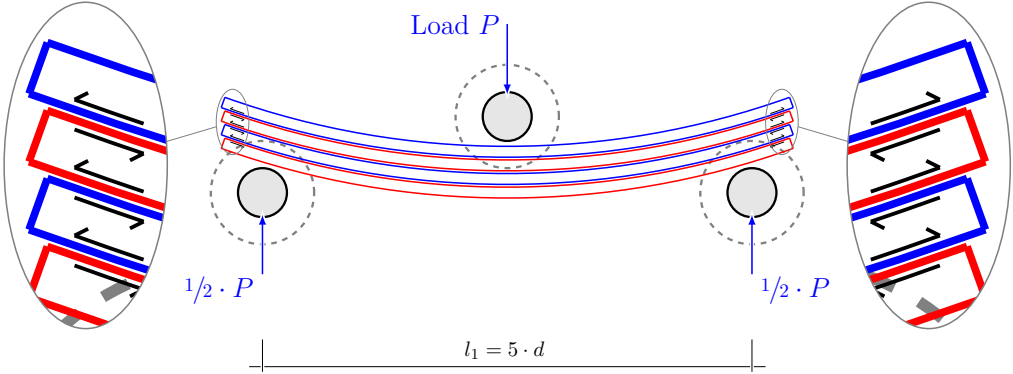


Figure 4.12: Horizontal shear test — methodology

the built fixture for horizontal shear test shown in Figure 4.13 was used. The fixture consisted of two bar supports and a loading nose built on a steel beam. Both the loading nose as well as the two bottom supports were made from suitable hardened steel rods with a groove in the middle to fit the individual rebar sizes. These steel rods were held in place, with the help of a spring on each side of the rod (Kampmann et al., 2018). This setup was used for all conducted apparent horizontal

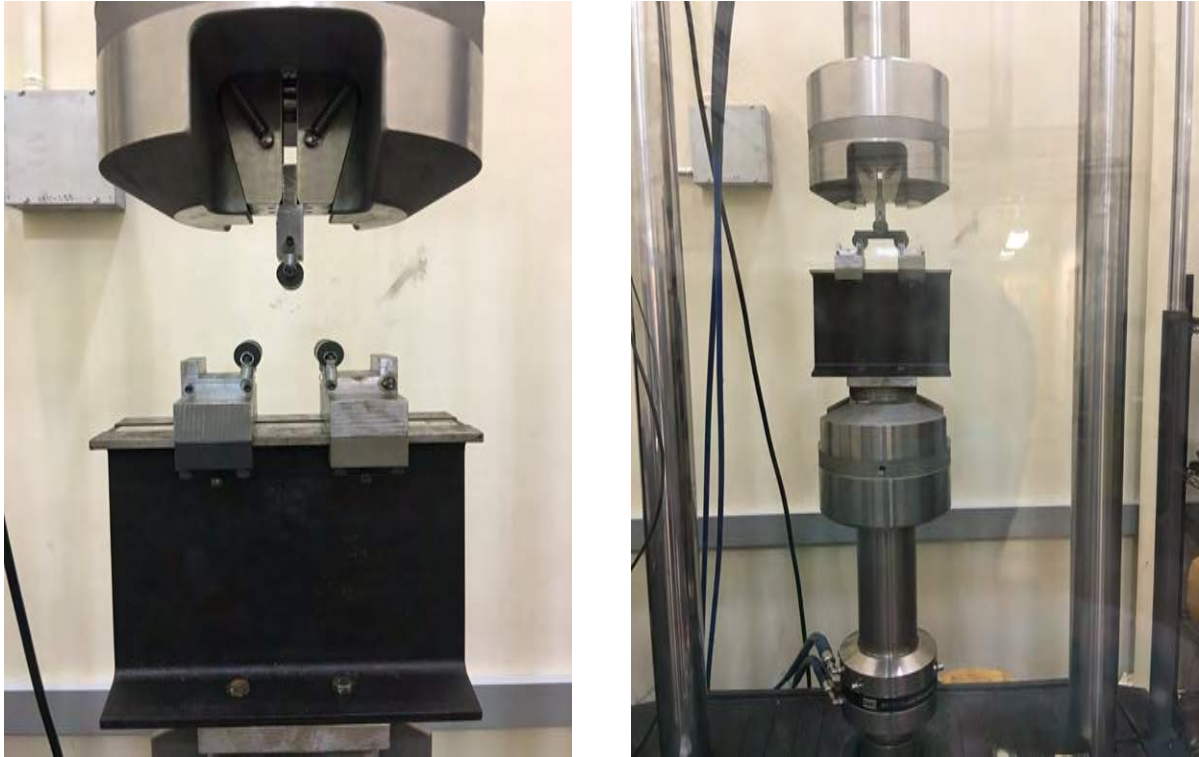


Figure 4.13: Horizontal shear test fixture

shear test, while the distance between the supports was adjusted, dependent on the tested rebar size/diameter.

#### 4.3.8 Test Fixture for Tensile Strength Tests

As mentioned above, an additional test fixture was needed to install the tensile specimens for proper load transfer. The standard load frame grips were not suitable for the tensile test experiments, and therefore, removed to directly attach the fixture to the load mechanism via threaded rod as shown in Figure 4.14. After installing the test fixtures at the bottom and at the upper cross-head, the tensile samples were installed by leading them through the slot of the bearing plates. Afterwards, the rebar was centered with locking plates to fix the specimen and to ensure proper alignment. The fixtures then transfer the load from the bearing plates to the cross section of the steel tube without touching the free portion of the BFRP rebar specimen. Due to this mechanism, the full load was transferred to the FRP rebars via friction between the cured expansive grout and the steel tube anchors. Figure 4.15 shows the installed fixture and the entire test setup. This setup was used to properly test all rebar types and sizes for tensile strength and elastic modulus.



(a) Bottom Plate



(b) Bottom Fixture

Figure 4.14: Bottom unit connected to actuator



Figure 4.15: Tensile fixture installed in load frame

#### 4.3.9 Test Fixture for Bond-to-Concrete Test

The test fixture for the bond-to-concrete test was designed to accommodate the requirements listed in ASTM D7913 (ASTM International, 2014). As seen in Figure 4.16, the fixture was divided into two sub fixtures: an upper and a lower fixture component. The upper fixture was designed to slide the concrete cube into place and to hold it in line with the thrust of the test frame. The lower part of the fixture was attached to the bottom of the test frame and designed to accommodate the steel tube anchor. Both the top and bottom parts of the fixture consisted of four uniformly threaded

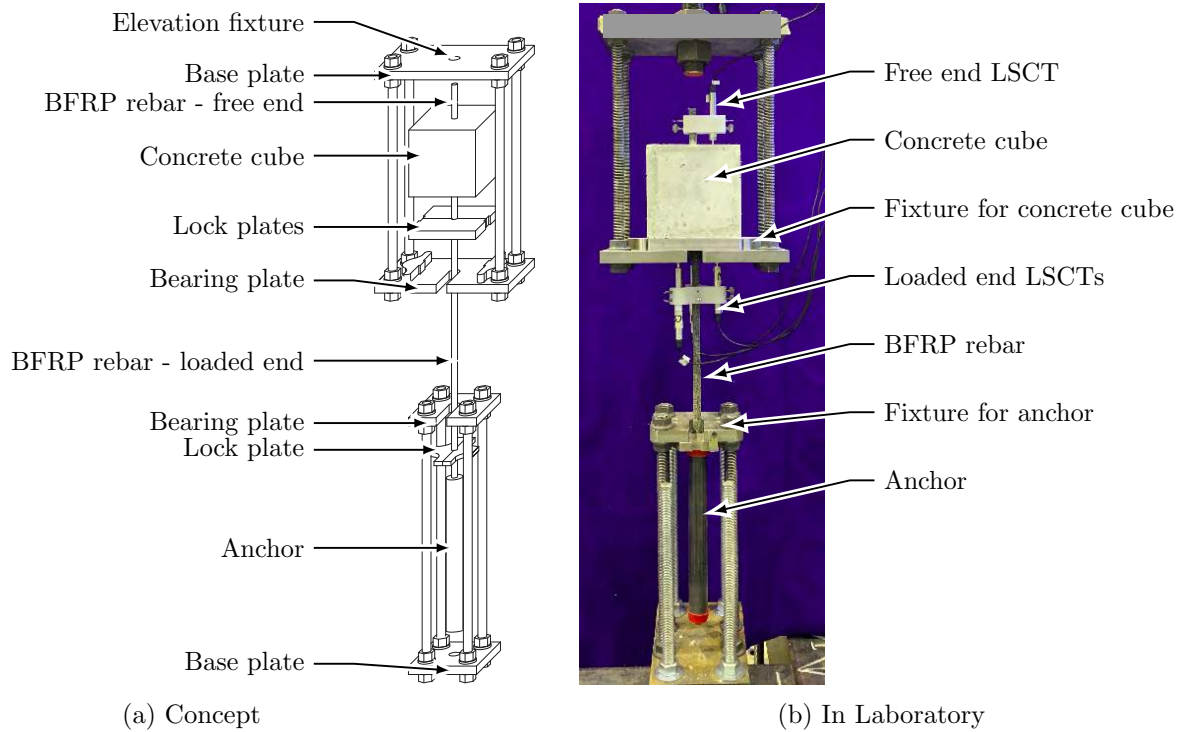


Figure 4.16: Bond-to-concrete experimental setup

rods connecting the top and bottom plates of the fixtures as seen in Figure 4.16. This design was used to conduct all pullout experiments.

### Casting Concrete Cubes for Bond-to-Concrete Tests

According to ASTM D7913 (ASTM International, 2014), the test specimen for pullout testing can either be single casted (vertical or horizontal), or two FRP bars casted into one horizontal prism (ganged horizontal specimens). The horizontal prism has to be separated into two halves before conducting the pullout test. This test setup is primarily used to evaluate the “top bar effect,” which occurs due to moisture migration in curing concrete and which can negatively affect bond strength in concrete reinforcing bars. Because the top bar effect was not part of this research project, the specimen were single casted. For this study, 30 pullout specimens embedded with #3 and #5 rebars were prepared via horizontal casting with combined molds using form dividers according ASTM D7913 (ASTM International, 2014), as shown in Figure 4.17. For easy removal without disturbing the embedded bars, melamine-coated particle boards were used and the edges of each mold were sealed with silicon to guarantee a watertight mold. Because the embedment length is given by the mold, the bond length had to be controlled by bond breakers made from plastic tubing

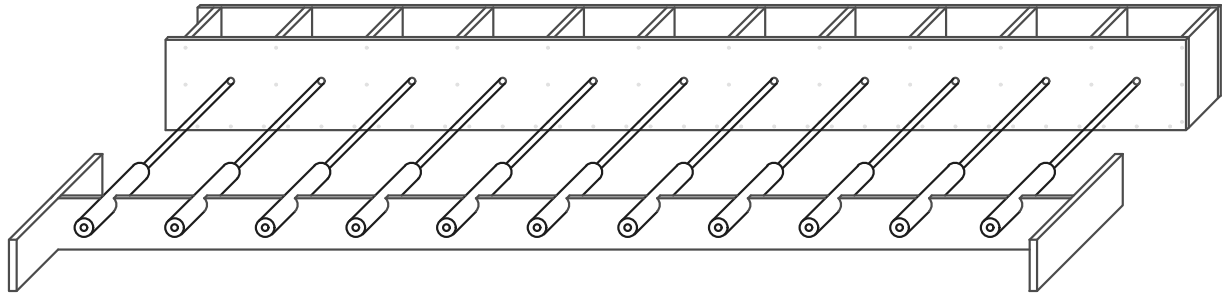


Figure 4.17: Schematic of the mold



Figure 4.18: Fixing the rebar and the plastic tube

with an inner diameter that was large enough to just accommodate the individual rebar size. To prevent the BFRP rebar and the plastic tubes from moving, the rebars were held in place with a screw (at the free end) and the tubes were taped to the mold (c.f. 4.18) before the concrete was poured into the molds. Each BFRP rebar was cut to a length that provided enough space for the measurement system and to prevent the rebar from unnecessary bending while installing the steel anchor at the opposite end. For consistency, one single operator placed the concrete in three layers of approximately equal thickness, while a different single operator rodded each layer 25 times with a 16 mm 5/8 in. diameter tamping rod. After each layer was consolidated, a third operator tapped the mold for each specimen with a rubber mallet 5 times. As soon as the top layer was completely consolidated, the free surface was struck off and leveled with a trowel, before it was covered to prevent evaporation according to ASTM C192 (ASTM International, 2018). For curing, the specimens remained covered in the molds for 17 days, but were removed thereafter to install the anchors at the load end (around the BFRP rebars) according to ASTM D7205 (ASTM-International, 2015a). In line with test procedure ASTM C39 (ASTM-International, 2004), the

compressive strength of five test cylinders (152.4 mm × 304.8 mm or 6 in. × 12 in.) was obtained at the day of pullout testing ( $\geq 28$  days) with a mean compressive strength of 51 MPa (7396 psi), a standard deviation of 1.39 MPa (201.38 psi), and a coefficient of variation of less than 2.7%.

### 4.3.10 Load Frame

To properly determine the tensile strength of BFRP rebars, a displacement-controlled testing machine with a large enough working space and load capacity was required. The High Performance Material Institute (HPMI) in Tallahassee is provided an MTS Landmark testing system (floor sanding) with a model 370 Load Frame, which was manufactured in 2009 and had a maximum work space capacity of approximately 2002 mm (78.8 in.) and a maximum load capacity of 500 kN (110 kip) (MTS Landmark Testing Solutions, 2015). The used Model 647.50A grips — which were used for the shear strength tests — could apply a clamping pressure up to 69 MPa (10 ksi) with wedges inside the grip mechanism of a 4 in. (101.6 mm) width. Figure 4.19 shows an overview of the testing machine and the laboratory setup. In the foreground, the computer with the MTS process-

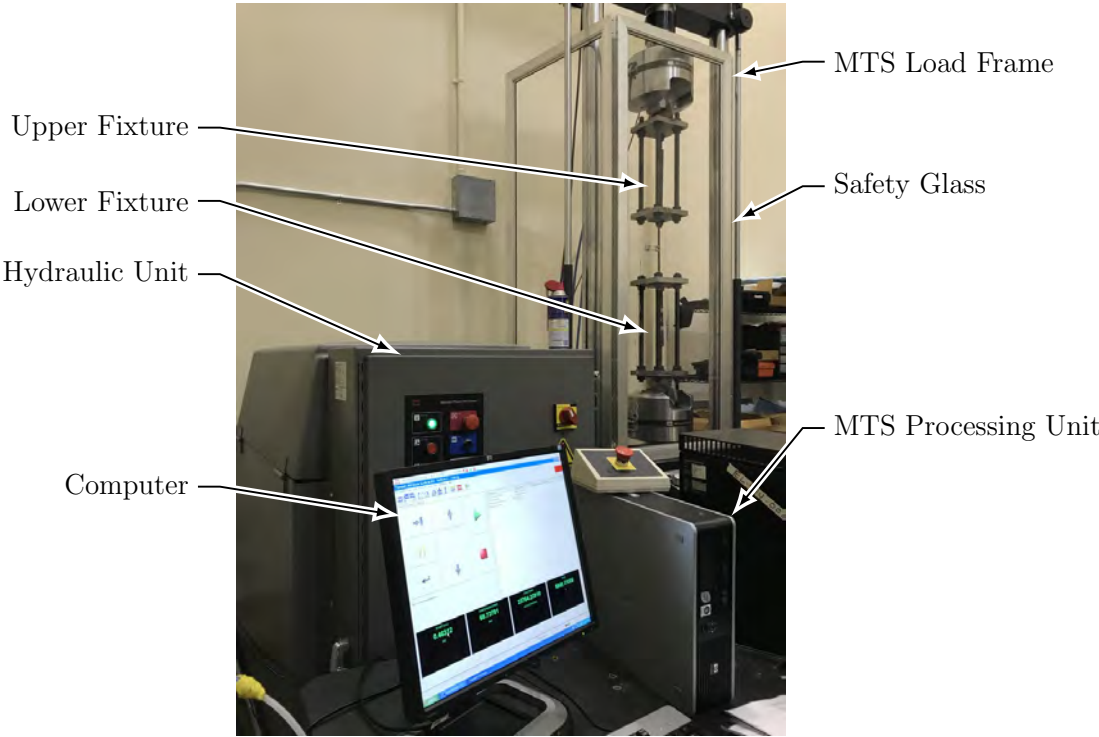


Figure 4.19: Laboratory setup in the HPMI

ing unit is shown. Behind the computer, the hydraulic unit is set to run the MTS load frame. As

shown, the tensile test fixture is installed in the test frame, which was located behind safety glass. The properly calibrated machine had a load measuring system (load cell) with a precision of  $\pm 1\%$  of the measured load. The provided hydraulic pressure to drive the actuator, which applied the load to the gripped specimens, was a detached system next to the testing frame. The load and/or displacement applications for the system were controlled via the MTS FlexTest 60 Controller, which was connected to all sensors, hydraulic, and electrical components, to properly drive the test and to collect the raw data. Furthermore, the controller was connected to the computer and to the MTS control panel (shown in Figure 4.20) to operate the machine and to monitor the test procedure. With the control panel, it was possible to adjust the position of the cross bar and to open or close



Figure 4.20: MTS control panel

the grips with the desired pressure. For fine adjustments, a handset was provided next to the control panel. To control the load and displacement settings, the computer system featured the “MTS TestWorks 4” software. The software interface allowed a proper operation of the machine, including the definition of test parameters and live monitoring of the test results. In addition, the program had an export function to retrieve the gathered raw test data.

**4.3.11 Extensometer**

To accurately record the stretch of the outermost rebar fibers while testing the ultimate tensile strength, an extensometer was used to determine the localized specimen strains. Figure 4.21 shows the used MTS model 634.12-25 extensometer which has a gauge length of 1.00 in. (25.4 mm). After an initial load of about 1 kN was applied, the extensometer was installed in the middle section of the free specimen length with rubber bands ensuring proper contact between the measuring parts of the extensometer and the surface of the rebar.



Figure 4.21: MTS extensometer

## 4.4 Test Procedures

This section details how each specific test procedure was conducted and which standard test method was followed to evaluate the individual rebar property.

### 4.4.1 Cross-Sectional Area Test — Specific Gravity (Relative Density)

The test procedure to determine the density and specific gravity (relative density) of plastics by displacement methods is described to explain how the rebar diameter (or cross section) was specified for each product. The cross-sectional properties were measured according to ASTM D 792 (ASTM-International, 2015b), while the density of each specimen was calculated via the buoyancy principle. A clean specimen was conditioned for 40 h prior to testing in a temperature range from 21 °C to 25 °C (70 °F to 74 °F) at a relative humidity between 40 % and 60 %. The specimen was then cut to the desired length of 25 mm (1 in.) using an electric precision saw. The length of each curtailed specimen was measured 3 times, at 120° intervals perpendicular to the longitudinal axis of the FRP rebar, and the average value was noted for density calculations. Afterwards, the weight of dry and conditioned specimen was measured using an electronic balance and recorded to the nearest 0.05 g (0.0017 oz.). The recorded weight of the curtailed specimen was measured to be no less than 10 g (0.352 oz.) and the value was used as the initial specimen weight, ( $W_i$ ), needed for density calculations. A glass beaker of known volume was used as an immersion vessel to hold the water in which the sample was submerged. However, the immersion vessel was tared to obtain the weight of the sample under buoyancy only. The temperature of the water bath was monitored for each test and constant water temperatures of 21 °C to 25 °C (70 °F to 74 °F) were maintained throughout all experiments. A corrosion-resistant copper wire was used as a sample holder and attached to the

fixture that was independent of the water bath/vessel but introduced the forces to the scale, the specimen was carefully attached to one end of the copper wire. Then, the weight of the specimen along with the copper wire was measured and recorded (Specimen + wire,  $W_{s+w}$ ). The immersion vessel was placed on the support (independent of the weighing mechanism), and the specimen was completely submerged in the water with the help of the copper wire. To remove any entrapped air or air bubbles at the surface of the FRP rebar, the specimen was carefully rubbed with the wire across the surface and submerged in a rotating motion. Any water that was displaced onto the scale was wiped without disturbing the immersion vessel. The weight of the submerged specimen was measured and recorded as final weight ( $W_f$ ). Density measurements were determined via the buoyancy principle and the cross-sectional dimensions were calculated by dividing the determined volume by the measured specimen length. For reliability of test results and to obtain representative values for the BFRP rebar product as a whole, the test was repeated five times for specimens taken from different sections of the production lot and the average value was assigned.

#### **4.4.2 Fiber Content Test — Ignition Loss**

The procedure for ignition loss test for cured reinforced resins is explained here to describe how the fiber content for the tested basalt FRP rebars was determined. ASTM D 2584 -11 (ASTM-International, 2011) outlines this procedure and details the required conditions. Similar to the specimen preparation for the cross-sectional dimension experiments, the specimens for this procedure were also conditioned in a temperature range from 21 °C to 25 °C (70 °F to 74 °F) at a relative humidity between 40 % and 60 %, for at least 40 hours prior to testing. The conditioned sample was then cut to the desired length of 25 mm (1 in.) with a precision of 0.05 mm (0.0019 in.). The weight of the conditioned sample ( $W_s$ ), was then recorded to the nearest 0.05 g (0.0017 oz.) using an electronic balance. This weight was used as the 100 % reference value for calculating the fiber and resin contents (relative to the initial weight). Likewise, a clean and oven-dried crucible was weighed ( $W_c$ ) to the nearest 0.05 g (0.0017 oz.) to obtain the initial weight of the sample holder. The FRP rebar specimen was transferred to the crucible and the total weight of the specimen and the crucible ( $W_i$ ) was recorded to the nearest 0.05 g (0.0017 oz.). To burn off all resin, the crucible (of known mass) along with the specimen were exposed to a temperature of 542 °C to 593 °C (1000 °F to 1100 °F) in a muffle furnace until the specimens reached a constant weight. The crucible was then

carefully removed from the muffle furnace and allowed to cool down to room temperature, before the cooled crucible including the remaining material was weighed using a precision electronic balance. This weight was recorded as final weight ( $W_f$ ). Because the rebar products were made with sand at the surface for bond enhancement, the weight of the sand ( $W_s$ ) was recorded and subtracted from the initial weight of the crucible and the specimen to obtain comparable and absolute fiber content percentages. Because fibers (and sand) are not susceptible to loss on ignition, the reduction in weight due to the burning process is equivalent to the weight of resin, and hence, the percentage of fibers was determined through the difference in weight before and after the burning process. For reliability of test results and to obtain representative values for the BFRP rebar product as a whole, the test was repeated five times for specimens taken from different sections of the production lot and the average value was assigned.

#### 4.4.3 Moisture Absorption Test

The test procedure described in ASTM D 5229 (ASTM, 2014) defines the standard method for determining the moisture absorption characteristics of FRP and is an indicator of porosity. This paragraph explains how the porosity of the tested rebars was determined and calculated. ASTM D 5229 offers seven different test procedures (A through E, Y, and Z) to assign moisture absorption properties for FRP in different environments. Procedure A is most commonly used, and was used for this research project. Each specimen was first oven dried for 48 h to eliminate moisture entrapped in the pores or at the surface. The dried and conditioned specimens were placed in storage bags to ensure that no moisture contaminated the specimens. Three diameter measurements were taken at 120° intervals, perpendicular to the longitudinal axis of the FRP rebar, and those measurements were recorded to the nearest 0.001 mm ( $\frac{4}{10\,000}$  in.). Then, each specimen was weighed with a precision of 0.05 g (0.0017 oz.) in its dry state and recorded as  $W_i$ . The specimens were then submerged in distilled water. The water along with the submerged specimens were stored in an air-circulated oven to maintain a temperature of 50 °C (122 °F) throughout the entire duration of the conditioning. First weight measurements to record  $W_1$  after water conditioning were taken after two weeks. To obtain additional measurements, the specimens were removed from the water bath in two-week intervals (continuous conditioning) and surface dried with a fresh paper towel until no free water remained on the surface of the FRP rebar. All intermediate measurements and the final weight of each specimen

( $W_f$ ) were measured and recorded to the nearest 0.05 g (0.0017 oz.). This procedure was repeated and weight gains were monitored until three consecutive two-week measurements did not differ by more than 0.02 % from one another. For reliability of test results and to obtain representative values for the BFRP rebar product as a whole, the test was repeated five times for specimens taken from different sections of the production lot and the average value was assigned.

#### 4.4.4 Transverse Shear Strength Test

ASTM D 7617 (ASTM-International, 2012b) was used in the process of testing and analyzing the transverse shear strength data. Before testing, the specimens were conditioned according to the ASTM D 5229 (ASTM, 2014). The conditioned specimen were then cut to a minimum length of 225 mm (8.85 in.) so that they fit in the shearing apparatus, which is a device that produces double shear on the FRP rebar specimen. The conditioned and curtailed bars were placed inside the shear test device and loaded with a displacement rate such that the test continued for at least 1 minute, but not more than 10 minutes until the force reached 70 % of the ultimate load. The transverse shear strength was determined using the ultimate load and the nominal cross-sectional area of the specimen.

#### 4.4.5 Apparent Horizontal Shear Test

The FRP rebar products were tested for the apparent horizontal shear properties and this test was conducted according to ASTM D 4475 (ASTM-International, 2012a) standards. First, the diameter at the center of the specimen was recorded and the specimens were conditioned at a temperature range from 21 °C to 25 °C (69.8 °F to 77 °F) and a moisture content between 40 % and 60 % before they were cut to a length of approximately five times the diameter. The horizontal shear strength was assessed through a three-point load test over a span length that was short enough to avoid bending failure. The load was applied at the center of specimen with a displacement rate of  $1.3 \frac{\text{mm}}{\text{min}}$  ( $0.05 \frac{\text{in.}}{\text{min}}$ ) until the shear failure was reached via horizontal delamination (failure of the resin or resin-fiber interface). The ultimate load and the break type (number of fracture surfaces) were recorded and analyzed. For reliability of test results and to meet the requirements listed in FDOT Specifications, Section 932, a minimum of five specimen per sample were tested.

#### 4.4.6 Tensile Strength and Modulus Test

The rebars were tested according to the ASTM D7205, which describes a specific test method for specimen preparation and testing of FRP rebars. It details how to anchor and grip the rebar specimen via steel pipe anchors at both ends, which is necessary because of the low shear and crushing strength of FRP rebars as such anchors prevent the rebar from failing in shear before reaching the ultimate tensile strength. Otherwise, the grip mechanism of standard test machines would lead to a premature (transverse) failure of the specimen. The anchors for this research project were potted with expansive grout to transfer the force from the testing machine into the rebar through compression and friction between the rebar surface and the grout. The dimensions of the anchors relate to the rebar diameter and the free specimen length between the anchors was set to 40 times the rebar diameter. After the grout in the anchors was cured for a minimum of seven days, the specimens were fixed in the MTS test frame. After the specimen was placed into the fixture and aligned properly by the locking plates, the crossbar of the machine was locked for safety purposes. Subsequently, the handset was used for the fine adjustment. An initial load of 1 kN (0.225 kip) was applied to the bar by using the setting wheel of the handset. The next step was to place the extensometer with two little rubber bands in the middle of the free specimen length of the rebar. When the extensometer was fixed, the safety pin was pulled out and the extensometer connected to the computer was ready to measure the displacement. Then, safety glass was placed on the top of the table of the load frame to protect the laboratory staff from chipping fibers caused by the failure of the rebars. The specimen was installed in the MTS Load Frame and the test was set up and configured with the program MTS TestWorks 4 to control and start the tests. The load had been zeroed before the samples were hung into the fixture to gain proper results without additional forces of the fixtures' dead weight. The rates were chosen to target a failure time between 60 s (1 min) and 600 s (10 min) as defined by ASTM D 7205 / D 7205 (ASTM-International, 2015a). To test the setup, some test specimens were produced in addition to the experimental program. After starting the test program, the force versus displacement and the strain data were monitored continuously at a 10 Hz frequency. According to ASTM D 7205, the tensile chord modulus of elasticity should be calculated from the strain range of the lower half of the stress-strain curve, with the start point being a strain of 0.1% and the end point being a strain of 0.3%. To protect the extensometer, it was removed around 10% displacement before the sample failed and possibly

damaged the extensometer. The testing machine stopped automatically when the force dropped by 85 %. This procedure was performed on 40 specimens.

#### 4.4.7 Bond-to-Concrete Strength Test

The bond-to-concrete properties of the rebars were evaluated via pullout testing according to ASTM D7913 (ASTM International, 2014). The bond strength experiments were conducted under standard laboratory conditions within  $(23 \pm 2)^\circ\text{C}$  [ $(73 \pm 5)^\circ\text{F}$ ] and  $(50 \pm 10)\%$  relative humidity, using a 300 kN (66 kip) hydraulically controlled load frame. First, the specimens were cleaned and installed in the test frame and an initial seating load of 272 kN (600 lbs.) was applied to generate sufficient stiffness in the system. Then the LSCTs, which were needed to measure the rebar slip at both ends (the so-called free and load ends). Once the setup was made safe, a static force was continuously applied via a displacement rate of  $0.75 \frac{\text{mm}}{\text{min}}$  ( $0.03 \frac{\text{in.}}{\text{min}}$ ) and the raw data was recorded with 1000 Hz until the measured force decreased significantly (more than 50 %) and the slippage at the free end of the bar measured at least 2.5 mm (0.1 in.). After each test was completed, the concrete block was split open to analyze the failure mode and to measure the precise bond length of each specimen. For repeatability, a minimum of five specimen per sample group were tested.

### 4.5 Data Acquisition and Data Analysis

All raw data for tensile strength and shear strength tests were recorded with MTS TestWorks software, and the raw data for the bond-to-concrete experiments were recorded using LabView software with high data rates. For all experiments, the measurements were written to file at 10 Hz (using appropriate filters). For efficient data analysis and data presentation, the high-speed data was filtered and reduced using R-statistics<sup>3</sup> and R-Studio<sup>4</sup> software packages. However, all reported numerical maximum and minimum values are based on the raw data and were calculated before any filter was applied.

To properly analyze and evaluate the BFRP rebar samples (specimen groups), the individual specimen results were determined and categorized, before statistical values (minimum, maximum, average, standard deviation and coefficient of variation) for the relevant specimen groups were

---

<sup>3</sup>R.app GUI 1.70 (7434 El Capitan build), S. Urbanek & H.-J. Bibiko, R Foundation for Statistical Computing, 2016

<sup>4</sup>Version 1.1.383 2009-2017 RStudio, Inc.

individually calculated using R-static software. The mean and other statistical values for each BFRP rebar sample were calculated based on a minimum of five individual specimen results.

# Chapter 5

## Results

### 5.1 Introduction

The performance evaluation of basalt fiber reinforced polymer (BFRP) rebars is summarized in this chapter. The following results were obtained at the FAMU-FSU College of Engineering in the High Performance Materials Institute (HPMI). All tests were conducted in accordance with the relevant American Society for Testing and Materials (ASTM) test protocol. The collected raw data were analyzed with the engineering software R-statistics<sup>1</sup> and R-Studio<sup>2</sup>. The results are presented throughout this chapter in tables and graphs for visual representation. For clarity, each property was individually studied and presented separately. At the end of the chapter, a summary of the test results is provided to comprehensively present each specific product, document its performance, and to compare it to the acceptance criteria in FDOT 932, AC 454, and ASTM D 7957 (for glass based FRP rebars).

### 5.2 Cross-Sectional Properties

The effective rebar diameter was measured according to the ASTM D 792-13. Due to the variety of FRP rebars on the market and depending on the proprietary production methods, rebars from different manufacturers with different surface enhancement may vary significantly and deviate from the given nominal diameter. Table 5.1 below lists the results of water displacement method according

---

<sup>1</sup>R.app GUI 1.70 (7434 El Capitan build), S. Urbanek & H.-J. Bibiko, R Foundation for Statistical Computing, 2016

<sup>2</sup>Version 1.1.383 2009-2017 RStudio, Inc.

to the ASTM D 792-13 of all the rebar products.

Table 5.1: Statistical evaluation of diameter measurements for rebar size # 3 and # 5

Rebar		Min Value	Max Value	Mean Value	Standard Deviation	CoV †
Type	Size	mm	mm	mm	mm	%
A	#3	10.23	10.24	10.28	0.02	0.22
B	#3	10.78	10.87	10.94	0.06	0.58
C-1	#3	9.92	9.95	9.99	0.03	0.32
C-2	#3	10.16	10.18	10.25	0.02	0.23
A	#5	16.64	16.71	16.78	0.05	0.31
B	#5	17.51	17.65	17.98	0.18	1.05
C-1	#5	17.05	17.14	17.40	0.14	0.86
C-2	#5	16.90	17.26	17.64	0.23	1.73

† Coefficient of Variation

### 5.3 Fiber Content

The fiber content by weight of the rebars was calculated according to ASTM D 2584 -11 (ASTM-International, 2011). The measured fiber content results are plotted in the Figure 5.1. The bar chart was generated to compare the different rebar types against each other and to compare the different rebar sizes. Each row in the plot indicates a specific rebar size, while each column represents a different rebar type. The bars represent individual specimens. The red hatched part of the bars indicates the fiber content in percentage, the blue crosshatched part represents the percentage of resin, and the black part represents the amount of sand that was applied to the rebar surface to increase the bond-to-concrete performance. Since the weight of the sand surface enhancement has a relative higher contribution (percentage wise) on smaller specimens, the percentage weight on # 3 rebars is higher than # 5 rebars as presented in bar chart. The 100 % values for these rebars are based on total specimen weight minus the sand content. The dashed line at the 70 % mark shows the currently accepted minimum fiber content for FRP rebars. It can be seen that all individual rebar specimens met the minimum requirement for the fiber content. The only marginal exception was specimen d of rebar Type A, # 3, however, that specimen still passed the acceptance criteria. Overall, the measured fiber content results show that the production quality was consistent for all rebar types and sizes (within each rebar product).

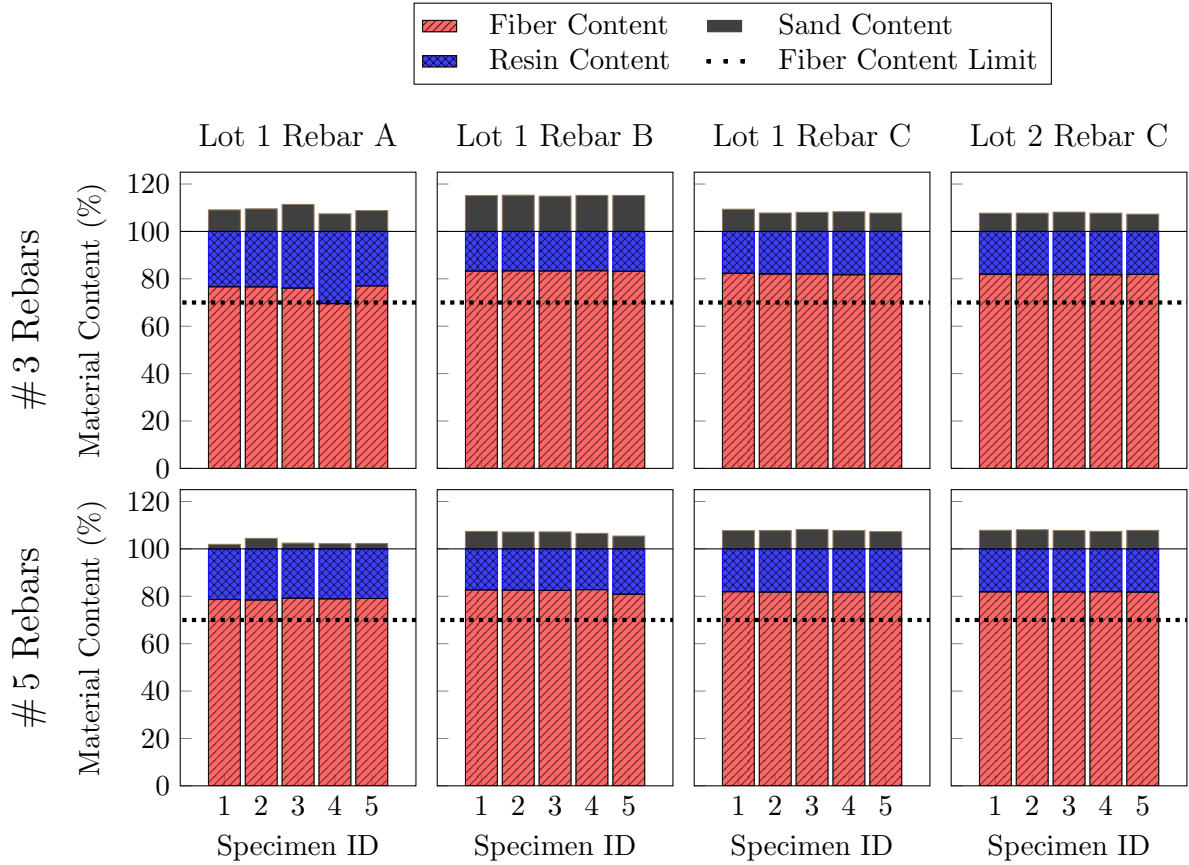


Figure 5.1: Fiber content percentage of rebars from all manufacturers

The following Figure 5.2 and 5.3 exemplify the rebar appearance after the loss on ignition test procedure. While the specimens shown in the figure were type C rebar materials, the appearance of the rebars after the test were similar for all rebar types. The following Figure 5.3 presents exemplary closeup pictures for individual test specimens of rebar types A through C. These pictures show # 3 rebars, but # 5 rebars were similar in appearance after completion of the lost on ignition experiments.

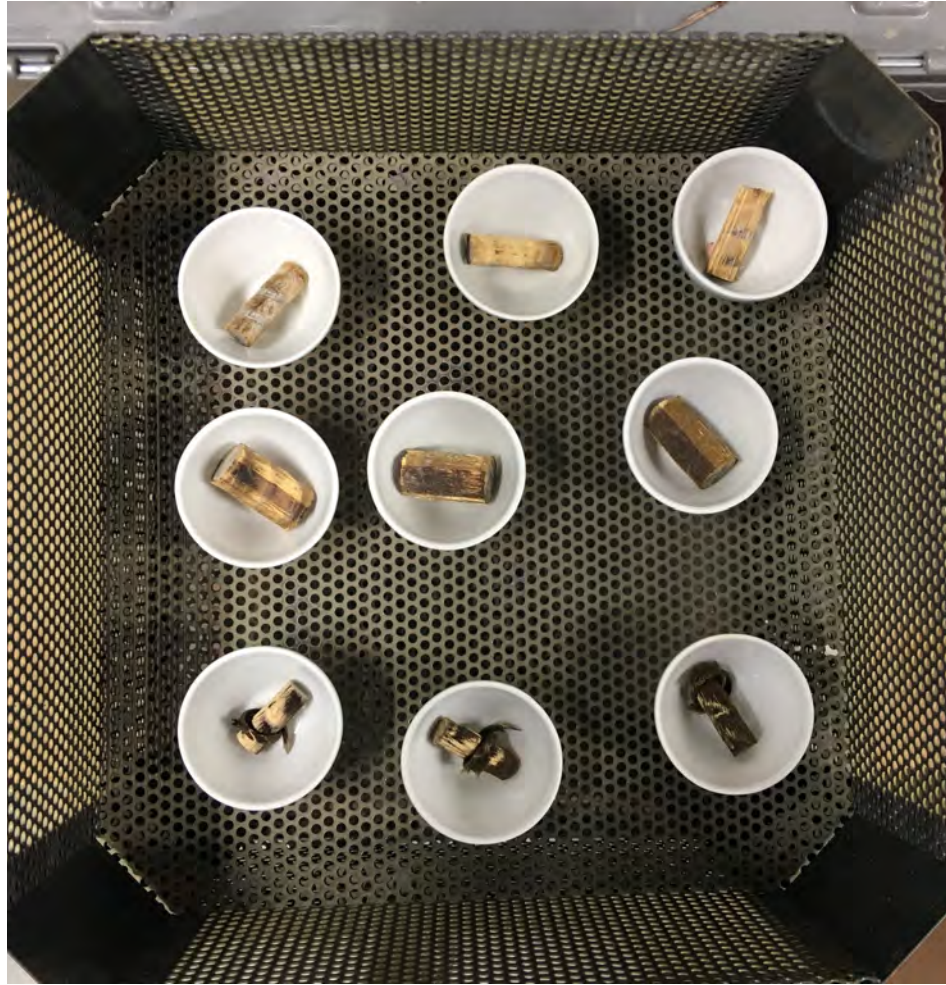


Figure 5.2: Fiber content specimen of rebar type C # 3, 5 after test



(a) Type A

(b) Type B

(c) Type C

Figure 5.3: Fiber content specimen of rebar # 3 after test

### 5.4 Moisture Absorption

The moisture absorption property of rebars was tested in accordance with ASTM D 5229 (ASTM, 2014). The graph plotted in Figure 5.4 represents weight change of the rebar specimen stored in distilled water over a test period of 98 d. It can be seen in the graph that all rebar types showed comparable moisture absorption behavior, except # 5 rebar from type C with epoxy resin. All the rebar types satisfied the AC454 limitations for the absorption limit of 0.25 % in first 24 hours of exposure except # 5 rebar from type C.

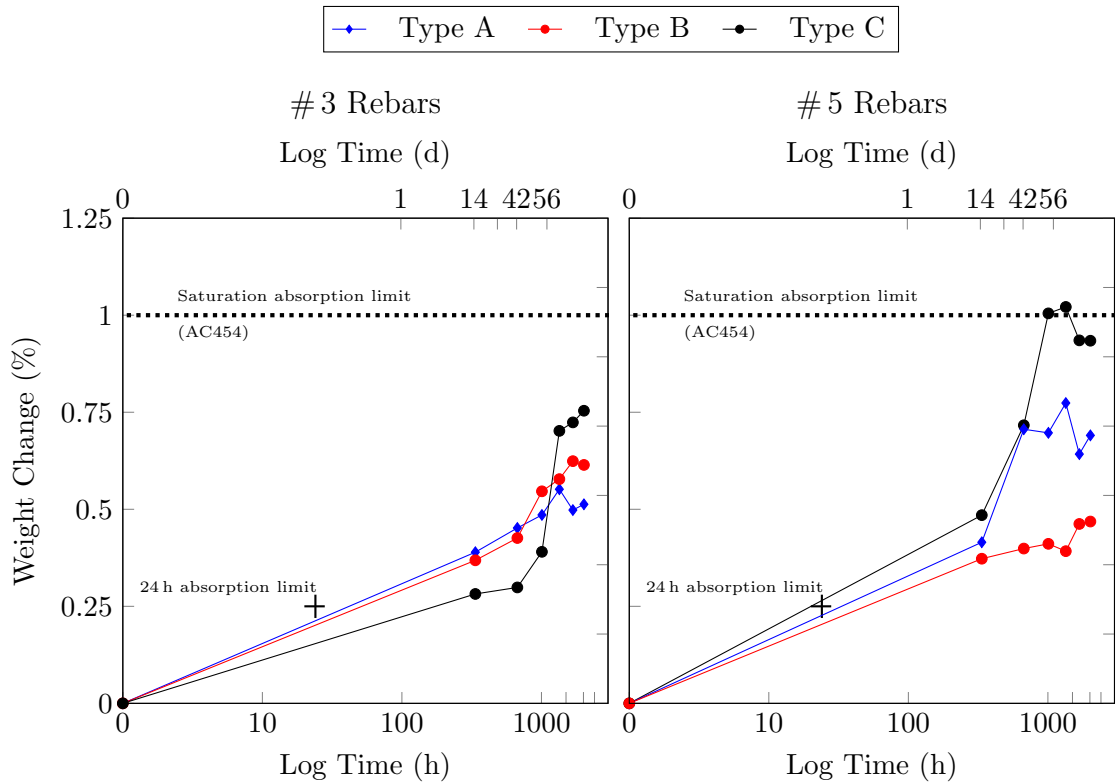


Figure 5.4: Moisture absorption results of rebars from all manufacturers

### 5.5 Transverse Shear Test

ASTM D 7617 (ASTM-International, 2012b) was used in the process of testing and analyzing the transverse shear strength of the rebars. Tested and processed data are plotted in the following sections 5.5.1 and 5.5.2.

### 5.5.1 Load vs. Displacement

The graphs plotted in Figures 5.5, 5.6, 5.7, and 5.8 show the load vs. displacement behavior of transverse shear behavior of #3 and #5 rebars from all manufacturers. The x-axis of the graph represents the cross-head extension or the relative displacement between the edges of the directly sheared specimen, while the y-axis shows the measured force throughout the load application period.

The Graph in figure 5.5 shows a linear behavior until it reaches the ultimate failure load. It

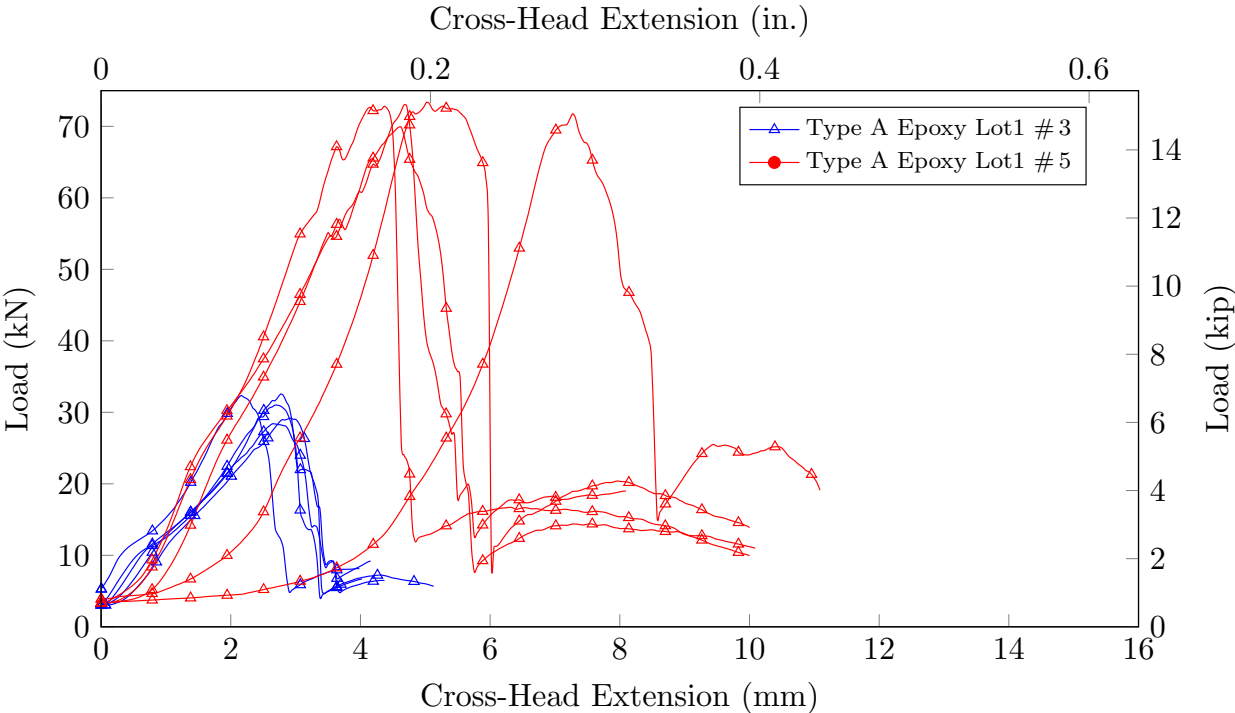


Figure 5.5: Extension vs. transverse shear load behavior of type A rebars Lot 1 size 3 and 5

can be seen that #5 sized rebar sustained higher load in comparison with #3 rebars. All the #3 rebars sustained a consistent load while #5 rebars sustained same peak load but the extension of the rebars varied. The graph in Figure 5.6 shows a comparison between the load and the displacement for transverse shear strength of #3 and #5 rebars lot 1 from type B rebar. It can be seen that the graph had a linear behavior until it reached the ultimate failure load. All the rebars sizes sustained a consistent load with similar extension. The graph in Figure 5.7 presents a comparison between the load and the displacement for of transverse shear strength of #3 and #5 rebars lot 1 from type C rebar. The graph shows a linear behavior until it reached 90% of the ultimate failure load.

The visualized data in Figure 5.8 show the load vs. displacement behavior for transverse shear

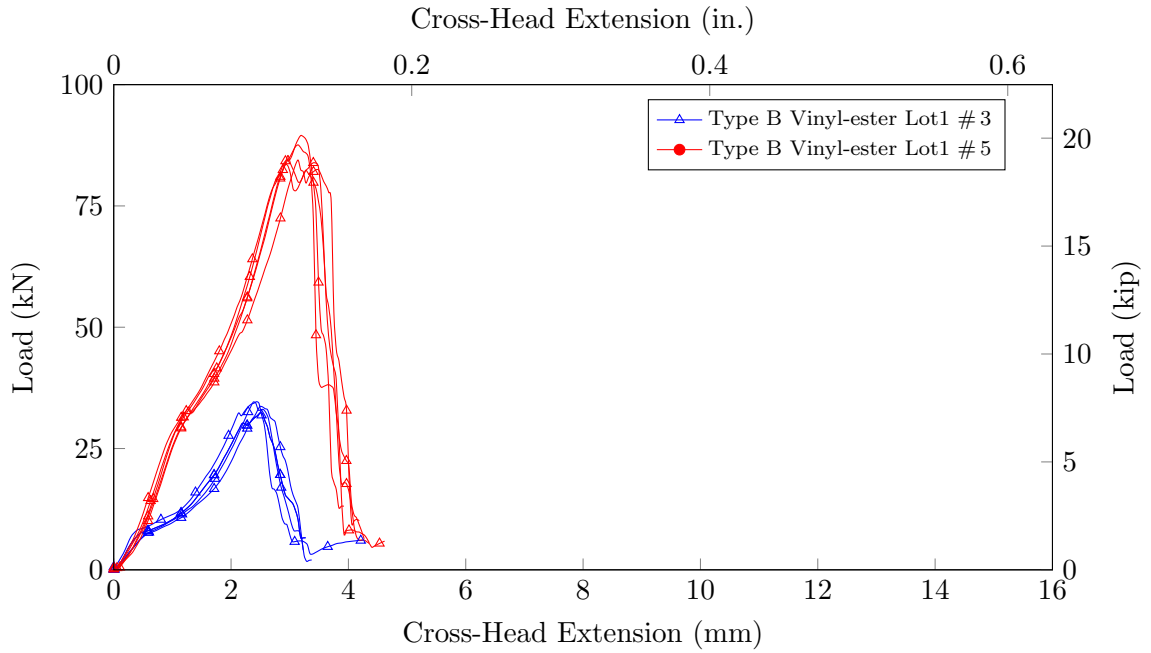


Figure 5.6: Extension vs. transverse shear load behavior of type B rebars Lot 1 size 3 and 5

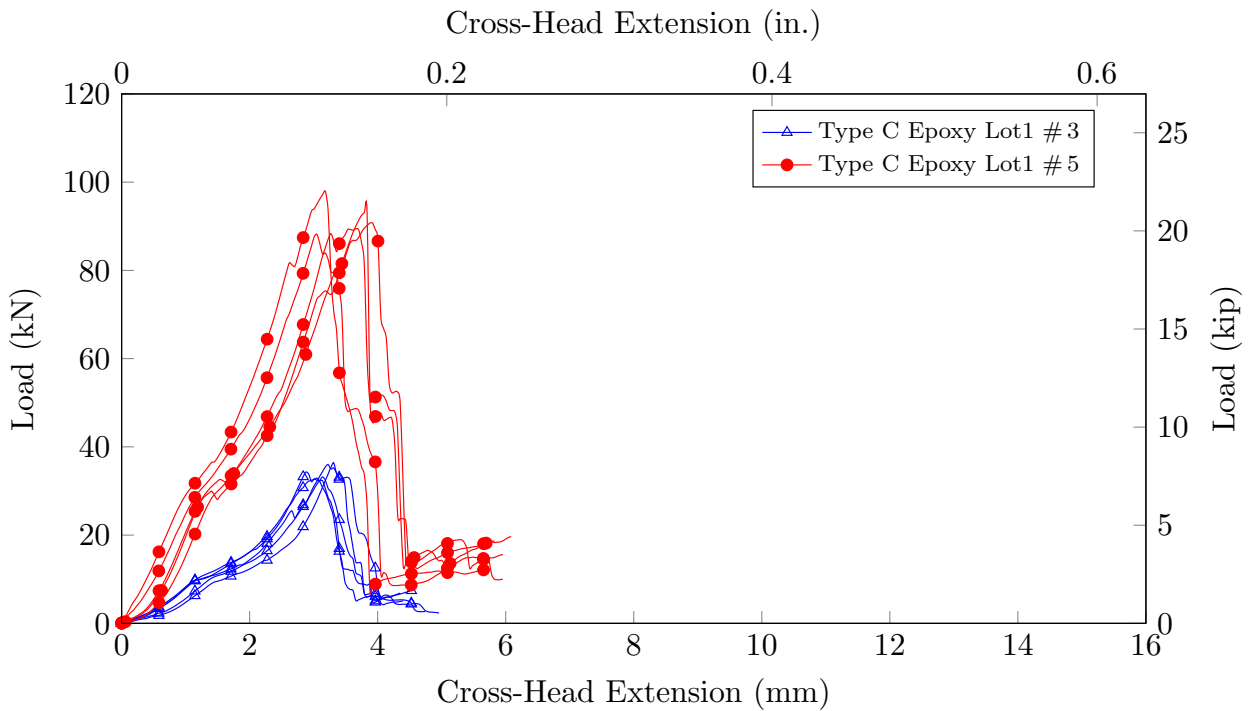


Figure 5.7: Extension vs. transverse shear load behavior of type C rebars Lot 1 size 3 and 5

strength of #3 and #5 rebars lot 2 from type C rebar. It can be seen that the material behaved linearly until 90% of the ultimate failure load was reached.

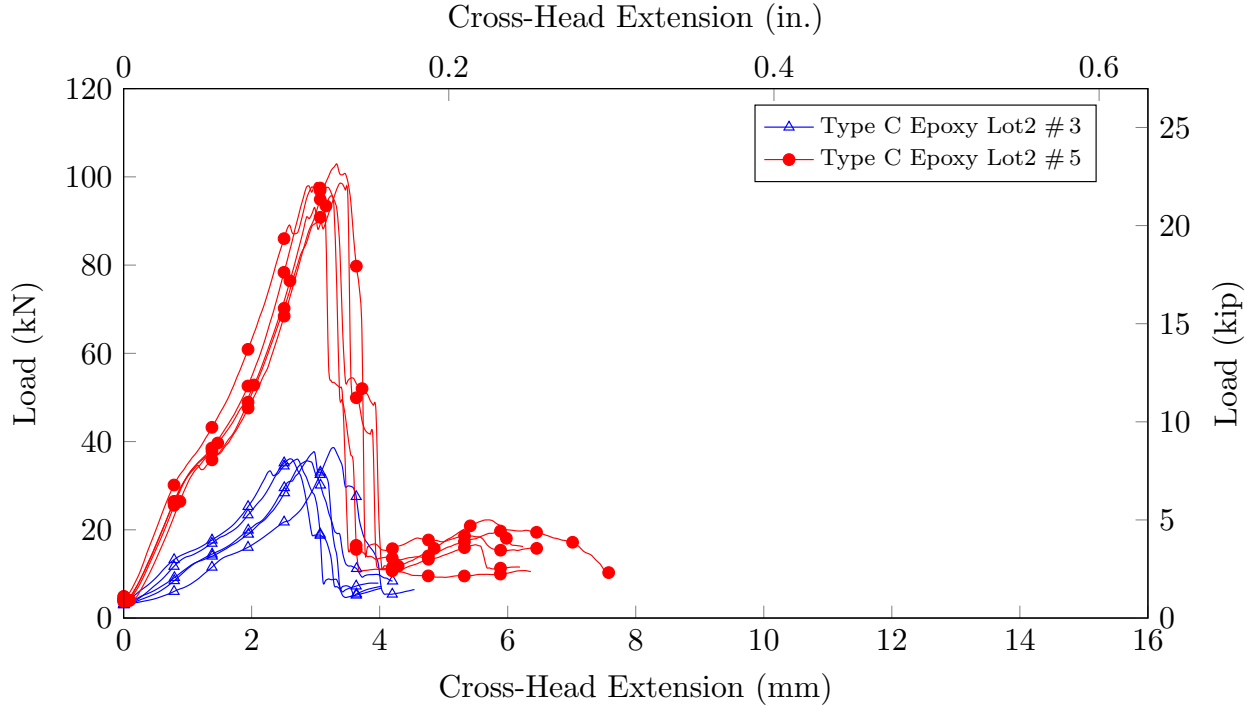


Figure 5.8: Extension vs. transverse shear load behavior of type C rebars Lot 2 size 3 and 5

### 5.5.2 Stress vs. Displacement

Transverse shear results are presented in Figures 5.9, 5.10, 5.11, and 5.12 compare the stress vs. displacement behavior of transverse shear test of # 3 and # 5 rebars from all rebar manufacturer. The data along the x-axis represents the cross-head extension or the direct shear displacement, while the y-axis signifies the measured shear stress.

The data in Figure 5.9 show that the material behaved nearly linearly until the ultimate failure load was reached. It can be seen in Figure 5.9 that the stress vs. strain behavior of both the rebars is close but not identical-especially because it varied significantly for rebar number # 5.

The graph in Figure 5.10 presents the stress vs. displacement behavior of transverse shear test of rebar type C lot 1. From the post failure stress vs. strain behavior of rebar type C as shown in Figure 5.10, it can be seen that the rebars underwent similar failure behavior.

The graph in Figure 5.11 presents the stress vs. displacement behavior of transverse shear test of rebar type C lot 1. The graphs display a mostly linear behavior until the ultimate failure load was reached. Figure 5.12 shows the stress vs. displacement behavior of transverse shear test of rebar type C lot 2. It can be seen that the data represented a nearly linear behavior until the ultimate

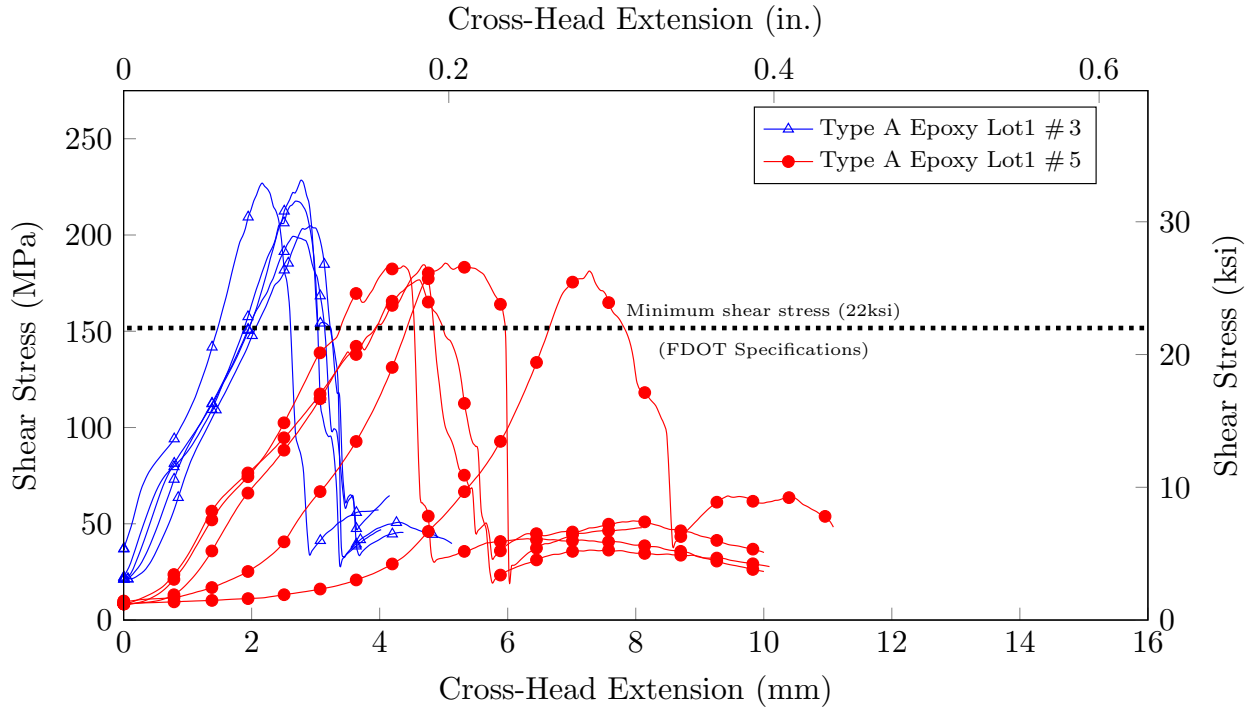


Figure 5.9: Transverse shear stress vs. extension behavior of rebar type A Lot 1 size 3 and 5

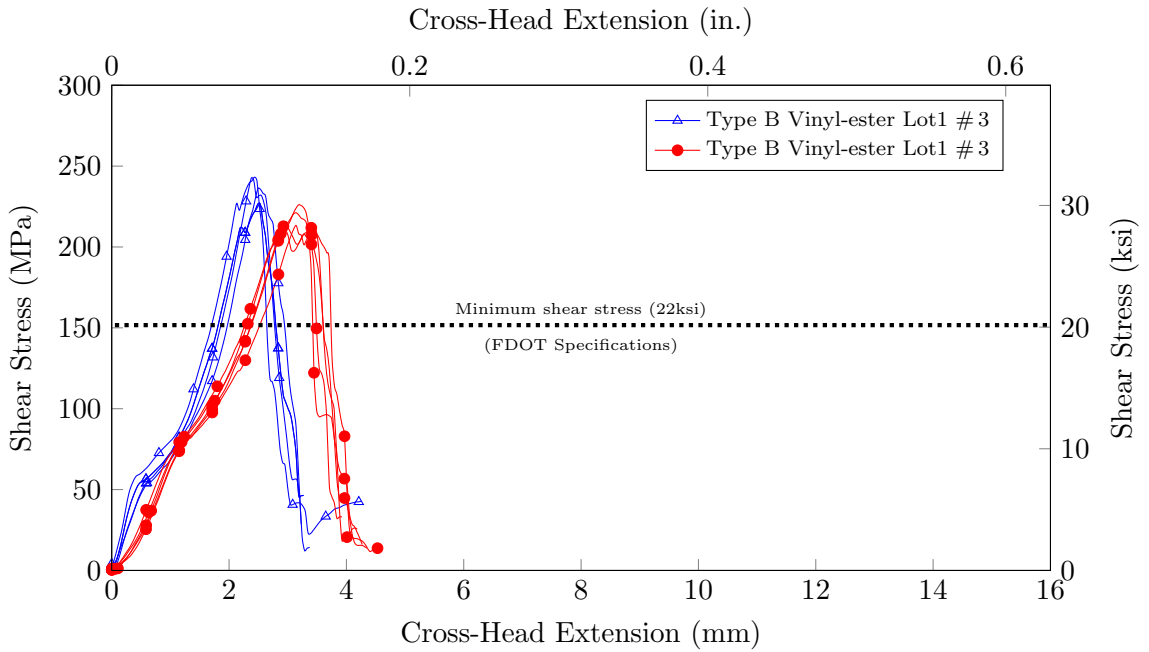


Figure 5.10: Transverse shear stress vs. extension results of rebar type B Lot 1 size 3 and 5

failure load was attained. The stress vs. strain behavior of failed rebar specimen from both lots of type C in Figures 5.11 and 5.12 show that, although the ultimate failure capacity of the rebars varied significantly, all the rebar samples failed in an identical manner.

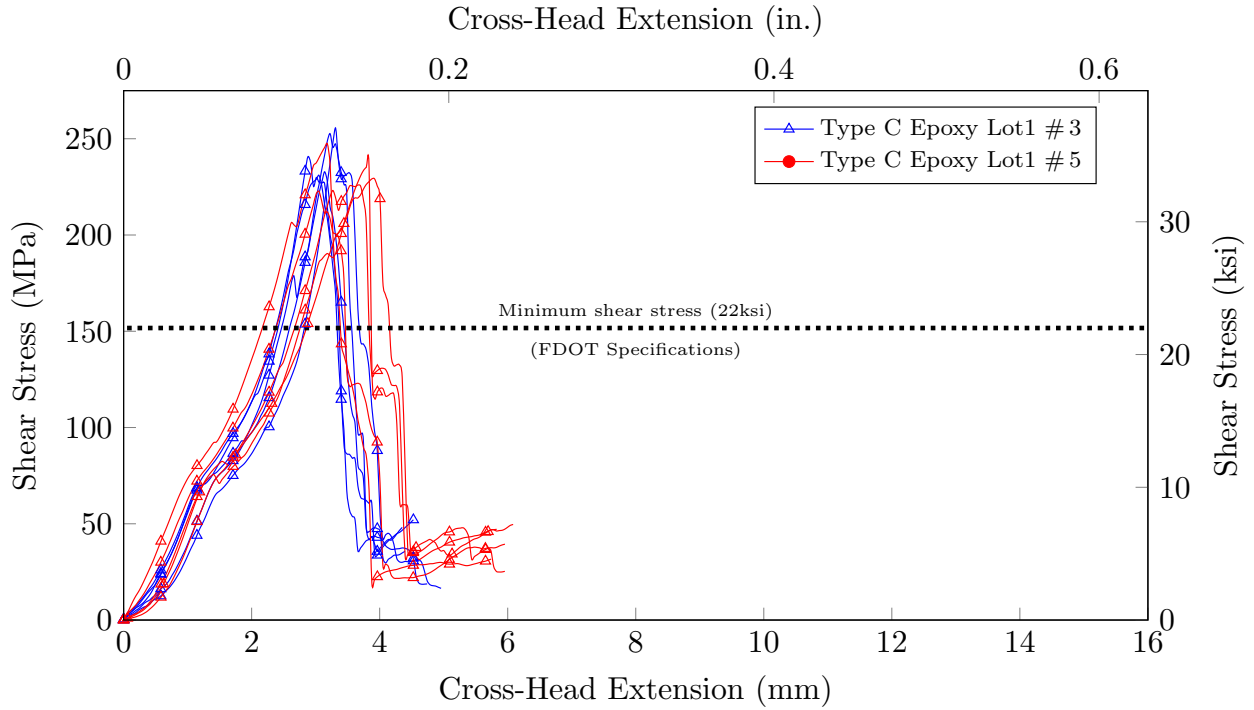


Figure 5.11: Transverse shear stress vs. extension behavior of type C Lot 1 size 3 and 5

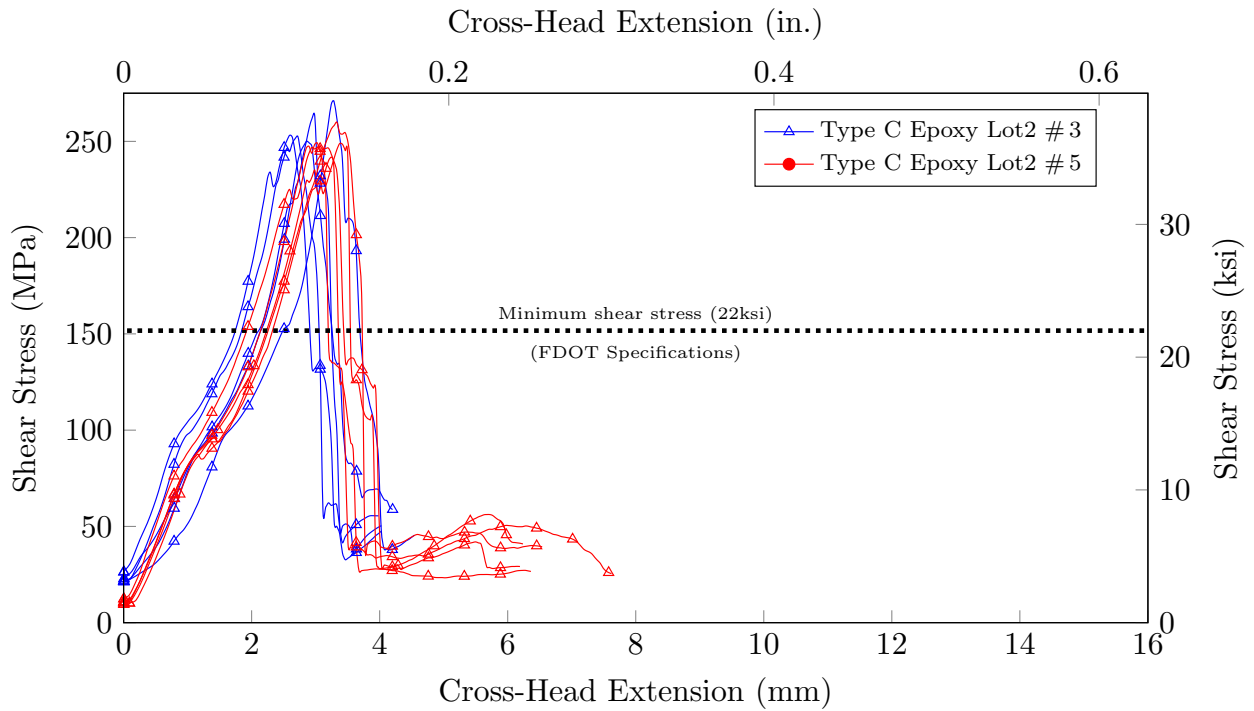


Figure 5.12: Transverse shear stress vs. extension behavior of type C Lot 2 size 3 and 5

## 5.6 Modes of Failure

To study the failure process, the failed BFRP rebars were analyzed in detail to observe the failure pattern of outer fibers and inner fibers. Therefore Figure 5.13 exemplifies the failure patterns of the tested BFRP specimen in response to the applied transverse shear loads. Figure 5.13 shows that the failure mode for all the rebars was identical irrespective of the sizes and types. The test fixture was designed so that direct shear stresses are applied perpendicular to the longitudinal axis of the rebars and a “scissor-like” failure occurs at the center of the specimen as dictated in ASTM standards. After a detailed analysis of failed specimens, it was seen that similar to GFRP rebars, BFRP rebar samples also tried to bend throughout the test, although fibers were aligned in the longitudinal direction.



(a) Type A #3



(b) Type A #5



(c) Type B #3



(d) Type B #5



(e) Type C #3



(f) Type C #5

Figure 5.13: Failure pattern for tested rebar after transverse shear test

## 5.7 Summary of Transverse Shear Properties

The results of the statistical evaluation for the transverse shear strength properties of the tested products are listed in the following Table 5.2. A total of 30 specimen, five for each rebar type and size, were tested. The average and all other statistical values were calculated based on a sample size of five specimen, and the corresponding results are shown in the table. For numerical comparison and concluding values, Table 5.2 lists the minimum shear stress ( $\wedge$ ), the maximum shear stress ( $\vee$ ), the average shear stress ( $\mu$ ), the standard deviation ( $\sigma$ ), and the coefficient of variation (CV) for each individual test sample.

Table 5.2: Transverse Shear test statistical values for each sample group (US Customary Units)

Sample Group				Statistical Values				
Manuf. Type	Resin Type	Size #	Lot No.	Shear Stress				
				$\wedge$ ksi	$\vee$ ksi	$\mu$ ksi	$\sigma$ ksi	CV %
Rebar A	Epoxy	3	1	29.1	33.2	31.4	1.9	6.00
Rebar A	Epoxy	5	1	25.7	26.9	26.5	0.5	1.94
Rebar B	Vinyl-ester	3	1	33.3	35.8	34.5	1.2	3.51
Rebar B	Vinyl-ester	5	1	30.8	32.9	31.7	0.8	2.62
Rebar C	Epoxy	3	1	33.6	37.5	35.2	1.6	4.64
Rebar C	Epoxy	3	2	36.5	39.8	37.7	1.4	3.71
Rebar C	Epoxy	5	1	32.4	35.9	33.7	1.4	4.14
Rebar C	Epoxy	5	2	35.3	38.0	36.5	1.0	2.71

It can be seen in Tables 4.3 and 4.4 that all the BFRP rebar samples are satisfying the minimum required criteria for GFRP transverse shear stress.

## 5.8 Apparent Horizontal Shear Test

The FRP rebar products were tested for horizontal shear properties. The horizontal shear test was conducted according to the ASTM D 4475 (ASTM-International, 2012a) standards.

### 5.8.1 Load vs. Displacement

The graphs in Figures 5.14, 5.15, 5.16, and 5.17 plot the load vs. displacement behavior of short span 3 point bending. Each rebar type is shown individually — and every specimen within the relevant sample is displayed — to compare # 3 and # 5 from the same manufacturer. The x-axis of the graph represents the cross-head frame displacement, and the y-axis represents the applied load.

The graph in Figure 5.14 shows a nearly linear behavior until it reached the ultimate failure load. Following the peak load, a descending branch proceeds with individual peaks and falls. The

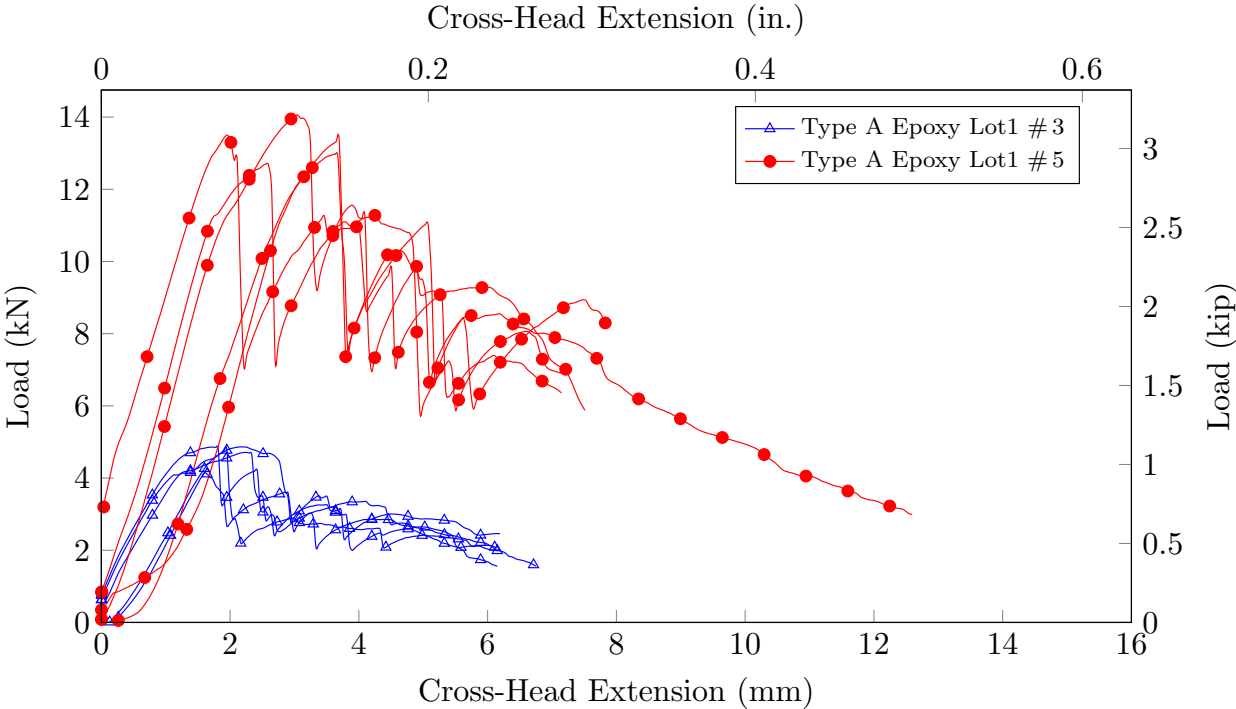


Figure 5.14: Extension vs. horizontal shear load behavior of rebar type A Lot 1 size 3 and 5

peaks and falls represent individual layers of fibers engaged and failing in tension located in the lower part of the specimen experiencing pure tension, while the upper part is in compression.

Extension vs. Horizontal shear behavior of rebar type B can be seen in the graph in Figure 5.15. Similar to type A, # 5 type B rebar sustained more load in comparison with # 3 rebars. The failure

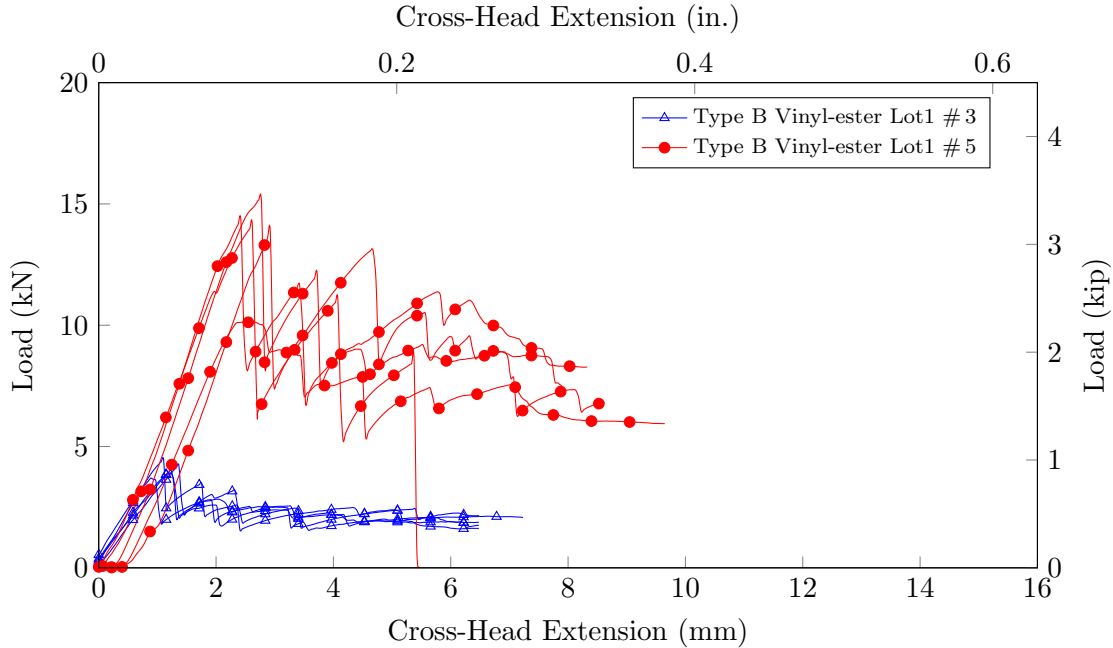


Figure 5.15: Extension vs. horizontal shear load behavior of rebar type B Lot 1 size 3 and 5

pattern of both rebars was similar and identical to type A rebar failure pattern.

The graphs shown in Figures 5.16 and 5.17 show the load vs. displacement behavior of rebar type C Lot 1 and 2. The graphs show a linear behavior until it reached 90% of the ultimate failure load. It can be seen in Figures 5.16 and 5.17 that the failure behavior of type C rebar is identical irrespective of production lot and rebar size. After a detailed analysis, we can see the shear lag effect in the rebars similar to other two types.

### 5.8.2 Stress vs. Displacement

To provide clarity and to compare the transverse shear strength performance of the two rebar sizes, stress vs. strain behavior of rebar is shown in this section via graphs. The following graphs in Figures 5.18, 5.20, and 5.21 show the comparison of the stress vs. cross-head behavior for the tested BFRP rebars. The x-axis of graph represents the cross-head extension, while the y-axis signifies the measured shear stresses. As expected, there is a significant difference in peak load between rebar sizes of type A rebar. Nevertheless, the resultant horizontal shear stress is approximately the same regardless of the rebar size. The stress vs. strain behavior of rebar type B shows that the failure pattern was identical for both the sizes but #5 rebars sustained more stress in comparison with #3 rebars.

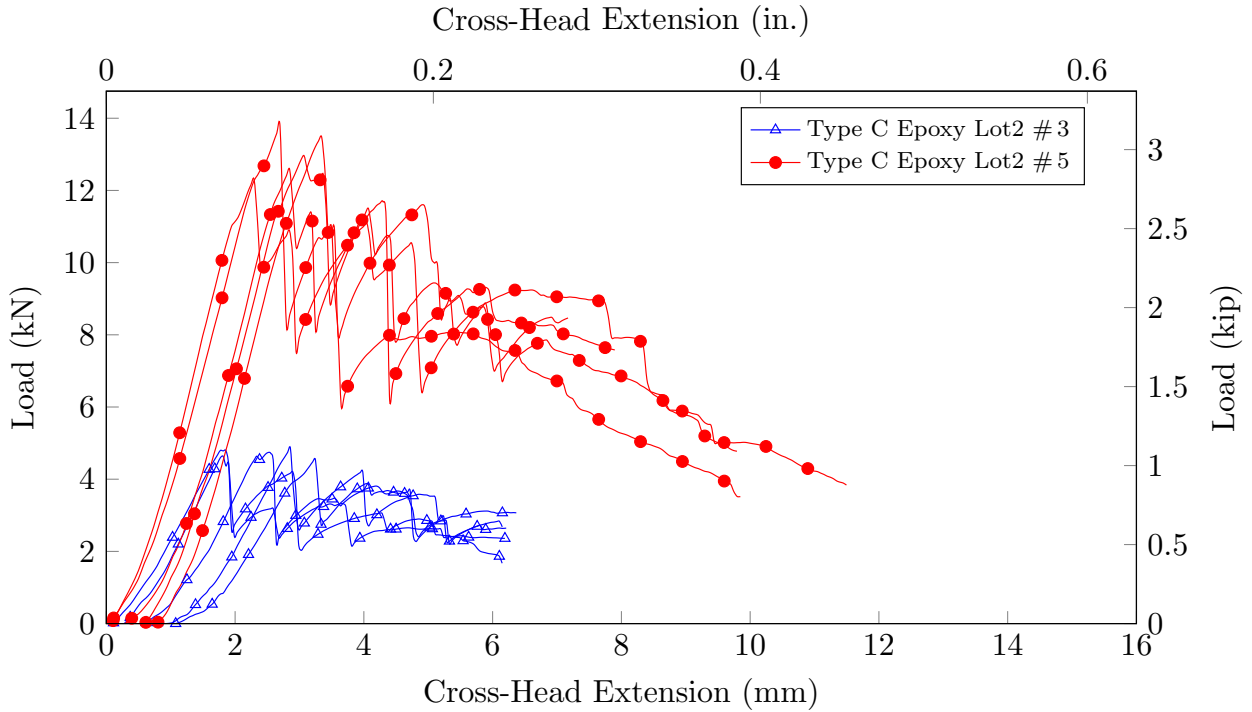


Figure 5.16: Extension vs. horizontal shear load behavior of type C Lot 1 size 3 and 5

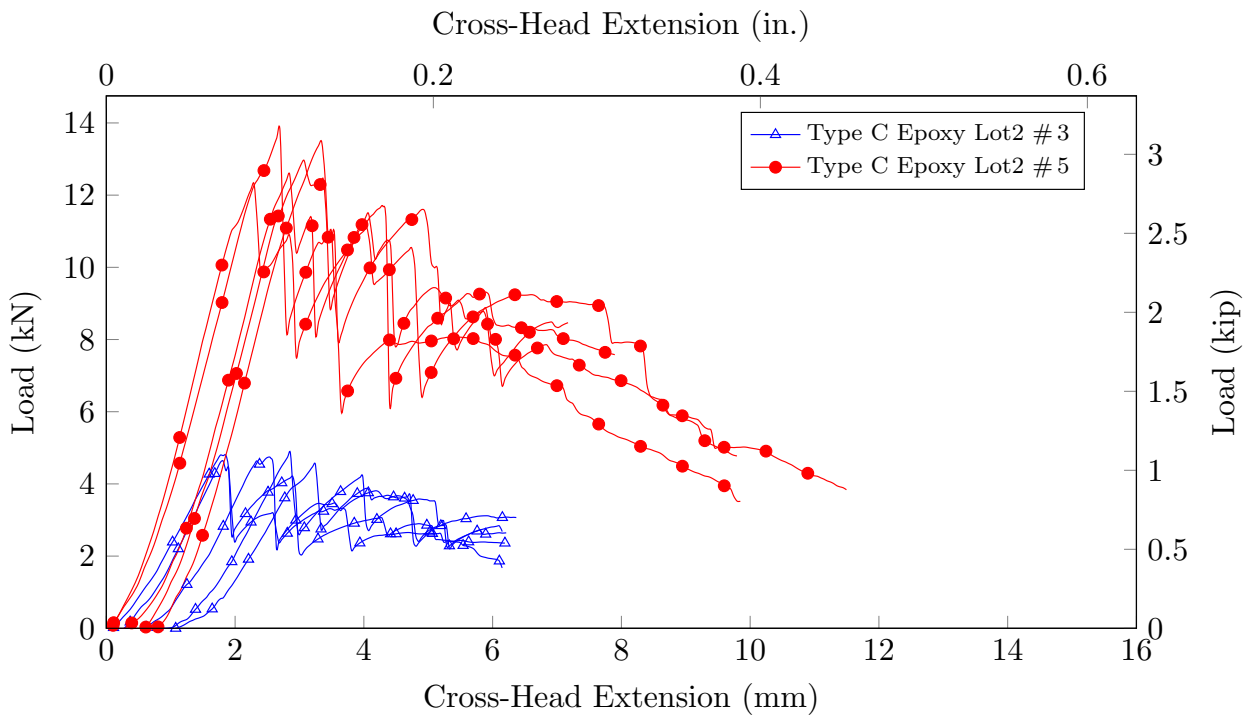


Figure 5.17: Extension vs. horizontal shear load behavior of type C Lot 2 size 3 and 5

The graphs in Figures 5.20 and 5.21 compare the stress vs. displacement behavior of horizontal shear test of # 3 and # 5 rebars from lot 1 and 2 of type C rebars. Figures 5.20 and 5.21 show

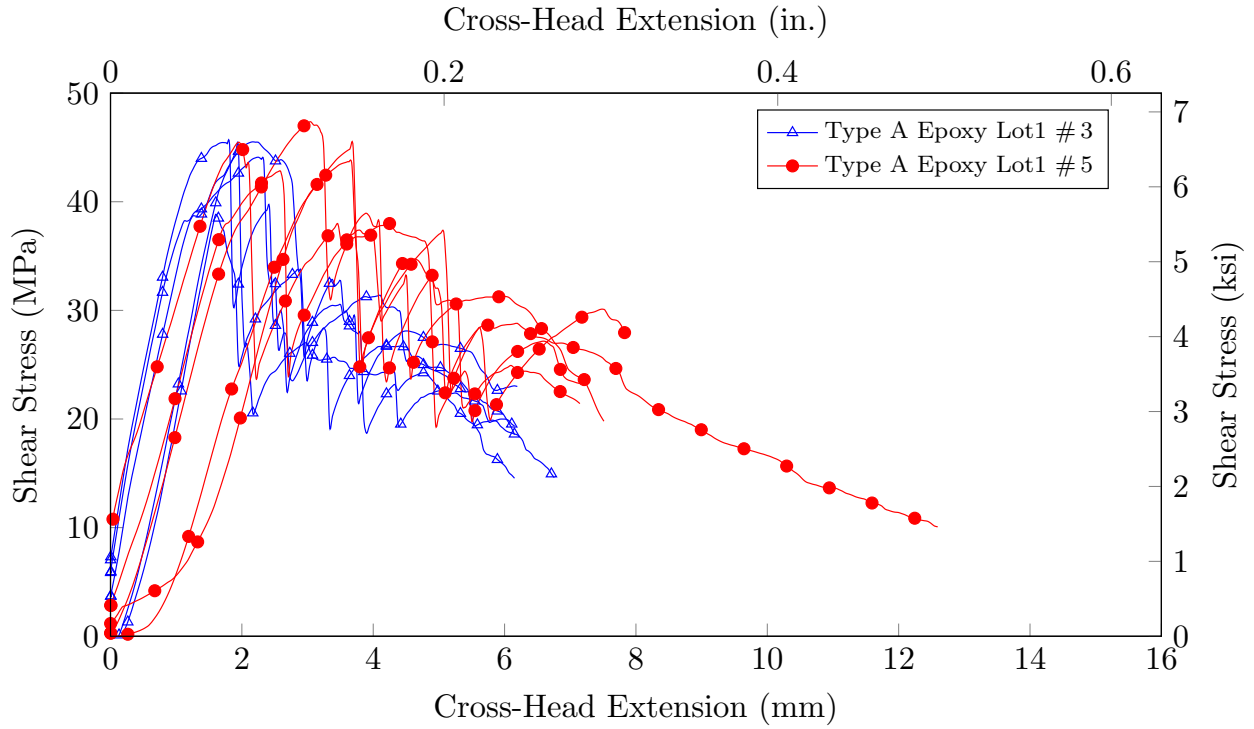


Figure 5.18: Horizontal shear stress vs. extension behavior of rebar type A Lot 1 size 3 and 5

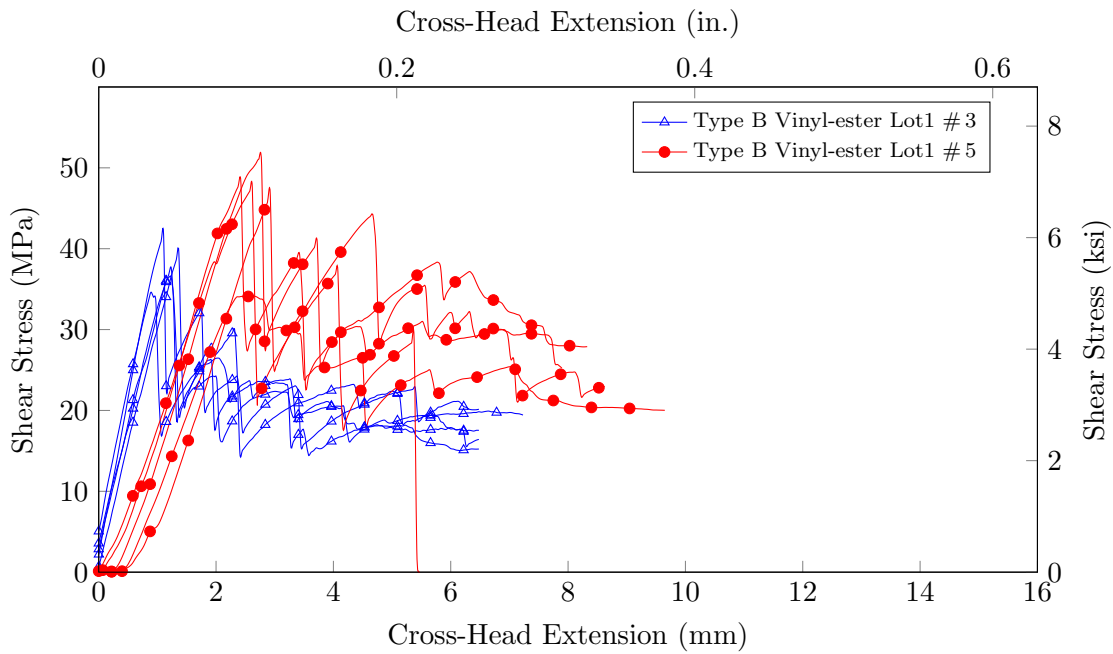


Figure 5.19: Horizontal shear stress vs. extension behavior of rebar type B Lot 1 size 3 and 5

that all the rebars of type C underwent similar stress and strain irrespective of lot and size.

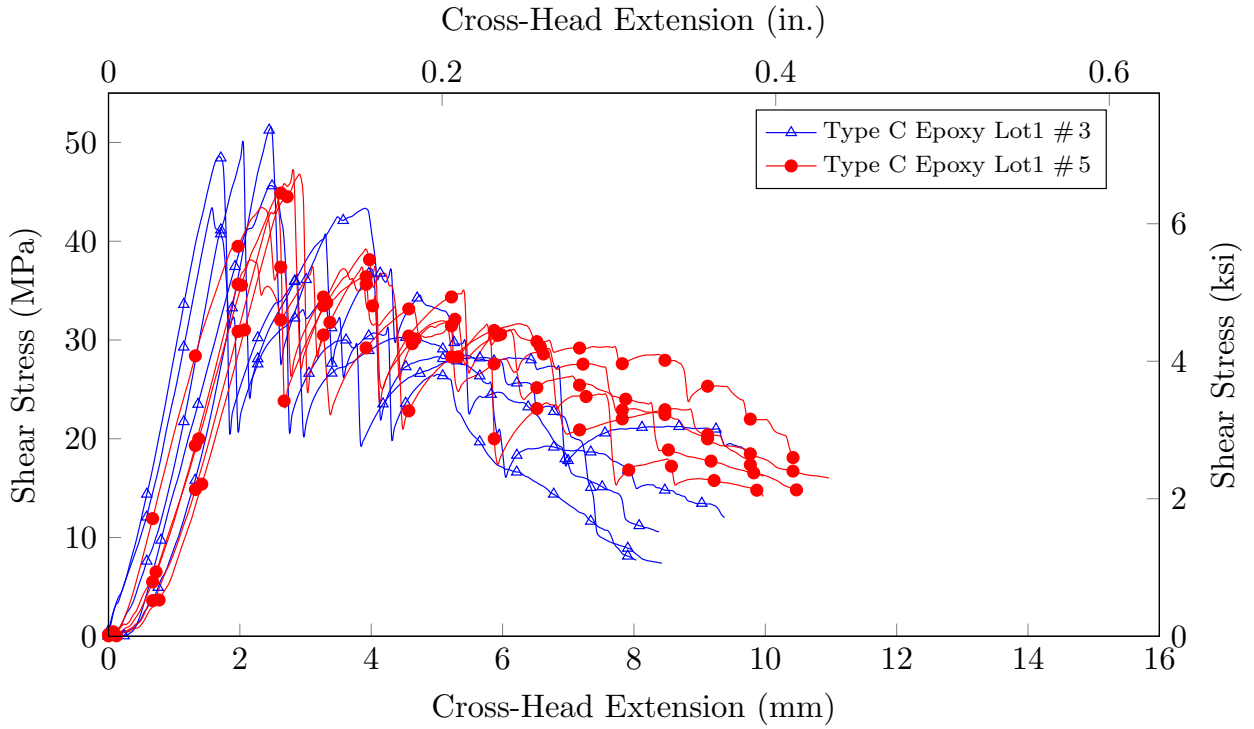


Figure 5.20: Horizontal shear stress vs. extension behavior of rebar type C Lot 1 size 3 and 5

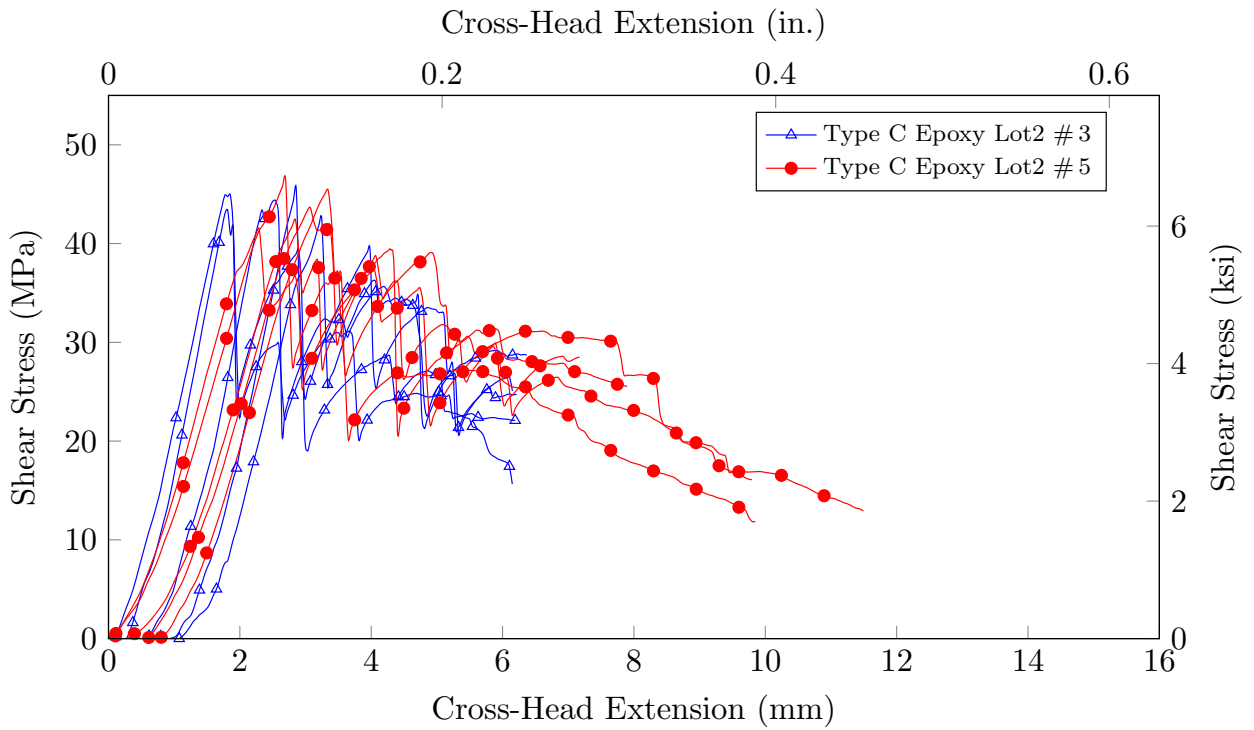


Figure 5.21: Horizontal shear stress vs. extension behavior of rebar type C Lot 2 size 3 and 5

### 5.9 Modes of Failure

To study the shear lag effect of BFRP rebars, failure modes of the tested rebars were analyzed. Figure 5.22 shows the failed BFRP specimen after completion of the horizontal shear test. All the



(a) Type A #3



(b) Type A #5



(c) Type B #3



(d) Type B #5



(e) Type C #3,



(f) Type C #5

Figure 5.22: Failure pattern for tested rebar after horizontal shear test

tested specimens failed due to the apparent horizontal shear force, resulting in horizontal failure planes as observed from the perpendicular cracks to the applied load, through the depth of the cross section. After the peak load, secondary cracks were generated representing the horizontal shear failure plane as each inter-laminar layer of fibers is engaged in tension and then failing in fiber-matrix interface.

### 5.10 Summary of Horizontal Shear Strength Properties

The statistical values for the horizontal shear strength properties of the tested products are listed in the following Table 5.3. A total of 30 specimens, five for each type and each size, were tested in total. The average of five specimens was assigned to each sample (specimen group) as shown in the table. All BFRP rebar samples satisfied the minimum acceptance criteria for the horizontal shear strength of glass FRP rebars according to FDOT Specifications 932, with the ultimate values shown in Tables 4.3 and 4.4.

Table 5.3: Horizontal Shear test statistical values for each sample group (US Customary Units)

Sample Group				Statistical Values				
Manuf. Type	Resin Type	Size #	Lot No.	Shear Stress				
				$\wedge$ ksi	$\vee$ ksi	$\mu$ ksi	$\sigma$ ksi	CV %
Rebar A	Epoxy	3	1	5.8	6.7	6.4	0.4	5.90
Rebar A	Epoxy	5	1	6.2	6.9	6.5	0.3	3.89
Rebar B	Vinyl-ester	3	1	5.1	6.1	5.6	0.4	6.80
Rebar B	Vinyl-ester	5	1	5.0	7.5	6.6	1.0	14.46
Rebar C	Epoxy	3	1	6.4	7.5	7.0	0.5	6.57
Rebar C	Epoxy	3	2	6.2	6.7	6.5	0.2	2.79
Rebar C	Epoxy	5	1	5.6	6.8	6.4	0.5	7.98
Rebar C	Epoxy	5	2	6.0	6.8	6.4	0.3	4.99

For numerical comparison and concluding values, Table 5.3 lists the minimum shear stress ( $\wedge$ ),

the maximum shear stress ( $\wedge$ ), the average shear stress ( $\mu$ ), the standard deviation ( $\sigma$ ), and the coefficient of variation (CV) for each individual test sample.

### 5.11 Tensile Test

The rebars were tested according to the ASTM D 7205 (ASTM-International, 2015a) to evaluate the tensile properties. The obtained and processed data of the tensile strength test are shown in this section via graphs and table.

#### 5.11.1 Load vs. Displacement Behavior

To compare the load vs. displacement behavior of the different rebar samples and specimens, the graphs in the Figure 5.23, 5.24, 5.29, and 5.30 plot the recorded test data. As shown, the x-axis of the graph represents the cross-head extension — which has to be interpreted with care because it includes the elastic deformation of the load frame and the test fixtures — and the y-axis indicates the applied and measured load. Figure 5.23 shows that # 5 rebar type A sustained higher failure

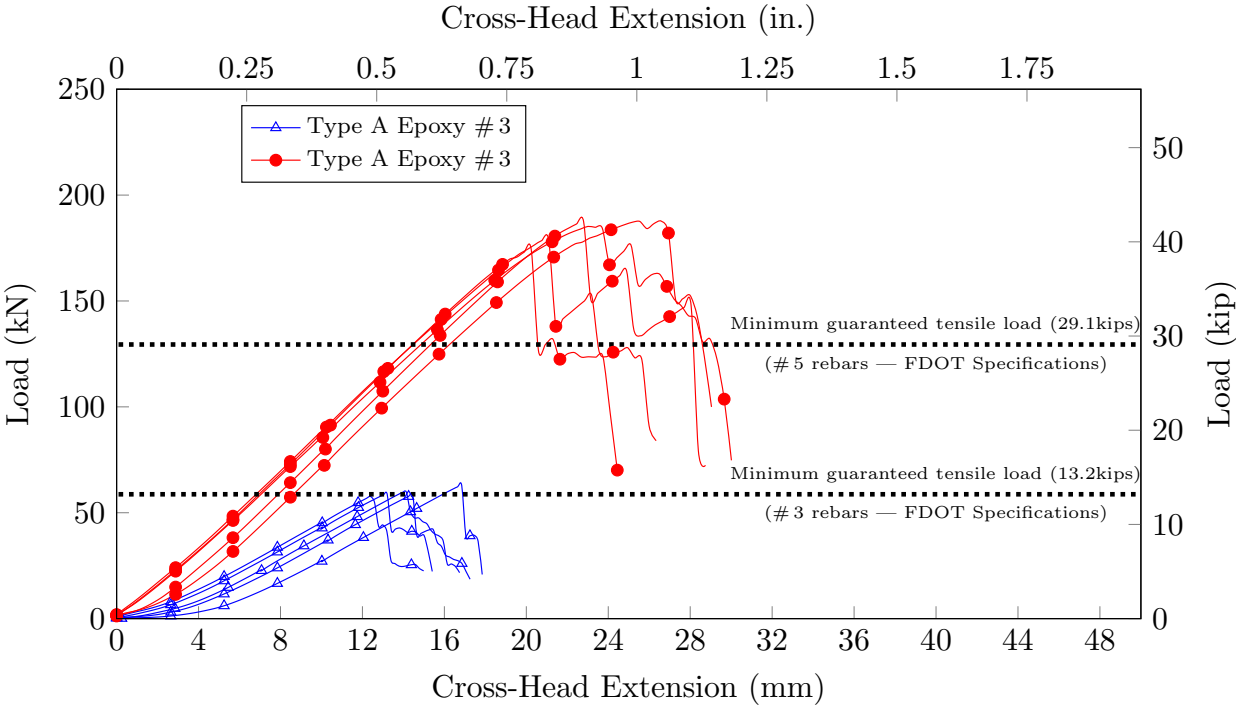


Figure 5.23: Tensile strength vs. displacement behavior of rebar type A Lot 1 size 3 and 5

load in comparison with # 3 rebars. And the extension of rebar # 5 was almost twice that of the # 3

rebars extension. Figure 5.24 shows that the extension of # 5 was more than twice in comparison

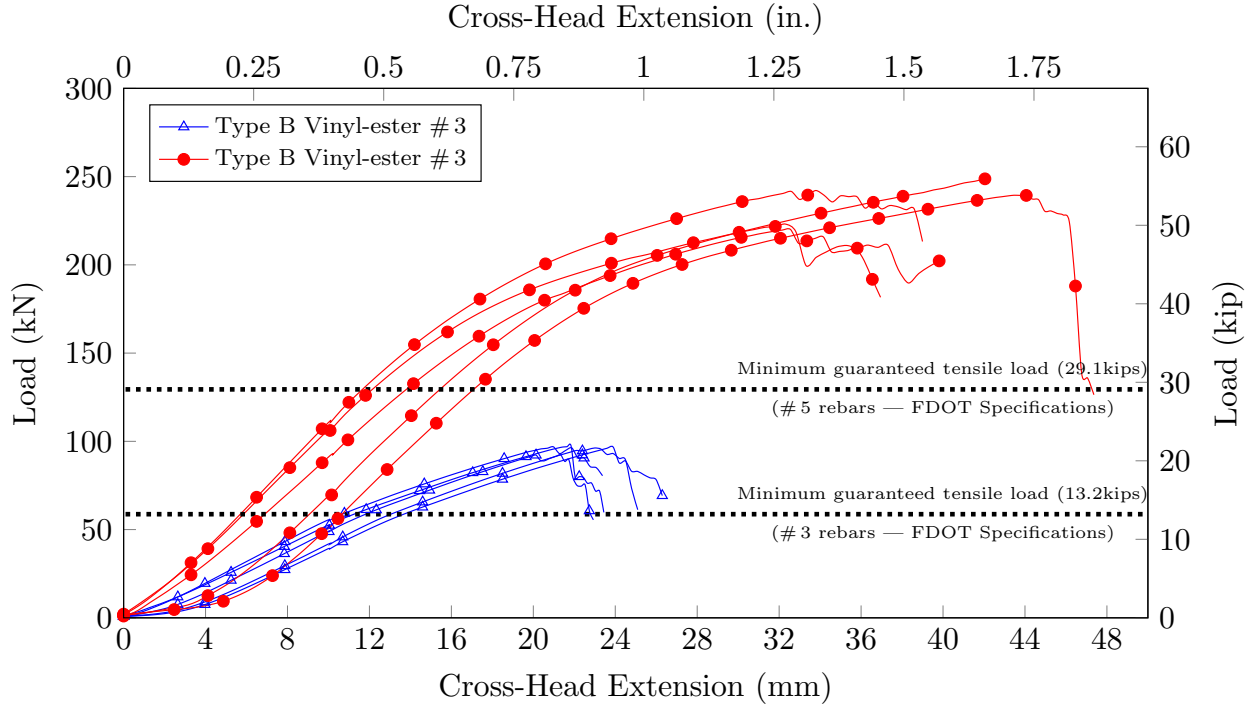


Figure 5.24: Tensile strength vs. displacement behavior of rebar type B Lot 1 size 3 and 5

with # 3 rebars and the peak load was much higher. All the rebars failed in similar fashion. After

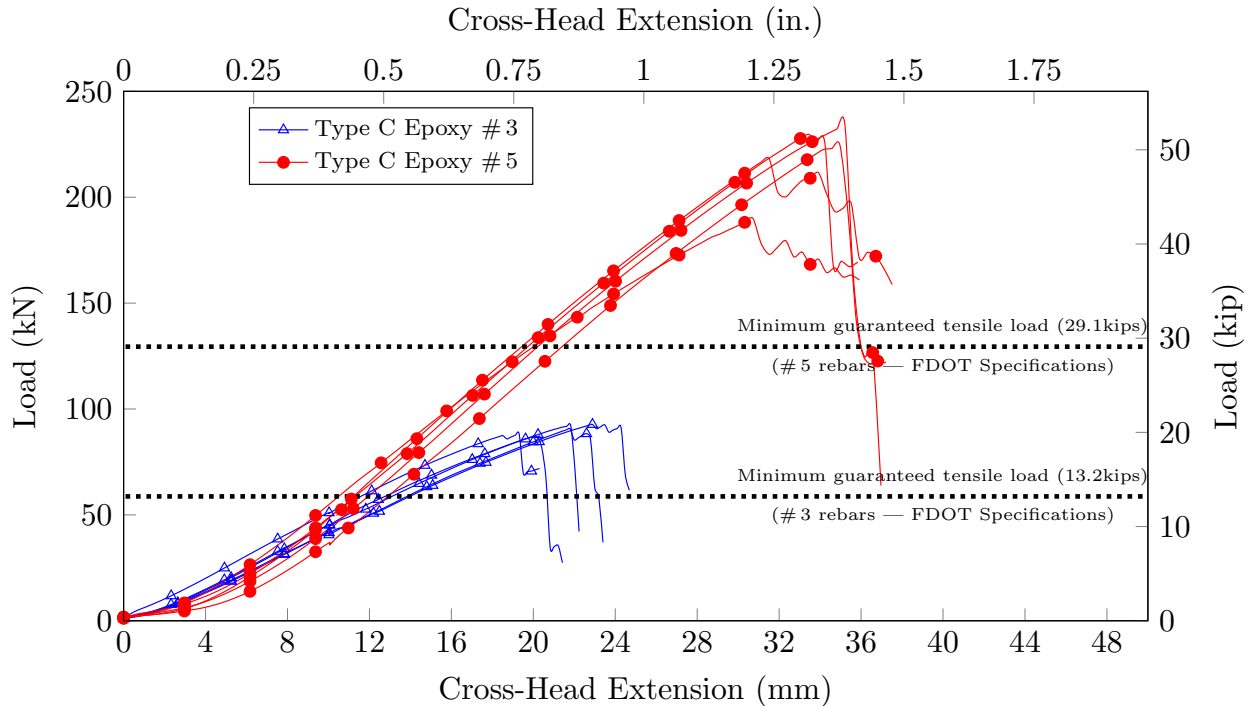


Figure 5.25: Tensile strength vs. displacement behavior of rebar type C Lot 1 size 3 and 5

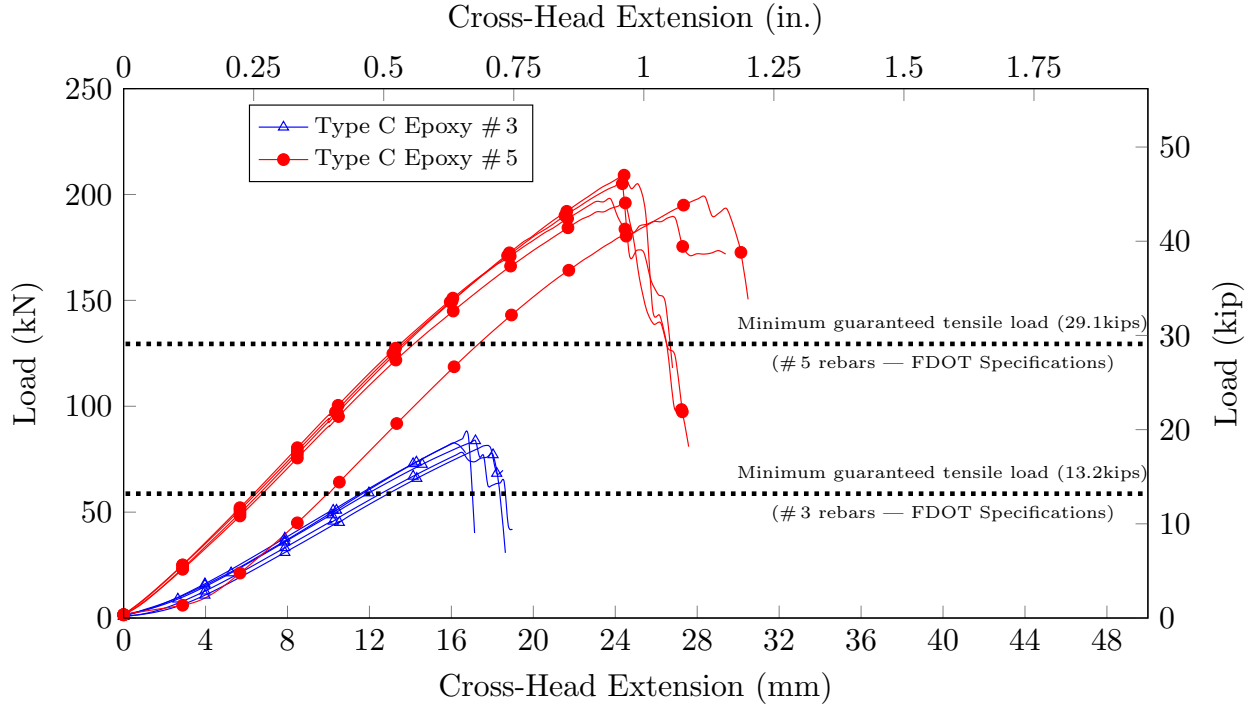


Figure 5.26: Tensile strength vs. displacement behavior of rebar type C Lot 2 size 3 and 5

comparing Figures 5.25 and 5.26, it can be seen that the rebars of the same size from both the lots of type C sustained the same peak load and failed in the same mode. Post failure extension of #5 rebars was almost twice in comparison with #3 rebars.

### 5.11.2 Stress vs. Strain Behavior

The stress-strain behavior of the failed rebars of all types was plotted to quantify and compare the elastic moduli of the tested BFRP rebars. The data in the Figures 5.27, 5.28, 5.29, and 5.30 were plotted to compare the stress vs. strain behavior of the different rebar types. Accordingly, the x-axis shows the applied stress while the y-axis represents the outermost surface strain that was measured with an external extensometer (c.f. Chapter 4, section 4.3). The post failure results plotted in the graph in Figure 5.27 show that although the load capacities of the different sized rebars vary in large scale, the slope of the stress-strain curve is identical for all the rebars.

It can be seen in Figure 5.28 that the post failure results, also known as stress-strain behavior of rebar type B are nonidentical for both the rebar sizes.

The post failure stress-strain behavior of rebar type C as shown in Figures 5.29 and 5.30 show that the slopes of #3 bars from different lots are identical but slopes of #5 bars are not identical.

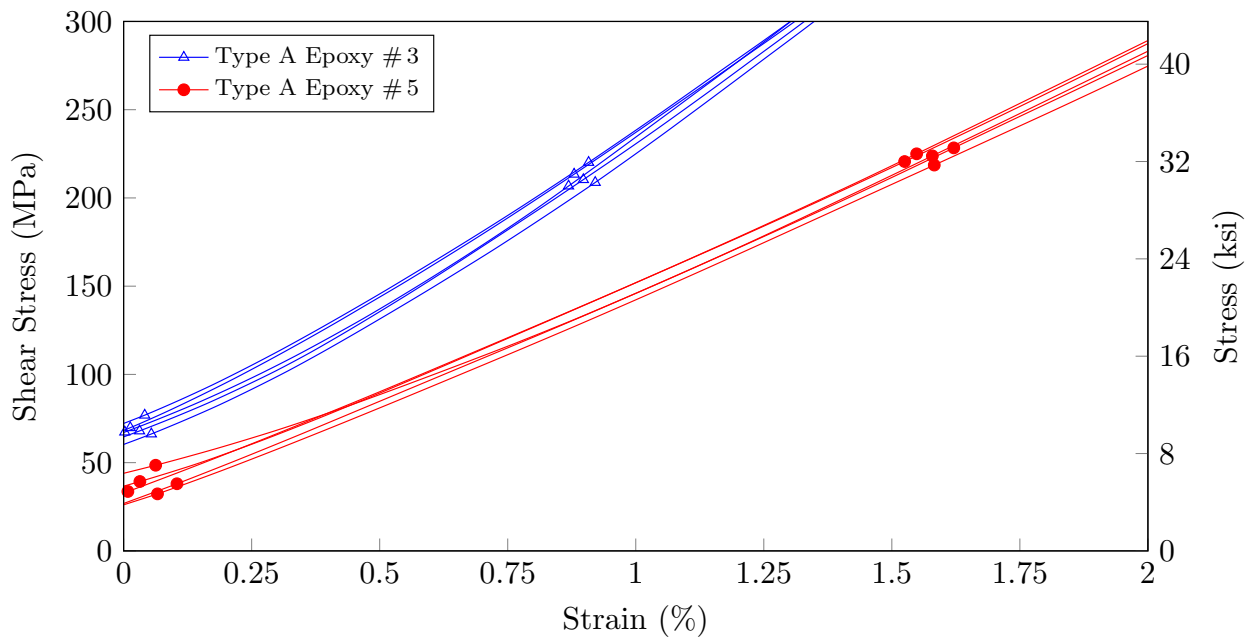


Figure 5.27: Tensile stress vs. strain behavior of rebar type A Lot 1 rebar size 3 and 5

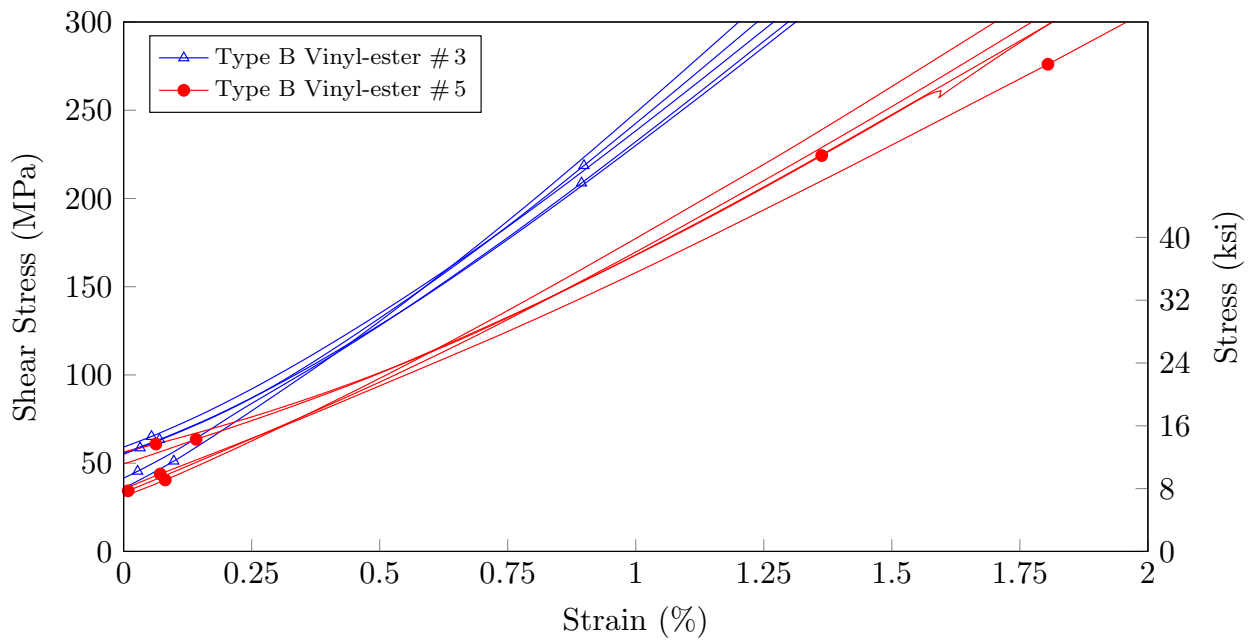


Figure 5.28: Tensile stress vs. strain behavior of rebar type B Lot 1 rebar size 3 and 5

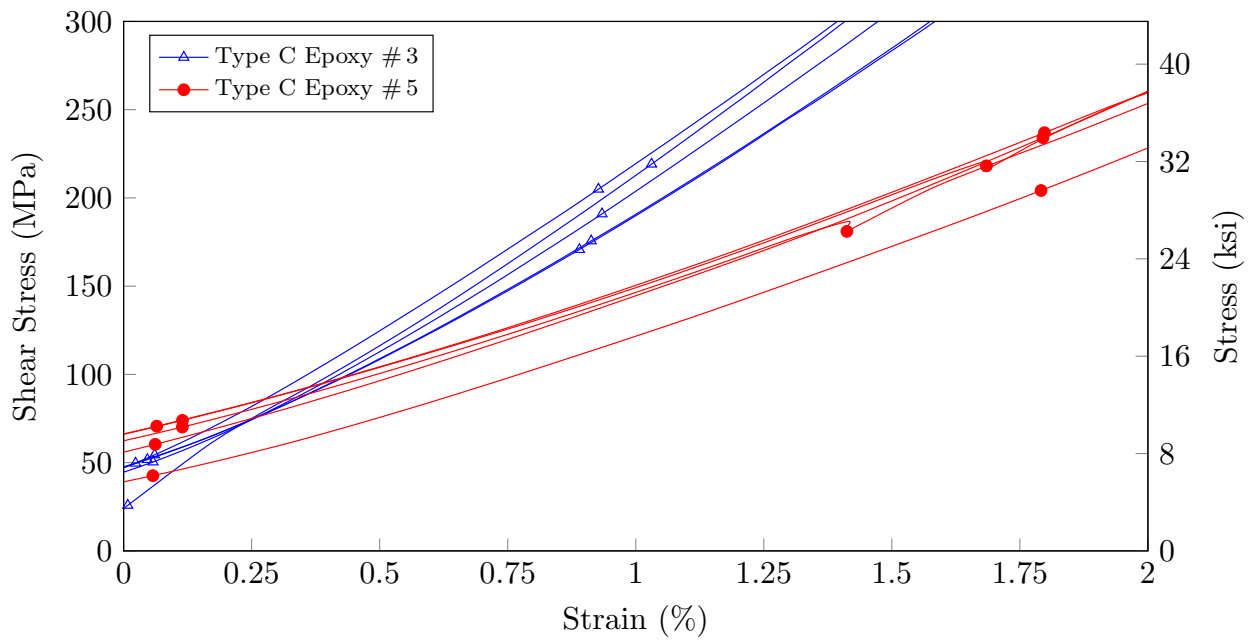


Figure 5.29: Tensile stress vs. strain behavior of rebar type C Lot 1 rebar size 3 and 5

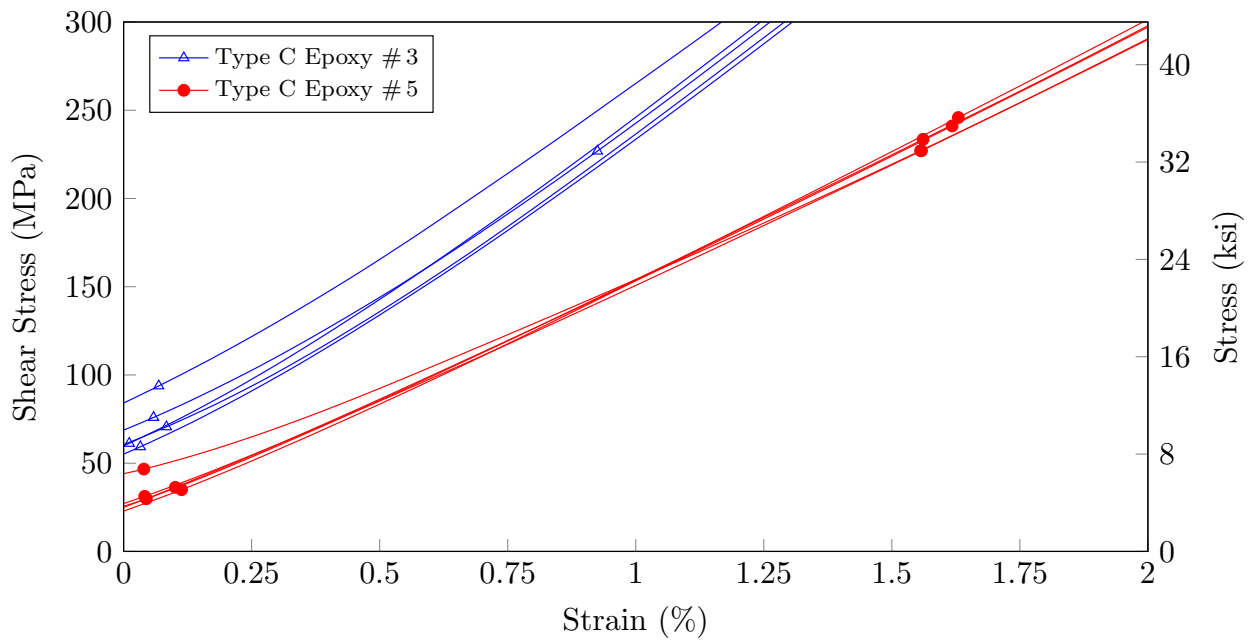


Figure 5.30: Tensile stress vs. strain behavior of rebar type C Lot 2 rebar size 3 and 5

## 5.12 Modes of Failure

According to ASTM D 7205, three different failure modes may occur during a tensile strength test. The first and expected one is the tensile rupture outside of the anchor pipes. Due to insufficient sample preparation or test procedure issues, two more failure modes may occur. The rebar could slip within the grouted anchor (rebar slippage) or the anchor could slip out of the fixture/grips (anchor slippage). Therefore, the last two described failure modes lead to unusable results when defining the material characteristics. However, for this research project, no specimen failed due to rebar or anchor slippage. Hence, tensile rupture of the BFRP rebar was the recorded failure mode for each bar that was tested.

Figure 5.31a and 5.32a show the failed specimens of type A rebars. It can be seen that all specimens, regardless of their diameter, displayed similar failure pattern. The fibers formed a brush type of failure and all specimens suffered fiber delamination throughout the entire free specimen length. Figure 5.31b and 5.32b present the post failure pattern of type B rebar specimens. It is shown that all the rebar sizes had an identical failure. The fibers were delaminated and a distinct brush-like failure was observed. Similarly, Figure 5.31c and 5.32c # 5 rebars exemplify the failure mode of type C rebars. All the specimens from two lots failed in a similar manner. After the peak load was reached, a bundle of outer fibers failed and brushed out over the entire free specimen length. After the first load drop, this behavior continued at each additional sudden load drop until delamination reached the center of the rebar, and the specimen eventually separated into two parts along the rebar axis.



(a) Type A



(b) Type B



(c) Type C

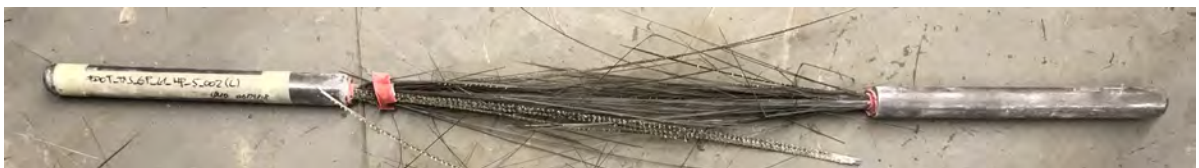
Figure 5.31: # 3 rebar final failure pattern after tensile test



(a) Type A



(b) Type B



(c) Type C

Figure 5.32: # 5 rebar final failure pattern after tensile test

### 5.13 Summary of Tensile Properties

The results of the statistical evaluation for the measured tensile properties of all products along with the elastic modulus property are listed in the following Table 5.4. A total of 40 specimen, 5 per rebar size and type, were tested and analyzed to determine the results shown in the table. For numerical comparison and concluding values, Table 5.4 lists the minimum tensile stress ( $\wedge$ ), the maximum tensile stress ( $\wedge$ ), the average tensile stress ( $\mu$ ), the standard deviation ( $\sigma$ ), and the coefficient of variation (CV) for each individual test sample.

Table 5.4: Tensile strength test statistical values for each sample group (US Customary Units)

Sample group				Statistical values									
Manf. Type	Resin Type	Size #	Lot No.	Tensile Strength					Elastic Modulus				
				$\wedge$ ksi	$\vee$ ksi	$\mu$ ksi	$\sigma$ ksi	CV %	$\wedge$ ksi	$\vee$ ksi	$\mu$ ksi	$\sigma$ ksi	CV %
Rebar A	Epoxy	3	1	118.8	128.1	121.7	3.8	3.14	6742	7735	7238	3145	57.37
Rebar A	Epoxy	5	1	127.8	137.9	134.2	4.3	3.23	7639	7990	7753	147	1.90
Rebar B	Vinyl-ester	3	1	188.8	198.8	196.3	4.2	2.15	7542	7999	7808	179	2.29
Rebar B	Vinyl-ester	5	1	161.9	183.2	172.5	9.2	5.32	7810	8301	7946	201	2.53
Rebar C	Epoxy	3	1	178.2	189.3	183.9	4.8	2.61	5385	7659	7154	990	13.84
Rebar C	Epoxy	5	1	139.6	171.8	161.2	12.9	7.97	7346	7933	7640	3312	62.88
Rebar C	Epoxy	3	2	161.3	175.0	169.2	5.0	2.97	6531	7881	7200	516	7.16
Rebar C	Epoxy	5	2	143.9	153.4	147.7	4.0	2.73	7065	8138	7479	410	5.48

## 5.14 Bond-to-Concrete Strength

The bond stress  $\tau_{max}$  (MPa or lbs./in.<sup>2</sup>) for a circular bar diameter  $d$  (mm or in.) is given by Equation 5.1, in which  $F$  represents the recorded pullout load (N or lbs.) and  $L$  is the accurately measured bond length (mm or in.).

$$\tau_{max} = \frac{F}{d\pi L} \quad [inMPa \text{ or } psi] \quad (5.1)$$

This formula was used to determine the bond behavior development and is the basis for the following graphs; Figures 5.39, 5.40, 5.33, 5.34, 5.36, and 5.37 depict the measured bond stresses along the rebar surfaces relative to the rebar slip at the free end. For clarity, the post failure measurements (at the onset of a 50% load drop) were removed from these graphs. All tested specimens failed at the rebar-concrete interface in bond slip, without splitting the concrete open or without tensile failure. The bond capacity and the failure behavior of the BFRP rebar-concrete interface were affected by the surface enhancement features.

## 5.15 Bond Stress vs. Slip at Free End

The graphs in this section compare the bond stress vs. slip at free end of rebar. Graphs in Figure 5.41, 5.35, and 5.38 portray bond stresses vs slip at free end of the rebars of both the sizes.

The x-axis of the graph signifies the measured bond stress, while the y-axis represents the slip of rebar at the free end.

Generally, from the graphs in Figures 5.33 to 5.41, it can be seen that each rebar type resulted in a consistent but distinct failure mode with ultimate stresses that were characteristic for each rebar type. All of the sand-coated rebars (Type-A and B) showed a soft failure while the rebars with a deformed surface (Type-C) failed suddenly with abrupt pullout.

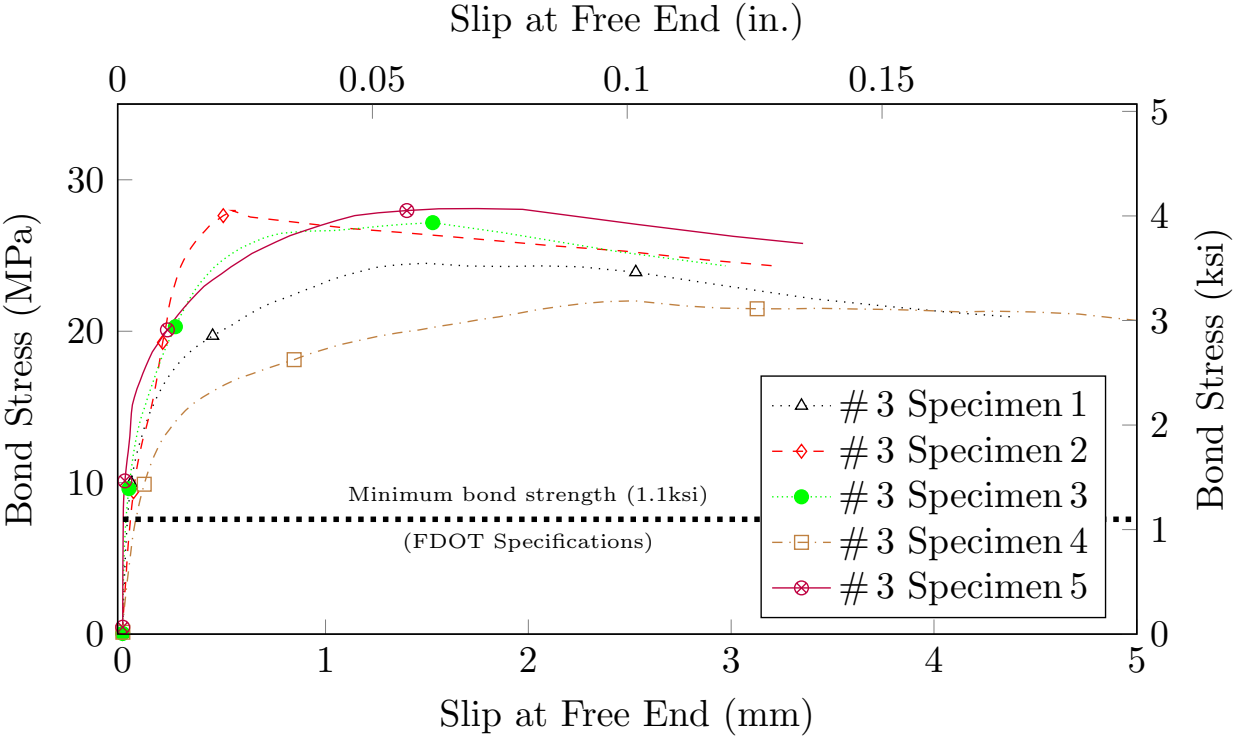


Figure 5.33: Free end slip behavior of the tested rebar type A Lot 1 #3

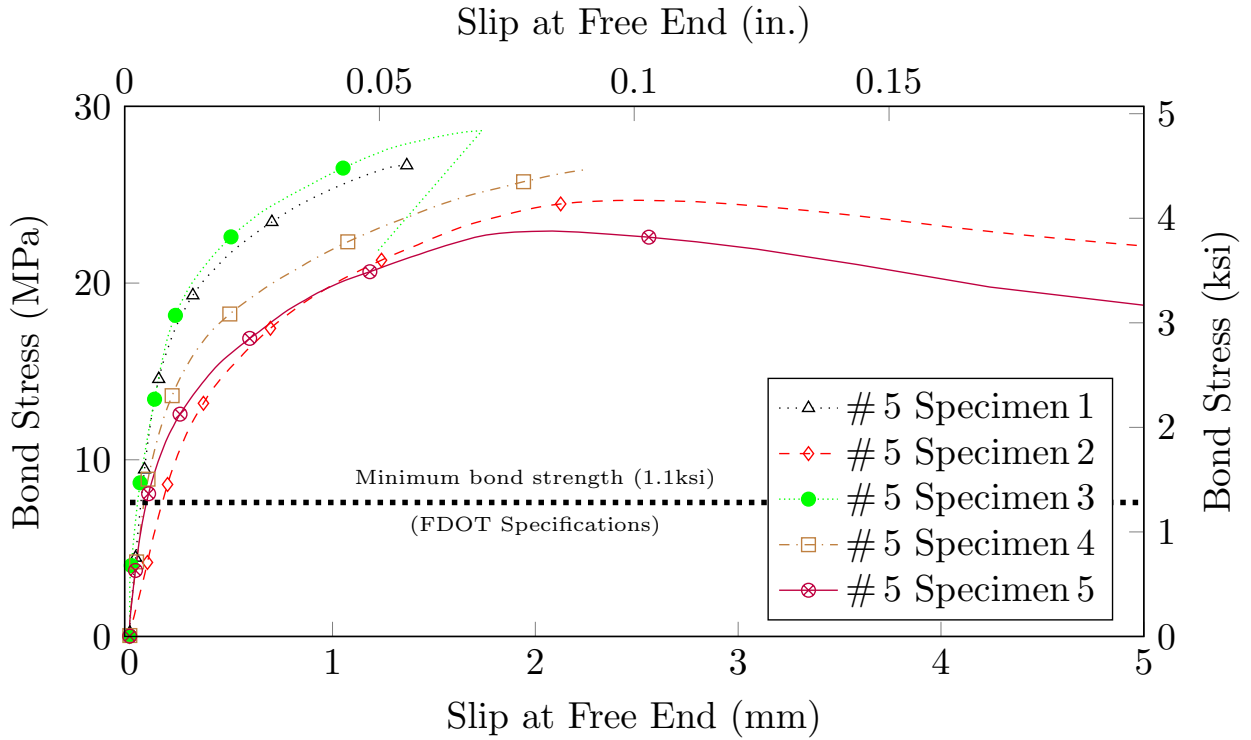


Figure 5.34: Free end slip behavior of the tested rebar type A Lot 1 # 5

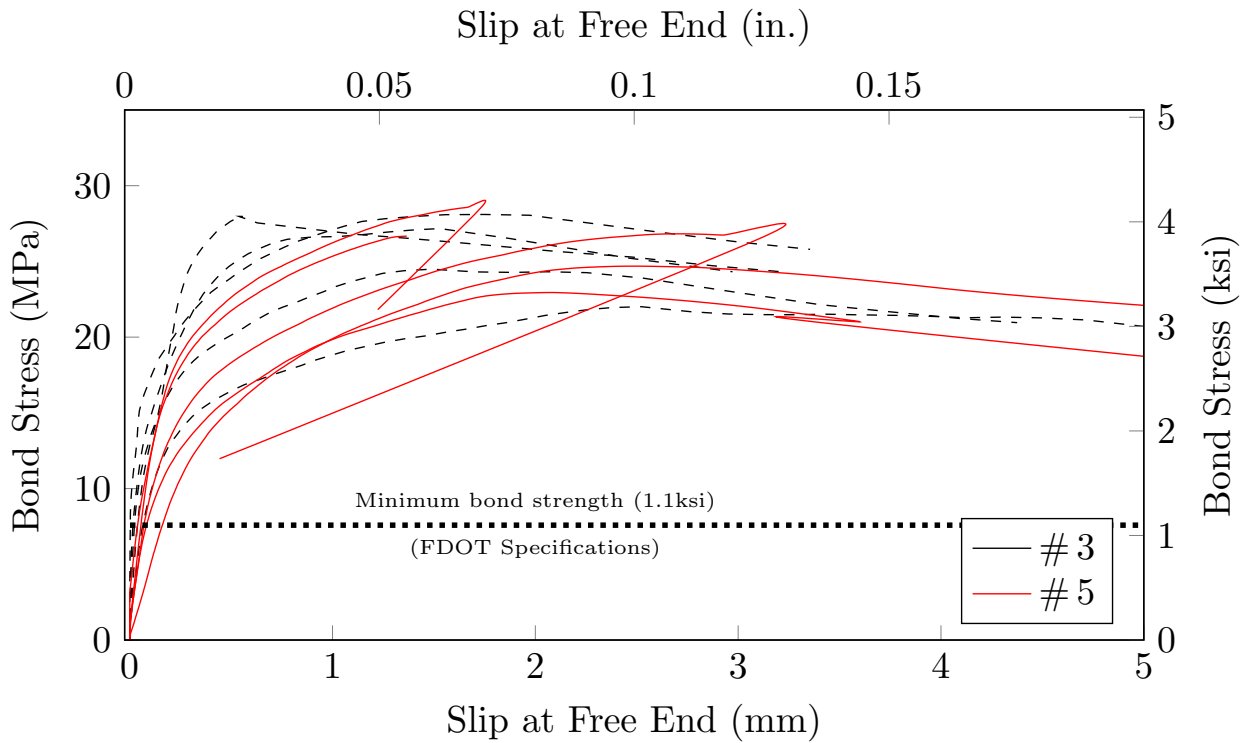


Figure 5.35: Free end slip behavior of the tested rebar type A Lot 1 # 3 and # 5

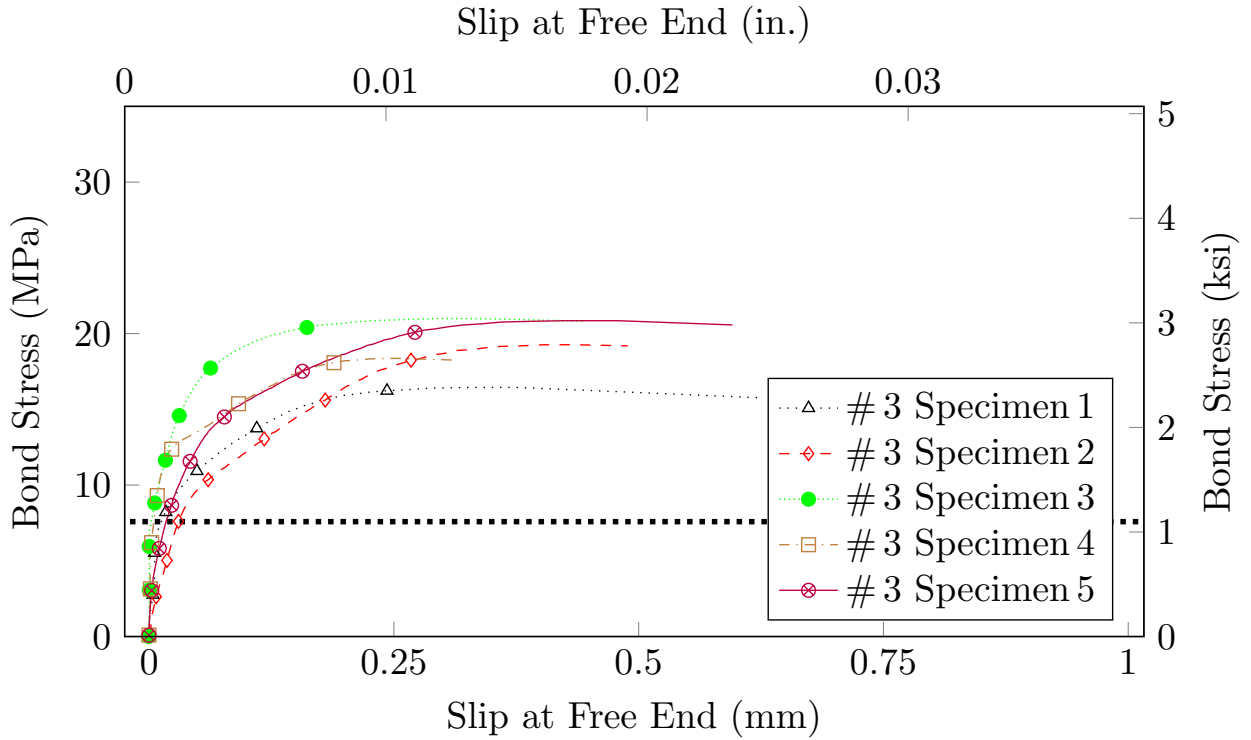


Figure 5.36: Free end slip behavior of the tested rebars type B Lot 1 # 3

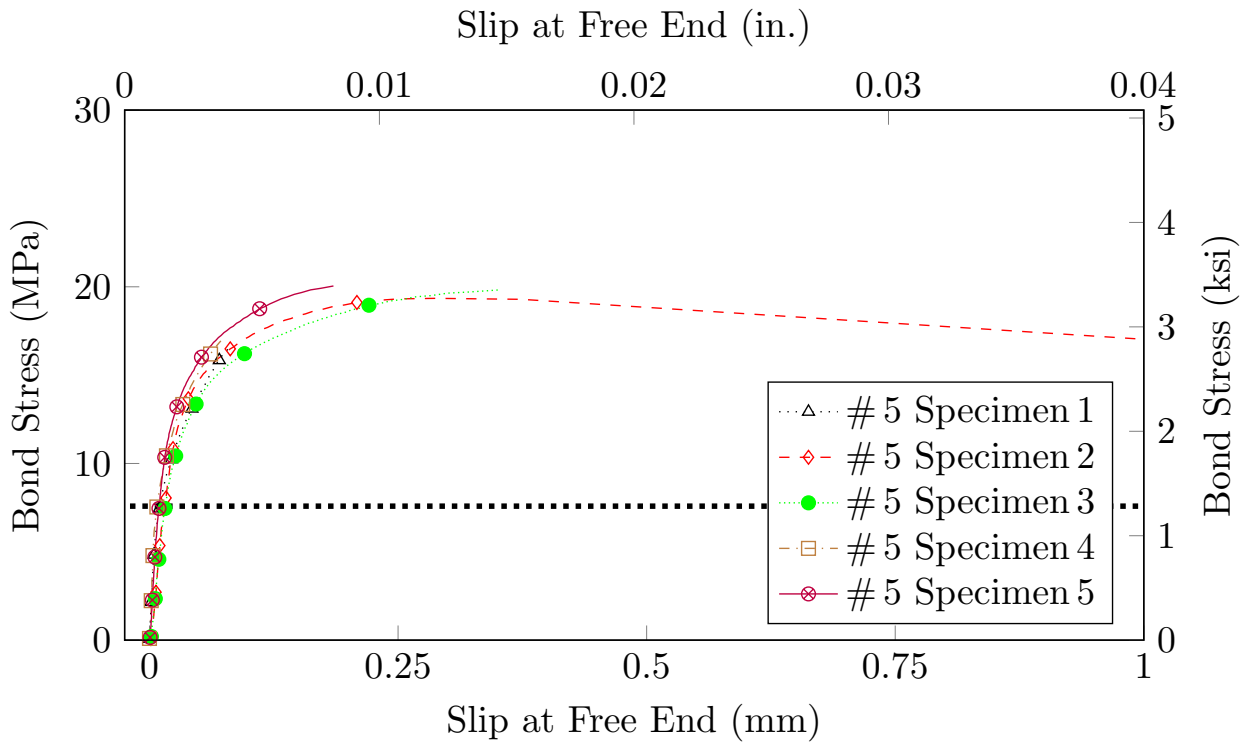


Figure 5.37: Free end slip behavior of the tested rebars type B Lot 1 # 5

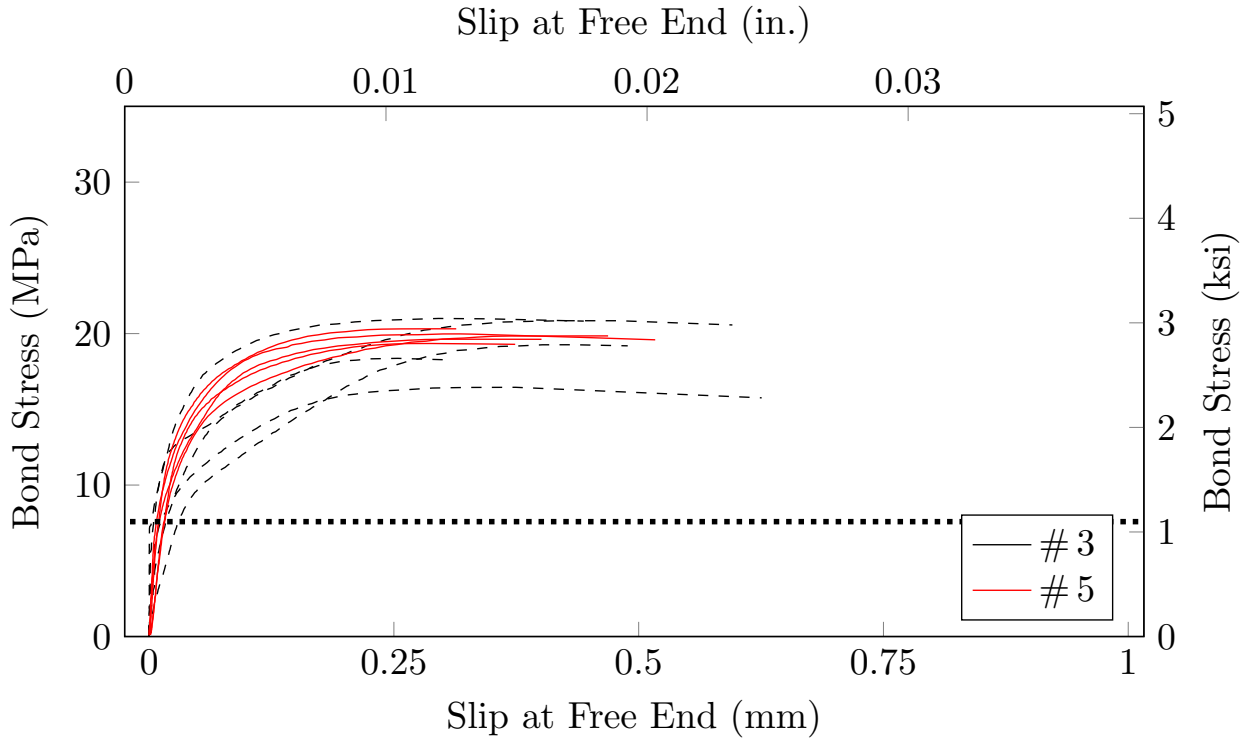


Figure 5.38: Free end slip behavior of the tested rebars type B Lot 1 #3 and #5

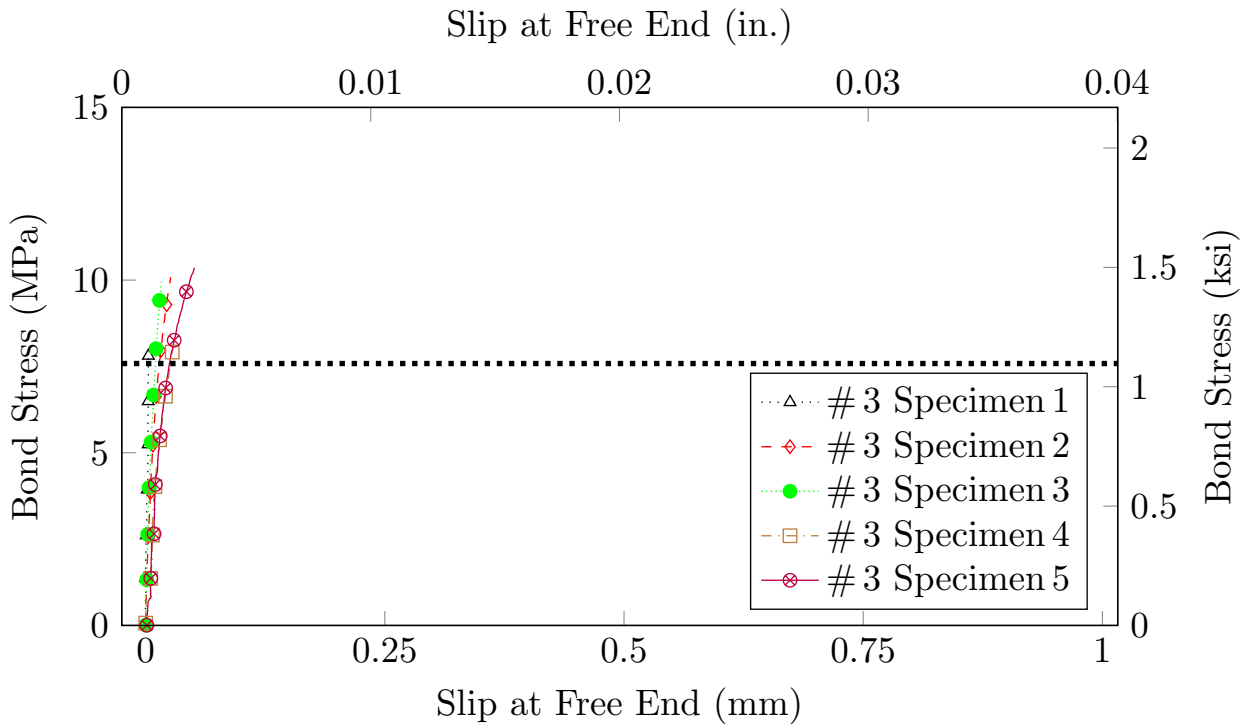


Figure 5.39: Free end slip behavior of the tested rebar type C Lot 1 #3

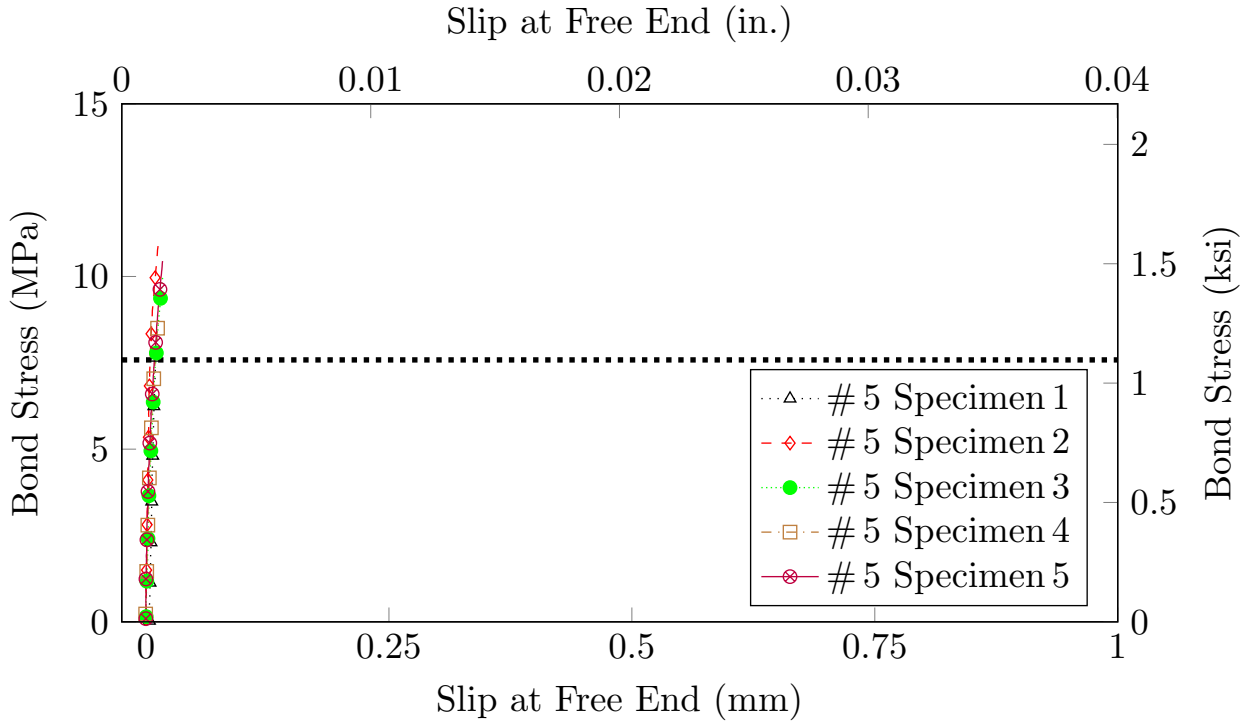


Figure 5.40: Free end slip behavior of the tested rebar type C Lot 1 # 5

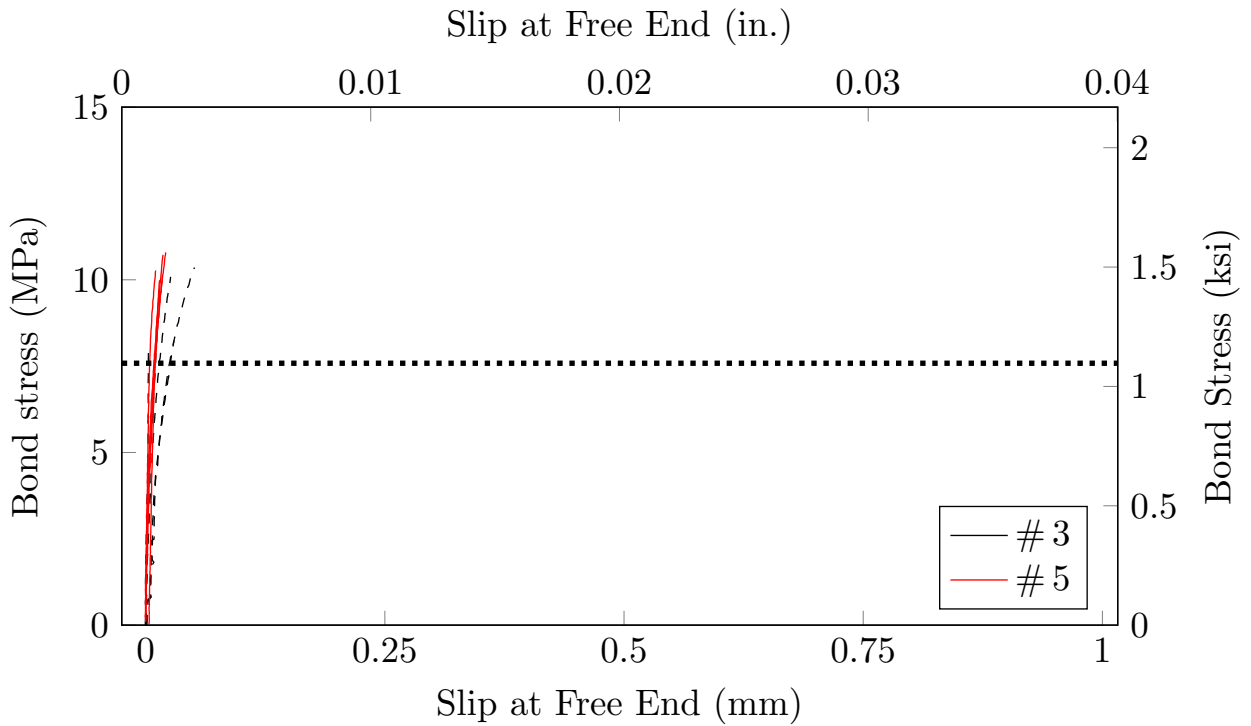


Figure 5.41: Free end slip behavior of the tested rebar type C Lot 1 # 3 and # 5

### 5.16 Modes of Failure

After the pullout tests were completed, the concrete blocks were split in half to further evaluate the failure mode by analyzing the surface of the rebar and the concrete. Figures 5.42, 5.43, 5.44, 5.45, 5.46, and 5.47 depict the different failure modes as they were observed after pullout testing. It

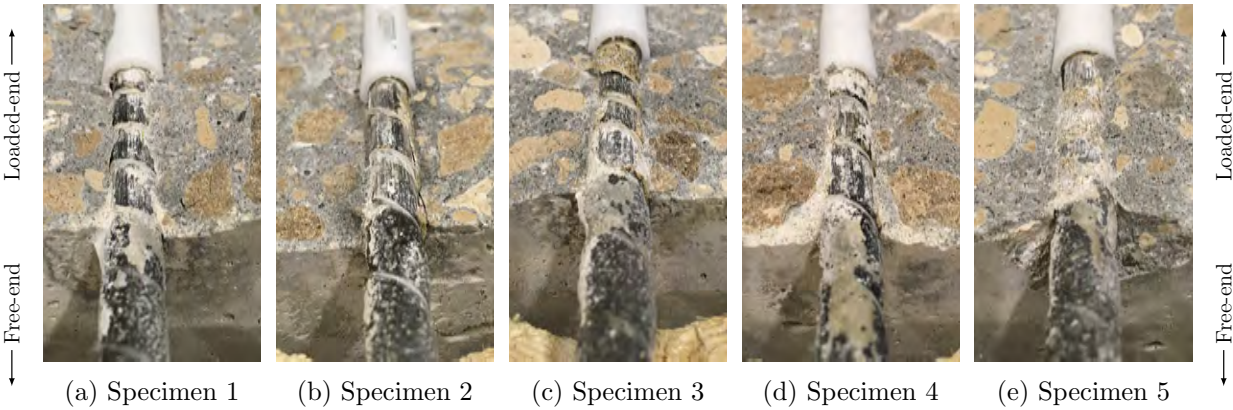


Figure 5.42: Overview rebar surface after bond strength test on type A Lot 1 rebar # 3

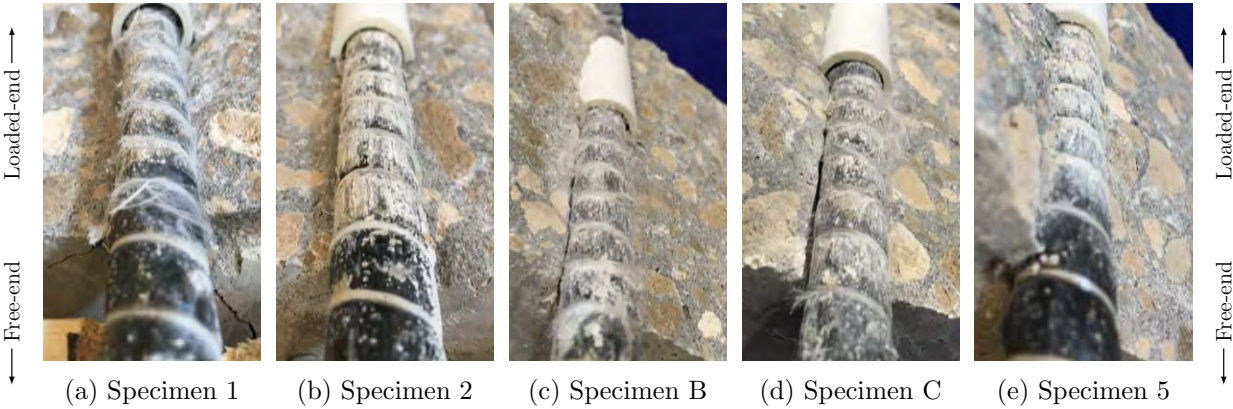


Figure 5.43: Overview rebar surface after bond strength test on type A Lot 1 rebar # 5

was noted that the rebar surface of all manufacturers was significantly damaged at the loaded end. For rebar type A only the sand layer was pulled off from the concrete and the surface deformed slightly, but the helical wraps remained in place. For rebar type B the layer between rebar and sand coat, which was made of fiber mesh, was entirely peeled off from the rest of the rebar. For rebar type C, de-bonding of the entire sand coat was observed (sand delamination). Close to the unloaded end, the surface layer of the rebar did not peel off, and most parts of the sand-coated layer remained well-adhered to the bar.

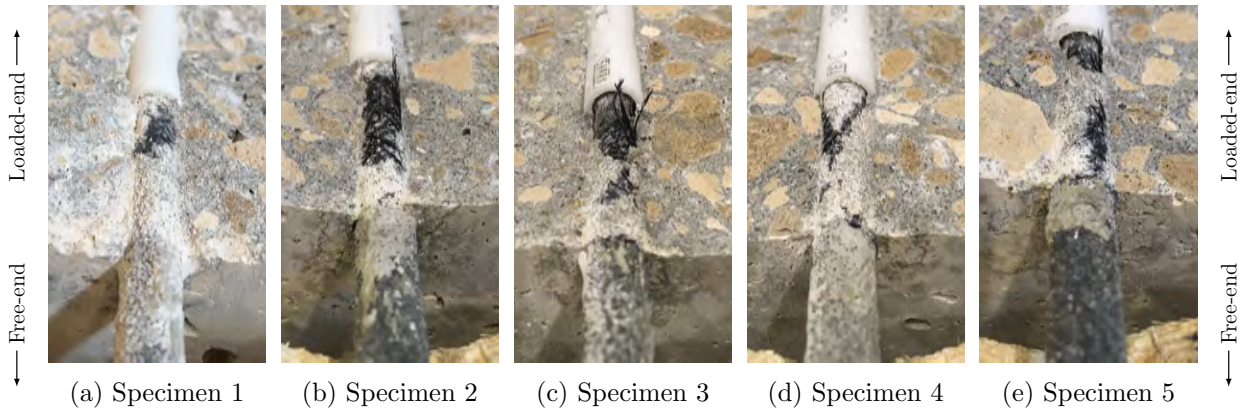


Figure 5.44: Overview rebar surface after bond strength test on type B Lot 1 rebar # 3

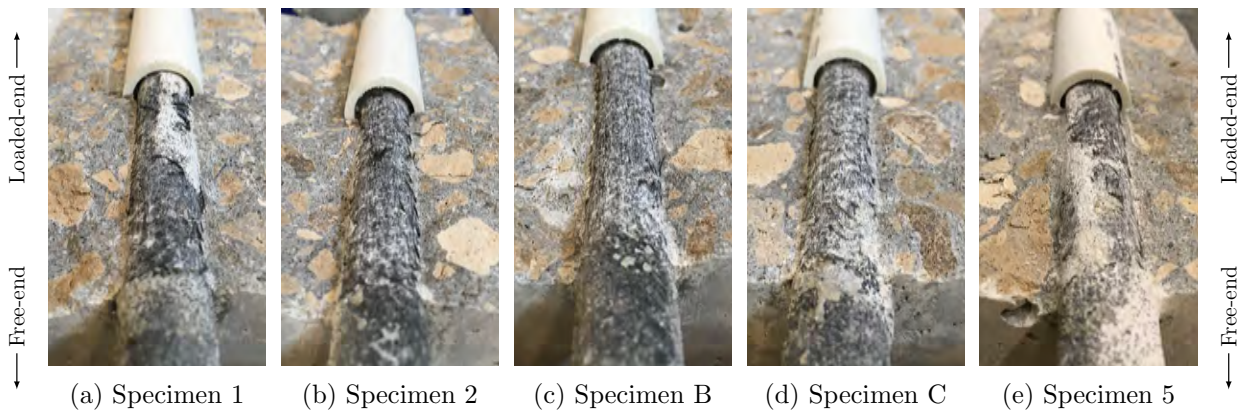


Figure 5.45: Overview rebar surface after bond strength test on type B Lot 1 rebar # 5

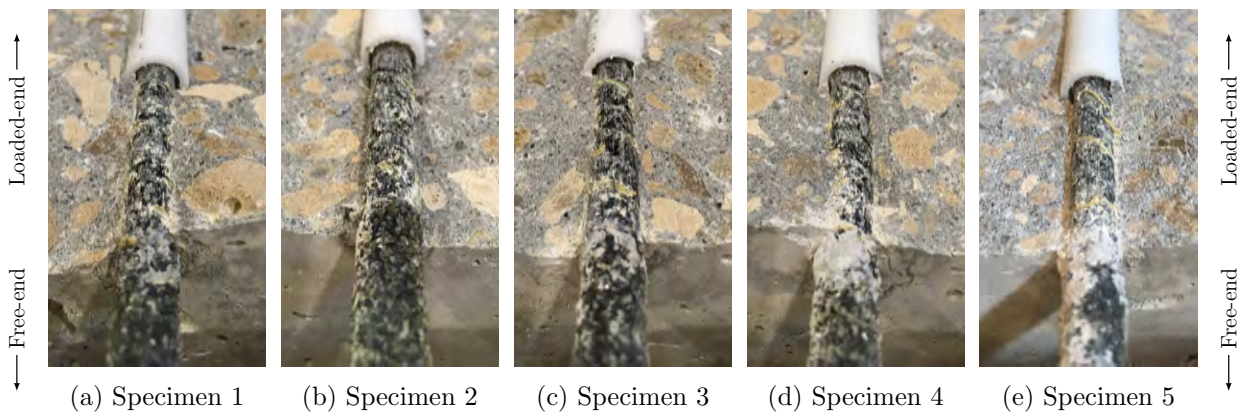


Figure 5.46: Overview rebar surface after bond strength test on type C Lot 1 rebar # 3

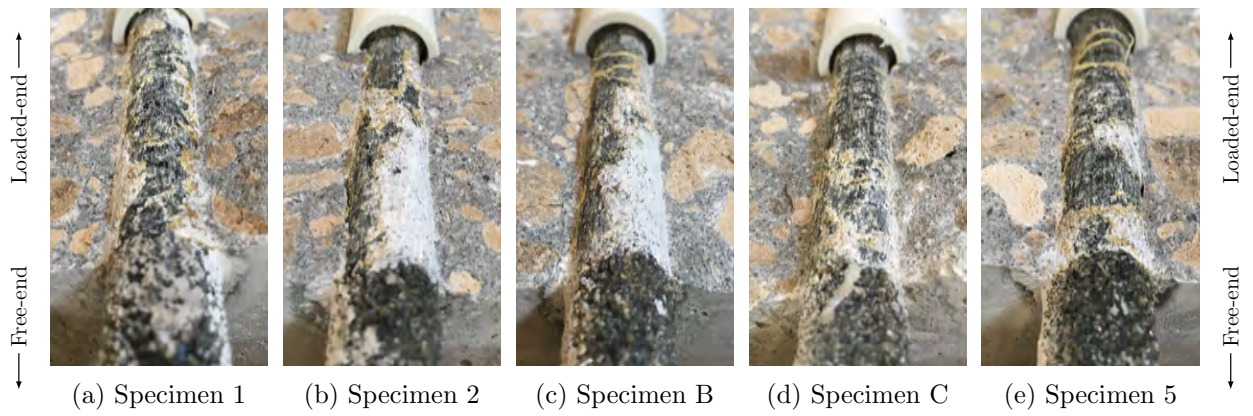


Figure 5.47: Overview rebar surface after bond strength test on type C Lot 1 rebar # 5

## 5.17 Summary of Bond-to-Concrete Strength

The statistical values for the bond strength properties of the tested products are listed in the following Table 5.5. A total of 30 specimens, five for each type and each size, were tested in total. The average of five specimens was assigned to each sample (specimen group) as shown in the table. All BFRP rebar samples satisfied the minimum acceptance criteria for the bond strength of glass FRP rebars according to FDOT Specifications 932, with the ultimate values shown in Tables 4.3, and 4.4. For numerical comparison and concluding values, Table 5.5 lists the minimum bond stress ( $\wedge$ ), the maximum bond stress ( $\vee$ ), the average bond stress ( $\mu$ ), the standard deviation ( $\sigma$ ), and the coefficient of variation (CV) for each individual test sample.

Table 5.5: Bond-to-concrete strength test statistical values for each sample

Sample Group				Statistical Values				
Manuf. Type	Resin Type	Size #	Lot No.	$\wedge$ ksi	$\vee$ ksi	$\mu$ ksi	$\sigma$ ksi	CV %
Type A	Epoxy	3	1	3.20	4.08	3.77	0.38	0.10
Type A	Epoxy	5	1	3.33	4.16	3.77	0.32	0.08
Type B	Vinyl-ester	3	1	2.39	3.05	2.79	0.27	0.10
Type B	Vinyl-ester	5	1	2.81	2.95	2.88	0.05	0.02
Type C	Epoxy	3	1	2.24	2.43	2.33	0.08	0.03
Type C	Epoxy	5	1	2.89	3.01	2.96	0.04	0.02

## 5.18 BFRP Rebar Performance

This section summarizes the material performance of the evaluated BFRP rebar samples based on the available acceptance criteria for glass FRP rebars, as shown in Tables 4.3, and 4.4, based on three different specifications. Tables 5.6 and 5.7 summarizes and compares the results for the type A rebar met or exceeded the acceptance criteria. The acceptance criteria for fiber content properties of #3 and #5 rebar samples of type B are shown in Table 5.8 and Table 5.9 respectively.

Table 5.10 details the obtained results and the acceptance criteria for #3 of type C rebar. It can be seen that the cross section properties and fiber content properties of the rebar fell within

Table 5.6: Acceptance criteria for rebar type A #3

Test Method	Test Description	Unit	Per diameter		FDOT 932-3/2017		AC454		ASTM D7957	
			Nom.	Exp.	Criteria	✓/✗	Criteria	✓/✗	Criteria	✓/✗
ASTM D 792	Measured Cross-Sectional Area	in. <sup>2</sup>	0.11	0.15	0.104 – 0.161	✓	0.104 – 0.161	✓	0.104 – 0.161	✓
ASTM D 2584	Fiber Content	% wt.	75.17	75.17	≥ 70	✓	≥ 70	✓	≥ 70	✓
ASTM D 570	Moist. Absorption Short Term @50 °C	%	0.2	0.2	≤ 0.25	✓	≤ 0.25	✓	≤ 0.25	✓
ASTM D 570	Moist. Absorption Long Term @50 °C	%	0.55	0.55	≤ 1.0	✓	n/a	n/a	≤ 1.0	✓
ASTM D 7617	Min. Guaranteed Transverse Shear	ksi	29.1	n/a	≥ 22	✓	≥ 22	✓	≥ 19	✓
ASTM D 4475	Horizontal Shear Stress	ksi	5.75	n/a	n/a	n/a	≥ 5.5	✓	n/a	n/a
ASTM D 7205	Min. Guaranteed Tensile Load	kip	13.4	13.4	≥ 13.2	✓	≥ 13.2	✓	≥ 13.2	✓
ASTM D 7205	Min. Guaranteed Tensile Strength	ksi	121.7	105.2	n/a	n/a	n/a	n/a	n/a	n/a
ASTM D 7205	Tensile Modulus	ksi	7306	6313	≥ 6,500	✓	≥ 6,500	✓	≥ 6,500	✓
ASTM D 7205	Max. Strain	%	1.66	1.66	n/a	n/a	n/a	n/a	n/a	n/a
ACI440. 3R,B.3	Bond-to-Concrete Strength	ksi	3.20	2.64	≥ 1.1	✓	≥ 1.1	✓	≥ 1.1	✓

Table 5.7: Acceptance criteria for rebar type A #5

Test Method	Test Description	Unit	Per diameter		FDOT 932-3/2017		AC454		ASTM D7957	
			Nom.	Exp.	Criteria	✓/✗	Criteria	✓/✗	Criteria	✓/✗
ASTM D 792	Measured Cross-Sectional Area	in. <sup>2</sup>	0.307	0.25	0.288 – 0.388	✓	0.288 – 0.388	✓	0.288 – 0.388	✓
ASTM D 2584	Fiber Content	% wt.	78.4	78.4	≥ 70	✓	≥ 70	✓	≥ 70	✓
ASTM D 570	Moist. Absorption Short Term @50 °C	%	0.18	0.18	≤ 0.25	✓	≤ 0.25	✓	≤ 0.25	✓
ASTM D 570	Moist. Absorption Long Term @50 °C	%	0.77	0.77	≤ 1.0	✓	n/a	n/a	≤ 1.0	✓
ASTM D 7617	Min. Guaranteed Transverse Shear	ksi	25.7	n/a	≥ 22	✓	≥ 22	✓	≥ 19	✓
ASTM D 4475	Horizontal Shear Stress	ksi	6.22	n/a	n/a	n/a	≥ 5.5	✓	n/a	n/a
ASTM D 7205	Min. Guaranteed Tensile Load	kip	41.2	41.2	≥ 29.1	✓	≥ 32.2	✓	≥ 29.1	✓
ASTM D 7205	Min. Guaranteed Tensile Strength	ksi	137.9	121.0	n/a	n/a	n/a	n/a	n/a	n/a
ASTM D 7205	Tensile Modulus	ksi	7749	6989	≥ 6,500	✓	≥ 6,500	✓	≥ 6,500	✓
ASTM D 7205	Max. Strain	%	1.78	1.78	n/a	n/a	n/a	n/a	n/a	n/a
ACI440. 3R,B.3	Bond-to-Concrete Strength	ksi	3.33	2.89	≥ 1.1	✓	≥ 1.1	✓	≥ 1.1	✓

the acceptance ranges, whereas the moisture absorption of the rebar exceeded specifications. The rebar met and exceeded all acceptance ranges for all evaluated strength parameters. The following Table 5.11 shows that #5 rebar of type C were within the acceptance range for cross section, fiber content, and shear properties, whereas the modulus of elasticity was lower than the required minimum.

Table 5.8: Acceptance criteria for rebar type B # 3

Test Method	Test Description	Unit	Per diameter		FDOT 932-3/2017		AC454		ASTM D 7957	
			Nom.	Exp.	Criteria	✓/✗	Criteria	✓/✗	Criteria	✓/✗
ASTM D 792	Measured Cross-Sectional Area	in. <sup>2</sup>	0.110	0.14	0.104 – 0.161	✓	0.104 – 0.161	✓	0.104 – 0.161	✓
ASTM D 2584	Fiber Content	% wt.	83.3	83.3	≥ 70	✓	≥ 70	✓	≥ 70	✓
ASTM D 570	Moist. Absorption Short Term @50 °C	%	0.2	0.2	≤ 0.25	✓	≤ 0.25	✓	≤ 0.25	✓
ASTM D 570	Moist. Absorption Long Term @50 °C	%	0.644	0.644	≤ 1.0	✓	n/a	n/a	≤ 1.0	✓
ASTM D 7617	Min. Guaranteed Transverse Shear	ksi	33.3	26.0	≥ 22	✓	≥ 22	✓	≥ 19	✓
ASTM D 4475	Horizontal Shear Stress	ksi	5.1	3.98	n/a	n/a	≥ 5.5	n/a	n/a	n/a
ASTM D 7205	Min. Guaranteed Tensile Load	kip	20.9	20.9	≥ 13.2	✓	≥ 13.2	✓	≥ 13.2	✓
ASTM D 7205	Min. Guaranteed Tensile Strength	ksi	183.6	148.9	n/a	n/a	n/a	n/a	n/a	n/a
ASTM D 7205	Tensile Modulus	ksi	7542	5957	≥ 6,500	✓	≥ 6,500	✓	≥ 6,500	✓
ASTM D 7205	Max. Strain	%	2.5	2.5	n/a	n/a	n/a	n/a	n/a	n/a
ACI440. 3R,B.3	Bond-to-Concrete Strength	ksi	2.39	2.02	≥ 1.1	✓	≥ 1.1	✓	≥ 1.1	✓

Table 5.9: Acceptance criteria for rebar type B # 5

Test Method	Test Description	Unit	Per diameter		FDOT 932-3/2017		AC454		ASTM D 7957	
			Nom.	Exp.	Criteria	✓/✗	Criteria	✓/✗	Criteria	✓/✗
ASTM D 792	Measured Cross-Sectional Area	in. <sup>2</sup>	0.307	0.372	0.288 – 0.388	✓	0.288 – 0.388	✓	0.288 – 0.388	✓
ASTM D 2584	Fiber Content	% wt.	82.28	82.28	≥ 70	✓	≥ 70	✓	≥ 70	✓
ASTM D 570	Moist. Absorption Short Term @50 °C	%	0.18	0.18	≤ 0.25	✓	≤ 0.25	✓	≤ 0.25	✓
ASTM D 570	Moist. Absorption Long Term @50 °C	%	0.501	0.501	≤ 1.0	✓	n/a	n/a	≤ 1.0	✓
ASTM D 7617	Min. Guaranteed Transverse Shear	ksi	30.8	25.3	≥ 22	✓	≥ 22	✓	≥ 19	✓
ASTM D 4475	Horizontal Shear Stress	ksi	5.0	4.09	n/a	n/a	≥ 5.5	n/a	n/a	n/a
ASTM D 7205	Min. Guaranteed Tensile Load	kip	49.7	49.7	≥ 29.1	✓	≥ 32.2	✓	≥ 29.1	✓
ASTM D 7205	Min. Guaranteed Tensile Strength	ksi	144.9	133.6	n/a	n/a	n/a	n/a	n/a	n/a
ASTM D 7205	Tensile Modulus	ksi	7819	6448	≥ 6,500	✓	≥ 6,500	✓	≥ 6,500	✓
ASTM D 7205	Max. Strain	%	2.07	2.07	n/a	n/a	n/a	n/a	n/a	n/a
ACI440. 3R,B.3	Bond-to-Concrete Strength	ksi	2.81	2.34	≥ 1.1	✓	≥ 1.1	✓	≥ 1.1	✓

Table 5.10: Acceptance criteria for rebar type C # 3

Test Method	Test Description	Unit	Per diameter		FDOT 932-3/2017		AC454		ASTM D 7957	
			Nom.	Exp.	Criteria	✓/✗	Criteria	✓/✗	Criteria	✓/✗
ASTM D 792	Measured Cross-Sectional Area	in. <sup>2</sup>	0.110	0.109	0.104 – 0.161	✓	0.104 – 0.161	✓	0.104 – 0.161	✓
ASTM D 2584	Fiber Content	% wt.	82.035	82.035	≥ 70	✓	≥ 70	✓	≥ 70	✓
ASTM D 570	Moist. Absorption Short Term @50 °C	%	0.20	0.20	≤ 0.25	✓	≤ 0.25	✓	≤ 0.25	✓
ASTM D 570	Moist. Absorption Long Term @50 °C	%	0.75	0.75	≤ 1.0	✓	n/a	n/a	≤ 1.0	✓
ASTM D 7617	Min. Guaranteed Transverse Shear	ksi	33.59	33.59	≥ 22	✓	≥ 22	✓	≥ 19	✓
ASTM D 4475	Horizontal Shear Stress	ksi	6.38	6.38	n/a	n/a	≥ 5.5	✓	n/a	n/a
ASTM D 7205	Min. Guaranteed Tensile Load	kip	19.68	19.68	≥ 13.2	✓	≥ 13.2	✓	≥ 13.2	✓
ASTM D 7205	Min. Guaranteed Tensile Strength	ksi	163.38	163.38	n/a	n/a	n/a	n/a	n/a	n/a
ASTM D 7205	Tensile Modulus	ksi	6.933	6.933	≥ 6,500	✓	≥ 6,500	✓	≥ 6,500	✓
ASTM D 7205	Max. Strain	%	2.34	2.34	n/a	n/a	n/a	n/a	n/a	n/a
ACI440. 3 R,B.3	Bond-to-Concrete Strength	ksi	2.24	1.98	≥ 1.1	✓	≥ 1.1	✓	≥ 1.1	✓

Table 5.11: Acceptance criteria for rebar type C # 5

Test Method	Test Description	Unit	Per diameter		FDOT 932-7/2017		AC454		ASTM D 7957	
			Nom.	Exp.	Criteria	✓/✗	Criteria	✓/✗	Criteria	✓/✗
ASTM D 792	Measured Cross-Sectional Area	in. <sup>2</sup>	0.307	0.353	0.288 – 0.388	✓	0.288 – 0.388	✓	0.288 – 0.388	✓
ASTM D 2584	Fiber Content	% wt.	81.8	81.8	≥ 70	✓	≥ 70	✓	≥ 70	✓
ASTM D 570	Moist. Absorption Short Term @50 °C	%	0.25	0.25	≤ 0.25	✓	≤ 0.25	✓	≤ 0.25	✓
ASTM D 570	Moist. Absorption Long Term @50 °C	%	1.17	1.17	≤ 1.0	✗	n/a	n/a	≤ 1.0	✗
ASTM D 7617	Min. Guaranteed Transverse Shear	ksi	32.38	28.115	≥ 22	✓	≥ 22	✓	≥ 19	✓
ASTM D 4475	Horizontal Shear Stress	ksi	5.56	4.826	n/a	n/a	≥ 5.5	✗	n/a	n/a
ASTM D 7205	Min. Guaranteed Tensile Load	kip	42.82	42.82	≥ 29.1	✓	≥ 32.2	✓	≥ 29.1	✓
ASTM D 7205	Min. Guaranteed Tensile Strength	ksi	119.6	121.16	n/a	n/a	n/a	n/a	n/a	n/a
ASTM D 7205	Modulus	ksi	5710	5836	≥ 6,500	✗	≥ 6,500	✗	≥ 6,500	✗
ASTM D 7205	Max. Strain	%	2.12	2.07	n/a	n/a	n/a	n/a	n/a	n/a
ACI440. 3 R,B.3	Bond-to-Concrete Strength	ksi	2.89	2.37	≥ 1.1	✓	≥ 1.1	✓	≥ 1.1	✓

## Chapter 6

# Discussion

To support the development of basalt-specific acceptance criteria for FDOT Specifications Section 932, this research was conducted with a focus on the biomechanical properties of readily available BFRP rebars. A test matrix — to address the cross-sectional properties, fiber content, moisture absorption, transverse shear strength, horizontal shear strength, tensile properties, and bond-to-concrete characteristics for three dissimilar rebars including two sizes (# 3 and # 5) — was developed to evaluate the essential material properties for BFRP rebar characterization. Based on established test standards and acceptance criteria for glass FRP (GFRP) rebars, BFRP rebars were classified for performance, and it was found that all test samples (specimen groups) from rebar types A, B, and # 3 rebar samples from type C satisfied the minimum requirements for GFRP rebars. Rebar # 5 of type C satisfied all criteria except the maximum moisture absorption and minimum elastic modulus criteria. In the following, these findings are discussed in further detail and studied in context of the available and relevant literature to provide BFRP rebar implementation recommendations and suggestions for future design specifications.

### 6.1 Research Significance

BFRP rebars are still considered new in civil engineering construction in the United States, but it has been successfully used around the world in demonstration and low-risk projects (Singha, 2012; Patnaik, 2009; Elgabbas et al., 2016). Before using new or emerging materials for infrastructure projects, the physical and mechanical properties must be evaluated and compared to acceptance criteria. In the case of emerging materials, acceptance criteria might not have been fully established

yet and research is needed to characterize a variety of products to determine general market quality and to define adequate limiting values. In this report, recommendations for physical properties such as cross-sectional dimensions, fiber content, and moisture absorption properties for BFRP rebars are proposed. In addition, recommendations for minimum mechanical properties, including the apparent horizontal shear strength, the transverse shear strength, the tensile properties, and the bond-to-concrete characteristics are suggested. These suggestions are based on experimental material evaluations, the above presented analyses, and the accompanying literature. These efforts were necessary because acceptance criteria for the specific use of BFRP rebars in the U.S. are still missing. More specifically, FDOT Specifications Section 932 provides defined minimum criteria for glass and carbon based FRP rebars, but values for BFRP rebars have not been implemented yet. Likewise, while some design codes like international building code AC454 (International Code Council, 2017) generally allow the use of BFRP rebars for engineering structures, some design guidelines in the USA, such as AASHTO LRFD guidelines (AASHTO, 2012, 2018), already provide specific procedures for the structural design with glass and carbon FRP rebars — using defined adjustment factors — explicit values for basalt have not been proposed yet. Accordingly, this research project was needed to initiate the development of BFRP rebar specific acceptance criteria and to open the discussion about adjustment factors for another rebar alternative.

## **6.2 Critical Analysis of Major Findings**

Because various material properties were experimentally evaluated throughout this research project and each property has its one specific relevance, these properties are individually discussed in the following subsections.

### **6.2.1 Cross-Sectional property**

The cross-sectional properties were measured according to ASTM D 792 (ASTM-International, 2015b), and it is an important characteristic because rebars are classified based on that diametric size and the strength requirements are dependent on the actual rebar size (in form of the nominal diameter). For traditional steel rebars, the tensile strength of rebar is directly related to effective area. While this is not ultimately true for FRP rebars — as only the fibers carry the tensile loads — it is a measurement that is needed due to design and detailing needs of reinforcement in con-

crete elements to this end, and in order to implement the use of FRP rebars, the same nominal geometry used in steel rebar is specified for FRP rebars with the exception of a range to account for different surface treatments, which for # 3 GFRP rebar is 0.11 in.<sup>2</sup>, with a minimum measured area of 0.104 in.<sup>2</sup> and a maximum measured area of 0.161 in.<sup>2</sup> For # 5 rebars, the nominal cross-sectional area is given as 0.31 in.<sup>2</sup>, with a minimum measured cross-sectional area of 0.228 in.<sup>2</sup> and a maximum of 0.338 in.<sup>2</sup>. All rebars shall be within that range to avoid errors in assumed centroid position for structural resistance calculations, any fit up errors in detailing such as spacing, cover or clearance, and consistency in product approval (Hurtado, 2018; AASHTO, 2018). Likewise, the production sequence for BFRP rebars and the load transfer is similar to glass fiber based rebars, which allows similar definitions for both rebar types (Kampmann et al., 2018).

### 6.2.2 Fiber Content

The experiments and the accompanying mathematical procedures to determine the fiber content percentage for FRP rebars are specified in material standard ASTM D 2584 -11 (ASTM-International, 2011). Fiber content (given in percent) plays a key role in the tensile behavior and load capacity of FRP rebars because induced stresses are mostly carried by the fibers, while the resin matrix must be stiff and elastic enough to transfer the loads between the individual fibers. The minimum fiber content percentage required for GFRP rebars according to FDOT Specifications Section 932, AC454 (International Code Council, 2017), and ASTM D7957 (ASTM-International, 2017) which follows ASTM D 2584 -11 (ASTM-International, 2011), is 70%. After careful evaluation on the tested samples, it was seen that two of the three BFRP rebar products exceeded the required minimum criteria by at least 10%. The third manufactured product exceeded the criteria by 5% on average. Further decrease in the fiber content percentage may affect the stress transfer capacity of the rebar. However, it appears reasonable to suggest a minimum fiber content percentage for BFRP rebars that is similar to that for GFRP products because the observed load carrying and stiffness behaviors were acceptable in the context of the measured fiber contents. As mentioned by You et al. (2015); ACI Committee 440 (2015), fiber contents less than 70% are not acceptable because the fiber-volume fraction significantly affects the tensile strength and quality of FRP rebars. Additional research and analyses are required to establish a precise correlation between fiber content percentage and its effects on the rebar strength to support any modifications of the GFRP specifications

for a BFRP specific minimum. For now, the 70 % minimum criteria seems to be appropriate for BFRP rebars as well and should be adopted in FDOT Specifications Section 932.

### **6.2.3 Moisture Absorption of BFRP rebar**

ASTM D 5229 (ASTM, 2014) details seven different test procedures (A through E, Y, and Z) for estimating moisture absorption properties for FRPs in different environments. Procedure A is most commonly used, and therefore, was followed for this research project. It is considered that the moisture absorption correlates to durability and the corresponding strength retention, where high moisture absorption values are indicative of a porous rebar that is more prone to degradation. According to FDOT Specifications Section 932, which follows ASTM D 5229 (ASTM, 2014) section 7.1, AC454 (International Code Council, 2017), and ASTM D 7957 (ASTM-International, 2017), the maximum short-term moisture absorption limit for GFRP rebars is 0.25 % by weight. In addition, the long-term moisture absorption specified by FDOT Specifications Section 932 and ASTM D 7957 (ASTM-International, 2017) is less than 1 %. After proper evaluation of the tested specimens, it was found that the long-term moisture absorption of BFRP rebars was less than 1 %. Kampmann et al. (2019) discussed the long term behavior of GFRP rebars, and it was found that the rebar strength and the micro structure durability is severely affected by an increased moisture absorption property. As increased moisture absorption affects the strength and strength retention of FRP rebars, it is reasonable to suggest that the BFRP rebar should follow the criteria established for GFRP moisture absorption properties (Kampmann et al., 2018). Nevertheless, it must be emphasized that basalt fibers contain approximately 7 % iron oxide, which makes them potentially more vulnerable in alkaline-chloride (concrete-saltwater) environments (Stekloplastics, 2014; Toni Schneider, 2015; Kochergin et al., 2013). Accordingly, a more critical moisture absorption value may eventually be necessary for BFRP rebars, but more research will be needed to support this claim. Until then, it is not advisable to use BFRP rebars in salty or submerged environments.

### **6.2.4 Transverse Shear Strength**

ASTM D 7617 (ASTM-International, 2012b) was followed to test and analyze the transverse shear data obtained from BFRP rebar testing. FRP rebars are weak in the transverse direction or perpendicular to the rebar longitudinal axis due to the unidirectionality of the fibers and the corresponding

low shear strength of the fibers. According to FDOT Specification Section 932, which is in agreement with AC454 (International Code Council, 2017), GFRP rebars are required to reach a minimum shear strength of 22 ksi before rupture. These values are more critical than the 19 ksi minimum transverse shear strength required by ASTM D 7957 (ASTM-International, 2017). After careful testing and analyses, the evaluated #3 BFRP rebars sustained shear stresses before ultimate failure ranging from 30 ksi to 36 ksi and #5 rebars sustained stresses between 26 ksi and 33 ksi. Based on the results obtained in this study, in comparison to other studies (Kampmann et al., 2018; Chen et al., 2007; ElSafty et al., 2014), BFRP rebars have a higher strength compared to GFRP rebars. This research suggests that the minimum transverse shear strength criteria for BFRP rebars can be equal to the specification for GFRP rebars, given that other rebar sizes have not been evaluated and the specification should remain equal regardless of the rebar size. The Authors suggest that with additional test data the specification for transverse shear strength may be increased up to 20%. This specification needs to be validated both for the average value as well as the guaranteed value, if BFRP products are considered for dowel applications as well, the higher shear strength of BFRP in comparison to GFRP can be beneficial (Brown and Bartholomew, 1993; Eddie, 1999).

### **6.2.5 Apparent Horizontal Shear Strength**

The horizontal shear test was conducted according to ASTM D 4475 (ASTM-International, 2012a) standards. AC454 (International Code Council, 2017) specifies a minimum of 5.5 ksi horizontal shear strength for GFRP bars. It has been noted that the FDOT Specifications and ASTM D 7957 (ASTM-International, 2017) currently does not include minimum horizontal shear strength requirements for rebars made from any fiber material. The horizontal shear failure, however, is an indicator of the resin strength and the resin-to-sizing-to-fiber interface and as such important for the load transfer mechanism. Ultimately, this mechanical property is a suitable quality control measure. After a manufacturer survey was conducted — as part of the literature review process, c.f. Section 3.3 — to identify common practices in the FRP rebar industry, it was noted that horizontal shear tests are one of the most common quality control methods that manufacturers use to ensure production consistency (because it is a mechanical test that can be conducted quickly). Accordingly, FDOT Specifications Section 932 would benefit from limiting minimum values for the acceptance of FRP rebars because it would provide a direct benefit to the manufacturing community and the inter-

section between FDOT and technology implementation; this quality control parameter could be directly targeted during production — and quickly evaluated. The horizontal shear strength of # 3, and # 5 GFRP rebars appears to range around 6 ksi (c.f. Kampmann et al. (2018)) with a minimum average of 5.2 ksi. Based on the experimental results obtained for this study, basalt FRP rebars with a size of # 3 and # 5 measure a minimum average apparent horizontal shear strength of 5.6 ksi and an absolute minimum value of 5.0 ksi. According to AC454 (International Code Council, 2017) and Canadian Standard Association (2018), the minimum horizontal shear strength of BFRP rebars should be 5.5 ksi. Hence, for now, a minimum requirement of 5.5 ksi for the apparent horizontal shear strength, tested on at least five specimens, appears to be an adequate addition to FDOT Specifications Section 932.

### **6.2.6 Tensile Properties**

The tensile strength and elastic modulus of BFRP rebars were evaluated based on procedures and methods detailed in ASTM D 7205 (ASTM-International, 2015a). Minimum guaranteed tensile load requirements for # 3 and # 5 GFRP rebars according to FDOT Specifications Section 932, AC454 (International Code Council, 2017), and ASTM D 7957 (ASTM-International, 2017) are 13.2 kip and 29.1 kip, respectively. Based on the findings from this research project and projects targeting glass fiber based rebars (Kampmann et al., 2018), on average BFRP rebars provide a relatively higher ultimate tensile load capacity and modulus — as compared to GFRP rebars (Benmokrane et al., 2015). It was noted that the minimum tensile load sustained by # 3 BFRP rebars is 19.7 kip and that of # 5 rebars was 42.8 kip . In addition, the elastic moduli of BFRP rebars were measured with a minimum of 8000 ksi (c.f. Table 5.4). The elastic moduli of GFRP rebar according to Kampmann et al. (2018) reached average values of approximately 7 ksi. All tested BFRP rebar types superseded the minimum strength criteria for GFRP rebars. According to research done by Patnaik (2009), BFRP rebars are stronger in tension and Wang et al. (2017) proved that long-term durability of BFRP rebars in harsh environments is higher in comparison to GFRP rebars. Wei et al. (2010) tested chemical durability of GFRP and BFRP rebars and found that BFRP rebars are durable and stronger in tension. Further detailed testing of a wide range of rebars from several manufacturers is required to fully study the strength properties of rebar and to properly define a minimum required criteria that is more critical than the one given for glass based FRP

rebars. However, if basalt fiber specific criteria are desirable for the tensile properties, the data in this research suggests that the minimum strength and elastic modulus should be similar for GFRP rebars.

### **6.2.7 Bond-to-Concrete Strength**

The bond-to-concrete strength of the rebar specimen was tested according to procedure described in ASTM D 7913 (ASTM International, 2014). The minimum guaranteed bond strength required for GFRP rebars according to FDOT Specifications Section 932, AC454 (International Code Council, 2017) and ASTM D 7957 (ASTM-International, 2017) is 1.1 ksi. Based on the measurements obtained in this research and a careful analyses of the results, the bond-to-concrete strength of # 3 rebars ranged from 2.2 ksi to 3.2 ksi and it varied between 2.8 ksi and 3.3 ksi for # 5 BFRP rebars. These results, in comparison to other studies (Kampmann et al., 2018; Chen et al., 2007; Brik, 2003; Li et al., 2017; Hassan et al., 2016), show that the bond-to-concrete strength of basalt FRP rebars is similar to the recorded bond strength of GFRP rebars. The bond strength of FRP rebars is a function of the geometric and surface enhancement features. As the surface for FRP rebars is either deformed or sand coated (or possibly both), it is reasonable to assume that the bond behavior of basalt FRP rebars is similar to the bond behavior of glass or other FRP rebars since equivalent friction is generated, irrespective of the fiber type. To this end, this research suggests that the minimum bond-to-concrete strength criteria for BFRP rebars should remain consistent with GFRP available specifications at a minimum guaranteed bond strength of 1.1 ksi.

## **6.3 Supplementary Findings**

Two of the three tested rebar types for this research included rebars made with epoxy resins. The mechanical performance of the rebars made from epoxy resin was higher than the rebars made from other resin. Through the state-of-the-production-practice review, it was noted that many/most basalt rebar producers across the globe uses epoxy resin in the manufacturing processes. It appears that epoxy resins are suitable for the production of basalt FRP rebars and that such constituent materials should be considered in future updates of FDOT Specifications Section 932. However, additional research with a focus on physical and mechanical properties in response to chemical durability for rebars made with different resins should be considered.

Comparing the findings from this research to the findings made in a previous study with a focus on GFRP (Kampmann et al., 2018), it can be seen that the maximum strain and elongation of BFRP rebars surpasses the maximum strains of glass fiber based rebars. The research completed by Wang et al. (2014) has also shown that the tensile strength retention of BFRP rebars is higher than the tensile strength retention of GFRP rebars. In addition, the maximum strain of BFRP is higher. Likewise, the elastic lengthening of BFRP tendons is higher than that of steel (Thorhallsson and Jonsson, 2012; Pearson et al., 2013) and it might be beneficial to evaluate basalt fiber materials for the use of prestressing tendons to make additional alternatives available that can be used for prestressed concrete elements that are completely steel- or corrosion-free.

## 6.4 BFRP Design Specifications

AASHTO-LRFD specifications for the design of concrete bridges reinforced with BFRP rebars are yet to be developed. Only ICC-ES Acceptance Criteria AC454 (International Code Council, 2017) provides referenced design recommendations and a method of acceptance for BFRP reinforcing under US building codes for alternative materials. The current FDOT Standard Specifications for Road and Bridge Construction Section 932, which details FRP internal reinforcement for concrete structures, does not include or address requirements or minimum criteria for basalt fiber rebars. This research project aims at addressing this knowledge gap by providing recommendations for BFRP rebar specifications. To this end, four different tests were conducted. The assigned guaranteed shear strengths and bond-to-concrete strengths of the tested rebars is the average value for the individual test sample (specimen group). In other words, the mean sample shear strength of the rebars is considered as guaranteed shear strength and mean bond-to-concrete strength is considered as the guaranteed bond-to-concrete strength (ASTM-International, 2012a,b; ASTM International, 2014). To summarize the guaranteed mechanical strength values for all rebar types evaluated in this study, the following Tables 6.1 and 6.2 list the shear and bond-to-concrete characteristics, as well as the tensile properties, respectively. Table 6.1 highlights the transverse shear strength, the horizontal shear strength, and the bond-to-concrete strength for the three different BFRP rebar types (A, B, C). The final results (per test group) were compared to the acceptance criteria for GFRP rebars as given in FDOT Specifications Section 932, such that the prevalent value for the GFRP acceptance criteria represent 100% and a value above 100% indicates a performance above the minimum

Table 6.1: Guaranteed shear and bond-to-concrete strength of rebars

	Rebar size	Lot	Transverse Shear			Horizontal Shear			Bond-to-Concrete		
			Strength			Strength			Strength		
			ksi	MPa	% <sup>†</sup>	ksi	MPa	% <sup>†</sup>	ksi	MPa	% <sup>†</sup>
Rebar A	# 3	1	35.20	242.7	160	7.00	48.31	n/a	2.33	16.09	212
	# 5	1	33.74	232.7	153	6.41	44.16	n/a	2.96	20.41	269
	# 3	2	37.67	259.7	171	6.49	44.71	n/a	1.92	13.22	174
	# 5	2	36.48	251.6	166	6.41	44.15	n/a	1.65	11.41	150
Rebar B	# 3	1	31.39	216.3	143	6.42	44.22	n/a	2.79	19.23	254
	# 5	1	26.51	182.8	120	6.53	45.00	n/a	2.88	19.85	262
Rebar C	# 3	1	34.48	237.2	157	5.56	38.38	n/a	3.77	26.00	343
	# 5	1	31.69	218.5	144	6.64	45.77	n/a	3.77	26.01	343

<sup>†</sup> Percentage comparison based on FDOT specifications section 932, where 100% is GFRP rebar acceptance criteria .

requirement (for GFRP rebars). According to ACI Committee 440 (2015), the guaranteed strength,  $f_{fu}^*$ , of GFRP rebars is defined as the experimentally obtained average tensile strength minus three times the measured standard deviation, as shown in equation 6.1, while the guaranteed elastic modulus,  $E_f = E_{f,ave}$ , is defined as the mean elastic modulus of a test sample (specimen group).

$$f_{fu}^* = f_{fu_{average}} - 3\sigma \quad (6.1)$$

Accordingly, the calculated value for  $f_{fu}^*$  corresponds to the 99<sup>th</sup> percentile (Rossini et al., 2018), such that the chance for material failure (before any design factors are applied) remains below 1%. The strength of commercially available GFRP rebars differs based on the fiber content and manufacturing techniques (Emparanza et al., 2017), and the guaranteed strength is typically experimentally determined at the time of (concrete) design. If a specific rebar product strength is not defined experimentally at that time, the manufacturer specified rebar strength ( $f'_{fu}$ ) is to be used (ACI Committee 440, 2015; Rossini et al., 2018). This specified design strength,  $f'_{fu}$ , is always less

than the guaranteed strength (c.f. equation 6.2) of the particular rebar lot that is to be used for construction.

$$f'_{fu} < f_{fu}^* \quad (6.2)$$

While most strength values for the basalt FRP rebars tested in this research showed that basalt rebars have a higher performance, the general material behavior appeared to be similar to the behavior of GFRP bars, and it is reasonable to assume that Equation 6.2 applies and can be used to calculate the guaranteed strength of basalt rebars. Accordingly, Table 6.2 lists the guaranteed strength values and elastic moduli for the three different BFRP rebar types (A, B, C) tested in this study, and the results are compared to criteria for GFRP rebar according to FDOT Specifications Section 932. The results in Table 6.2 show that both # 3 and # 5 type B rebars were the strongest

Table 6.2: Guaranteed strength and elastic modulus of rebars

		Tensile Strength								Elastic		
		Mean		Sta. Deviation		Guaranteed			Modulus			
		$\mu$		$\sigma$		$\mu - 3\sigma$			$E$			
Rebar size	Lot	ksi	MPa	ksi	MPa	ksi	MPa	% <sup>†</sup>	ksi	GPa	% <sup>†</sup>	
Rebar A	# 3	1	121.7	839	3.82	26.36	110.2	760	92	5482	37.80	84
	# 5	1	134.2	925	4.34	29.92	121.3	836	129	7735	53.46	119
Rebar B	# 3	1	196.3	1353	4.21	29.03	183.6	1266	153	7808	53.83	120
	# 5	1	172.5	1189	9.19	63.33	145.0	999	155	7946	54.79	122
Rebar C	# 3	1	183.9	1268	4.80	33.12	169.5	1168	141	7154	49.32	110
	# 5	1	161.2	1112	12.85	88.63	122.7	1074	131	5267	36.31	81
	# 3	2	169.2	1166	5.03	34.69	154.1	1062	128	7200	49.64	111
	# 5	2	147.8	1019	4.04	27.86	135.6	935	145	7480	51.57	115

<sup>†</sup> Percentage comparison based on FDOT specifications section 932, where 100% is GFRP rebar acceptance criteria.

among all tested rebar samples. But the standard deviation of # 3 type A rebars was the smallest, while the type C # 5 rebars measure the highest standard deviation. The graphs in Figures 6.1 and 6.2 visualize the Gaussian distribution for the measured tensile strength results for # 3 and # 5 rebar, respectively. The mean value and guaranteed tensile strength ( $\mu - 3\sigma$ ) are indicated on the

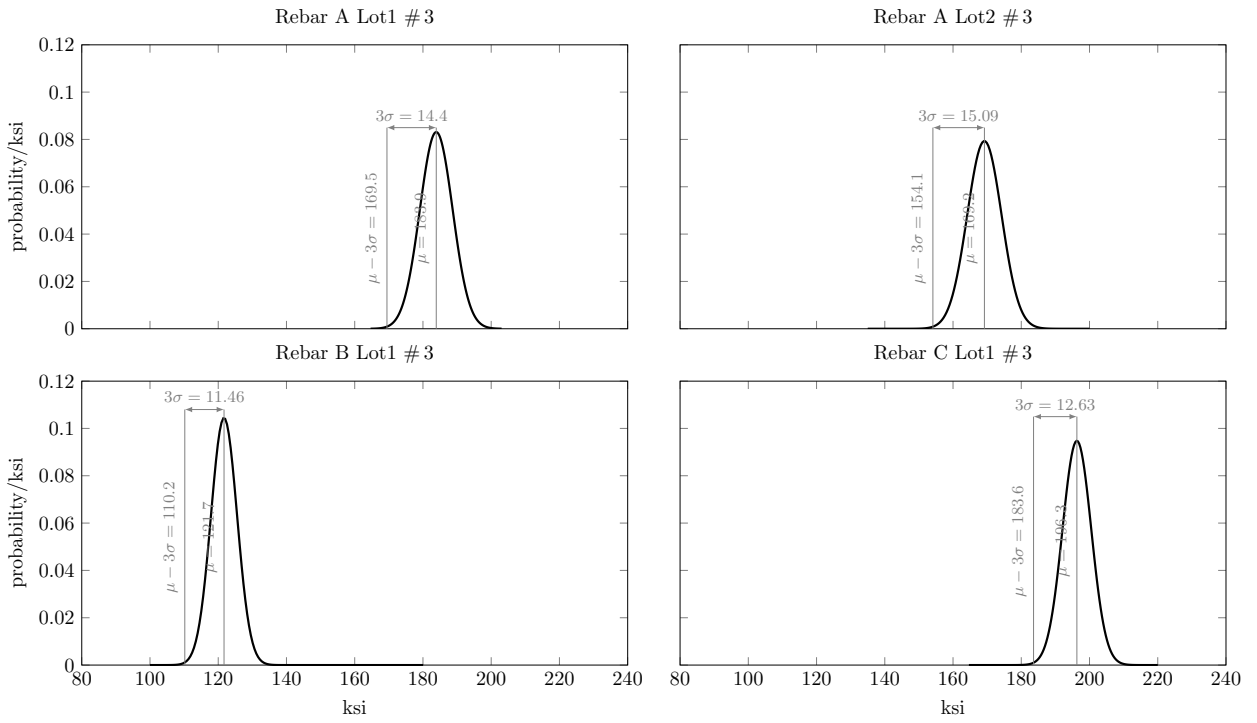


Figure 6.1: Gaussian distribution for tensile strength of #3 rebars

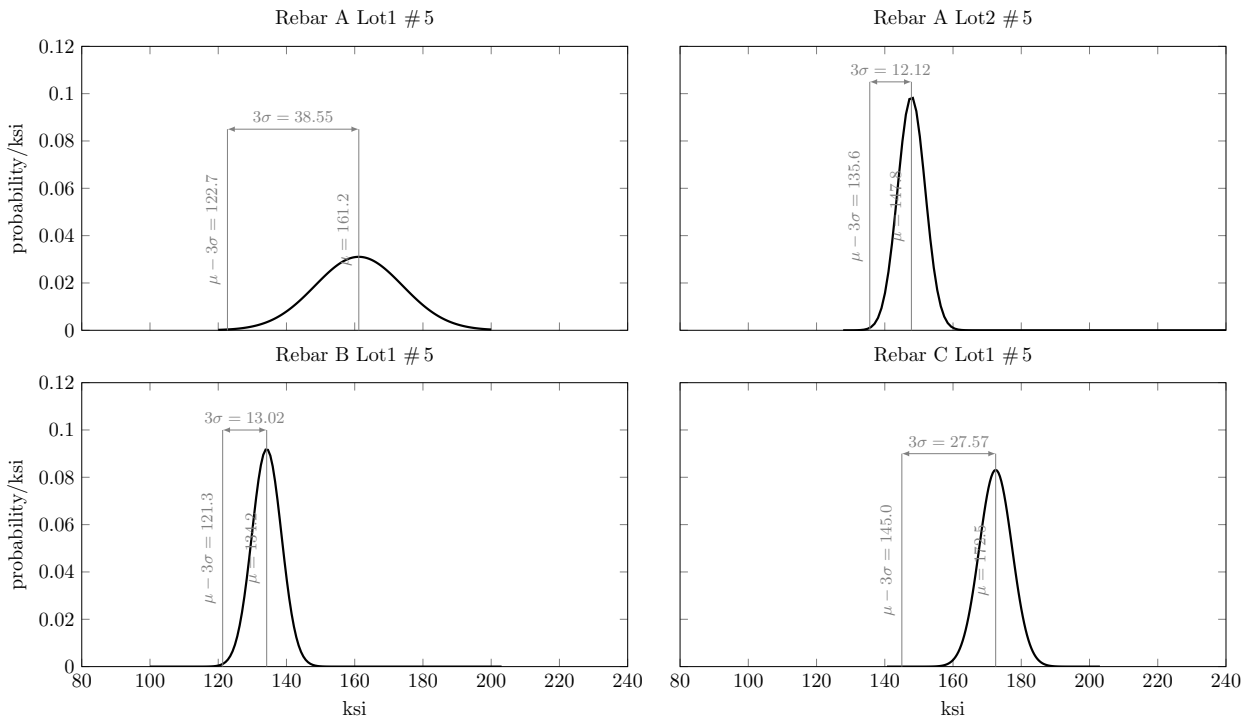


Figure 6.2: Gaussian distribution for tensile strength of #5 rebars

curves. It can be concluded that the guaranteed tensile strength of BFRP rebars can be derived similar to GFRP rebars.

#### 6.4.1 Design Guide Considerations

According to AASHTO-LRFD Bridge Design Guide Specifications for GFRP Reinforced Concrete and ACI 440.1R Guide for the Design and Construction of Structural Concrete Reinforced with Fiber-Reinforced Polymer (FRP) Bars, strength reduction factors must be applied to decrease the design strength of FRP to overcome strength degradations (c.f. Table 6.3). The guaranteed strength of FRP rebars must be reduced by applying the environmental factor ( $C_E$ ) (ACI Committee 440, 2015) to account for the strength loss due to exposure conditions. Likewise, the design strength for FRP rebars under sustained load must be reduced via the creep rupture factor ( $C_c$ ) to avoid premature failure due to creep (ACI Committee 440, 2015; du Béton, 2007). The fatigue reduction factor ( $C_f$ ) must be applied to properly define the strength of FRP rebars under cyclic loading. For the design of FRP rebar reinforced concrete structures, a reduction factor ( $C_b$ ) has to be applied to the bond-to-concrete strength values listed in Table 6.1 to account for the different surface enhancement properties, which may differ significantly in comparison to steel rebars (ACI Committee 440, 2015). ACI Committee 440 (2015) defines the bond reduction factor as the inverse of the bond coefficient ( $k_b$ ), which is larger than 1.0 for FRP rebars with a bond strength that is inferior to the bond strength for traditional steel rebars and less than 1.0 for FRP rebars with superior bond strength.

The brittle nature of FRPs implies a possibility of over-reinforced flexural members, which leads to concrete failure in the compression zone or to under-reinforced compression members, which may cause reinforcement rupture in the tension zone (ACI Committee 440, 2015; Rossini et al., 2018). The two failure modes — failure in the compression zone and rupture in the tension zone — are characterized by two different strength factors  $\phi_c$  and  $\phi_t$  respectively (ACI Committee 440, 2015; Rossini et al., 2018). As flexural members can sometimes undergo shear failure, the strength reduction factor  $\phi_s$  is incorporated in the design; in other words, the nominal shear resistance of the designed member shall be reduced to factored shear resistance (Rossini et al., 2018). These factors are applied during the design phase to reduce the estimated nominal moment of a reinforced concrete member. Table 6.3 provides an overview of these factor and exemplifies how each factors

is applied in the design procedures according to ACI Committee 440 (2015); AASHTO (2018). The

Table 6.3: Reduction factors

Reduction factor	Equation used in design
Environmental factor ( $C_E$ )	$f_{fd} = C_E f'_{fu}$
Creep rupture factor ( $C_c$ )	$f_{f,c} = C_c f_{fd} = C_E C_c f'_{fu}$
Fatigue rupture factor ( $C_f$ )	$f_{f,f} = C_f f_{fd} = C_E C_f f'_{fu}$
Bond reduction factor ( $C_b$ )	$(C_b) = 1/k_b$
Factor for compression-controlled failures ( $\phi_c$ )	$M_r = \phi_c M_n$
Factor for tension-controlled failures ( $\phi_t$ )	$M_r = \phi_t M_n$
Factor for shear-controlled failures ( $\phi_s$ )	$V_r = \phi_s V_n$

results obtained through this research can be used to initiate the development of the bond factor for BFRP rebars in concrete structures. A detailed research focusing on the reduction factors and long-term durability of BFRP rebars in harsh environments is suggested because this would inform future iterations of the AASHTO LRFD bridge specifications for BFRP rebars and also helps with updates to ACI 440 codes for the implementation of BFRP design specifications.

## 6.5 Research Limitations

This research project was focused toward a BFRP rebar market analysis and the performance evaluation of three different BFRP rebar products. It was found that numerous readily available rebar types exist, with a range of strength properties, and that those properties are dependent on the different raw materials and surface enhancement features (chosen by the manufacturer). While an effort was made to evaluate representative and commonly available BFRP rebar products, this study was limited to the specific material compositions used by the three selected manufacturers. Likewise, for economical considerations, only the two most common rebar sizes were tested. Only one manufacturer was able to supply material from two lots, while the other two manufacturers were still developing their production lines and only supplied materials from their pilot productions. The results obtained from this research are currently used by the manufacturers to improve the quality of production of the rebars. Accordingly, it must be noted that the presented conclusions have to

be interpreted with care when using other products or different material compositions. While the findings seem adequate and applicable in the context of the BFRP rebar technology, it is emphasized that the derived conclusions are not universal. Because acceptance criteria for BFRP rebar are still under development for FDOT Specifications Section 932, all obtained results were benchmarked relative to the existing acceptance criteria for GFRP rebars.

BFRP rebars are intended for use in harsh environments. Therefore, a long-term durability analysis of these rebars must be done because those aspects could not be addressed through this research project. Only BFRP rebar material properties were tested, while the application behavior of these rebars in concrete elements such as beams, columns, and slabs was not studied here. The presented findings provide insight and initial guidance for the adoption of BFRP rebars in FDOT Specifications and suggestions for future iterations of design guidelines. But the authors explicitly advise acting with caution when extrapolating the findings and conclusions to other or future FRP rebar materials.

## 6.6 Future and Further Directions

It is noted that no long-term tests were performed throughout this project and that additional durability analyses for BFRP rebars in extreme environments shall be conducted. It appears vital because of the unique chemical composition of basalt fibers and the interaction they can potentially undergo in saline-rich environments heterodyned with high pH concentrations. This may be one of the most important aspects for a proper life cycle of concrete structures reinforced with BFRP rebars in aggressive environments (e.g.; coastal bridges) because of the highly basic conditions of the rebar surrounding cementitious paste.

Lu et al. (2015) compared virgin to aged, pultruded BFRP plates and rebars to measure the effect of thermal aging (at 135 °C and 300 °C for four hours) on the longitudinal tensile strength and the interlaminar shear properties. It was found that the degradation process of aged rebars immersed in alkaline solution and distilled water accelerated due to thermal aging. Similarly, Altalmas et al. (2015) studied the bond-to-concrete durability properties of sand coated basalt fiber reinforced polymer (BFRP) rebars and glass fiber reinforced polymer (GFRP) rebars via accelerated conditioning in acidic, saline, and alkaline solutions for 30 days, 60 days, and 90 days. The results showed that the bond strength retention was reduced for rebars immersed in acid solution, alkaline,

and saline environments, as compared to un-aged rebars; all rebars failed in interlaminar shear. Wang et al. (2017) tested tensile strength and Young's modulus properties of BFRP and GFRP rebars exposed to seawater and sea sand concrete (SWSSC). The rebars were exposed to normal SWSSC (N-SWSSC), and high performance SWSSC (HP-SWSSC) at room temperature, 40 °C, 48 °C, and 50 °C for 21 days, 42 days, and 63 days. When compared to HP-SWSSC, N-SWSSC was more aggressive on both BFRP and GFRP bars due to the high alkali ion concentration. In high temperature environments, the GFRP rebars were more durable than the BFRP rebars because of the different resins. Based on the SEM, 3D X-ray, and CT-results, the resin properties of GFRP bars were more stable in SWSSC conditions than the resin used for the tested BFRP rebars. In research projects conducted by Benmokrane et al. (2017) and Kajorncheappunngam et al. (2002), the long-term durability in alkali environments at accelerated temperatures for rebars made with different resins was evaluated. It was seen that the performance of epoxy resins was comparably good and acceptable.

Wei et al. (2011) studied degradation of basalt fiber-epoxy resin and glass fiber-epoxy resin composites in seawater, and it was found that the bending and tensile strength decreased with increased immersion times. This study also emphasized that the chemical stability of BFRP rebars can be improved by lowering the  $Fe^{+2}$  ions in basalt rock and durability of rebar in seawater can be increased.

As mentioned before and based on the above listed research studies, it is suggested to conduct degradation analyses of BFRP rebars in harsh environments. Furthermore, because the microstructure porosity and the moisture absorption of FRP rebars are closely related, SEM analysis of basalt fiber rebar specimens after long-term moisture absorption tests should be performed to evaluate the rebar properties at the micro level and to define its vulnerability to degradation. New products should be characterized via SEM technology, such that the findings and images can be stored for comparison to future iterations of specific product lines. The development of a product database is highly suggested. It appears that long-term durability performance of BFRP rebars in concrete structures has not been sufficiently studied yet. To fully embrace this technology, it is important to study the flexural and shear properties of BFRP rebar reinforced concrete beams after exposing them to aggressive environments for extended periods. Therefore, it is suggested to evaluate the performance of BFRP rebars and strength retention in concrete elements exposed to

different environmental conditions.

# Chapter 7

## Conclusions

To provide a concise overview of the tasks performed for this research project, a brief summary of the experimental work and the analysis is provided in this chapter, before the final conclusion and future recommendations — based on the overall findings and the discussion presented in Chapter 6 — are listed here.

### 7.1 Summary

This project was conducted to evaluate the performance of three commercially available BFRP rebar products to assist the Florida Department of Transportation in the development of acceptance criteria for basalt based fiber reinforced polymer (BFRP) reinforcing bars for the extension of FDOT Specifications Section 932 — Nonmetallic Accessory Materials for Concrete Pavement and Concrete Structures. Three high-quality rebar products from different established FRP rebar producers were selected to evaluate two of the most commonly used rebar sizes (# 3 and # 5) and to fully characterize the relevant material properties. It was the goal to study the effects of different material constituents and surface enhancement properties. For the purpose of this research, a total of three different physical properties (cross-sectional dimensions, moisture absorption, and fiber content) and four mechanical strength characteristics (transverse shear strength, apparent horizontal shear strength, tensile strength and elastic modulus, and bond-to-concrete strength) were experimentally quantified for virgin state BFRP rebars. Because acceptance criteria for basalt FRP rebars does not yet exist in the US, the findings were compared to the prevalent minimum criteria for glass FRP rebars. The measured and analyzed data showed that two of the three re-

bar products (Type A and B), irrespective of their size, met the GFRP rebar criteria defined in FDOT Specifications Section 932. The other rebar Type C met all performance criteria for the #3 rebar size, but rebar size #5 did not meet the acceptance criteria for moisture absorption or elastic modulus properties. Performance differences were noted for rebar products from different manufacturers because of dissimilarities in material production and surface enhancement properties. However, basalt fiber rebar products appear to be a viable alternative as a non-corrosive rebar option for future FDOT construction projects, and the data gathered throughout this research showed that high-quality BFRP rebars are available in the American market. A standardized use of such rebars seem feasible based on appropriate acceptance criteria because BFRP rebars outperform the already accepted/established GFRP rebars. While the development of acceptance criteria for BFRP rebars has been initiated through this project, and an implementation of this alternative reinforcing technology should be strongly considered by the FDOT, more critical BFRP-specific performance criteria — beyond GFRP performance criteria — can be developed in future projects to further differentiate the various fiber types and to take full advantage of the available material characteristics.

## 7.2 Conclusions

Based on the research findings which were obtained through a comprehensive literature review, a BFRP rebar market analysis, material characterization, and the discussion points presented throughout this report, the following conclusions were drawn:

- A variety of BFRP rebar types and sizes, with dissimilar physical and strength properties, are currently available in the market. The strength properties of different types of rebars vary vastly based on the manufacturer type, raw materials, and surface enhancement property. While manufacturer reported properties vary, BFRP rebars appear to be [notably] stronger than GFRP rebars.
- The fiber content of BFRP rebars appears to be well-controlled throughout the manufacturing process, and it is nearly identical between various products (or the tested rebar types). This property was notably consistent with minimal coefficients of variations, which indicates high-quality products.

- Differences in performance of rebars were observed based on the moisture absorption property, specifically for the material that did not satisfy the maximum absorption criteria. It appears that the rebar strength is inversely proportional to moisture absorption property because of the related porosity that potentially leads to material imperfections.
- The transverse shear strength of BFRP rebars appears to be measurably stronger than the the transverse shear strength of GFRP rebars. The data showed that BFRP outperformed the minimum GFRP criteria by at least 116 %.
- Because the apparent horizontal shear strength is dependent on the quality of the resin and the resin-fiber interface — and less influenced by the fiber itself — this property was not significantly different from measurements usually obtained for GFRP products. Nevertheless, this property is a valuable quality control parameter that is used by many manufacturers around the world to quickly recognize/address production inconsistencies. As such, FDOT Specifications Section 932 should adopt a minimum threshold value.
- The size effect or shear lag for BFRP rebars with sizes between # 3 and # 5 is notably higher. These phenomenon occurred because BFRP rebars are a product of composite materials and they are produced in multiple layers. Due to the test procedure, the external fibers are stretched the most, while the inner layers stretch less towards the rebar core and can only be fully utilized after the outer fibers fail.
- Similar to GFRP rebars, for BFRP rebars which were manufactured with helical wraps — as surface enhancement property — the helically wrapped fibers ruptured before the longitudinal fibers failed in tension.
- The bond-to-concrete property of BFRP rebars is highly dependent on the surface enhancement features and the rebar geometry. Due to the geometric interlocking effect, helically wrapped rebars (in addition to being sand coated) measured the highest absolute bond-to-concrete strength, while the rebar slip was significantly minimized — in comparison to the measured slip for sand coated rebars.
- The minimum criteria for bond-to-concrete of  $\geq 1.1$  ksi appears to be at the lower limit, because all rebars tested in this study outperformed this criteria by more than 200 %, with

individual rebar types beyond 300 %.

- Based on the performance analysis of the tested BFRP rebars and an evaluation of all obtained results in context of FDOT Specifications Section 932, AC454, and ASTM 7957, it can be concluded that the tested materials are generally stronger than comparable GFRP rebars.
- The elastic modulus and tensile strength criteria for BFRP rebars can be set higher than the existing criteria for GFRP rebars in FDOT Specifications Section 932.

### 7.3 Further Recommendations

Because FRP rebars are desirable for use in harsh environments and material properties generally degrade in aggressive media (ACI Committee 440, 2015; du Béton, 2007), the long-term chemical durability performance of BFRP rebars, including their raw material components, have to be studied and evaluated in various alkaline and saline environments before minimum material and design criteria can be ultimately defined. As discussed in Section 6.4.1, for the implementation of BFRP rebar technology in future design codes, such as AASHTO design guidelines, ACI, or state design requirements, the following suggestions are made.

- The bond strength results obtained through this research project can be used in the development of a bond factor ( $C_b$ ) for BFRP rebars, and this factor can be directly implemented in ACI 440 and AASHTO-bridge design guide specifications.
- Additional studies with a focus on bond-to-concrete properties of BFRP rebars and the bond degradation over time in harsh environments is recommended to full development of a suitable bond reduction factor ( $C_b$ ) that is specific to BFRP rebars.
- Because BFRP rebars are thought of as a preferable alternative in harsh environments, it is important to study the long-term chemical durability properties of such rebars before the environmental reduction factor ( $C_E$ ) for BFRP rebars can be independently defined.

# References

- AASHTO (2012). *Guide Specifications for Design of Bonded FRP Systems for Repair and Strengthening of Concrete Bridge Elements*. American Association of State Highway and Transportation Officials.
- AASHTO (2018). *AASHTO LRFD Bridge Design Guide Specifications for GFRP-Reinforced Concrete Bridge Decks and Traffic Railings*. American Association of State Highway and Transportation Officials.
- ACI Committee 440 (2006). *Guide for the Design and Construction of Structural Concrete Reinforced with FRP Bars*, (440.1R). American Concrete Institute.
- ACI Committee 440 (2007). *Report on Fiber-Reinforced Polymer (FRP) Reinforcement for Concrete Structures*, (440R). American Concrete Institute.
- ACI Committee 440 (2008a). *Guide for the Design and Construction of Externally Bonded FRP Systems for Strengthening Concrete Structures*, (440.2R). American Concrete Institute.
- ACI Committee 440 (2008b). *Specification for Carbon and Glass Fiber-Reinforced Polymer Bar Materials for Concrete Reinforcement*, (440.6). American Concrete Institute.
- ACI Committee 440 (2012). *Guide Test Methods for Fiber-Reinforced Polymer (FRP) Composites for Reinforcing or Strengthening Concrete and Masonry Structures*, (440.3R). American Concrete Institute.
- ACI Committee 440 (2013). *Specification for Carbon and Glass Fiber-Reinforced Polymer (FRP) Materials Made by Wet Layup for External Strengthening of Concrete and Masonry Structures*, (440.8-13). American Concrete Institute.

- ACI Committee 440 (2015). “*Guide for the design and construction of structural concrete reinforced with fiber-reinforced polymer (frp) bars.*” Report No. ACI 440.1R-15, American Concrete Institute.
- Altalmas, A., Refai, A. E., and Abed, F. (2015). “Bond degradation of basalt fiber-reinforced polymer (bfrp) bars exposed to accelerated aging conditions.” *Construction and Building Materials*, 81, 162–171.
- ASTM (2014). *Standard Test Method for Moisture Absorption Properties and Equilibrium Conditioning of Polymer Matrix Composite Materials*, (D5229). ASTM International, West Conshohocken, PA.
- ASTM-International (2004). *Standard Test Method for Compressive Strength of Cylindrical Concrete Specimens*, (C 39/C 39 M). West Conshohocken, PA.
- ASTM-International (2011). *Standard Test Method for Ignition Loss of Cured Reinforced Resins*, (D2584-11). West Conshohocken, PA.
- ASTM-International (2012a). *Standard Test Method for Apparent Horizontal Shear Strength of Pultruded Reinforced Plastic Rods By the Short-Beam Method*, (D4475 - 02 (REAPPROVED 2008)). West Conshohocken, PA.
- ASTM-International (2012b). *Standard Test Method for Transverse Shear Strength of Fiber-reinforced Polymer Matrix Composite Bars*, (D7617/D7617M - 11). West Conshohocken, PA.
- ASTM International (2014). *Standard Test Method for Bond Strength of Fiber-Reinforced Polymer Matrix Composite Bars to Concrete by Pullout Testing*, (D7913/D7913M). West Conshohocken, PA.
- ASTM International (2014). *Standard Test Method for Bond Strength of Fiber-Reinforced Polymer Matrix Composite Bars to Concrete by Pullout Testing*, (D7913/D7913M). ASTM International, West Conshohocken, PA.
- ASTM-International (2015a). *Standard Test Method for Tensile Properties of Fiber Reinforced Polymer Matrix Composite Bars*, (D7205/D7205M – 06 Reapproved 2011). West Conshohocken, PA.

- ASTM-International (2015b). *Standard Test Methods for Density and Specific Gravity (Relative Density) of Plastics by Displacement*, (D792-13). West Conshohocken, PA.
- ASTM-International (2017). *Standard Specification for Solid Round Glass Fiber Reinforced Polymer Bars for Concrete Reinforcement*, (ASTM D7957 / D7957M – 17). West Conshohocken, PA.
- ASTM International (2018). *Standard Practice for Making and Curing Concrete Test Specimens in the Laboratory*, (C192/C192M). West Conshohocken, PA.
- Aubourg, P., Crall, C., Hadley, J., Kaverman, R., and Miller, D. (1991). *Engineered Materials Handbook*, (Vol. 4). ASM International.
- Bagherpour, S. (2012). (*Polyester*). InTech.
- Bagherpour, S., Bagheri, R., and Saatchi, A. (2009). “Effects of concentrated hcl on the mechanical properties of storage aged fiber glass polyester composite.” *Materials and Design*, 30(2), 271–274.
- Benmokrane, B. (2018). “*Development of New Edition of CSA S807 Standard — Specifications for Fiber Reinforced Polymers.*” Report No. to be assigned, Canadian-CSA Specifications for Fiber Reinforced Polymers.
- Benmokrane, B., Ali, A. H., Mohamed, H. M., ElSafty, A., and Manalo, A. (2017). “Laboratory assessment and durability performance of vinyl-ester, polyester, and epoxy glass-frp bars for concrete structures.” *Composites Part B: Engineering*, 114, 163–174.
- Benmokrane, B., Elgabbas, F., Ahmed, E. A., and Cousin, P. (2015). “Characterization and comparative durability study of glass/vinylester, basalt/vinylester, and basalt/epoxy frp bars.” *Journal of Composites for Construction*, 19(6), 04015008.
- Benmokrane, B., Wang, P., Ton-That, T. M., Rahman, H., and Robert, J.-F. (2002). “Durability of glass fiber-reinforced polymer reinforcing bars in concrete environment.” *Journal of Composites for Construction*, 6(3), 143–153.
- Best, M. G. (2003). *Igneous and metamorphic petrology*, (2nd Edition). Wiley-Blackwell.
- Borges, S. G., Ferreira, C. A., Andrade, J. M., and Prevedello, A. L. (2015). “The influence of bath temperature on the properties of pultruded glass fiber reinforced rods.” *Journal of Reinforced Plastics and Composites*, 34(15), 1221–1230.

- Brik, V. B. (2003). “*Advanced concept concrete using basalt fiber/bf composite rebar reinforcement.*”  
Final report for highway-idea project 86, Innovations Deserving Exploratory Analysis Programs.
- Brown, V. and Bartholomew, C. (1993). “Frp dowel bars in reinforced concrete pavements.” *Special Publication, 138*, 813–830.
- Busel, J. P. (2016). “*Introduction to fiber reinforced polymer (frp) composites in infrastructure.*”  
Report no., American Composites Manufacturers Association.
- Canadian Standard Association (2010). *Specifications for Fibre Reinforced Polymers*, (CAN/CSA-S807).
- Canadian Standard Association (2018). *Specifications for Fibre Reinforced Polymers*, (CAN/CSA-S807).
- Castro, F. and Carino, N. J. (1998). “Tensile and nondestructive testing of frp bars.” *Journal of Composites for Construction*.
- Chen, Y., Davalos, J. F., Ray, I., and Kim, H. Y. (2007). “Accelerated aging tests for evaluations of durability performance of FRP reinforcing bars for concrete structures.” *Composite Structures*, 78(1), 101–111.
- Colombo, C., Vergani, L., and Burman, M. (2012). “Static and fatigue characterisation of new basalt fibre reinforced composites.” *Composite Structures*, 94, 1165–1174.
- Dhé, P. (1923). “*Tipping crucible for basalt furnaces.*” Patent 1,462,446, United States Patent Office.
- du Béton, F. I. (2007). “Frp reinforcement in rc structures.” *Task Group*, 9, 151.
- Eddie, D. (1999). “Frp dowels for concrete pavements. Master’s thesis, University of Manitoba.
- Ehrenstein, G. W. (2006). *Faserverbund-Kunststoffe: Werkstoffe - Verarbeitung - Eigenschaften*, (2. Edition). Carl Hanser Verlag GmbH and Co. KG.
- Elgabbas, F., Vincent, P., Ahmeda, E. A., and Benmokrane, B. (2016). “Experimental testing of basalt-fiber-reinforced polymer bars in concrete beams.” *Composites Part B*, 91, 205–218.

- ElSafty, A., Benmokrane, B., Rizkalla, S., Mohamed, H., and Hassan, M. (2014). “*Degradation assessment of internal continuous fiber reinforcement in concrete environment.*” Report no., Florida Department of Transportation.
- Emparanza, A. R., Kampmann, R., and y Basalo, F. D. C. (2017). “State-of-the-practice of global manufacturing of frp rebar and specifications.” *The 13th International Symposium on Fiber-Reinforced Polymer Reinforcement for Concrete Structures (FRPRCS-13)*, American Concrete Institute Anaheim, CA.
- Fallaha, S., Knight, C., and Nolan, S. (2017). “FDOT GFRP-RC implementation - current status, projects and challenges. First International Workshop on Glass Fibre Reinforced Polymer (GFRP) Bar for Concrete Structures (IWGFRP-1), July 18, 2017.
- Faruk, O., Tjong, J., and Sain, M. (2017). (*Lightweight and Sustainable Materials for Automotive Applications*). Tyler & Francis Group, LCC.
- Fiore, V., Scalici, T., Bella, G. D., and Valenza, A. (2015). “A review on basalt fibre and its composites.” *Composites Part B*, 74, 74–94.
- Florida Department of Transportation (2015). “*Fiber reinforced polymer guidelines (frpg).*” Structural Manual Topic No. 625-020-018 Volume 4, FDOT.
- G., N. and D., V. (2011). *Wendehorst Baustoffkunde Grundlagen - Baustoffe - Oberflächenschutz*, (Vol. 27). Vieweg+Teubner Verlag.
- Gieben, N. (2017). “An analysis of the free specimen length for tensile testing of glass fiber reinforced polymer (gfrp) reinforcement bars according to astm 7205. Master’s thesis, FH Münster University of Applied Sciences.
- Hassan, M., Benmokrane, B., ElSafty, A., and Fam, A. (2016). “Bond durability of basalt-fiber-reinforced-polymer (bfrp) bars embedded in concrete in aggressive environments.” *Composites Part B*, 106, 262–272.
- Hurtado, D. (2018). “*Fdot standard specification for road and bridge construction.*” Report no., Florida Department of Transportation.

- International Code Council (2017). *Fiber-reinforced Polymer (FRP) Bars for Internal Reinforcement of Concrete Members*. 500 New Jersey Avenue, NW.
- International Code Council Evaluation Services (2016). “Acceptance criteria for glass fiber-reinforced polymer (GFRP) bars for internal reinforcement of concrete members.” Acceptance criteria 454, ICCES.
- International Code Council Evaluation Services (2017). “Acceptance criteria for glass fiber-reinforced polymer (GFRP) bars for internal reinforcement of concrete members.” Acceptance criteria 454, ICCES.
- Ipbüker, C., Nulk, H., Gulik, V., Biland, A., and Tkaczyk, A. H. (2014). “Radiation shielding properties of a novel cement-basalt mixture for nuclear energy applications.” *Nuclear Engineering and Design*, 284, 27–37.
- ISC (2014). *Fibre-Reinforced polymer bar for concrete reinforcement general specifications*, (GOST 31938-2012). Interstate Council for Standardization, Metrology and Certification (ISC).
- Jamshaid, H. and Mishra, R. (2016). “A green material from rock: basalt fiber — a review.” *The Journal of The Textile Institute*, 107(7), 923–937.
- Joshi, S. C., Lam, Y., and Tun, U. W. (2003). “Improved cure optimization in pultrusion with pre-heating and die-cooler temperature.” *Composites Part A*, 34, 1151–1159.
- Kajorncheappunngam, S., Gupta, R. K., and GangaRao, H. V. (2002). “Effect of aging environment on degradation of glass-reinforced epoxy.” *Journal of composites for construction*, 6(1), 61–69.
- Kampmann, R., De Caso Y Basalo, F., and Ruiz Emparanza, A. (2018). “Performance evaluation of glass fiber reinforced polymer (gfrp) reinforcing bars embedded in concrete under aggressive environments.” Technical Report BDV30 TWO 977-18, Florida Department of Transportation.
- Kampmann, R., Ruiz Emparanza, A., Telikapalli, S., Suhrheinrich, J., and De Caso Y Basalo, F. (2019). “The correlation between moisture absorption and tensile strength retention of glass fiber reinforced polymer rebars.” *2nd International Workshop on Glass Fibre Reinforced Polymer (GFRP) Bars for Concrete Structures*.

- Kocaoza, S., Samaranayakeb, V., and Nanni, A. (2004). “Tensile characterization of glass frp bars.” *Composites Part B*, 36, 127–134.
- Kochergin, A., Granovskaya, N., Kochergin, D., Savchenko, V., and Galimov, N. (2013). “Ways to supply gabbro-basalt raw materials to mineral fiber producers.” *Glass and Ceramics*, 69(11-12), 405–408.
- Li, C., Gao, D., Wang, Y., and Tang, J. (2017). “Effect of high temperature on the bond performance between basalt fibre reinforced polymer (bfrp) bars and concrete.” *Construction and Building Materials*, 141, 44–51.
- Lu, Z., Xian, G., and Li, H. (2015). “Effects of exposure to elevated temperatures and subsequent immersion in water or alkaline solution on the mechanical properties of pultruded bfrp plates.” *Composites Part B: Engineering*, 77, 421–430.
- Maitre, R. W. L. (2002). (*Igneous Rocks: A Classification and Glossary of Terms: Recommendations of the International Union of Geological Sciences Subcommittee on the Systematics of Igneous Rocks*). 2nd. Cambridge University Press.
- Markets and Markets (2016). “Frp rebar market by resin type, by fiber type, by application — global forecasts to 2021.” *PR Newswire Association LLC*.
- MTS Landmark Testing Solutions (2015). *Versatile, high-performance servohydraulic systems for static and dynamic material and component testing*, (12/15). MTS Systems Corporation, 14000 Technology Drive Eden Prairie, MN 55344-2290 USA.
- Nanni, A., De Luca, A., and Jawaheri Zadeh, H. (2014). (*FRP Reinforced Concrete Structures – Theory, Design and Practice*). CRC Press.
- Patnaik, A. (2009). “Applications of basalt fiber reinforced polymer (bfrp) reinforcement for transportation infrastructure.” Report no., The University of Akron.
- Pavlovski, D., Mislavsky, B., and Antonov, A. (2007). “Cng cylinder manufacturers test basalt fibre.” *REINFORCEDplastics*, 36–39.
- Pearson, M., Donchev, T., and Salazar, J. (2013). “Long-term behaviour of prestressed basalt fibre reinforced polymer bars.” *Procedia Engineering*, 54, 261–269.

- Rarnalaishnan, V. and Tolmare, N. S. (1998). “*Performance evaluation of 3-d basalt fiber reinforced concrete & basalt rod reinforced concrete.*” IDEA Program Final Report, Contract No. NCHRP-45, Transportation Research Board National Research Council.
- Rossini, M., Matta, F., Nolan, S., Potter, W., and Nanni, A. (2018). “Aashto design specifications for gfrp-rc bridges.” *Italian Concrete Days*, Associazione Italiana Calcestruzzo Armato e Precompresso (AICAP) & Collegio .
- Ruelke, T. (2014). “*Non metallic accessory materials for concrete pavement and concrete structures.*” Section 932, Florida Department of Transportation.
- Schesser, D., Yang, Q. D., Nanni, A., and Giancaspro, J. W. (2014). “Expansive grout-based gripping systems for tensile testing of large-diameter composite bars.” *Journal of Materials in Civil Engineering*, 26(2), 250–258.
- Singha, K. (2012). “A short review on basalt fiber.” *International Journal of Textile Science*, 1(4), 19–28.
- Slyter, G. (1938). “*Method and apparatus for making glass wool.*” Patent 2,133,235, United States Patent Office.
- Stekloplastics, D. (2014). “Stekloplastic visit to iceland.” *Communication with Stekloplastics Boris Gromkov and Natalya Demenia with Birgir Jóhannesson.*
- Thorhallsson, E. and Jonsson, B. S. (2012). “Test of prestressed concrete beams with bfrp tendons.” *Reykjavik University.*
- Toni Schneider, G. L. (2015). “Lipex gmbh, germany.” *Communication with Toni Schneider, Gert Lichblau with Birgir Jóhannesson.*
- Vincent, P., Ahmed, E., and Benmokrane, B. (2013). “Characterization of basalt fiber-reinforced polymer (bfrp) reinforcing bars for concrete structures.” *Specialty Conference on Material Engineering & Applied Mechanics, 3rd*, MEC–111–1 – MEC–111–10.
- Wallenberger, F. T., Watson, J. C., Li, H., and PPG Industries Inc. (2001). “*Glass fibers.*” ASM Handbook 21, ASM International.

- Wang, X., Wang, Z., Wu, Z., and Cheng, F. (2014). “Shear behavior of basalt fiber reinforced polymer (frp) and hybrid frp rods as shear resistance members.” *Construction and Building Materials*, 73, 781–789.
- Wang, Z., Zhao, X.-L., Xian, G., Wu, G., Raman, R. S., Al-Saadi, S., and Haque, A. (2017). “Long-term durability of basalt- and glass-fibre reinforced polymer (bfrp/gfrp) bars in seawater and sea sand concrete environment.” *Construction and Building Materials*, 139, 467–489.
- Wei, B., Cao, H., and Song, S. (2010). “Tensile behavior contrast of basalt and glass fibers after chemical treatment.” *Materials and Design*, 31, 4244–4250.
- Wei, B., Cao, H., and Song, S. (2011). “Degradation of basalt fibre and glass fibre/epoxy resin composites in seawater.” *Corrosion Science*, 53(1), 426–431.
- Wu, G., Dong, Z.-Q., Wang, X., Zhu, Y., and Wu, Z.-S. (2014). “Prediction of long-term performance and durability of bfrp bars under the combined effect of sustained load and corrosive solutions.” *Journal of Composites for Construction*, 19(3), 04014058.
- You, Y.-J., Kim, J.-H. J., Kim, S.-J., and Park, Y.-H. (2015). “Methods to enhance the guaranteed tensile strength of gfrp rebar to 900 mpa with general fiber volume fraction.” *Construction and Building Materials*, 75, 54 – 62.
- Zych, T. and Wojciech, K. (2012). “Study on the properties of cement mortars with basalt fibres.” *Brittle Matrix Composites 10*, 155–166.

# Appendices

# Appendix A

## Individual Specimen Results

This appendix supplements the results chapter to present the individual test results for every tested specimen and the corresponding statistical results that were determined for each control and test group (of relevant specimen sets). The tables with individual specimen results are sorted by rebar type, size, lot, and specimen count. Dependent on the test procedure, the tables for the individual test results list the most essential (e.g. maximum specimen strength, displacement at maximum strength, etc.) data, while the statistical tables present the minimum ( $\wedge$ ), maximum ( $\wedge$ ), mean ( $\mu$ ), standard deviation ( $\sigma$ ), and coefficient of variation (CV) values. For the purpose of this research project, a wide variety of physical and mechanical tests were conducted on five specimens per sample of BFRP rebar materials. All statistical results that are presented in the main text above are based on those five individual specimen results.

### A.1 Density and Cross-Sectional Dimension Test

The following Table A.1 lists all specimen measurements and results that were determined to derive the BFRP rebar diameters according to ASTM D792 (ASTM-International, 2015b). The diameter and the cross-sectional area of the rebars were calculated from the measured density and the individual specimen volume and lengths.

Table A.1: Diameter measurements for each individual specimen

Specimen				Specimen Length				Weight				
Manuf. Type	Lot No.	Size #	Specimen No.	L1 mm	L2 mm	L3 mm	Average mm	a g	a+s g	b g	s g	$\delta$ M g
A	1	3	1	31.30	31.30	31.40	31.30	5.22	13.01	10.36	7.80	2.57
A	1	3	2	32.10	32.10	31.90	32.10	5.32	13.13	10.44	7.81	2.63
A	1	3	3	30.00	30.00	30.00	30.00	5.00	12.81	10.27	7.81	2.46
A	1	3	4	32.30	32.30	32.40	32.30	5.37	13.17	10.48	7.80	2.67
A	1	3	5	31.20	31.10	31.20	31.20	5.18	12.99	10.37	7.81	2.57
A	1	5	1	31.20	31.40	31.20	31.20	13.60	21.40	14.61	7.80	6.80
A	1	5	2	31.20	31.20	31.20	31.20	13.73	21.54	14.69	7.81	6.88
A	1	5	3	31.10	31.00	31.10	31.10	13.64	21.45	14.62	7.81	6.81
A	1	5	4	33.00	33.20	32.90	33.00	14.43	22.24	15.06	7.81	7.26
A	1	5	5	31.00	30.80	30.80	31.00	13.49	21.30	14.51	7.81	6.70
B	1	3	1	27.90	28.10	28.00	27.90	5.02	12.82	10.40	7.79	2.61
B	1	3	2	29.90	29.70	29.70	29.90	5.39	13.21	10.61	7.82	2.79
B	1	3	3	30.20	30.40	30.30	30.20	5.46	13.26	10.63	7.80	2.83
B	1	3	4	28.90	29.00	29.00	28.90	5.17	12.97	10.47	7.80	2.67
B	1	3	5	29.00	29.00	29.00	29.00	5.22	13.03	10.45	7.81	2.63
B	1	5	1	30.50	30.50	30.80	30.50	14.35	22.16	15.56	7.81	7.75
B	1	5	2	30.40	30.50	30.30	30.40	14.26	22.07	15.17	7.81	7.36
B	1	5	3	30.80	30.70	30.70	30.80	14.42	22.22	15.26	7.79	7.46
B	1	5	4	31.00	30.90	30.90	31.00	14.55	22.37	15.33	7.82	7.51
B	1	5	5	29.70	29.70	29.80	29.70	13.87	21.67	14.94	7.80	7.14
C	1	3	1	25.50	25.27	25.12	25.30	3.98	11.77	9.77	7.80	1.97
C	1	3	2	25.14	25.19	25.27	25.20	3.98	11.78	9.76	7.80	1.96
C	1	3	3	25.58	25.33	25.21	25.37	3.98	11.78	9.77	7.81	1.96
C	1	3	4	25.13	25.12	25.27	25.17	3.94	11.74	9.74	7.80	1.95
C	1	3	5	25.70	25.36	25.23	25.43	3.93	11.73	9.76	7.80	1.96
C	1	5	1	25.57	25.35	25.38	25.43	11.41	19.02	13.64	7.61	6.03
C	1	5	2	25.30	25.47	25.69	25.49	11.15	18.94	13.59	7.80	5.79
C	1	5	3	25.39	25.58	25.49	25.49	11.17	18.97	13.60	7.79	5.81
C	1	5	4	25.35	25.36	25.41	25.37	11.25	19.05	13.65	7.80	5.86
C	1	5	5	25.34	25.48	25.34	25.39	11.15	18.95	13.60	7.80	5.80
C	2	3	1	30.80	30.80	30.70	30.80	4.85	12.65	10.30	7.80	2.50
C	2	3	2	31.00	30.90	30.80	31.00	4.90	12.69	10.32	7.80	2.53
C	2	3	3	31.10	31.10	31.10	31.10	4.93	12.74	10.34	7.81	2.53
C	2	3	4	30.30	30.10	30.30	30.30	4.75	12.55	10.25	7.80	2.45
C	2	3	5	31.80	31.80	31.70	31.80	5.00	12.80	10.37	7.80	2.57
C	2	5	1	31.00	30.90	31.00	31.00	9.00	16.79	15.34	7.79	7.54
C	2	5	2	31.40	31.60	31.40	31.40	9.15	16.95	14.84	7.80	7.04
C	2	5	3	30.50	30.60	30.60	30.50	8.81	16.61	14.73	7.80	6.93
C	2	5	4	30.40	30.40	30.70	30.40	8.87	16.67	15.01	7.80	7.21
C	2	5	5	30.30	30.30	30.40	30.30	8.79	16.59	14.96	7.80	7.16

The specific gravity was calculated by dividing the measured dry mass of the sample by the weight of the submerged specimen. Subsequently, the density of the samples was determined by multiplying the specific gravity and the density of the water in which the specimen was submerged. Because the density of every substance depends on its temperature, the water temperature was monitored as described in ASTM. The water temperature measured 19.8° (67.6 °F) for this project, and hence, the distilled water had a density of 998.25 kg/m<sup>3</sup> (62.319 lbs./ft<sup>3</sup>). Then, the volume of the submerged

rebar section was determined by dividing the dry mass of the sample by the density of the water. Afterwards, the volume of the rebar sample was divided by the average length of the sample to calculate the cross-sectional area. Finally, the diameter was calculated based on the assumption that the shape of the rebars was round.

## A.2 Fiber Content Test

The relative amount of constituent materials were determined based on weight measurements after lost on ignition tests. The percentage of fiber content is listed in Table A.2 along with the relative resin and sand (surface coating) quantities.

c

Table A.2: Fiber content test results for each individual specimen

Specimen				Contents		
Manuf. Type	Lot No.	Size #	Spec No.	Fiber %	Resin %	Sand %
A	1	3	1	76.6	23.4	9.1
A	1	3	2	76.6	23.4	9.5
A	1	3	3	76.1	23.9	11.4
A	1	3	4	69.5	30.5	7.4
A	1	3	5	77.0	23.0	8.8
A	1	5	1	78.6	21.4	1.9
A	1	5	2	78.4	21.6	4.4
A	1	5	3	79.2	20.8	2.4
A	1	5	4	78.9	21.1	2.2
A	1	5	5	79.1	20.9	2.3
B	1	3	1	83.3	16.7	15.1
B	1	3	2	83.3	16.7	15.3
B	1	3	3	83.3	16.7	14.9
B	1	3	4	83.4	16.6	15.2
B	1	3	5	83.2	16.8	15.2
B	1	5	1	82.7	17.3	7.4
B	1	5	2	82.6	17.4	7.1
B	1	5	3	82.5	17.5	7.2
B	1	5	4	82.8	17.2	6.5
B	1	5	5	80.8	19.2	5.4
C	1	3	1	82.3	17.7	9.4
C	1	3	2	82.1	18.0	7.8
C	1	3	3	82.1	17.9	8.1
C	1	3	4	81.7	18.3	8.3
C	1	3	5	82.0	18.0	7.8
C	1	5	1	81.9	18.1	7.7
C	1	5	2	81.8	18.3	7.7
C	1	5	3	81.8	18.2	8.2

Continued on next page ...

Table A.2: Fiber content test results for each individual specimen

Specimen				Contents		
Manuf. Type	Lot No.	Size #	Spec No.	Fiber %	Resin %	Sand %
C	1	5	4	81.7	18.3	7.7
C	1	5	5	81.9	18.2	7.3
C	2	3	1	82.4	17.6	8.3
C	2	3	2	82.6	17.4	8.8
C	2	3	3	82.4	17.6	7.8
C	2	3	4	82.1	17.9	7.7
C	2	3	5	82.2	17.8	7.7
C	2	5	1	81.9	18.1	7.8
C	2	5	2	81.9	18.2	8.1
C	2	5	3	81.8	18.2	7.7
C	2	5	4	81.9	18.1	7.4
C	2	5	5	81.7	18.3	7.8

For rebar types that included sand as part of the surface enhancement, the weight of sand was subtracted before the fiber and resin content percentage were calculated to achieve comparable results throughout all tested rebar types, independent on the surface enhancement.

### A.3 Transverse Shear Test

The following Table A.3 displays the most important measurements and results related to the transverse shear strength test for every individual rebar specimen.

Table A.3: Transverse shear test results (ultimate values) for each individual specimen

Specimen				Transverse		Displacement	
Manuf. Type	Lot No.	Size #	Spec No.	Shear Strength		at Shear Strength	
				ksi	MPa	in.	mm
A	1	3	1	29.77	205	0.115	2.92
A	1	3	2	33.01	228	0.085	2.16
A	1	3	3	29.07	200	0.110	2.79
A	1	3	4	31.87	220	0.107	2.72
A	1	3	5	33.22	229	0.110	2.80
A	1	5	1	26.95	186	0.198	5.04
A	1	5	2	26.73	184	0.172	4.38
A	1	5	3	26.38	182	0.287	7.29
A	1	5	4	25.68	177	0.182	4.62
A	1	5	5	26.84	185	0.185	4.69
B	1	3	1	35.58	245	0.097	2.46

Continued on next page ...

Table A.3: Transverse shear test results (ultimate values) for each individual specimen

Specimen				Transverse		Displacement	
Manuf.	Lot	Size	Spec	Shear Strength		at Shear Strength	
Type	No.	#	No.	ksi	MPa	in.	mm
B	1	3	2	33.26	229	0.099	2.51
B	1	3	3	33.26	229	0.099	2.51
B	1	3	4	35.78	247	0.095	2.42
B	1	3	5	34.52	238	0.099	2.51
B	1	5	1	31.13	215	0.124	3.14
B	1	5	2	32.85	226	0.126	3.19
B	1	5	3	30.79	212	0.116	2.96
B	1	5	4	31.50	217	0.118	2.99
B	1	5	5	32.17	222	0.124	3.14
C	1	3	1	34.08	235	0.125	3.17
C	1	3	2	35.39	244	0.114	2.91
C	1	3	3	33.59	232	0.121	3.07
C	1	3	4	37.47	258	0.130	3.31
C	1	3	5	36.79	254	0.127	3.22
C	1	3	6	33.87	234	0.132	3.36
C	2	3	1	36.95	255	0.103	2.61
C	2	3	2	36.74	253	0.107	2.72
C	2	3	3	39.82	275	0.129	3.27
C	2	3	4	38.35	264	0.118	2.99
C	2	3	5	36.49	252	0.113	2.86
C	2	5	1	36.17	249	0.120	3.04
C	2	5	2	37.99	262	0.132	3.35
C	2	5	3	36.71	253	0.119	3.03
C	2	5	4	35.29	243	0.128	3.26
C	2	5	5	36.26	250	0.134	3.40

The shear strength results (based on the nominal diameter) and the corresponding cross-head displacements — measured at the same moment at which the maximum test load was reached and recorded — are provided.

## A.4 Horizontal Shear Test

Similar to the previous section, the following Table A.4 lists the maximum measured data for all specimens that were tested for horizontal shear strength.

Table A.4: Horizontal shear test results (ultimate values) for each individual specimen

Specimen				Horizontal		Displacement	
Manuf.	Lot	Size	Spec	Shear Strength		at Shear Strength	
Type	No.	#	No.	ksi	MPa	in.	mm
A	1	3	1	6.66	45.9	0.086	2.18
A	1	3	2	6.64	45.8	0.066	1.68
A	1	3	3	5.75	39.7	0.064	1.62
A	1	3	4	6.45	44.5	0.088	2.25
A	1	3	5	6.57	45.3	0.078	1.97
A	1	5	1	6.62	45.6	0.076	1.94
A	1	5	2	6.54	45.1	0.147	3.72
A	1	5	3	6.23	42.9	0.101	2.56
A	1	5	4	6.89	47.5	0.120	3.05
A	1	5	5	6.36	43.8	0.142	3.62
B	1	3	1	6.07	41.9	0.044	1.11
B	1	3	2	5.35	36.9	0.049	1.24
B	1	3	3	5.11	35.2	0.036	0.90
B	1	3	4	5.49	37.9	0.049	1.25
B	1	3	5	5.81	40.0	0.055	1.39
B	1	5	1	6.91	47.7	0.104	2.65
B	1	5	2	4.98	34.4	0.094	2.38
B	1	5	3	7.00	48.2	0.095	2.42
B	1	5	4	6.81	47.0	0.116	2.95
B	1	5	5	7.49	51.6	0.110	2.78
C	1	3	1	6.70	46.2	0.098	2.48
C	1	3	2	7.15	49.3	0.067	1.69
C	1	3	3	6.38	44.0	0.063	1.59
C	1	3	4	7.52	51.9	0.098	2.48
C	1	3	5	7.29	50.2	0.082	2.08
C	1	5	1	6.35	43.8	0.092	2.35
C	1	5	2	6.82	47.0	0.112	2.84
C	1	5	3	6.78	46.7	0.116	2.96
C	1	5	4	6.52	44.9	0.101	2.58
C	1	5	5	5.56	38.3	0.084	2.14
C	2	3	1	6.20	42.8	0.128	3.24
C	2	3	2	6.62	45.7	0.071	1.80
C	2	3	3	6.66	45.9	0.113	2.87
C	2	3	4	6.45	44.5	0.072	1.82
C	2	3	5	6.48	44.7	0.100	2.53
C	2	5	1	6.36	43.8	0.121	3.06
C	2	5	2	6.18	42.6	0.113	2.87
C	2	5	3	6.62	45.6	0.132	3.35
C	2	5	4	6.82	47.0	0.108	2.74
C	2	5	5	6.04	41.6	0.091	2.31

The given strength values were determined based on the measured maximum loads and the nominal (not measured) cross-sectional dimensions. The displacement at shear strength represents the cross-head extension that was measured at the instant in time at which the maximum failure load was

recorded. Accordingly, this value is indicative of the ultimate defection of the shear specimen that lead to resin failure and slip between the fibers.

## A.5 Tensile Test

The longitudinal tensile properties for all tested specimens are listed in Table A.5.

Table A.5: Tensile strength test results (ultimate values) for each individual specimen

Manuf. Type	Specimen			Tensile		Elastic	
	Lot	Size	Spec	Strength		Modulus	
	No.	#	No.	ksi	MPa	ksi	GPa
A	1	3	1	122	844	5760	39.72
A	1	3	2	120	828	6996	48.24
A	1	3	3	119	819	6917	47.69
A	1	3	4	128	883	6812	46.72
A	1	3	5	119	822	7735	53.33
A	1	5	1	128	881	7800	53.78
A	1	5	2	132	908	7645	52.71
A	1	5	3	138	949	7692	53.04
A	1	5	4	136	938	7639	52.67
A	1	5	5	138	951	7990	55.09
B	1	3	1	189	1302	7735	53.33
B	1	3	2	199	1371	7928	54.66
B	1	3	3	198	1365	7542	52.00
B	1	3	4	197	1361	7837	54.03
B	1	3	5	198	1367	7999	55.15
B	1	5	1	176	1211	7868	54.25
B	1	5	2	162	1116	7819	53.91
B	1	5	3	178	1226	8301	57.23
B	1	5	4	183	1263	7837	54.03
B	1	5	5	164	1131	7907	54.52
C	1	3	1	189	1306	7630	52.61
C	1	3	2	187	1290	7659	52.81
C	1	3	3	180	1238	7535	51.95
C	1	3	4	178	1229	5385	37.13
C	1	3	5	185	1276	7559	52.12
C	1	5	1	172	1184	4126	28.45
C	1	5	2	160	1107	6834	53.45
C	1	5	3	169	1168	7933	54.70
C	1	5	4	165	1137	6534	45.05
C	1	5	5	140	962	7739	53.36
C	2	3	1	171	1178	6990	48.19
C	2	3	2	170	1175	7509	51.78
C	2	3	3	168	1159	6531	45.03
C	2	3	4	175	1207	7881	54.34
C	2	3	5	161	1112	7088	48.87

Continued on next page ...

Table A.5: Tensile strength test results (ultimate values) for each individual specimen

Specimen				Tensile		Elastic	
Manuf.	Lot	Size	Spec	Strength		Modulus	
Type	No.	#	No.	ksi	MPa	ksi	GPa
C	2	5	1	153	1058	8138	56.11
C	2	5	2	146	1006	7242	49.93
C	2	5	3	145	1001	7404	51.05
C	2	5	4	150	1037	7065	48.71
C	2	5	5	144	992	7549	52.05

Specifically, the table presents the maximum tensile stresses and the corresponding elastic moduli, both based on the nominal cross-sectional dimensions.

## A.6 Bond-to-Concrete Test

The individual measured bond strength test results are listed in Table A.6 to report both the bond stresses and the rebar bond slippage for each specimen.

Table A.6: Bond-to-Concrete strength test results for each individual specimen (Imperial Units)

Specimen				Bond Stress			Bond Slippage		
Manuf. Type	Lot No.	Size #	Spec No.	at Specific Slippage			Ult. ksi	at Maximum Stress	
				$\frac{2}{1000}$ in. ksi	$\frac{4}{1000}$ in. ksi	$\frac{1}{100}$ in. ksi		Free End in.	Load End in.
A	1	3	1	1.55	1.93	2.54	3.56	0.059	0.080
A	1	3	2	1.31	1.87	3.30	4.07	0.022	0.070
A	1	3	3	1.68	2.12	2.90	3.95	0.060	0.085
A	1	3	4	0.94	1.39	2.01	3.20	0.100	0.123
A	1	3	5	2.21	2.50	3.01	4.08	0.067	0.082
A	1	5	1	1.01	1.71	2.62	3.89	0.054	0.074
A	1	5	2	0.36	0.70	1.55	3.59	0.097	0.119
A	1	5	3	1.24	1.75	2.73	4.16	0.070	0.092
A	1	5	4	0.82	1.37	2.13	3.89	0.105	0.110
A	1	5	5	0.82	1.22	1.83	3.33	0.083	0.106
B	1	3	1	1.60	1.94	2.35	2.39	0.015	0.020
B	1	3	2	1.42	1.77	2.60	2.80	0.017	0.023
B	1	3	3	2.45	2.79	3.03	3.05	0.013	0.018
B	1	3	4	1.96	2.28	2.66	2.67	0.010	0.017
B	1	3	5	1.81	2.26	2.86	3.03	0.018	0.021
B	1	5	1	2.01	2.54	2.83	2.85	0.014	0.026

Continued on next page . . .

Table A.6: Bond-to-Concrete strength test results for each individual specimen (Imperial Units)

Specimen				Bond Stress				Bond Slippage	
Manuf. Type	Lot No.	Size #	Spec No.	at Specific Slippage			Ult. ksi	at Maximum Stress	
				$\frac{2}{1000}$ in. ksi	$\frac{4}{1000}$ in. ksi	$\frac{1}{100}$ in. ksi		Free End in.	Load End in.
B	1	5	2	2.14	2.49	2.80	2.81	0.012	0.024
B	1	5	3	1.98	2.37	2.79	2.88	0.017	0.027
B	1	5	4	2.21	2.66	2.89	2.90	0.013	0.023
B	1	5	5	2.29	2.66	2.94	2.95	0.012	0.035
C	1	3	1	2.06	2.28	2.42	2.43	0.009	0.016
C	1	3	2	1.90	2.22	2.34	2.35	0.008	0.011
C	1	3	3	2.04	2.28	2.38	2.39	0.009	0.016
C	1	3	4	1.62	2.21	2.27	2.27	0.008	0.013
C	1	3	5	1.49	1.89	2.23	2.24	0.010	0.012
C	1	5	1	2.43	2.78	3.00	3.01	0.011	0.038
C	1	5	2	2.30	2.59	2.94	2.96	0.011	0.027
C	1	5	3	2.30	2.59	2.95	2.98	0.013	0.030
C	1	5	4	2.29	2.71	2.96	2.97	0.012	0.028
C	1	5	5	2.18	2.45	2.84	2.89	0.015	0.024

Because ACI 440.3R suggests documenting the slippage behavior through the bond stress measurements at specific rebar slip instances, the table presents not just the ultimate bond stress (strength) but also the bond stresses that corresponded to slip values of  $\frac{2}{1000}$  in.,  $\frac{4}{1000}$  in., and  $\frac{1}{100}$  in. For clarity, the table lists all results in imperial units only.

Similar to the previous table, Table A.7 documents the bond-to-concrete measurement results for all tested specimens per ASTM requirements.

Table A.7: Bond-to-Concrete strength test results for each individual specimen (Metric Units)

Specimen				Bond Stress				Bond Slippage	
Manuf. Type	Lot No.	Size #	Spec No.	at Specific Slippage			Ult. MPa	at Maximum Stress	
				$\frac{5}{100}$ mm MPa	$\frac{1}{10}$ mm MPa	$\frac{1}{4}$ mm MPa		Free End mm	Load End mm
A	1	3	1	10.7	13.3	17.5	24.5	1.49	2.02
A	1	3	2	9.1	12.9	22.8	28.0	0.56	1.77
A	1	3	3	11.6	14.6	20.0	27.2	1.53	2.16
A	1	3	4	6.5	9.6	13.9	22.1	2.54	3.13
A	1	3	5	15.3	17.3	20.7	28.2	1.69	2.09
A	1	5	1	6.9	11.8	18.0	26.8	1.38	1.89
A	1	5	2	2.5	4.8	10.7	24.7	2.48	3.02

Continued on next page ...

Table A.7: Bond-to-Concrete strength test results for each individual specimen (Metric Units)

Specimen				Bond Stress			Bond Slippage		
Manuf. Type	Lot No.	Size #	Spec No.	at Specific Slippage			Ult. MPa	at Maximum Stress	
				$\frac{5}{100}$ mm MPa	$\frac{1}{10}$ mm MPa	$\frac{1}{4}$ mm MPa		Free End mm	Load End mm
A	1	5	3	8.6	12.1	18.8	28.7	1.78	2.34
A	1	5	4	5.7	9.4	14.7	26.9	2.67	2.79
A	1	5	5	5.6	8.4	12.6	23.0	2.11	2.70
B	1	3	1	11.0	13.4	16.2	16.5	0.37	0.50
B	1	3	2	9.8	12.2	17.9	19.3	0.42	0.58
B	1	3	3	16.9	19.3	20.9	21.0	0.32	0.45
B	1	3	4	13.5	15.7	18.4	18.4	0.25	0.44
B	1	3	5	12.5	15.6	19.7	20.9	0.45	0.54
B	1	5	1	13.9	17.5	19.5	19.7	0.36	0.65
B	1	5	2	14.7	17.2	19.3	19.4	0.31	0.62
B	1	5	3	13.7	16.4	19.3	19.9	0.43	0.68
B	1	5	4	15.2	18.3	19.9	20.0	0.32	0.59
B	1	5	5	15.8	18.4	20.3	20.4	0.30	0.88
C	1	3	1	14.2	15.7	16.7	16.7	0.24	0.40
C	1	3	2	13.1	15.3	16.1	16.2	0.20	0.29
C	1	3	3	14.0	15.7	16.4	16.4	0.24	0.40
C	1	3	4	11.2	15.2	15.6	15.7	0.21	0.32
C	1	3	5	10.3	13.1	15.4	15.4	0.24	0.30
C	1	5	1	16.8	19.2	20.7	20.8	0.28	0.96
C	1	5	2	15.8	17.9	20.2	20.4	0.28	0.68
C	1	5	3	15.9	17.8	20.3	20.5	0.34	0.75
C	1	5	4	15.8	18.7	20.4	20.5	0.29	0.71
C	1	5	5	15.1	16.9	19.6	19.9	0.37	0.62

However, other than the previous table, Table A.7 offers the test results in metric units. Accordingly, the relevant bond stresses are tabulated for measurements corresponding to 0.05 mm, 0.10 mm, and 0.25 mm of rebar slip.

## **Appendix B**

### **FDOT Materials Manual, Section 12.1 – BFRP Rebar Producer updates**

(16 pages)

## **Section 12.1**

### **Volume II**

# **FIBER REINFORCED POLYMER COMPOSITES**

### **12.1.1 PURPOSE**

This procedure provides guidance for the development and implementation of the quality control plan for the manufacture, storage, and transportation of fiber reinforced polymer composites for Florida Department of Transportation (FDOT) projects. Fiber reinforced polymer composites, hereinafter referred to as composites, include ~~for example:~~ glass, carbon, ~~aramid,~~ and basalt reinforced polymeric materials.

### **12.1.2 AUTHORITY**

Code of Federal Regulations (CFR), Federal-Aid Policy Guide (FAPG), Subchapter G – Engineering and Traffic Operations, Part 637 – Construction Inspection and Approval, Subpart B – Quality Assurance Procedures for Construction

Sections 20.23(3)(a) and 334.048(3), Florida Statutes.

### **12.1.3 REFERENCES**

Design Standards, Topic No. 625-010-003, Florida Department of Transportation

Florida Department of Transportation Standard Specifications for Road and Bridge Construction

American Society for Testing and Materials (ASTM) Standard Test Methods and Specifications, Philadelphia, Pennsylvania

American Association of State Highway and Transportation Officials (AASHTO), Part I Specifications, and Part II Tests, Washington, D.C.

Field Sampling and Testing Manual, Florida Department of Transportation

US Department of Transportation Federal Aviation Administration, Advisory Circular AC No. 21-26A

## 12.1.4 SCOPE

This procedure is used by composite producers to perform the required inspections and testing of composites during and after manufacturing. These requirements and activities pertain to the inspections, measurements and necessary tests to substantiate that materials and composites are in conformity with the contract documents. The quality control plans provide the guidelines utilized by producers to consistently manufacture quality composite products in conformance with the **FDOT Specifications** and other **Contract Documents**.

## 12.1.5 GENERAL INFORMATION

Producers are responsible for the production, inspection, documentation, storage and shipment of the composites. The composites delivered to the project shall meet the requirements of the **FDOT Specifications** and other **Contract Documents**.

## 12.1.6 PLANT QUALIFICATION PROCESS

### 12.1.6.1 General

Prepare the proposed Quality Control Plan (QCP) in accordance with **Materials Manual Section 5.6**.

The QCP shall include procedures that ensure the quality of all incoming raw materials, the control of in-process manufacturing, and testing performed to evaluate the end product for conformity to contract requirements. In addition, the QCP shall include test standards to be used for nondestructive and destructive evaluations, visual inspection techniques during the manufacturing process, and product final acceptance. These standards define the acceptance or rejection criteria of manufacturing induced defects.

### 12.1.6.2 Review of Plant's Proposed Quality Control Plan

Submit the proposed QCP to the State Materials Office (SMO). Upon the producer's submittal of their QCP, the SMO will review the proposed QCP and make the necessary arrangements for the initial manufacturing facility qualification review in accordance with **Section 12.1.6.3**.

In the QCP, include the work experience, qualifications, and responsibilities of the production and quality control personnel. Identify

the on-site Production Manager, General Manager, Quality Control Inspectors/Technicians, and Quality Control Manager. Identify the responsibilities for monitoring key quality attributes and quality control data. Include the applicable information required in **FDOT Specifications Section 105**. Include a copy of any available repair methods frequently utilized to repair minor deficiencies.

#### 12.1.6.3 Manufacturing Facility Qualification Review

The Department will perform an initial qualification review of producers that intend to manufacture composites for the Department. An initial review is required for producers that submit their QCP and also for producers that have not provided products for the Department in excess of one year. In addition, routine manufacturing facility qualification reviews will be performed at least annually for all active producers.

#### 12.1.6.4 Maintenance of Producer's Qualification

Upon the Department's satisfactory review of the proposed QCP, in compliance with **Materials Manual Section 5.6**, and satisfactory manufacturing facility qualification reviews, the SMO will accept the proposed QCP and include the producer the Department's **Production Facility Listing**. Any changes to a QCP must be submitted to the SMO and accepted prior to manufacturing product for the Department.

Producers that are on the Department's **Production Facility Listing** will be inspected in accordance with **FDOT Specifications Section 105** and the **Materials Manual**.

### 12.1.7 FUNCTIONS AND RESPONSIBILITIES OF COMPOSITE PRODUCER

#### 12.1.7.1 General

Producers are responsible for the quality of their finished composites. Facilities and qualified personnel must be provided to perform specified inspections and tests and maintain an acceptable QCP in compliance with the requirements specified herein and in applicable **FDOT Specifications Section 973**.

#### 12.1.7.2 Quality Control Manager

The Quality Control Manager shall ensure that the quality of the products

at each manufacturing facility meets the quality requirements of the contract documents. The Quality Control Manager may serve in more than one manufacturing facility. The responsibilities of the Quality Control Manager include, but are not limited to, the following:

- A. Maintain the quality control approval label and apply it to acceptable composites, or designate a qualified Quality Control Technician, who is working under the direct supervision of the Quality Control Manager to apply the plant approval label.
- B. Be present, or designate a Quality Control Technician/Inspector working under the direct supervision of the Quality Control Manager to be present during the production of all composites that will be shipped to Department projects.
- C. Perform and/or supervise the quality control testing and inspection.
- D. Ensure that the producer has a sufficient number of Quality Control Technician(s)/Inspector(s) to maintain adequate inspection and testing during the production of composites for Department projects. In lieu of permanent staff, testing at the plant may be performed by an engineering consulting firm or laboratory meeting the requirements of FDOT **Specifications Section 105**.
- E. Ensure that the testing equipment is maintained and calibrated in accordance with the applicable test methods and **Specifications**.
- F. Ensure that all inspections are performed by a qualified technician. Each composite product shall be inspected before shipment to the project site. Implement effective controls including Non-Destructive Inspection (NDI) techniques that result in a product meeting the **Contract Documents**. These control processes shall be included in the QCP and approved by the Department. The following shall be addressed:
  1. A QCP including approved NDI procedures to be used.
  2. Periodic qualification of personnel conducting inspections. This includes regularly scheduled vision examinations and inspection of a standard with a known defect.
  3. Establish realistic acceptance standards for use by process and final inspection personnel.

4. Calibration of equipment used in the inspection. Include any standard with known defects that is used for comparison. The calibration procedure shall provide for periodic requalification of any such equipment at specific time intervals.
  5. An internal audit program that validates the effectiveness of the NDI.
- G. Ensure that all materials used in the manufacture of the composites are from sources that meet the **FDOT Specification** requirements.
  - H. Maintain a daily production log that, at a minimum, includes fiber lot numbers, resin lot numbers, composite lot numbers, sizes and number of composites produced.
  - I. Ensure that all composites are properly stored and marked with the producer's name and other information that is required in the applicable ASTM or AASHTO Standards.
  - J. Maintain the files of material certifications, test data, and inspection results.
  - K. Arrange meetings with the Verification Inspector as needed.
  - L. Provide certifications attesting to applicable specification compliance and include a detailed listing of the composite type, size and quantities.
  - M. Ensure that the composite joints/connections comply with any requirements of **FDOT Specifications**. In addition, perform any required testing on a periodic basis to ensure continuing compliance. Any testing required by the Department must be conducted in the presence of a representative of the Department.

## 12.1.8 QUALITY CONTROL OF ~~CERTIFIED~~ RAW MATERIALS

### 12.1.8.1 General

The producer shall have an incoming material acceptance plan that ensures raw materials purchased to produce composite products are in conformance with the **FDOT Specifications**. Laboratory test reports that document actual test results for each batch of material received must be provided for review and approval. A material supplier's test report alone is not adequate documentation to substantiate that materials satisfy all

**FDOT Specification** requirements. Samples of these materials shall be taken on a batch-to-batch basis and tested to verify the accuracy of suppliers' laboratory reports. Sample testing may be performed by the producer at their production facility or by an independent laboratory identified in the producer's QCP. Testing frequency shall be based on historical test results and may be decreased over time if results indicate that a source supplies consistent materials.

### 12.1.8.2 Fiber Reinforcements

The producer shall establish procedures in coordination with its material suppliers to control the quality of raw materials sources. For example, fibrous materials such as roving, tow, and fabric shall be tested for physical properties including tensile and modulus of elasticity. In addition, a means shall be developed to control the quality of fiber surface treatments, sizing, etc. —Department Verification Inspectors may take samples, at each facility, from randomly selected LOTs at any time. A LOT is the entire volume of fibers represented by the raw material supplier's test report or the fiber producer's lot number.

Each LOT of basalt fibers must meet the requirements of Table 1 when tested using X-ray fluorescence (XRF). In addition, the fibers must be coated (sized) with a chemical intended for, and compatible with both the fibers and the polymer matrix system.

<u>Table 1</u> <u>Chemical Constituent Requirements</u> <u>for Basalt Fibers</u>	
<u>Constituent/Parameter</u>	<u>Content by Weight %</u>
<u>SiO<sub>2</sub></u>	<u>50-60</u>
<u>Al<sub>2</sub>O<sub>3</sub></u>	<u>7-20</u>
<u>Fe<sub>2</sub>O<sub>3</sub> + FeO</u>	<u>7-15</u>
<u>CaO</u>	<u>6-12</u>
<u>MgO</u>	<u>3-9</u>
<u>Na<sub>2</sub>O</u>	<u>&lt; 5</u>

<u>Table 1</u> <u>Chemical Constituent Requirements</u> <u>for Basalt Fibers</u>	
<u>Constituent/Parameter</u>	<u>Content by Weight %</u>
<u>TiO<sub>2</sub></u>	<u>0.1-2</u>
<u>K<sub>2</sub>O</u>	<u>&lt; 5</u>
<u>MnO</u>	<u>&lt; 0.25</u>
<u>SO<sub>3</sub></u>	<u>&lt; 0.2</u>
<u>Acidity Modulus (M<sub>a</sub>),</u> <u>calculated using weight percentages of oxides by:</u>  <u>(SiO<sub>2</sub> + Al<sub>2</sub>O<sub>3</sub>)/(CaO + MgO)</u>	<u>&gt; 1.8</u>
<u>Viscosity Modulus (M<sub>v</sub>),</u> <u>calculated using molar ratios of oxides by:</u>  <u>(SiO<sub>2</sub> + Al<sub>2</sub>O<sub>3</sub>)/</u> <u>(2Fe<sub>2</sub>O<sub>3</sub> + FeO + CaO + MgO + K<sub>2</sub>O + Na<sub>2</sub>O)</u>	<u>2-3</u>

### 12.1.8.3 Polymer Matrix Systems

The producer shall require chemical characterization tests of the matrix material. The producer's material specification shall define the combinations of acceptable test techniques and test results required to adequately demonstrate the material's conformity and process capability. Techniques for chemical characterization are not universal, but are strongly dependent upon the resin formulation. Therefore, test methods adapted to each material shall be developed appropriately considering the sensitivity of the method to detect deviations in formulation.

A representative of the Department may obtain verification samples at the source or at the composite manufacturing facility. The polymer resins shall be stored such that contamination and environmental degradation do not occur. A certification for each LOT of resin is required and resins shall be identified by the resin producer's LOT number. A LOT is defined as the

entire volume of material produced under uniform conditions and represented by the LOT number.

#### A. Thermosetting Resins

A typical material specification for thermosetting resin systems identifies upper and lower limits on the concentration of reactive functional group(s), viscosity, color, and moisture content. The characterization tests shall measure and identify the amount of individual constituents of the resin system such as the basic epoxide, curing agent, accelerator, hardener, reaction time, and the conversion of reactants upon resin mixing. Also, storage, fiber impregnation, and other processes relevant to the production of finished products shall be identified.

#### B. Thermoplastic Resins

Thermoplastic resins typically require evaluation of the incoming material that includes monitoring the melt index and density to ensure conformity with material requirements. For post-consumer resins, additional requirements must be met. These include moisture content and quantification of any other contamination level, as well as meeting quality targets for the final products. The quality of the final product can be measured with a variety of test methods, including melt index, tensile strength, density, or quantitative chemical analysis: by color (colorimetry), differential scanning calorimetry (DSC), infrared spectroscopy.

#### 12.1.8.4 Preimpregnated Materials (Prepreg)

In applications where prepreg tape, fabric, or roving are primary constituents of the composite produced, it is necessary to test for the chemical, physical, and mechanical fiber and matrix dominated properties identified in the applicable prepreg material specification. QCP procedures previously described in **Section 12.1.6.1** for resins and fibers may be used to control the quality of incoming prepreg raw materials. Chemical characterization shall be performed on resin extracted from the prepreg material intended for production, where applicable.

#### 12.1.8.5 Adhesives

The QCP procedures recommended for structural adhesives are similar to those utilized for resin matrix systems; that is, the procedures shall

provide assurance that each incoming batch or lot conforms to the chemical, physical, and mechanical properties identified in the material specification.

#### **12.1.8.6 Coatings**

The producer of the coatings shall provide certification indicating compliance with the manufacturer's requirements. A copy of the certification of compliance shall be maintained by the producer in the Quality Control file. The Verification Inspector may sample the coating material at any time.

### **12.1.9 QUALITY CONTROL OF COMPOSITE MANUFACTURING**

The QCP shall establish, implement, and verify that (1) the parameters affecting material integrity and process capability are operating under controlled conditions; and (2) individual items, batches, or LOTS conform to specified quality standards. To ensure that the QCP objectives have been met, process procedures shall clearly define specific materials, tooling, equipment, cure cycle parameters, quality standards, operator qualifications, storage and handling requirements, traceability records, and any other relevant documents or requirements.

The producer shall develop integrated quality and production control procedures for operations that define product configuration, selection of materials, tooling and facility equipment, calibration, sequence of manufacturing operations, critical in-process parameters and processing tolerances, and conformity to quality standards.

The producer shall establish a program to properly train and qualify operators. This program shall measure operator performance to production standards and provide for qualification as necessary.

Before production, manufacturing processes shall be qualified by demonstrating that the combination of materials, tooling, equipment, procedures, and other controls making up the process will produce parts having consistent material properties that conform to design requirements. As part of the process qualification, appropriate destructive inspection and NDI of appropriate tool proofing specimens shall be conducted to determine conformity to specified design requirements. Destructive tests of specimens verify conformity to the specified physical and mechanical properties. NDI of specimens verifies that discrepancies caused by manufacturing procedures remain within allowable limits.

### **12.1.9.1 Fabrication Equipment**

Inspect manufacturing equipment daily and at the beginning of each production run. Inspect all components that are an integral part of the manufacturing equipment. Check all adjustable components for proper adjustment for the type and size of composite being produced.

### **12.1.9.2 Calibration of Equipment**

Ensure that all equipment is checked and calibrated for compliance with the requirements of applicable ***FDOT Specifications***. Calibrations must be performed at least annually or more frequently if conditions merit.

### **12.1.9.3 Quality Control of Composite Manufacturing Process**

After the initial process qualification, testing for conformity to design requirements shall continue regularly to ensure that the manufacturing process, materials, and associated tooling continue to operate in a state of control and produce conforming product.

A. The following are manufacturing controls unique to the manufacturing of parts such as laminate and wet layup, filament winding, pultrusion, and other molding methods that a QCP shall include:

#### **1. Laminate layup**

- a. Standards and methods shall be established to ensure the proper orientation, stacking, and nesting of the plies during lay up operations. The programs that control tape head and table motions, and tape feed and tape stacking, shall be addressed in the QCP. Standards shall be established for such in-process variables as tape orientation, gaps, and overlap.
- b. For automatic and hand layup methods, controls shall be established for in-process variables that affect the cured laminate quality, for example, resin content, ply compaction, laminate density, porosity that may result from debulking, pre-bleeding, and bagging operations.

#### **2. Wet layup**

- a. Procedures shall be established to ensure the correct material selection, orientation and stacking, or nesting of the plies during wet layup operations.

- b. Procedures shall be established to control in-process variables such as resin content, aeration, and air pockets.
  3. Filament winding.
    - a. Preimpregnated filaments for dry winding shall be stored and handled according to procedures similar to those for other prepreg materials to ensure that the material's original properties have been maintained, especially material flow and tack to ensure proper bonding for subsequent winding operations.
    - b. Establish procedures to ensure that the working life of the resin system exceeds the anticipated winding time and to ensure gelation does not take place before completion of winding.
    - c. Establish procedures to control machine-dominant parameters such as feed rate, feeder arm and mandrel motions, mandrel dwell angle, number of circuits per pattern, total number of circuits for complete coverage, number of plies per layer, winding angle, fiber tension and alignment, bandwidth, fiber/resin ratio, etc.
    - d. Establish procedures to control process variables during the winding operation such as resin viscosity, fiber wetting, fiber tension, fiber bandwidth and alignment, air entrapment, degree of compaction, fiber damage, etc.
  4. Pultrusion.
    - a. Establish procedures to control pultrusion start-up, steady state, and shutdown operations including compliance of material produced during start-up and shutdown operations.
    - b. Establish process procedures that define operating limits for important process parameters critical to product quality such as line speed, die temperature profile for the particular operating conditions and resin system, clamping pull-through lead, resin temperature, die input temperature, material orientation for preform operation, and material tension.
  5. Other Molding Methods.

- a. For techniques such as resin injection, compression, and transfer molding processes, specifications shall define the limits for all critical process parameters that determine product quality. Such parameters are, for example, resin mix, feed-rate and feed temperature, mold temperature, and back pressure or vacuum. In addition, molding process specifications shall identify the timing and sequence of automatic operations. These critical parameters shall be defined in the process specification and identified in the associated production records.

#### B. Curing process.

1. Develop procedures to control the critical parameters of the process, namely chemical reactions of the resin and consolidation of the plies to achieve manufacturing consistency and quality parts that are of uniform consolidation, within void tolerances, and of correct fiber volume.
2. Procedures shall define the relationship of the variables (time, temperature, pressure) in the cure cycle (and post-cure cycles) that control compaction and consolidation and cure reaction. These control variables shall include the acceptable limits and the appropriate action to be taken when such limits are exceeded. For example, submit cured parts through the QCP for evaluation and disposition.

## 12.1.10 QUALITY CONTROL TESTING AND INSPECTION OF COMPOSITES

### 12.1.10.1 General

Perform the quality control inspections and/or testing specified in the applicable AASHTO and ASTM Standards for each type of composite, unless modified by the Specifications. Additional tests applicable to specific composite products shall be identified by the producer as part of their quality control/quality assurance program.

### 12.1.10.2 Quality Control Tests

The QCP shall include the test methods, inspections, and minimum frequencies that are used as the basis of acceptance for each type of composite. Dimensional checks for length, width, thickness, and diameter shall be made and recorded at the minimum frequency of twice daily.

Composite density (i.e. weight per linear foot) shall be either continuously monitored or determined twice daily. Tests of composite stiffness, environmental crack resistance and impact resistance shall be made for each production run or whenever production of a new lot begins or supply changes or when the manufacturing process changes. The Director, Office of Materials may approve or direct modifications to the frequency of tests based on the performance history of the producer.

Index tests derived from existing test methods may be developed and implemented by the producer for quality control/quality assurance purposes subject to the approval of the Director, Office of Materials.

### **12.1.10.3 Test on Composite Joints/Connections**

When requested by the Department, perform a joint/connection test in accordance with ASTM D-4762, as applicable, at the pressures appropriate for the application. Perform these tests in the presence of the Quality Control Manager. Notify the SMO with enough prior notice to witness the testing.

## **12.1.11 APPEARANCE AND INSPECTION OF ~~FINAL~~ FINISHED COMPOSITES**

Perform final inspection of the finished composites, before the application of the quality control approval label. Final acceptance requirements and QCP procedures shall provide added assurance that the completed structure meets its functional and design requirements. Minor deficiencies may be repaired in accordance with the repair methods included as part of the approved QCP, or by approval of the Director, Office of Materials.

Acceptance of a LOT of composite components:

- A. All tests and inspection results shall meet the requirements of the contract documents.

Final acceptance records shall provide evidence that the following production and QCP activities have been completed:

1. Incoming material acceptance;
2. Production and assembly controls;
3. Maintenance of tooling and facility equipment;

4. Calibration of inspection and laboratory test equipment;
  5. Inspection acceptance of functional characteristics at detail and assembly levels;
  6. Nondestructive inspection acceptance;
  7. Configuration control; and
  8. Any other requirements
- B. The producer has completed all patching and repair work.
- C. The Quality Control Manager has labeled the composites.
- D. The list of the composites and producer's certification statement is included with each shipment of the composites to the project site.
- E. Prior to shipment, a certification, notarized by the producer, is sent to the project indicating that the composites meet contract documents.

### 12.1.12 HANDLING AND STORAGE

Composite materials and structures require specific handling procedures to protect them from damage during production and storage. Accordingly, procedures for handling and storing composite materials and structures shall be established and followed. These procedures shall be an integral part of the producer's QCP and shall provide protection during receiving inspection, material storage, material handling, manufacturing process, cure cycle, final inspection, and final product storage. Clearly identify rejected components and do not store them in the same area with compliant composites.

### 12.1.13 QUALITY CONTROL LABELS

The producer's Quality Control Manager shall affix a label to each section of composite, indicating that the manufactured composite meets the requirements of the ~~contract—documents~~ Contract Documents. The producer's QC approval label shall be indelible and legible, and applied to each composite before its shipment from the manufacturing facility to the project site.

The label shall include the producer's identity, LOT number and the date of final quality control inspection. The date of final quality control inspection

shall be written in indelible ink or be mechanically imprinted. The label shall consist of a pre-printed polymer sticker or as may be approved by the Director, Office of Materials. An example of the label shall be included in the QCP.

#### **12.1.14 SHIPMENT**

Address the producer's shipping policy as part of the QCP.

Ensure that each shipment of composites to the project site is accompanied with a signed or stamped delivery ticket providing the description and the list of the products. The list of the products with each delivery ticket shall include as a minimum, project number, date shipped, lot numbers, identification and quantity.

#### **12.1.15 DOCUMENTATION**

The Quality Control Manager shall maintain the following documentation for a period of three years after the delivery of the composites to the project site. The documentation shall as a minimum include the following items:

- A. A copy of the QCP
- B. Approved design/shop drawings (if applicable)
- C. Applicable ASTM and AASHTO Standards
- D. ***FDOT Specifications and Design Standards***
- E. The names of all quality control personnel and qualifications
- F. All material certification records
- G. Equipment calibration records, including composite forming machines and test equipment
- H. LOT numbers for the materials and composites produced
- I. Number and type of composites in each LOT
- J. All applicable test data
- K. Record of the list of the delivered composites

- L. Record of all deficiencies found as a result of quality control/quality assurance activities and the corrective action taken. A copy of the deficiency reports shall also be maintained for the three-year period as described above.

## 12.1.16 TRAINING

The producer shall establish and implement a training program for all personnel that perform testing of product used for Department projects. The training must include knowledge of all **Specifications** related to the products being manufactured. All training shall be documented and provided to the Department upon request. The producer's training must be approved by the Department.

## 12.1.17 FORMS

- 12.1.17.1. There are no forms associated with this procedure.

## **Appendix C**

### **FDOT Materials Specification - Section 932-3 BFRP Rebar updates**

(11 pages)



*Florida Department of Transportation*

RON DESANTIS  
GOVERNOR

605 Suwannee Street  
Tallahassee, FL 32399-0450

KEVIN J. THIBAUT, P.E.  
SECRETARY

August 23, 2019

Khoa Nguyen  
Director, Office of Technical Services  
Federal Highway Administration  
3500 Financial Plaza, Suite 400  
Tallahassee, Florida 32312

Re: State Specifications Office  
Section: **932**  
Proposed Specification: **9320300 Nonmetallic Accessory Materials for Concrete Pavement and Concrete Structures.**

Dear Mr. Nguyen:

We are submitting, for your approval, two copies of the above referenced Supplemental Specification.

The changes are proposed by Steve Nolan of the State Structures Design Office to add basalt (BFRP) rebar as an equivalent option to GFRP rebar.

Please review and transmit your comments, if any, within two weeks. Comments should be sent via email to [stefanie.maxwell@dot.state.fl.us](mailto:stefanie.maxwell@dot.state.fl.us).

If you have any questions relating to this specification change, please call me at 414-4130.

Sincerely,

Signature on file

Daniel Strickland, P.E.  
State Specifications Engineer

DS/dt

Attachment

cc: Florida Transportation Builders' Assoc.  
State Construction Engineer

## NONMETALLIC ACCESSORY MATERIALS FOR CONCRETE PAVEMENT AND CONCRETE STRUCTURES.

(REV ~~6-26-197-8-198-23-19~~)

SUBARTICLE 932-3 is deleted and the following substituted:

### 932-3 Fiber Reinforced Polymer (FRP) Reinforcing Bars.

**932-3.1 General:** Obtain FRP reinforcing bars from producers currently on the Department's Production Facility Listing. Producers seeking inclusion on the list shall meet the requirements of Section 105.

Use only solid, round, thermoset basalt fiber reinforced polymer (BFRP), glass fiber reinforced polymer (GFRP) or carbon fiber reinforced polymer (CFRP) reinforcing bars. Bars shall be manufactured using pultrusion, variations of pultrusion, or other suitable processes noted in the producer's Quality Control Plan, subject to the approval of the State Materials Office (SMO). For BFRP and CFRP bars only vinyl ester or epoxy resin systems are permitted. For GFRP, use only bars manufactured using vinyl ester resin systems and glass fibers classified as E-CR that meet the requirements of ASTM D578.

**932-3.2 Bar Sizes and Loads:** The sizes and loads of FRP reinforcing bars shall meet the requirements in Table 3-1. The measured cross-sectional area, including any bond enhancing surface treatments, shall be determined according to Table 3-2.

Bar Size Designation	Nominal Bar Diameter (in)	Nominal Cross Sectional Area (in <sup>2</sup> )	Measured Cross-Sectional Area (in <sup>2</sup> )		Minimum Guaranteed Tensile Load (kips)	
			Minimum	Maximum	<u>BFRP and GFRP Bars</u>	CFRP Bars
2	0.250	0.049	0.046	0.085	6.1	10.3
3	0.375	0.11	0.104	0.161	13.2	20.9
4	0.500	0.20	0.185	0.263	21.6	33.3
5	0.625	0.31	0.288	0.388	29.1	49.1
6	0.750	0.44	0.415	0.539	40.9	70.7
7	0.875	0.60	0.565	0.713	54.1	-
8	1.000	0.79	0.738	0.913	66.8	-
9	1.128	1.00	0.934	1.137	82.0	-
10	1.270	1.27	1.154	1.385	98.2	-

**932-3.3 Material Requirements:** Producers shall submit to the State Materials Office (SMO), a test report of the physical and mechanical property requirements in Table 3-2 and Table 3-3 as applicable for the types and sizes of FRP reinforcing produced. Qualification testing shall be conducted by an independent laboratory approved by the Department for performing the FRP test methods.

Three production LOTS shall be randomly sampled at the production facility by a designee of the ~~State Materials Office~~. The minimum number of specimens per production LOT shall be as indicated in Table 3-2 and Table 3-3. The coefficient of variation (COV) for each test result shall be less than 6%. Outliers shall be subject to further investigation per ASTM E178. If the COV exceeds 6%, the number of test specimens per production LOT may be doubled, a maximum of two times, to meet the COV requirement. Otherwise, the results shall be rejected. A production LOT is defined as a LOT of FRP reinforcing produced from start to finish with the same constituent materials used in the same proportions without changing any production parameter, such as cure temperature or line speed.

Property	Test Method	Requirement	Specimens per LOT
Fiber Mass Fraction	ASTM D2584 or ASTM D3171	$\geq 70\%$	5 <sup>n</sup>
Short-Term Moisture Absorption	ASTM D570, Procedure 7.1; 24 hours immersion at 122°F	$\leq 0.25\%$	5 <sup>m</sup>
Long-Term Moisture Absorption	ASTM D570, Procedure 7.4; immersion to full saturation at 122°F	$\leq 1.0\%$	5 <sup>m</sup>
Glass Transition Temperature (T <sub>g</sub> )	ASTM D7028 (DMA) or ASTM E1356 (DSC; T <sub>m</sub> )/ASTM D3418 (DSC; T <sub>mg</sub> )	$\geq 230^\circ\text{F}$  $\geq 212^\circ\text{F}$	3 <sup>m</sup>
Total Enthalpy of Polymerization (Neat Resin)	ASTM E2160	Identify the resin system used for each bar size and report the average value of three replicates for each system	--
Degree of Cure	ASTM E2160	$\geq 95\%$ of Total polymerization enthalpy	3 <sup>n</sup>
Measured Cross-Sectional Area	ASTM D7205	Within the range listed in Table 3-1	10 <sup>n</sup>
Guaranteed Tensile Load <sup>a</sup>		$\geq$ Value listed in Table 3-1	
Tensile Modulus		$\geq 6,500$ ksi for <b>BFRP and GFRP</b> $\geq 18,000$ ksi for CRFP	
Alkali Resistance with Load	ASTM D7705; 3 months test duration, followed by tensile strength per ASTM D7205	$\geq 70\%$ Tensile strength retention	5 <sup>m</sup>
Transverse Shear Strength	ASTM D7617	$> 22$ ksi	5 <sup>n</sup>
<b>Horizontal Shear</b>	<b>ASTM D4475</b>	<b><math>\geq 5.5</math> ksi</b>	<b>5<sup>n</sup></b>

Property	Test Method	Requirement	Specimens per LOT
<b>Strength<sup>p</sup></b>			
Bond Strength to Concrete, Block Pull-Out	ACI 440.3R, Method B.3 or ASTM D7913	>1.1 ksi	5 <sup>m</sup>

a – Guaranteed tensile load shall be equal to the average test result from all three lots minus three standard deviations.  
n – Tests shall be conducted for all bar sizes produced.  
m – Tests shall be conducted for the smallest, median, and largest bar size produced.  

**p – Only required for BFRP bars.**

**932-3.3.1 Additional Requirements for Bent FRP Bars:** For all bars produced by bending straight solid FRP bars before the resin is fully cured, the minimum inside bend radius shall be at least three times the nominal diameters for bar sizes 2 through 8; and four times the nominal diameters for sizes 9 and 10.

The straight portion of a bent FRP reinforcing bar shall be extracted with sufficient length for tensile testing according to Table 3-3. When the bent shape does not allow for the tensile testing of one of its straight portions, test specimens produced at the same time during the same production LOT shall be used.

Property	Test Method	Requirement	Specimens per LOT
Fiber Mass Fraction – Bent Portion <sup>b</sup>	ASTM D2584 or ASTM D3171	≥70%	5 <sup>m</sup>
Short-Term Moisture Absorption – Bent Portion <sup>b</sup>	ASTM D570, Procedure 7.1; 24 hours immersion at 122°F	≤0.25%	5 <sup>m</sup>
Long-Term Moisture Absorption – Bent Portion <sup>b</sup>	ASTM D570, Procedure 7.4; immersion to full saturation at 122°F	≤1.0%	5 <sup>m</sup>
Glass Transition Temperature – Bent Portion <sup>b</sup>	ASTM E1356 (DSC; $T_m$ ) /ASTM D3418 (DSC; $T_{mg}$ )	≥212°F	3 <sup>m</sup>
Degree of Cure – Bent Portion <sup>b</sup>	ASTM E2160	≥95% of Total polymerization enthalpy	3 <sup>m</sup>
Measured Cross-Sectional Area – Straight Portion	ASTM D7205	Within the range listed in Table 3-1	5 <sup>m</sup>
Guaranteed Tensile Load <sup>a</sup> – Straight Portion		≥ Value listed in Table 3-1	

Property	Test Method	Requirement	Specimens per LOT
Tensile Modulus – Straight Portion		≥6,500 ksi for <b>BFRP and GFRP</b> ≥18,000 ksi for CRFP	
Alkali Resistance without Load – Straight Portion	ASTM D7705; 3 months test duration, followed by tensile strength per ASTM D7205	≥ 80% Tensile strength retention	5 <sup>m</sup>
Strength of 90° Bends	ACI 440.3, Method B.5 or ASTM D7914	> 60% Guaranteed tensile load listed in Table 3-1	5 <sup>m</sup>
Transverse Shear Strength – Straight Portion	ASTM D7617	>22 ksi	5 <sup>m</sup>
<b>Horizontal Shear Strength<sup>p</sup></b>	<b>ASTM D4475</b>	<b>&gt;5.5 ksi</b>	<b>5<sup>m</sup></b>

a – Guaranteed tensile load shall be equal to the average test result from all three lots minus three standard deviations.  
b – Bent portion specimens shall be extracted from a central location within a 90° bend.  
m – Tests shall be conducted for the smallest, median, and largest bent bar size produced.  
p – Only required for BFRP bars.

**932-3.4 Material Acceptance:** Submit to the Engineer, a certification for each production LOT from the producer of the FRP reinforcing bars, confirming that the requirements of this Section are met. The certifications shall conform to the requirements of Section 6.

**932-3.4.1 Sampling:** The Engineer will select a minimum of six straight bars with minimum lengths of 7 feet each and a minimum of five bent bars from each shipment, representing a random production LOT, per bar size of FRP reinforcing for testing in accordance with Table 3-4. Testing shall be conducted, at the Contractor's expense, by a Department approved independent laboratory. Each test shall be replicated a minimum of three times per sample. Submit the test results to the Engineer for review and approval prior to installation. Sampling and Testing will not be required for bars to be used solely as reinforcement for sheet pile bulkheads, but LOT samples will still be selected and retained by the Engineer until final acceptance of the work.

Property	Test Method	Requirement	Test Required for Straight Bar	Test Required for Bent Bar
Fiber Mass Fraction	ASTM D2584 or ASTM D3171	≥70%	Yes	Yes – bent portion <sup>b</sup>
Short-Term Moisture Absorption	ASTM D570, Procedure 7.1; 24 hours immersion at 122°F	≤0.25%	Yes	Yes – bent portion <sup>b</sup>

Glass Transition Temperature	ASTM D7028 (DMA) or ASTM D3418 (DSC; mg)	$\geq 230^{\circ}\text{F}$ $\geq 212^{\circ}\text{F}$	Yes	Yes – bent portion <sup>b</sup>
Degree of Cure	ASTM E2160	$\geq 95\%$ of Total polymerization enthalpy	Yes	Yes – bent portion <sup>b</sup>
Measured Cross-sectional Area	ASTM D7205	Within the range listed in Table 3-1	Yes	Yes – straight portion
Guaranteed Tensile Load <sup>a</sup>		$\geq$ Value listed in Table 3-1	Yes	No
Tensile Modulus		$\geq 6,500$ ksi for <b>BFRP</b> <b>and</b> GFRP $\geq 18,000$ ksi for CFRP	Yes	No

a – Guaranteed tensile load shall be equal to the average test result from all three lots minus three standard deviations.

b – Bent portion specimens shall be extracted from a central location within a 90° bend.

## NONMETALLIC ACCESSORY MATERIALS FOR CONCRETE PAVEMENT AND CONCRETE STRUCTURES.

(REV 8-23-19)

SUBARTICLE 932-3 is deleted and the following substituted:

### 932-3 Fiber Reinforced Polymer (FRP) Reinforcing Bars.

**932-3.1 General:** Obtain FRP reinforcing bars from producers currently on the Department's Production Facility Listing. Producers seeking inclusion on the list shall meet the requirements of Section 105.

Use only solid, round, thermoset basalt fiber reinforced polymer (BFRP), glass fiber reinforced polymer (GFRP) or carbon fiber reinforced polymer (CFRP) reinforcing bars. Bars shall be manufactured using pultrusion, variations of pultrusion, or other suitable processes noted in the producer's Quality Control Plan, subject to the approval of the State Materials Office (SMO). For BFRP and CFRP bars only vinyl ester or epoxy resin systems are permitted. For GFRP, use only bars manufactured using vinyl ester resin systems and glass fibers classified as E-CR that meet the requirements of ASTM D578.

**932-3.2 Bar Sizes and Loads:** The sizes and loads of FRP reinforcing bars shall meet the requirements in Table 3-1. The measured cross-sectional area, including any bond enhancing surface treatments, shall be determined according to Table 3-2.

Bar Size Designation	Nominal Bar Diameter (in)	Nominal Cross Sectional Area (in <sup>2</sup> )	Measured Cross-Sectional Area (in <sup>2</sup> )		Minimum Guaranteed Tensile Load (kips)	
			Minimum	Maximum	BFRP and GFRP Bars	CFRP Bars
2	0.250	0.049	0.046	0.085	6.1	10.3
3	0.375	0.11	0.104	0.161	13.2	20.9
4	0.500	0.20	0.185	0.263	21.6	33.3
5	0.625	0.31	0.288	0.388	29.1	49.1
6	0.750	0.44	0.415	0.539	40.9	70.7
7	0.875	0.60	0.565	0.713	54.1	-
8	1.000	0.79	0.738	0.913	66.8	-
9	1.128	1.00	0.934	1.137	82.0	-
10	1.270	1.27	1.154	1.385	98.2	-

**932-3.3 Material Requirements:** Producers shall submit to the State Materials Office (SMO), a test report of the physical and mechanical property requirements in Table 3-2 and Table 3-3 as applicable for the types and sizes of FRP reinforcing produced. Qualification testing shall be conducted by an independent laboratory approved by the Department for performing the FRP test methods.

Three production LOTS shall be randomly sampled at the production facility by a designee of the SMO. The minimum number of specimens per production LOT shall be as indicated in Table 3-2 and Table 3-3. The coefficient of variation (COV) for each test result shall be less than 6%. Outliers shall be subject to further investigation per ASTM E178. If the COV exceeds 6%, the number of test specimens per production LOT may be doubled, a maximum of two times, to meet the COV requirement. Otherwise, the results shall be rejected. A production LOT is defined as a LOT of FRP reinforcing produced from start to finish with the same constituent materials used in the same proportions without changing any production parameter, such as cure temperature or line speed.

Property	Test Method	Requirement	Specimens per LOT
Fiber Mass Fraction	ASTM D2584 or ASTM D3171	$\geq 70\%$	5 <sup>n</sup>
Short-Term Moisture Absorption	ASTM D570, Procedure 7.1; 24 hours immersion at 122°F	$\leq 0.25\%$	5 <sup>m</sup>
Long-Term Moisture Absorption	ASTM D570, Procedure 7.4; immersion to full saturation at 122°F	$\leq 1.0\%$	5 <sup>m</sup>
Glass Transition Temperature (T <sub>g</sub> )	ASTM D7028 (DMA) or ASTM E1356 (DSC; T <sub>m</sub> )/ASTM D3418 (DSC; T <sub>mg</sub> )	$\geq 230^\circ\text{F}$  $\geq 212^\circ\text{F}$	3 <sup>m</sup>
Total Enthalpy of Polymerization (Neat Resin)	ASTM E2160	Identify the resin system used for each bar size and report the average value of three replicates for each system	--
Degree of Cure	ASTM E2160	$\geq 95\%$ of Total polymerization enthalpy	3 <sup>n</sup>
Measured Cross-Sectional Area	ASTM D7205	Within the range listed in Table 3-1	10 <sup>n</sup>
Guaranteed Tensile Load <sup>a</sup>		$\geq$ Value listed in Table 3-1	
Tensile Modulus		$\geq 6,500$ ksi for BFRP and GFRP $\geq 18,000$ ksi for CRFP	
Alkali Resistance with Load	ASTM D7705; 3 months test duration, followed by tensile strength per ASTM D7205	$\geq 70\%$ Tensile strength retention	5 <sup>m</sup>
Transverse Shear Strength	ASTM D7617	$> 22$ ksi	5 <sup>n</sup>
Horizontal Shear	ASTM D4475	$> 5.5$ ksi	5 <sup>n</sup>

Table 3-2 Physical and Mechanical Property Requirements for Straight FRP Reinforcing Bars			
Property	Test Method	Requirement	Specimens per LOT
Strength <sup>p</sup>			
Bond Strength to Concrete, Block Pull-Out	ACI 440.3R, Method B.3 or ASTM D7913	>1.1 ksi	5 <sup>m</sup>

a – Guaranteed tensile load shall be equal to the average test result from all three lots minus three standard deviations.  
n – Tests shall be conducted for all bar sizes produced.  
m – Tests shall be conducted for the smallest, median, and largest bar size produced.  
p – Only required for BFRP bars.

**932-3.3.1 Additional Requirements for Bent FRP Bars:** For all bars produced by bending straight solid FRP bars before the resin is fully cured, the minimum inside bend radius shall be at least three times the nominal diameters for bar sizes 2 through 8; and four times the nominal diameters for sizes 9 and 10.

The straight portion of a bent FRP reinforcing bar shall be extracted with sufficient length for tensile testing according to Table 3-3. When the bent shape does not allow for the tensile testing of one of its straight portions, test specimens produced at the same time during the same production LOT shall be used.

Table 3-3 Physical and Mechanical Property Requirements for Bent FRP Reinforcing Bars			
Property	Test Method	Requirement	Specimens per LOT
Fiber Mass Fraction – Bent Portion <sup>b</sup>	ASTM D2584 or ASTM D3171	≥70%	5 <sup>m</sup>
Short-Term Moisture Absorption – Bent Portion <sup>b</sup>	ASTM D570, Procedure 7.1; 24 hours immersion at 122°F	≤0.25%	5 <sup>m</sup>
Long-Term Moisture Absorption – Bent Portion <sup>b</sup>	ASTM D570, Procedure 7.4; immersion to full saturation at 122°F	≤1.0%	5 <sup>m</sup>
Glass Transition Temperature – Bent Portion <sup>b</sup>	ASTM E1356 (DSC; $T_m$ ) /ASTM D3418 (DSC; $T_{mg}$ )	≥212°F	3 <sup>m</sup>
Degree of Cure – Bent Portion <sup>b</sup>	ASTM E2160	≥95% of Total polymerization enthalpy	3 <sup>m</sup>
Measured Cross-Sectional Area – Straight Portion	ASTM D7205	Within the range listed in Table 3-1	5 <sup>m</sup>
Guaranteed Tensile Load <sup>a</sup> – Straight Portion		≥ Value listed in Table 3-1	

Property	Test Method	Requirement	Specimens per LOT
Tensile Modulus – Straight Portion		≥6,500 ksi for BFRP and GFRP ≥18,000 ksi for CRFP	
Alkali Resistance without Load – Straight Portion	ASTM D7705; 3 months test duration, followed by tensile strength per ASTM D7205	≥ 80% Tensile strength retention	5 <sup>m</sup>
Strength of 90° Bends	ACI 440.3, Method B.5 or ASTM D7914	> 60% Guaranteed tensile load listed in Table 3-1	5 <sup>m</sup>
Transverse Shear Strength – Straight Portion	ASTM D7617	>22 ksi	5 <sup>m</sup>
Horizontal Shear Strength <sup>p</sup>	ASTM D4475	>5.5 ksi	5 <sup>m</sup>

a – Guaranteed tensile load shall be equal to the average test result from all three lots minus three standard deviations.  
b – Bent portion specimens shall be extracted from a central location within a 90° bend.  
m – Tests shall be conducted for the smallest, median, and largest bent bar size produced.  
p – Only required for BFRP bars.

**932-3.4 Material Acceptance:** Submit to the Engineer, a certification for each production LOT from the producer of the FRP reinforcing bars, confirming that the requirements of this Section are met. The certifications shall conform to the requirements of Section 6.

**932-3.4.1 Sampling:** The Engineer will select a minimum of six straight bars with minimum lengths of 7 feet each and a minimum of five bent bars from each shipment, representing a random production LOT, per bar size of FRP reinforcing for testing in accordance with Table 3-4. Testing shall be conducted, at the Contractor's expense, by a Department approved independent laboratory. Each test shall be replicated a minimum of three times per sample. Submit the test results to the Engineer for review and approval prior to installation. Testing will not be required for bars to be used solely as reinforcement for sheet pile bulkheads, but LOT samples will still be selected and retained by the Engineer until final acceptance of the work.

Property	Test Method	Requirement	Test Required for Straight Bar	Test Required for Bent Bar
Fiber Mass Fraction	ASTM D2584 or ASTM D3171	≥70%	Yes	Yes – bent portion <sup>b</sup>
Short-Term Moisture Absorption	ASTM D570, Procedure 7.1; 24 hours immersion at 122°F	≤0.25%	Yes	Yes – bent portion <sup>b</sup>

Glass Transition Temperature	ASTM D7028 (DMA) or ASTM D3418 (DSC; mg)	$\geq 230^{\circ}\text{F}$  $\geq 212^{\circ}\text{F}$	Yes	Yes – bent portion <sup>b</sup>
Degree of Cure	ASTM E2160	$\geq 95\%$ of Total polymerization enthalpy	Yes	Yes – bent portion <sup>b</sup>
Measured Cross-sectional Area	ASTM D7205	Within the range listed in Table 3-1	Yes	Yes – straight portion
Guaranteed Tensile Load <sup>a</sup>		$\geq$ Value listed in Table 3-1	Yes	No
Tensile Modulus		$\geq 6,500$ ksi for BFRP and GFRP $\geq 18,000$ ksi for CFRP	Yes	No

a – Guaranteed tensile load shall be equal to the average test result from all three lots minus three standard deviations.

b – Bent portion specimens shall be extracted from a central location within a 90° bend.

## **Appendix D**

### **Bridge Engineering Institute – 2019 Conference Papers**

- a. Basalt FRP-RC Standardization for Florida DOT Structures;
- b. Effect of the Fiber Content on the Tensile Strength Properties of Basalt Fiber Reinforced Polymer Rebars;
- c. Bond-to-Concrete Characteristic of Basalt Fiber-Reinforced Polymer Rebars for Design Code Implementation

(29 pages)



# BEI-2019

## Bridge Engineering Institute Conference

### July 22-25, 2019

### Honolulu, Hawaii, USA

Edited by

Yail J. Kim

Isamu Yoshitake

Vanissorn Vimonsatit

Xuhui He

Yongcheng Ji

BEI

An International Technical Society



Bond Behavior of FRP Bars in Air-Entrained Concrete.....	487
<i>Sandor Solyom, Anna Szijarto, and György L. Balázs</i>	
Heavy CFRP Fabric Deployment for Repair of Impacted PC Bridge Girder on Interstate 64 in Kentucky.....	492
<i>Abheetha Peiris and Issam Harik</i>	
Development of Efficient Anchorage Systems for Flexural Strengthening of Concrete Bridge Planks using FRP Materials.....	496
<i>Bahaa Al-Atta, Robin Kalfat, Riadh Al-Mahaidi, and Alaa Al-Mosawe</i>	
Strengthening of Concrete Bridge Girders with Concavely-Curved Soffit Using Fiber Reinforced Polymer.....	502
<i>Khattab Al-Ghrery, Robin Kalfat, Nazar Oukaili, Alaa Al-Mosawe, and Riadh Al-Mahaidi</i>	
Application of FRP for Strengthening of Precast Segmental Bridge Construction of Motorway No. 6 in Thailand.....	510
<i>Sukit Yindeesuk, Phanthira Chanachompu, and Panatchai Chetchotisak</i>	
Basalt FRP-RC Standardization for Florida DOT Structures.....	514
<i>Steven Nolan, Chase Knight, and Raphael Kampmann</i>	
Basalt Characterization from Commercial Quarries on Hawaii Island and Feasibility Study Results for a Continuous Basalt Fiber Manufacturing Operation.....	524
<i>Rodrigo Romo and Kyla Defore</i>	
Effect of the Fiber Content on the Tensile Strength Properties of Basalt Fiber Reinforced Polymer Rebars.....	527
<i>Alvaro Ruiz Emparanza, Raphael Kampmann, Francisco De Caso, and Antonio Nanni</i>	
The Use of Geopolymer Concrete and GFRP Materials for an Innovative Wharf Structure...	532
<i>Thomas Glasby, John Day, Michael Kemp, and Rohan McElroy</i>	
Bond-to-Concrete Characteristic of Basalt Fiber Reinforced Polymer Rebars.....	551
<i>Raphael Kampmann, Tim Schneider, and Srichand Telikapalli</i>	



## Basalt FRP-RC Standardization for Florida DOT Structures

Steven Nolan<sup>1\*</sup>, Chase Knight<sup>2</sup>, and Raphael Kampmann<sup>3</sup>

<sup>1</sup> Florida Department of Transportation – State Structures Design Office, Tallahassee, FL. USA; email: Steven.Nolan@dot.state.fl.us

<sup>2</sup> Florida Department of Transportation – State Materials Office, Gainesville FL. USA; email: Chase.Knight@dot.state.fl.us

<sup>3</sup> FAMU-FSU, Tallahassee FL. USA; email: kampmann@eng.famu.fsu.edu

\*: corresponding author

**Keywords:** basalt, BFRP, composite reinforcing, corrosion-resistant, rebar, standards

**Abstract:** Fiber-reinforced polymer bars are emerging as a viable economical solution to eliminate corrosion degrading of reinforced concrete (RC) structures caused by chloride attack in both coastal and cold weather locations. The corrosion mechanism is similar in these divergent environments due to the presence of chlorides: within seawater along the coastal fringe of 20 states; and within deicing chemicals used in most of the other US states. Significant improvements in manufacturing techniques and resin matrix materials have occurred in recent years enabling exploitation of the superior properties of Basalt FRP rebar that is now available. The Canadian Standards Association will shortly be adopting BFRP rebar for concrete structures in their next update to the Canadian Highway Bridge Design Code. FDOT under their Transportation Design Innovation initiative is committed to providing resilient, sustainable, cost effective and scalable solutions to the aging infrastructure challenge. The provision of multiple material options for corrosion-resistant rebar is foreseen as a positive development to encourage competition, further innovation and provide a redundant supply chain for FRP materials, especially as wider deployment occurs. A significant amount of inferior BFRP products are reportedly now available on the world market due to the lack of standards, underlying the need and urgency for establishing robust standards in the US. This paper describes the need and development of standard (guide) design specifications, and standard material and construction specifications for basalt fiber-reinforced polymer (BFRP) bars for the internal reinforcement of structural concrete on FDOT projects.

### 1. Introduction

Fiber-reinforced polymer bars are emerging as a viable economical solution to eliminate corrosion degradation of reinforced concrete (RC) structures caused by chloride attack in both coastal and cold weather locations. Although Paul Dh'e first produced basalt fibers in the United States, in 1923 (Dh'e, 1923; Colombo et al., 2012), the technology did not gain traction in the US due to initial production difficulties and more profitable opportunities with glass fibers. Specifically, after the manufacturing process for glass fibers was successfully industrialized in Toledo, Ohio, by Games Slayter in 1933 (Slayter, 1938), the major fiber producers in the US abandoned basalt fiber research in favor of glass products (Faruk et al., 2017). Extensive research on basalt fibers was later conducted in the former Soviet Union, during the cold war (Jamshaid and Mishra, 2016), for military purposes in a search for ballistic resistant textiles.



After the Soviet Union collapse in 1991, these research projects were declassified (in 1995) and released for civilian applications. In consequence, basalt fibers are a recent development in the engineered construction industry and most basalt fiber producing companies are still located in countries that use to be associated with the Eastern Bloc (Zych and Wojciech, 2012).

## 2. Basalt FRP Rebar Manufacturing

Significant improvements in FRP manufacturing techniques and resin matrix materials have occurred in recent years enabling exploitation of the superior properties of Basalt FRP rebars. Different processes have been developed to combine the basalt fibers and resin for the efficient production of fiber reinforced polymer rebar. The typical production method is pultrusion, however the production method is not yet standardized leading to different rebar products from each manufacturer. Pultrusion is a relatively simple and reliable process for the manufacture of BFRP bars, particularly for the straight rods. Other production processes are available as discussed in Patnaik, 2009, potentially less reliable, but possibly better suited for complicated bent shapes or mesh products.

Pultrusion is a continuous molding process combining fibers and thermosetting resin, with a constant cross-sectional architecture. The fibers are continuously pulled from rovings, passing through a wetting operation (impregnated) usually in a liquid resin bath. Inside the pultrusion die, a controlled temperature promotes resin hardening while the heat activates the curing or polymerization of the thermoset resin. The fixed cross section of the pultrusion-dies, ensure tight dimensional control of FRP rebar. Inside the heating die, the rebar reacts chemically and solidifies under an exothermic reaction morphing from a heterogenous liquid stage to a gel stage, until finally the solid state is reached. To achieve a sufficient bond between concrete and the rebar in its end use, an additional process is required to provide surface enhancement features (You et al., 2015). Surface enhancement includes: formed ribs; machined grooves; sand coating; helical wrap; or combinations of these. The final product is cut to length at the end of the pultrusion process is only constrained by logistics such as storage and transporting limitations. Coiling is also possible when smaller diameters are produced (ACI Committee 440, 2007).

Various studies have identified possible weaknesses in existing products and provide recommendations for standardization requirements. Scanning electron microscope (SEM) analysis can be used to show qualitatively when porosity and voids are present with FRP rebars. Based on these observations ElSafty et al. (2014) recommended improvements to the manufacturing process to reduce and/or eliminate these defects. Borges et al. (2015), studied the influence of resin bath temperature on the properties of pultruded FRP rebars with polyester resin. It was shown that temperatures between 86°F to 122°F (30°C to 50°C) were suitable for the production process. Higher temperatures lead to a low viscosity and inadequate wetting of the fibers before entering the heating die. The recommended curing temperature for resins is about 350°F (177°C) according to Joshi et al., 2003. More commonly, epoxy based resins are the preference for BFRP due to improved durability and mechanical performance in a concrete bound environment.



### 3. Standards for BFRP-RC

A significant amount of BFRP products are reportedly now available on the world market, with a wide range of performance properties due to the lack of uniform standards. This highlights the need and urgency for establishing robust standards in the US to ensure reliability and instill confidence in asset owners and designers. Some significant progress has already been completed for developing a US based code of practice using the current GFRP rebar Guide Specifications as a framework (AASHTO 2018, ACI 2015).

The American Concrete Institute Committee 440 (ACI 440) initially led the North American effort to address the technical implementation for FRP rebars by developing and publishing test methods, specifications, and design guidelines (ACI Committee 440, 2006, 2008a, 2008b, 2012, 2013, 2015). The 2008 version of ACI 440 (ACI Committee 440, 2008b) and the 2010 version of the Canadian Standards Association (CSA) Specifications for Fiber Reinforced Polymers (CAN/CSA, 2010) were developed to standardize glass, carbon, and aramid FRP bars. CSA has recently led the western effort for developing specifications and design guidelines for BFRP. The new CSA S807-19 (CAN/CSA, 2019) standard will include FRP bars made from basalt fibers, which highlights the current interest of this material and the confidence of a commercialized availability (Vincent et al., 2013). Similarly, ASTM Committees D30 and D20 have addressed the emergence of FRP rebar technology by developing test methods (ASTM-International, 2015) intended to characterize GFRP rebar, that can also be applied to BFRP rebar. Recently, ASTM D7957-17 was published with specific guidelines for solid round glass fiber reinforced polymer bars for concrete reinforcement (ASTM-International, 2017). In addition, the FDOT has developed documents to regionally aid in the design and implementation of FRP rebar, specifically expanding Specifications Section 932 (FDOT, 2014 & 2018), and implementing the Fiber Reinforced Polymer Guidelines (FDOT, 2015).

While different production techniques and processes exist today in the FRP rebar market, the established acceptance criteria allow manufacturers to target specific properties. Nevertheless, BFRP rebars have been produced before these acceptance criteria were available, and so manufacturers have often followed very individual mechanical properties and proprietary production sequences. Accordingly, the market is currently very diverse with unique products, and new manufacturers can enter the market quickly due to relatively low start-up costs.

It is therefore desired to add BFRP rebar specific criteria to the AASHTO guidelines and specifications as soon as practical to ensure product reliability, encourage US manufacturing, and increase competition and redundancy in the material supply chain. Transportation agencies and asset owners are becoming increasingly interested in BFRP composites because of broader exposure in the western hemisphere and production technology improvements which have led to improved mechanical properties such as: fatigue endurance; creep rupture resistance; strength; and elastic modulus. The environmental benefits of lower embodied energy and a longer service life compared to steel are also gaining interest. Some recent guideline and specification developments for BFRP rebar are summarized in the following:

### 3.1. AC454 - 2015

The International Code Council Evaluation Services, approved the proposed addition of BFRP rebar to their Acceptance Criteria AC454 “Fiber-Reinforced Polymer Bars for Internal Reinforcement of Concrete Members” (ICC-ES, 2014) in 2015. This allows structures designed according to the requirements of the International Building Code (IBC), and most state adopted versions of this model code, to be realized with BFRP rebar technology.

### 3.2. State Transportation Innovation Council (STIC) Incentive Project, 2018 - 2019

FDOT under their Transportation Design Innovation (TDI) initiative provides guidance for FRP technology infrastructure solutions (<https://www.fdot.gov/structures/innovation/FRP.shtm>). One goal of the TDI initiative is to provide multiple material options (including the adoption of BFRP) for corrosion-resistant rebar, which encourages market competition and product innovation, and should provide a redundant supply chain of FRP materials as wider deployment occurs. The FHWA funded STIC Incentive project (STIC-0004-00A) is developing standard design (guide) specifications, and standard material and construction specifications for BFRP rebars for 2020 adoption.

### 3.3. CAN/CSA 807 & S6 - 2019

The Canadian Standards Association will be adopting BFRP rebar for concrete structures in the next update to their “Specifications for fibre-reinforced polymers” (CAN/CSA 807-19), followed by adoption in the Canadian Highway Bridge Design Code (CAN/CSA S6-19)

**Table 2A**  
**Grades of FRP straight bars and grids corresponding to their minimum modulus of elasticity, GPa**

Designation	Grade I		Grade II		Grade III	
	Individual bars	Bars in a grid	Individual bars	Bars in a grid	Individual bars	Bars in a grid
AFRP	50	40	70	60	90	80
BFRP	50	40	60	50	70	60
CFRP	80	70	110	100	140	130
GFRP	40	30	50	40	60	50

**Fig. 1.** Proposed grades of FRP bars per CAN/CSA S807-19 public review copy

## 4. BFRP-RC Structures

Some recent examples of structures that have been successfully constructed with BFRP rebar in Florida, are summarized below:

### 4.1. Port Miami Tunnel Entrance Walls (Watson Island), Miami - 2014

BFRP reinforcement bars #2.5 and #4 (8 mm and 12 mm) were utilized in Watson Island Retaining Walls 5 and 6 (Fig. 2) as an FDOT demonstration project, with a research plan for monitoring long-term performance and durability. The retaining walls were originally designed with Grade 60 carbon-steel reinforcement. The contractor initiated redesign, proposed BFRP

bars in substantial conformance with the AASHTO LRFD Bridge Design Guide Specifications for GFRP-RC Bridge Decks and Traffic Railings (2009). The wall shape, dimensions, and class of concrete remained the same as the original plans. An FDOT research plan includes extraction of cores to evaluate any changes in the physical and chemical properties of BFRP rebar, concrete, and interfaces between them. Sampling and analysis for this research project is scheduled to begin in 2019.

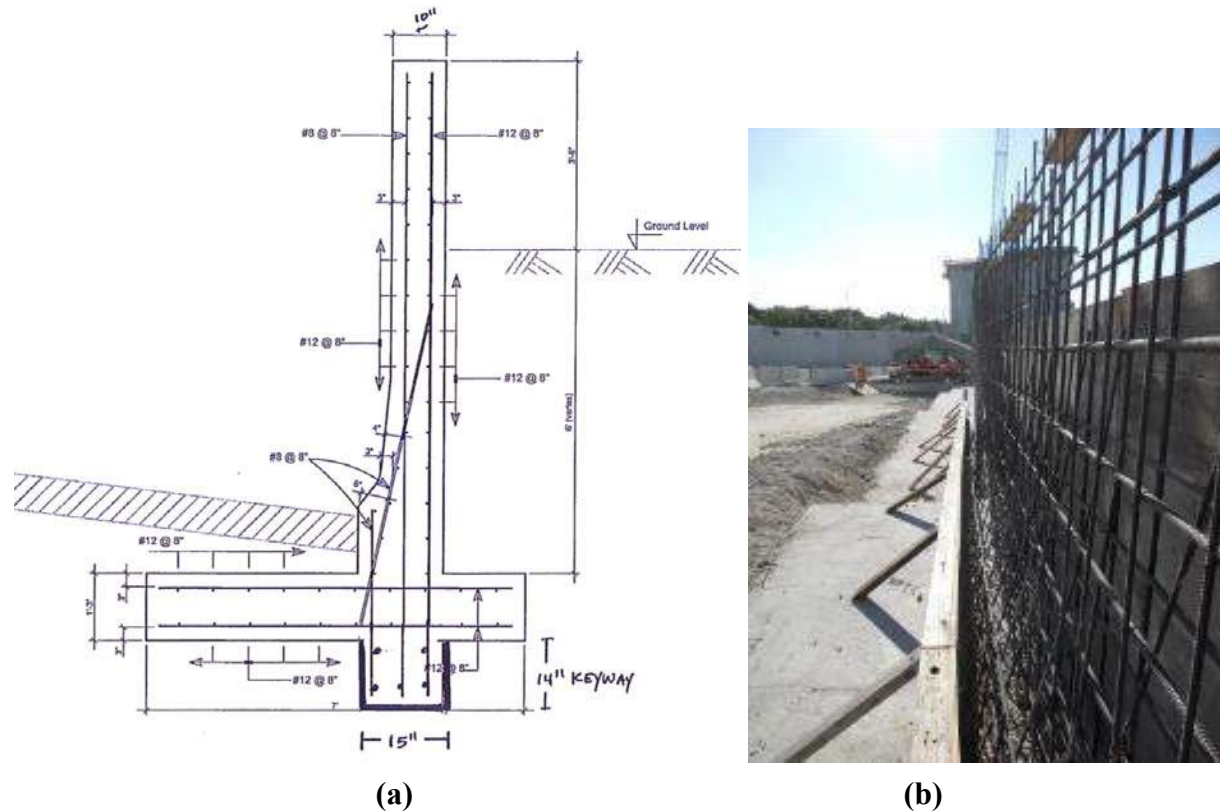


**Fig. 2.** (a) Typical Cross-section of Retaining Walls 5 and 6 with BFRP Reinforcement (Bar sizes in mm); (b) Wall 6 under construction.

#### 4.2. IROX Drainage Structures, Lee County - 2014

Five precast drainage structures (ditch bottom inlets and junction boxes) were constructed using BFRP rebar as a direct replacement for Grade 60 carbon-steel rebar as originally designed. The structures are inside or near retention ponds which experience seasonal wet/dry cycles. Fig. 3(a) shows the locations of three structures that were visually inspected in December 2018, with no external evidence of cracking or deterioration observed. Fig. 2(b) shows images of one of the retention pond structures.

#### 4.3. Innovation Pedestrian Bridge, Miami - 2016

This bridge on the University of Miami (UM) campus combines different FRP materials (basalt, glass, and carbon) and novel composite manufacturing technologies (continuous closed stirrups

and automated-preassembled cages) within the following elements: auger-cast piles; cast-in-place pile caps and back walls; precast prestressed girders; and, cast-in-place deck topping and curbs. FRP was deliberately chose to demonstrate UM’s commitment to innovation and sustainability for a pedestrian bridge and BFRP was heavily featured. Eight 40-foot long, 16-inch diameter auger-cast piles were reinforced with a prefabricated cage of six #6 BFRP bars and bespoke spirals. The cages (in the shape of an octagon) were prefabricated at the composite manufacturer’s plant and delivered to the site, ready for installation with only man-power.



**Fig. 3.** BFRP-RC drainage structures: (a) Plan view locations of 3 retention pond overflow

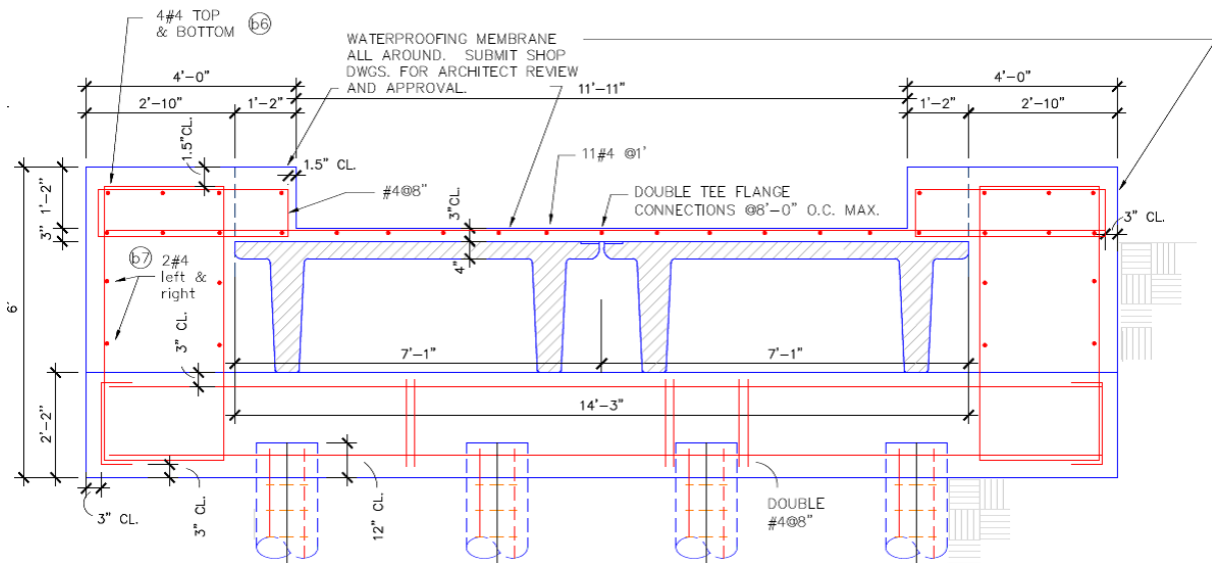


**Fig. 4.** (a) Typical cross-section of Innovation Bridge with BFRP reinforcement in the piles, caps, double-tee stems and flanges, deck overlay and curbs.

The pile caps and backwalls were mostly reinforced with closed (bespoke) BFRP stirrups and straight bars. The two double-tees girders were prestressed with CFRP strands and BFRP shear and supplemental reinforcing. The reinforcement grids for the stems and flanges were made of

pre-assembled interwoven BFRP bars (#3 and #4, respectively). The cast-in-place, 3-inch concrete deck topping was also reinforced with a grid of #3 BFRP bars in both directions while the curbs consisted of a combination of closed (bespoke) #4 BFRP transverse stirrups and straight longitudinal BFRP rebars.

#### 4.4. Halls River Bridge, Homosassa - 2018

The Halls River Bridge replacement project is the first of its kind for a vehicular bridge in Florida. The bridge was predominantly designed and constructed using a variety of non-metallic reinforcement materials. In addition, it features 400 linear feet of sacrificial test blocks constructed monolithically with the bulkhead-seawall coping along the north and south abutments. These test blocks are reinforced with several types of FRP rebars, including BFRP rebar (#5). The test blocks are designed to be removed for testing and analysis after various periods of exposure. Fig. 5 shows the typical positioning of the test blocks after construction. The test blocks allow for natural exposure to brackish water in the splash zone. The first set of test blocks were removed in November 2018 and are currently being evaluated as a benchmark for long-term comparison. An example Life-Cycle Cost (LCC) analysis was performed by Cadenazzi et al. 2018, to highlight the economic advantage of FRP in similar structures and environments.



**Fig. 5.** Typical position of test blocks: (a) High tide at HRB (test block outlined); (b) Benchmark test blocks cut and ready for extraction.

#### 5. Conclusion

Several demonstration projects in Florida, and many others around the world, have shown the versatility and practicality of BFRP rebar for structural applications. Commercial manufacturers have exhibited the capacity to accommodate a variety of geometric challenges and respond to asset owner's needs. Researchers have validated the mechanical properties, and while durability research continues, the current limits in the available GFRP-RC guide specifications appear appropriately conservative for initial deployment of BFRP-RC in the US. LCC analysis can currently be utilized by designers to show the benefits of BFRP-RC alternatives, while future refinement of the durability models can provide additional economy, as will industry innovation,



fueled by an increase in market share, and demand by asset owners for more sustainable infrastructure.

## 6. References

AASHTO (2012). Guide Specifications for Design of Bonded FRP Systems for Repair and Strengthening of Concrete Bridge Elements. American Association of State Highway and Transportations Officials

AASHTO (2018). LRFD Bridge Design Guide Specifications for GRFP-Reinforced Concrete. American Association of State Highway and Transportations Officials

ACI Committee 440 (2006). Guide for the Design and Construction of Structural Concrete Reinforced with FRP Bars, (440.1R-06). American Concrete Institute.

ACI Committee 440 (2007). Report on Fiber-Reinforced Polymer (FRP) Reinforcement for Concrete Structures, (440R). American Concrete Institute.

ACI Committee 440 (2008a). Guide for the Design and Construction of Externally Bonded FRP Systems for Strengthening Concrete Structures, (ACI 440.2R-08). American Concrete Institute.

ACI Committee 440 (2008b). Specification for Carbon and Glass Fiber-Reinforced Polymer Bar Materials for Concrete Reinforcement, (ACI 440.6-08). American Concrete Institute.

ACI Committee 440 (2012). Guide Test Methods for Fiber-Reinforced Polymer (FRP) Composites for Reinforcing or Strengthening Concrete and Masonry Structures, (ACI 440.3R-12). American Concrete Institute.

ACI Committee 440 (2013). Specification for Carbon and Glass Fiber-Reinforced Polymer (FRP) Materials Made by Wet Layup for External Strengthening of Concrete and Masonry Structures, (ACI 440.8-13). American Concrete Institute.

ACI Committee 440 (2015). Guide for the Design and Construction of Structural Concrete Reinforced with Fiber-Reinforced Polymer (FRP) Bars, (ACI 440.1R). American Concrete Institute.

ASTM-International (2017). Standard Specification for Solid Round Glass Fiber Reinforced Polymer Bars for Concrete Reinforcement, (ASTM D7957 / D7957M – 17). West Conshohocken, PA.

Borges, S. G., Ferreira, C. A., Andrade, J. M., and Prevedello, A. L. (2015). “The influence of bath temperature on the properties of pultruded glass fiber reinforced rods.” *Journal of Reinforced Plastics and Composites*, 34(15), 1221–1230.

Colombo, C., Vergani, L., and Burman, M. (2012). “Static and fatigue characterisation of new basalt fibre reinforced composites.” *Composite Structures*, 94, 1165–1174.



- CAN/CSA. (2010). Specifications for Fibre Reinforced Polymers: CAN/CSA-S807-10, Canadian Standard Association.
- CAN/CSA. (2019). Specifications for Fibre Reinforced Polymers: CAN/CSA-S807-19, Canadian Standard Association (in press).
- ElSafty, A., Benmokrane, B., Rizkalla, S., Mohamed, H., and Hassan, M. (2014). “Degradation assessment of internal continuous fiber reinforcement in concrete environment”, Florida Department of Transportation.
- Faruk, O., Tjong, J., and Sain, M. (2017). “Lightweight and Sustainable Materials for Automotive Applications.” Tyler & Francis Group, LCC.
- FDOT. (2014). “Nonmetallic Accessory Materials for Concrete Pavement and Concrete Structures”, Dev932FRP. FDOT Developmental Specification, Revision 7-16-14.
- FDOT. (2015). “Fiber reinforced polymer guidelines (FRPG).” Structures Manual - Volume 4. Florida Department of Transportation.
- FDOT. (2018). “FDOT Standard Specification for Road and Bridge Construction”, Section 932. Florida Department of Transportation.
- ICC-ES. (2014). “Acceptance Criteria for Glass Fiber-Reinforced Polymer (GFRP) Bars for Internal Reinforcement of Concrete Members.” Acceptance Criteria 454, International Code Council Evaluation Services
- ICC-ES. (2017). “Acceptance Criteria for Fiber-Reinforced Polymer (FRP) Bars for Internal Reinforcement of Concrete Members.” Acceptance Criteria 454, International Code Council Evaluation Services
- Jamshaid, H. and Mishra, R. (2016). “A green material from rock: basalt fiber - a review.” The Journal of The Textile Institute, 107(7), 923–937.
- Joshi, S. C., Lam, Y., and Tun, U. W. (2003). “Improved cure optimization in pultrusion with pre-heating and die-cooler temperature.” Composites Part A, 34, 1151–1159.
- Nanni, A., De Luca, A., and Jawaheri Zadeh, H. (2014). FRP Reinforced Concrete Structures – Theory, Design and Practice. CRC Press.
- Patnaik, A. (2009). “Applications of Basalt Fiber Reinforced Polymer (BFRP) Reinforcement for Transportation Infrastructure.” The University of Akron.
- Slyter, G. (1938). “Method and apparatus for making glass wool.” Patent 2,133,235, United States Patent Office.



Bridge Engineering Institute Conference 2019 (BEI-2019)  
Honolulu, Hawaii, USA, July 22-25, 2019



Vincent, P., Ahmed, E., and Benmokrane, B. (2013). "Characterization of basalt fiber-reinforced polymer (BFRP) reinforcing bars for concrete structures." Specialty Conference on Material Engineering & Applied Mechanics, 3rd, MEC-111-1 – MEC-111-10.

You, Y.-J., Kim, J.-H. J., Kim, S.-J., and Park, Y.-H. (2015). "Methods to enhance the guaranteed tensile strength of gfrp rebar to 900 mpa with general fiber volume fraction." Construction and Building Materials, 75, 54 – 62.

Zych, T. and Wojciech, K. (2012). "Study on the properties of cement mortars with basalt fibres." Brittle Matrix Composites 10, 155–166.



## Effect of the Fiber Content on the Tensile Strength Properties of Basalt Fiber Reinforced Polymer Rebars

Alvaro Ruiz Empananza<sup>1\*</sup>, Raphael Kampmann<sup>2</sup>, Francisco De Caso<sup>3</sup>, and Antonio Nanni<sup>4</sup>

<sup>1</sup> Department of Civil & Environmental Engineering, University of Miami, Miami (FL), USA.  
email: alvaro.ruiz@miami.edu

<sup>2</sup> Department of Civil & Environmental Engineering, FAMU-FSU College of Engineering,  
Tallahassee (FL), USA. email: kampmann@eng.famu.fsu.edu

<sup>3</sup> Department of Civil & Environmental Engineering, University of Miami, Miami (FL), USA.  
email: fdecaso@miami.edu

<sup>4</sup> Department of Civil & Environmental Engineering, University of Miami, Miami (FL), USA.  
email: nanni@miami.edu

\*: corresponding author

**Keywords:** BFRP; basalt fiber, fiber content; tensile strength; corrosion

**Abstract:** The long-term performance of steel reinforced concrete structures is limited by the corrosion of the steel reinforcing bars (rebars). Recently, continued efforts have emerged to implement alternative reinforcing materials in substitution of steel to extend the lifespan of concrete structures. The use of basalt fiber reinforced polymer (BFRP) rebars as internal reinforcement of has increased significantly in the last years, mainly due to the corrosion resistance and its beneficial mechanical properties. BFRP rebars are composite materials made of continuous basalt fibers embedded longitudinally in a resin matrix. The fiber to resin proportion is different for every commercially produced rebar type, with a minimum fiber content of 70% (by weight/mass) per ASTM D7957. The aim of this project was to evaluate the effect of the fiber content and its impact on the tensile strength properties of the BFRP rebars. Accordingly, the fiber mass content, the cross-sectional area, and the tensile strength of three different rebar types were tested and compared. Preliminary results show, that a direct relation exists between fiber to resin proportion, and the tensile strength of BFRP rebars.

### 1. Introduction

In the process of moving toward a sustainable and long-lasting infrastructure, composite materials are gaining importance to be used as internal reinforcement in concrete structures, substituting the traditional black steel to avoid corrosion issues. Composite rebars are fiber reinforced polymers (FRP) and compared to steel, they have higher strength (2-3 times higher), they are lightweight (4 times lighter), but most importantly, they don't suffer corrosion. To-date, the most commonly used fiber types are carbon (for pre-stress applications) and glass (for mild reinforcement); however, the use of basalt fibers is increasing exponentially due to relatively simpler production process compared to glass. Basalt fibers are produced using a continuous process similar to the glass fibers, but with the difference that the basalt fibers are extracted from a single raw material (melted basalt rock), while the glass fibers are made combining different constituents (silica sand, oxides of boron, aluminum, etc.). In addition, aramid fibers are also used by some manufacturers but are not as common as carbon, glass or basalt. Among the resins,

epoxy and vinyl-ester are the ones that are mainly used in the production of FRP rods (Nanni, De Luca and Zadeh, 2014). For the production of these composite materials, the quality of the raw materials (fibers and resin) is of high importance, but also the proportions of each constituent are critical. The fibers are the load carrying elements, while the resin is responsible for the strength transfer between the fibers, as well as for protecting them against damaged over time.

Due to the increase of the use of basalt fiber reinforced polymer (BFRP) rebars, many researchers around the world have worked on the characterization and durability assessment of these composite materials (Serbescu, Guadagnini and Pilakoutas, 2014; Wu *et al.*, 2014; Dong *et al.*, 2016, 2017; Wang, X. L. Zhao, *et al.*, 2017; Wang, X.-L. Zhao, *et al.*, 2017). However, to the best knowledge of the authors, the effect of the fiber/resin ratio on the strength properties of the BFRP rebars has not been documented in the literature. To-date, no material standard specification exists for BFRP rebars, but the one existing for glass FRP rebars, ASTM D7957 (ASTM International, 2017), sets the minimum fiber mass content to a minimum of 70%. To determine the fiber mass content, two methods are referenced in ASTM 7957: ‘ASTM D2584 - Standard Test Method for Ignition Loss of Cured Reinforced Resins’ (ASTM International, 2018) and the ‘ASTM D3171 - Standard Test Method for Constituent Content of Composite Materials’ (ASTM International, 2015). The aim of this paper is to correlate the fiber content of BFRP rebars with their tensile test properties.

## 2. Methodology

For the evaluation of the effect of the fiber content on the tensile test properties of BFRP rebars, rebars from three different manufacturers were tested (A, B, C). Two rebar sizes were evaluated: #3 and #5. Manufacturer A provided two rebar types per size (A-1 and A-2), made of different resins but same fibers. Manufacturer B provided # 3 rebars only, while manufacturer C provided # 5 rods only. Four different physio-mechanical properties were tested: cross-sectional area, fiber content, tensile strength and modulus of elasticity. The research scope included 5 repetitions per test (tensile test, fiber content test and cross-sectional area test), rebar type (A, B and C) and size (#3 and #5), leading to a total of 90 test repetitions. The specimen preparation and the tests were accomplished according to the relevant ASTM standards. ASTM D7205 was followed for the tensile tests: due to the low strength capacity on the transverse direction of the BFRP rebars compared to the longitudinal one, both specimen ends were protected using steel pipes filled with expansive grout. The fiber mass content tests were conducted according to ASTM D2584, while ASTM D792 was followed to evaluate the cross-sectional area. Figure 1 shows the test setup for both the tensile (left) and the fiber content (right) tests.

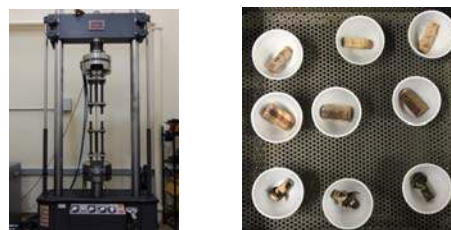


**Figure 1.** Tensile test setup (left) and fiber content test specimens being burnt inside the furnace (right)

### 3. Results and Discussion

The obtained results were analyzed and statistically evaluated and as summarized in Table 1. Both the tensile strength and E-Modulus were calculated using the measured area values. It can be seen that the physio-mechanical properties for the two types of rebars for manufacturer A, were similar, while they differed significantly from the rebars provided by manufacturers B and C.

**Table 1.** Summary of the experimental results

Rebar Size	Rebar Type	Measured Area		Fiber Content		Tensile Peak Load		Tensile Strength		E-Modulus	
		Mean	COV	Mean	COV	Mean	COV	Mean	COV	Mean	COV
		in <sup>2</sup>	%	%	%	kip	%	ksi	%	10 <sup>6</sup> psi	%
#3	A-1	77.29	0.49	71.78	0.32	17.19	5.70	146.63	5.70	6.99	3.10
	A-2	77.73	0.26	75.27	0.18	19.78	2.60	167.81	2.60	6.66	2.50
	B	55.56	0.45	75.48	1.12	14.06	3.70	166.79	3.70	7.94	3.80
#5	A-1	225.62	0.35	75.54	0.06	52.34	5.80	144.30	5.80	6.46	5.60
	A-2	231.00	0.85	75.49	0.06	49.15	8.00	140.28	8.00	5.74	7.00
	C	192.41	0.17	84.80	0.06	47.37	3.80	162.30	3.80	7.20	2.40

To better understand the correlation between the fiber content and the tensile properties of the BFRP rebars, the tensile strength and the E-Modulus were plotted with respect to the fiber content (see Figure 2 and 3). The average tensile strength values for the different rebar types are shown in Figure 2, grouped by rebar size. Each of the three data points per rebar size represents the average tensile peak stress with respect to the average fiber content of the five repetitions per rebar type. The maximum fiber content was obtained for manufacturer C (#5 rebars) with about 85%, while A-1 rebars had the least relative amount of fibers. However, all rebar types exceeded the minimum fiber content (70%) defined by ASTM D7957. In general, it can be inferred that the tensile capacity increases with increasing fiber content. These results indicate that the tensile strength is mainly governed by the amount of fibers, though a minimum amount of resin is needed to properly transfer the stress between fibers. For this reason, the resin type appears to also affect this property as it can be seen in rebar types A-1 and A-2, which had almost identical fiber contents but different resin types. However, the tensile strength for A-1 was about 6.5% higher than the one for A-2.

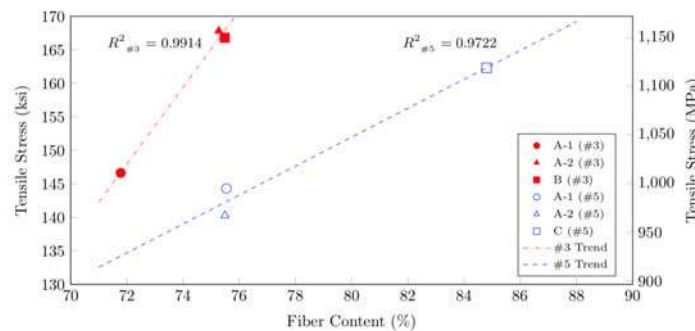


**Figure 12.** Tensile stress with respect to the fiber content

In Figure 3, the E-modulus was plotted versus the fiber content. In this case, based on the tested specimens, the authors did not find any relation between the E-modulus and the fiber content. In general, the E-modulus tended to increase with the increase of fiber content, though the values appeared to be more scattered.

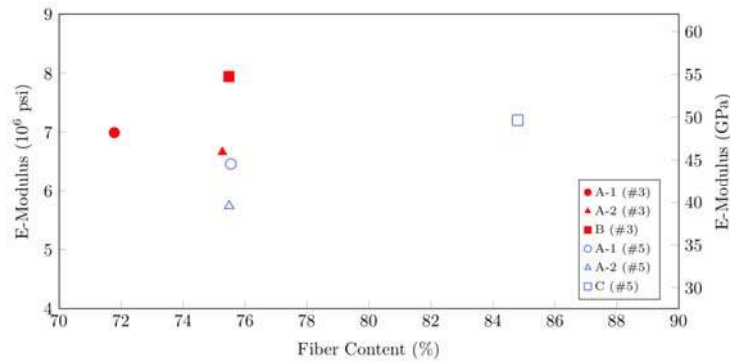


**Figure 13.** E-Modulus with respect to the fiber content

The resin type also appeared to affect the E-Modulus. Both #5 rebar types produced by manufacturer A (type A-1 and A-2) were produced using the same fiber type but different resins, and even if they had comparable fiber contents, the E-Modulus varied about 12.5% between each other.

#### 4. Conclusions

In this paper the correlation between the fiber content and the tensile properties of BFRP rebars was evaluated by testing dissimilar rebar types and sizes (#3 and #5) produced by three different manufacturers. For all rebar types and sizes, the cross-sectional area, the fiber content, the tensile strength, and the E-Modulus were calculated. From the obtained results it could be seen that a linear correlation exists between the tensile strength and the fiber content: the higher the fiber content, the higher the tensile capacity of the rebar. This leads to the conclusion that the tensile response of the BFRP rebars is directly related to the amount of fiber, though the resin type (responsible for the stress transfer between fibers) also has an effect. This was substantiated by the 6.5% difference in peak tensile stress for A-1 and A-2 rebars, which differed only by the resin type. The E-modulus also tended to increase with the increasing fiber content, though no clear trend was found. In this case too, the E-Modulus appeared to be affected by the resin type: a difference of about 12.5% was found between the E-Modulus of type A-1 and A-2 rebars.

To better assess the relation between the tensile properties and fiber content of BFRP rebars, more rebar types and sizes should be tested. In addition, tests on each of the constituents (fibers and resin) independently would be beneficial to assess the effect that these raw materials may have in the general performance of the rebars.

#### 5. Acknowledgments

The authors acknowledge the financial support of the Florida Department of Transportation (FDOT) and the guidance provided by its staff Chase C. Knight, Ph.D. and Steven Nolan, P.E.

## 6. References

ASTM International (2015) ‘ASTM D3171 - Standard Test Methods for Constituent Content of Composite Materials’. doi: 10.1520/D3171-15.2.

ASTM International (2017) *ASTM D7957 - Standard Specification for Solid Round Glass Fiber Reinforced Polymer Bars for Concrete Reinforcement*. doi: 10.1520/D7957.

ASTM International (2018) *ASTM D2584 - Standard Test Method for Ignition Loss of Glass Strands and Fabrics*. doi: 10.1520/D2584-11.2.

Dong, Z., Wu, G., Xu, B., Wang, X. and Taerwe, L. (2016) ‘Bond durability of BFRP bars embedded in concrete under seawater conditions and the long-term bond strength prediction’, *Materials and Design*, 92, pp. 552–562. doi: 10.1016/j.matdes.2015.12.066.

Dong, Z., Wu, G., Zhao, X. L. and Wang, Z. K. (2017) ‘A refined prediction method for the long-term performance of BFRP bars serviced in field environments’, *Construction and Building Materials*, 155, pp. 1072–1080. doi: 10.1016/j.conbuildmat.2017.07.154.

Nanni, A., De Luca, A. and Zadeh, H. (2014) *Reinforced Concrete with FRP Bars*. doi: 10.1201/b16669.

Serbescu, A., Guadagnini, M. and Pilakoutas, K. (2014) ‘Mechanical characterization of basalt FRP rebars and long-term strength predictive model’, *Journal of Composites for Construction*. American Society of Civil Engineers, 19(2), p. 4014037.

Wang, Z., Zhao, X.-L., Xian, G., Wu, G., Raman, R. K. S., Al-Saadi, S. and Haque, A. (2017) ‘Long-term durability of basalt-and glass-fibre reinforced polymer (BFRP/GFRP) bars in seawater and sea sand concrete environment’, *Construction and Building Materials*. Elsevier, 139, pp. 467–489.

Wang, Z., Zhao, X. L., Xian, G., Wu, G., Singh Raman, R. K. and Al-Saadi, S. (2017) ‘Durability study on interlaminar shear behaviour of basalt-, glass- and carbon-fibre reinforced polymer (B/G/CFRP) bars in seawater sea sand concrete environment’, *Construction and Building Materials*, 156, pp. 985–1004. doi: 10.1016/j.conbuildmat.2017.09.045.

Wu, G., Dong, Z., Wang, X., Zhu, Y. and Wu, Z. (2014) ‘Prediction of Long-Term Performance and Durability of BFRP Bars under the Combined Effect of Sustained Load and Corrosive Solutions’, *Journal of Composites for Construction*, 19(3), p. 4014058. doi: 10.1061/(ASCE)CC.1943-5614.0000517.

## Bond-to-Concrete Characteristic of Basalt Fiber Reinforced Polymer Rebars

Raphael Kampmann<sup>1\*</sup>, Tim Schneider<sup>2</sup>, and Srichand Telikapalli<sup>3</sup>

<sup>1</sup> FAMU-FSU College of Engineering, USA; email: [kampmann@eng.famu.fsu.edu](mailto:kampmann@eng.famu.fsu.edu)

<sup>2</sup> Fachhochschule Mnster, Germany; email: [tim.schneider@fh-muenster.de](mailto:tim.schneider@fh-muenster.de)

<sup>3</sup> FAMU-FSU College of Engineering, United States of America; email: [st15d@my.fsu.edu](mailto:st15d@my.fsu.edu)

\*: Corresponding author

**Keywords:** basalt; BFRP; bond; bond-to-concrete; surface enhancement

**Abstract:** Due to historical developments, fiber reinforced polymer (FRP) materials in the United States are mostly based on glass (GFRP) or carbon (CFRP) and the majority of reinforcing bars (rebars) for concrete structures are made with GFRP. Recently, basalt-based composites gained traction as these materials have been successfully used in Russia and China, and because U.S.- based FRP manufacturers and distributors have started to use basalt fibers for various rebar products. BFRP rebars are now considered because of the low production cost compared to CFRP rebars and due to improved chemical resistance, a higher tensile strength, and a higher modulus of elasticity compared to GFRP rebars. As the production of BFRP rebars is yet to be standardized, manufacturers around the world have produced various BFRP rebar types with different surface enhancements that affect the bond-to-concrete performance in various ways. For this study, it was the goal to evaluate the design-critical bond-to-concrete property for dissimilar BFRP rebar types through pullout tests according to ASTM D 7913 in an effort to characterize the bond performance of various surface conditions. The evaluated independent test variable was the bond interface — created through the various rebars types with sand coat, helical wraps and traditional steel lugs — while the measured dependent variables included the free-end slip, load-end slip, bond stress development, and interface stiffness. The results showed that the bond stiffness and rebar slip behavior are dependent on the surface enhancement features; while rebars with surface deformation presented a ductile rebar slip behavior, sand-coated surface lead to sudden failure. Likewise, the strength capacity of the BFRP rebar-concrete interface was affected by the surface enhancement features, and rebars with a deformed surface attained the highest bond capacity. Further, the type of resin affected the bond-to-concrete strength of BFRP rebars. Each rebar type lead to a distinctive failure interface and the failure modes suggested that the pullout behavior of BFRP rebars differs significantly from the pullout behavior of traditional steel rebars due to the transverse material stiffness.

### 1. Introduction

Throughout the past decades, concrete structures in coastal environments have deteriorated faster than expected. Besides a significant increase in traffic volume and traffic loads, exposure to salt-water and harsh environments has led to increased corrosion of traditional reinforcement bars. While corrosion results in tensile strength losses, the volumetric expansion of rust causes surface cracks and spalling, which destroy the protective (high pH) concrete layer. Generally, these effects lead to deterioration and may induce structural failure with significant financial implications and personal losses. To reduce these risks and to increase the service life of bridges

and infrastructure elements, noncorrosive internal reinforcement alternatives, such as fiber reinforced polymers (FRP) rebars, have been developed and they appear to be a viable option for concrete structures in harsh environments (Benmokrane and Ali, 2016; Vincent et al., 2013). FRP rebars are manufactured from different fiber types (glass, carbon, aramid or basalt), which are bound together with various resins, for example polyester, vinyl ester or epoxy (Sólyom and Balázs, 2015). Besides corrosion resistance, other benefits, such as high tensile strength, magnetic transparency, low unit weight (about one-third of steel), reduced transportation costs, ease of handling on the job site, etc., have sparked a great interest in the construction industry. Recent research projects and demonstration structures — e.g., Halls River Bridge replacement in Florida — have shown that FRP rebars are advantageous for many aspects and that the technology has the potential for standardized use in construction projects (Rossini et al., 2018). Similar to the Halls River Bridge replacement, most pilot projects in the United States are generally based on glass (GFRP) or carbon (CFRP) and the majority of rebars for concrete structures are GFRP based. Now, basalt FRP rebars are gaining more attention because of the low production cost compared to CFRP rebars and due to improved chemical resistance, a higher tensile strength, and a higher modulus of elasticity in comparison to GFRP rebars. Basalt (a volcanic rock) is the only needed raw ingredient for the production of basalt fibers; it turns into a molten mass at 1400 °C to 1500 °C and can be formed directly into continuous fibers. Due to the promising characteristics, numerous research projects are conducted to determine the material characteristics and mechanical properties of BFRP rebars (Elgabbas et al., 2013, 2016; Hassan M., 2016; Ali et al., 2019). The bond-to-concrete performance of these rebars is an important material characteristic and research topic because it determines the structural behavior of BFRP reinforced concrete. To ensure proper bond between the BFRP rebar and the concrete, a surface treatment is applied to the FRP rebars, which increases the friction at the bond interface, or improves the interlocking effect. Unlike for traditional black steel rebars, the production of BFRP rebars has not been standardized yet and manufacturers around the world have developed different BFRP rebar products with various surface types and features (sand-coated, helical wraps, lugs, etc.). While the bond-to-concrete behavior of various Glass FRP surface enhancements has already been evaluated in many studies (Fava et al., 2016; Yan and Lin, 2016; Yang and Xu, 2018; Jamal and Fu, 2018), this property has not been extensively defined for BFRP, and currently, it only can be assumed that Basalt FRP rebars perform similarly.

## 2. Problem Statement

The bond-to-concrete behavior is one of the most fundamental mechanical characteristics of FRP rebars that affects the quality and durability of concrete structure because it guarantees proper stress transfer between the two materials and ensures uniformity (Sólyom et al., 2015). While the bond-to-concrete performance of traditional black steel rebars (W. A. Slater, 1920; Bilek et al., 2017) and GFRP rebars (Gu et al., 2016; El-Nemr et al., 2016; Yan and Lin, 2016; Islam et al., 2015; Munoz, 2010) has been evaluated in detail, the bond-to-concrete performance of BFRP rebars has not been fully analyzed yet. This BFRP rebar knowledge gap is reflected in current structural design codes; most design standards allow the use of FRP rebars, but generally only permit glass and carbon fiber materials because adjustment factors for these rebar types are available already (AASHTO, 2018). Such adjustment factors are also needed to define the bond properties, because it is reasonable to assume that the diverse BFRP rebar surface treatments lead to dissimilar bond-to-concrete performances and that some surface features provide better

interlocking effects than others. To properly use and implement BFRP rebar technology for infrastructure projects, the bond-to-concrete performance of different rebar products must be evaluated and compared—relative to each other and to traditional steel rebars.

### 3. Research Significance

To provide additional data and knowledge for the bond behavior of basalt FRP rebars, this study aims to evaluate the bond-to-concrete performance of various BFRP rebars with different surface enhancements. Rebar pullout tests were conducted to quantify and compare the bond strength and bond stiffness due to various surface types and enhancement features. Thereby, this study provides important data for further development of specifications and guidelines for the design of FRP-reinforced structures to facilitate redundant material supply chains, additional alternatives, and market expansion.

### 4. Methodology

In an effort to characterize the bond-to-concrete performance of various BFRP rebar surface features and to evaluate dissimilar BFRP rebar types relative to each other and relative to the performance of traditional steel rebars, pullout tests according to ASTM D7913 (ASTM International, 2014) were conducted. For this study, # 3 rebars with a nominal diameter of  $3/8$  in. (10mm) and three different rebar types (A, B, and C) were tested, whereas one rebar type had two sub-variants (Type-A1 and Type-A2), each was made with a different resin (c.f. Table 1). Control group specimens were made from traditional black steel rebars and were tested to provide benchmark values.

**Table 1.** Properties of the tested Rebars

Rebar	Surface Treatment	Resin Type	Measured Diameter		Tensile Strength		Elastic Modulus	
			mm	in.	MPa	ksi	GPa	ksi
Type-A1	Sand coating	Epoxy (HE)	10.41	0.410	926	134.2	47.07	6827
Type-A2	Sand coating	Epoxy (HP)	10.19	0.401	1166	169.2	49.64	7200
Type-B	Helical Wrapped	Epoxy	10.25	0.403	839	121.7	37.80	5482
Type-C	Sand coating	Vinyl ester	10.88	0.428	1353	196.3	53.83	7808
Type-D <sup>1</sup>	Surface lugs	Black steel	9.53	0.375	276	40.0	200.00	29000

<sup>1</sup> Control group (black steel)

Each sample consisted of five specimens for each rebar type, and a total of 25 specimens were tested for this study. The bond interface created by the various rebars (sand-coated, helically grooved, and surface lugs) was defined as the independent test variable. Test constants according to ACI/ASTM were the bond length with five times the nominal diameter of the rebar (47.5mm or  $1\frac{7}{8}$  in.), the (via PVC-tubes) de-bonded rebar length, and the concrete properties. The measured dependent variables included the free-end slip, load-end slip, bond stress development, and interface stiffness. All rebar types, independent variables, and the relevant material properties are summarized in Table 1 to provide an overview of the entire test program. Besides the control group of steel rebars (Type-D) all values were experimentally evaluated. As shown in Figure 1, one rebar end was embedded inside the concrete cube — with a 200mm (8 in.) edge length — while the other end was encased in a steel anchor to protect it from transverse failure

due to rebar gripping. To guarantee an accurate bonding length of five times the nominal diameter (48mm or 1<sup>7</sup>/<sub>8</sub> in.), PVC tubes were installed as a bond blocker.

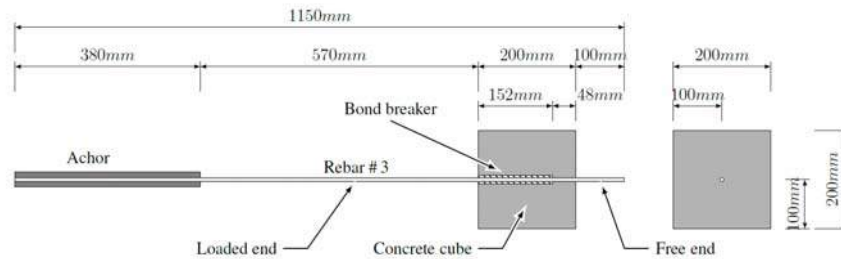


Fig. 1. Specimen with a rebar # 3

According to ASTM D7913 (ASTM International, 2014) the PVC tubes were used at the loaded ends of the rebar to minimize the stress concentration near the loading plate. The rebar displacement relative to the concrete cube was measured at both ends — the free end and the loaded end. While the free end slip was measured with one transducer, the relative displacement at the loaded end was recorded as the average value measured by three transducers in a 120° arrangement. All tests were displacement-controlled with a rate of 0.076 mm/min (0.3 in./min).

#### 4.1. Materials

Photos of the cross section and the surface enhancement for each experimentally tested rebar type (BFRP and steel) can be seen in Figure 2. As seen in the Figure 2, all rebar types had a round solid cross section, but the surface features varied.

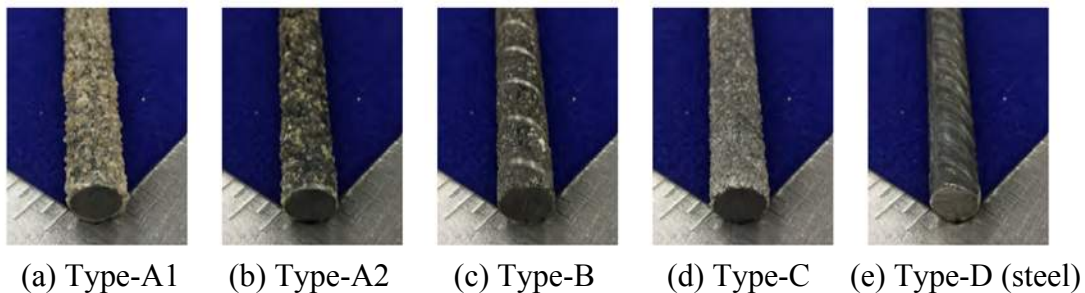


Fig. 2. Rebar overview

The major physical difference between the rebar types was the surface enhancement features because Type B was helically wrapped, sand coating was used for Types-A and C, and the tradition steel rebars had surface lugs. To reduce variances and to ensure consistency of test results, one single batch of ready-mixed concrete with a guaranteed compressive strength of 31.01 MPa (4500 psi) was used to produce all pullout cubes. Suwannee American type I cement (371 kg/m<sup>3</sup> or 625 lbs./yd<sup>3</sup>), A-mining/FDOT Sand (761 kg/m<sup>3</sup> or 1282 lbs./yd<sup>3</sup>), A-mining/FDOT# 57 Stone (801 kg/m<sup>3</sup> or 1350 lbs./yd<sup>3</sup>), A-mining/ FDOT# 89 stone (178 kg/m<sup>3</sup> or 300 lbs./yd<sup>3</sup>), tapwater (117 L or 31 gal.), air entrainment (0.015 L or 0.5 oz.), type A water reducer (0.46 L or 15.6 oz), and a retarder (0.28 L or 9.4 oz) were used to batch the concrete mixture.

## 4.2. Specimen Production and Preparation

For this study, 25 pullout specimens with embedded # 3 rebars were created via horizontal casting with combined molds using form dividers according ASTM D7913 (ASTM International, 2014). For consistency, one single operator placed the concrete in three layers of approximately equal thickness, while a different single operator rodded each layer 25 times with a 16mm 5/8 in. Diameter tamping rod. After each layer was consolidated, a third operator tapped the mold for each specimen with a rubber mallet 5 times. After the top layer was completely consolidated, the free surface was struck off and leveled with a trowel before it was covered to prevent evaporation according to ASTM C192 (ASTM International, 2002). For curing, the specimens remained covered in the molds for 17 days but were removed thereafter to install the anchors at the load end (around the BFRP rebars) according to ASTM D7205 (ASTM International, 2016). In line with test procedure ASTM C39 ASTM International (2003), the compressive strength of five test cylinders (152.4 mm × 304.8 mm or 6 in. × 12 in.) was obtained at the day of pullout testing (more mature than 28 days) with a mean compressive strength of 51 MPa (7396 psi), a standard deviation of 1.39 MPa (201.38 psi), and a coefficient of variation of less than 2.7 %.

## 4.3. Test Procedure

The bond-to-concrete properties were recorded according to ASTM D7913 ASTM International (2014), which provides a standard test method by means of pullout testing. The tests were conducted under standard laboratory conditions within (23±2) °C [(73±5) °F] and (50±10) % relative humidity, using a 300 kN (66 kip) hydraulically controlled load frame. To properly apply the pullout force to the specimen, the test fixtures shown in Figure 3 were designed. Before installing the LSCTs to measure the rebar slip at both ends, an initial seating load of 272 kN (600 lbs.) was applied to every specimen to generate sufficient stiffness in the system. The force was continuously applied and without shock, all values were recorded with 1000 Hz until the measured force decreased significantly (more than 50 %) and the slippage at the free end of the bar measured at least 2.5mm (0.1 in.). After each test was completed, the concrete block was split open to analyze the failure mode and to measure the precise bond length of each specimen. While the raw data was recoded in LabView software with high data rates, it was written to file at 10 Hz (using appropriate filters). For efficient data analysis and data presentation, the high-speed data was filtered and reduced using R-statistics<sup>1</sup> and R-Studio<sup>2</sup> software packages. The graphs presented in this paper display the filtered and reduced data, which was verified to match the original raw high-speed data. However, all reported numerical values are based on the raw data and were calculated before any filter was applied.

## 5. Results

The experimental results obtained through pullout testing are presented in Figure 4 and Table 2, while the modes of failure are shown in Figure 5. The bond stress  $\tau_{max}$  (MPa or psi) for a circular bar diameter  $d$  (mm or in.) is given by Equation 1 in which  $F$  represents the recorded pullout load (N or lbs.) and  $L$  is the accurately measured bond length (mm or in.).

<sup>1</sup>R.app GUI 1.70 (7434 El Capitan build), S. Urbanek & H.-J. Bibiko, R Foundation for Statistical Computing, 2016

<sup>2</sup>Version 1.1.383 2009-2017 RStudio, Inc.

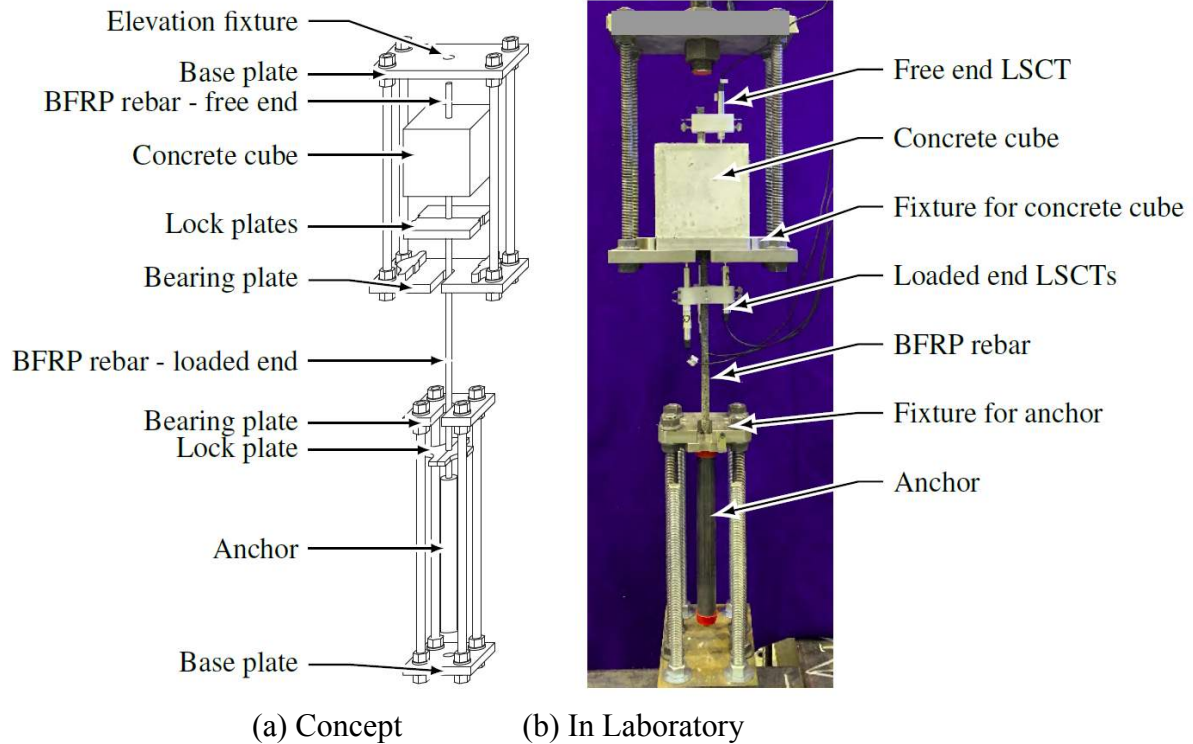


**Fig. 3.** Experimental Setup

$$\tau_{max} = \frac{F}{d\pi L} \quad [\text{MPa or psi}] \quad (1)$$

The bond stress vs. free end slip behavior is graphed in Figure 4 for all 25 specimens. For clarity, the post failure measurements (at the onset of the 50 % load drop) were removed from these graphs. All tested specimens failed at the rebar-concrete interface in bond rupture, without splitting the concrete open or without tensile failure. Generally, from the graphs it can be seen that each rebar type resulted in a consistent but distinct failure mode with ultimate stresses that were characteristic for each rebar type. Whereas most of the sand-coated rebars (Type-A1, A2 and B) failed suddenly with abrupt pullout, the rebars with a deformed surface (Type-C and Type-D [steel]) showed a soft failure. Likewise, the strength capacity of the BFRP rebar-concrete interface was affected by the surface enhancement features. While steel rebars attained the highest maximum strength values, they were seconded by helically wrapped rebars, which were followed by sand-coated rebars (c.f. Table 2). The initial slope (bond stiffness) of the steel specimens was notably variant with a wide envelope. However, all steel rebar specimens demonstrated a similarly ductile failure after reaching the peak bond stress.

For numerical comparison and concluding values, Table 2 lists the bond minimum stress ( $\wedge$ ), the maximum bond stress ( $\vee$ ), the average bond stress ( $\mu$ ), the standard deviation ( $\sigma$ ), and the coefficient of variation (CV) for each individual test sample.

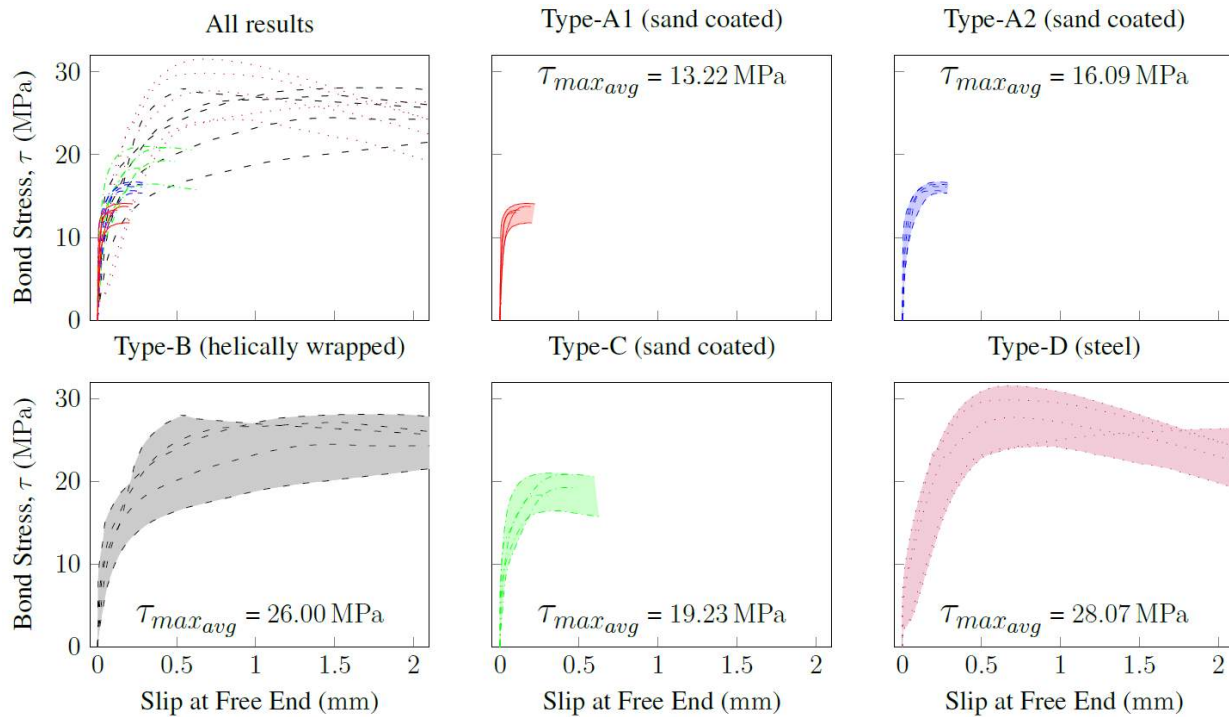


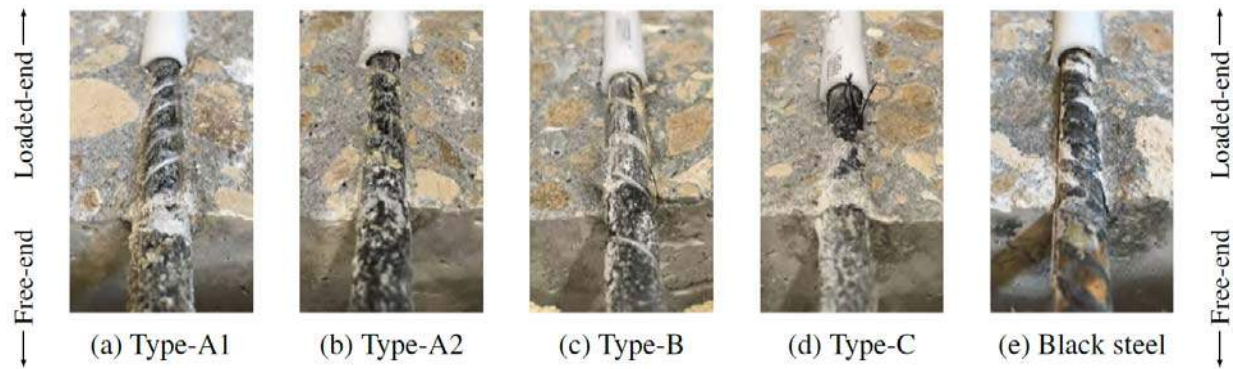
Fig. 4. Free end slip behavior of the tested rebars

Table 2. Bond-to-Concrete strength test statistical values for each sample

Sample Group		Statistical Values								
Rebar Type	Resin Type	Imperial				Metric				
		Λ	∇	μ	σ	Λ	∇	μ	σ	CV
		ksi	ksi	ksi	ksi	MPa	MPa	MPa	MPa	%
A	HE	1.71	2.05	1.92	0.13	11.81	14.15	13.22	0.90	0.07
A	HP	2.24	2.43	2.33	0.08	15.41	16.74	16.09	0.54	0.03
B	Epoxy	3.20	4.08	3.77	0.38	22.08	28.15	26.00	2.64	0.10
C	VinylEster	2.39	3.05	2.79	0.27	16.49	21.04	19.23	1.89	0.10
D	Steel	3.53	4.59	4.07	0.41	24.33	31.65	28.07	2.85	0.10

While Type-A1 and A2 measured the lowest mean bond strength (13.22 MPa or 1.92 ksi for Type-A1 and 16.09 MPa or 2.33 ksi for Type-A2), they also had the lowest variation between individual test results with a standard deviation of less than 1.0 MPa (0.13 ksi) and a CV of 7 % for Type-A1 and 3 % for Type-A2. All other rebar types had the same CV of 10%, whereas Type-D rebars (black steel) measured the highest mean bond strength (28.07 MPa or 4.07 ksi) followed by Type-B rebars (helically wrapped) with a mean bond strength of (26.00 MPa or 3.77 ksi) and Type C (sand-coated) with a mean bond strength of (19.23 MPa or 2.79 ksi). After the pullout tests were completed, the concrete blocks were split in half to further evaluate the failure

mode by analyzing the surface of the rebar and the concrete. Figure 5 exemplifies the different representative failure modes as they were observed for each rebar type.



**Fig. 5.** Overview rebar surface after testing

In Figure 5 can be seen that each rebar type produced different damages dependent on the surface enhancement features. For rebar Types-A1 and A2, de-bonding of the entire sand coat was observed (sand delamination). For rebar Type-B, only the sand layer was pulled off the concrete and the surface deformed slightly, but the helical wraps remained in place. For rebar Type-C, it was noted that the rebar surface was significantly damaged at the loaded end, and that the outer layer was entirely peeled off from the rest of the rebar. Close to the unloaded end, the surface layer of the rebar did not peel off, and most parts of the sand-coated layer remained well-adhered to the bar. The steel rebars did not suffer any visible damages, but fine concrete dust was noted at the surface of the rebar.

## 6. Analysis & Discussion

The results have shown that a different surface enhancement, as well as different resin types, lead to different bond behavior, and therefore, to different damages at the rebar surface. Besides the resin type, rebar Types-A1 and A2 were made from identical materials and with the same production techniques; however, the maximum bond stress of rebar Type-A2 was more than 20 % higher in comparison to the bond strength of rebar Type-A1. The results within each test sample were considerably consistent (CV of 7 % for rebar Type-A1 and 3 % for rebar Type-A2), which leads to the conclusion that the bond properties are affected by the resin. Similar to the observations made by Ahmed et al. (2018), the sand-coated rebars failed mainly due to damages at the bar surface in the form of abrasion. For these specimens, the concrete strength was high enough, such that the bond strength of FRP rebars was controlled by the shear strength between the fiber layers (Sólyom and Balázs, 2015; Fava et al., 2016), which also is depending on the resin type (Achillides and Pilakoutas, 2004). This uniform peeling off of the surface layer along the whole length of the embedded portion of the bar explains the abrupt failure of these specimens (Munoz, 2010). After delamination, the sanded surface becomes effectively smooth and increasing loads can no longer be resisted (Refai A., 2015). While also sand-coated, the failure mode of Type-C rebars was different, which is assumed to be due to different resin properties. As shown in Figure 5, rebar damages (delamination) were noted at the loaded end, but the sand coat at the free end remained intact. Because delamination was more pronounced

and concentrated at the loaded end, it appears that peeling started from there and moves toward the free end until failure. Due to the pullout test setup, the higher stresses appears at the loaded end, which explains the damage concentration on the rebar surface closest to that end (Refai A., 2015; Kabir and Islam, 2014). Before the bonded area can delaminate completely (moving toward the free end), the increasing bond stresses (due to surface reduction and increasing loads) cause failure at the concrete surface and the rebar is pulled in a sudden manner. Rebar Type-B (with helical wraps) had the highest bond strength of the tested BFRP rebar types (almost twice the average bond strength of rebar Type-A1). These rebars facilitated a softer failure and the fibers did not delaminate, but the rebar deformed slightly in the radial direction and the sand coat was partially rubbed off. Accordingly, it can be concluded that the Type-B rebars were squeezeed through the concrete, because of low transverse stiffness. For this rebar type, the bond strength is mostly generated through the geometrical interlocking effect or by friction between the rebar surface deformations and the concrete (Sólyom and Balázs, 2015; Aiello et al., 2007; Munoz, 2010). The helical wrapping may not be advantageous for rebar tensile strength because the outer layer of the fibers have to be straightened before the entire cross section can be fully activated, but if bond strength needs to be maximized, this interlocking effect appears to be advantages, because it lead to the highest load resistance during pullout testing compared to the other BFRP specimen types tested in this study. These helical wraps are closest to the ribs of the control group Type-D (black steel) specimens, which had an 8 % higher average bond stress than rebar Type-B. Also the bond stress vs. free-end-slip development of the control group was similar to rebar Type-B, but the peak bond stress of the steel rebars occurred earlier (at a lower free end displacement). This is because of the higher transverse stiffness of the steel rebar, which reduces rebar deformation, and therefore, the steel rebars cannot squeeze through the concrete. Instead, it crushed the surrounding concrete at the lugs within the bonded length (Fava et al., 2016). This also explains the concrete dust around the control group Type-D (steel) rebars that was not seen for any of the other rebar types. Generally rebars with a surface deformation (Type-B and Type-D) provided higher bond stress than rebars without a surface deformation (Aiello et al., 2007). These rebar types measured a larger free end slip when they reached the maximum capacity and failed in a ductile fashion, whereas the rebars without a surface deformation showed a more sudden failure. This phenomenon can be traced back to the larger interlock effect, created through the deformed surface of the rebars, which is activated by the slip of the rebar. Generally, pullout tests lead to compression within the concrete—which rarely occurs in practice when a rebar is in tension—and cause a reduction in bond stress of sand-coated rebars, while the opposite is true for deformed rebars (Aiello et al., 2007; Sólyom and Balázs, 2015).

## 7. Conclusions

For this research project, a total of 25 specimens with a nominal diameter of 10 mm ( $\frac{3}{8}$  in.) and different surface enhancements (sand-coated, helically wrapped and black steel) were tested according to ASTM D7913 (ASTM International, 2014) in an effort to quantify the bond strength of dissimilar basalt FRP rebars in concrete. Four BFRP rebar types with different surface enhancement features and one traditional steel rebar type were experimentally and statistically evaluated. The load displacement behavior, the failure behavior, and the fracture patterns of all samples (specimen groups) were systematically compared to each other. Based on the findings and the analysis conducted in this research, the following conclusions were drawn:

- Different surface enhancements lead to different bond-to-concrete behavior and performance. Rebars with surface deformations provided a higher bond strength than rebars without a surface deformation.
- The pullout failure mechanism of FRP rebars is significantly different from the pullout failure mechanism of traditional steel rebars, due to the differences in the material transverse stiffness. While the stiff lugs of steel rebars crush the surrounding concrete, BFRP rebars with surface deformations may squeeze through the concrete.
- Basalt FRP rebars with sand coating and without surface deformations predominantly fail due to delamination at the outer rebar surface.
- Sand-coated FRP rebars without surface deformations are more likely to fail in a sudden or brittle fashion, while rebars with surface deformations lead to a more ductile pullout failure behavior.
- The ultimate bond stress of deformed BFRP rebars occurs after significant slip, whereas rebars with sand coating and no surface deformations produce a high initial bond stiffness, but with reduced bond-to-concrete strength due to missing interlocking effects.
- If bond strength needs to be maximized, interlocking effects due to rebar surface deformations (e.g.: through helical wraps) should be considered.
- The resin type impacts the bond-to-concrete performance of BFRP rebars. Though all other constituent materials and production processes may be identical for a specific rebar type, from this study it appears that a variation in resin can lead to a 20% strength difference.

## 8. Acknowledgements

The authors would like to acknowledge the Florida Department of Transportation (FDOT) for a progressive approach to the implementation of emerging technologies in our infrastructure. Special thanks go to Steven Nolan and Chase Knight for their continues engagement, exceptional support, and outstanding expertise. The opinions, findings, and conclusions expressed in this publication are those of the authors and not necessarily those of the Florida Department of Transportation, or the US Department of Transportation.

## 9. References

- AASHTO (2018). AASHTO LRFD Bridge Design Guide specifications for GFRP-Reinforced Concrete. American Association of State Highway and Transportation Officials.
- Achillides, Z. and Pilakoutas, K. (2004). “Bond behavior of fiber reinforced polymer bars under direct pullout conditions.” *Journal of Composites for Construction*, 8(2), 173–181.
- Ahmed, S. A. S., Fahmy, M. F. M., and Wu, Z. (2018). “Experimental study and numerical modeling of cyclic bond and slip behavior of basalt frp bars in concrete.” *Journal of Composites for Construction*, 22(6), 04018050.
- Aiello, M., Leone, M., and Pecce, M. (2007). “Bond performances of frp rebars-reinforced concrete.” *Journal of Materials in Civil Engineering*, 19, 205–213.



Ali, A. H., Mohamed, H. M., Benmokrane, B., ElSafty, A., and Chaallal, O. (2019). “Durability performance and long-term prediction models of sand-coated basalt frp bars.” *Composites Part B: Engineering*, 157, 248 – 258.

ASTM International (2002). *Standard Practice for Making and Curing Concrete Test Specimens in the Laboratory*, (C192/C192M). West Consohocken, PA.

ASTM International (2003). *Standard Test Method for Compressive Strength of Cylindrical Concrete Specimens*, (C39/C39M). West Consohocken, PA.

ASTM International (2014). *Standard Test Method for Bond Strength of Fiber-Reinforced Polymer Matrix Composite Bars to Concrete by Pullout Testing*, (D7913/D7913M). West Consohocken, PA.

ASTM International (2016). *Standard Test Method for Tensile Properties of Fiber Reinforced Polymer Matrix Composite Bars*, (D2584-06(2016)). West Consohocken, PA.

Benmokrane, B. and Ali, A. (2016). “Durability of frp rebars in aggressive environments.” *International Workshop on Seawater Sea-sand Concrete (SSC) Structures Reinforced with FRP Composites* 13.

Bilek, V., Bonczková, S., Hurta, J., Pytlík, D., and Mrovec, M. (2017). “Bond strength between reinforcing steel and different types of concrete.” *Procedia Engineering*, 190, 243 – 247. *Structural and Physical Aspects of Construction Engineering*.

El-Nemr, A., Ahmed, E. A., Barris, C., and Benmokrane, B. (2016). “Bond-dependent coefficient of glassand carbon-frp bars in normal- and high-strength concretes.” *Construction and Building Materials*, 113, 77 – 89.

Elgabbas, F., Ahmed, E., and Benmokrane, B. (2013). “Basalt frp reinforcing bars for concrete structures.” *Fourth Asia-Pacific Conference on FRP in Structures (APFIS 2013)*.

Elgabbas, F., Vincent, P., Ahmeda, E. A., and Benmokrane, B. (2016). “Experimental testing of basalt-fiberreinforced polymer bars in concrete beams.” *Composites Part B*, 91, 205–218.

Fava, G., Carvelli, V., and Pisani, M. A. (2016). “Remarks on bond of gfrp rebars and concrete.” *Composites Part B: Engineering*, 93, 210 – 220.

Gu, X., Yu, B., and Wu, M. (2016). “Experimental study of the bond performance and mechanical response of gfrp reinforced concrete.” *Construction and Building Materials*, 114, 407–415.

Hassan M., Benmokrane B., E. A. (2016). “Bond durability of basalt-fiber-reinforced-polymer (bfrp) bars embedded in concrete in aggressive environments.” *Composites Part B*, 106, 262–272.

- Islam, S., Afefy, H. M., Sennah, K., and Azimi, H. (2015). “Bond characteristics of straight- and headedend, ribbed-surface, gfrp bars embedded in high-strength concrete.” *Construction and Building Materials*, 83, 283 – 298.
- Jamalan, M. H. and Fu, D. F. (2018). “Numerical analysis on bond strength of FRP re-bars under elevated temperature.” *IOP Conference Series: Materials Science and Engineering*, 371, 012013.
- Kabir, M. and Islam, M. M. (2014). “Bond stress behavior between concrete and steel rebar: Critical investigation of pull-out test via finite element modeling.” *International Journal of Civil and Structural Engineering*, 5, 80–90.
- Munoz, M. B. (2010). “Study of bond behaviour between frp reinforcement and concrete,” PhD thesis, Universitat de Girona.
- Refai A., Ammar M. A., M. R. (2015). “Bond performance of basalt fiber-reinforced polymer bars to concrete.” *Journal of Composites for Construction*.
- Rossini, M., Cadenazzi, T., Nolan, S., and Nanni, A. (2018). “Seacon and resilient frp-rc/pc solutions: The halls river bridge.” *Italian Concrete Days 2018*.
- Sólyom, S. and Balázs, G. (2015). “Bond strength of frp rebars.” *Concrete Structures*, 16, 62–68.
- Sólyom, S., Balázs, G., and Borosnyói, A. (2015). “Material characteristics and bond tests for frp rebars.” *Concrete Structures*, 16, 38–45.
- Vincent, P., Ahmed, E., and Benmokrane, B. (2013). “Characterization of basalt fiber-reinforced polymer (bfrp) reinforcing bars for concrete structures.” *Specialty Conference on Material Engineering & Applied Mechanics*, 3rd, MEC–111–1 – MEC–111–10.
- W. A. Slater, F. E. Richart, G. G. S. (1920). (Tests of Bond Resistance Between Concrete and Steel). Washington Government Printing Office.
- Yan, F. and Lin, Z. (2016). “Bond behavior of gfrp bar-concrete interface: Damage evolution assessment and fe simulation implementations.” *Composite Structures*, 155, 63 – 76.
- Yang, S. and Xu, X. (2018). “Discussion on bonding performance between FRP bars and concrete.” *IOP Conference Series: Earth and Environmental Science*, 189, 032031.

## **Appendix E**

### **BDV30 986-02 Draft Deliverable 2: BFRP-FRC Link Slab – Instrumentation & Monitoring Plan**

*(Minor changes requested,*

*43 pages)*

## **EXHIBIT A – SCOPE OF SERVICE**

Project Title: **BRIDGE DECK WITH LINK-SLAB**  
For FPID: **435390-1-52-01: US 41 from Midway Blvd to Enterprise**  
**Contract Number: BDV34 986-02**  
**Deliverable 2 - TASK 2 – RECOMMENDATIONS FOR BRIDGE**  
**INSTRUMENTATIONS AND MONITORING OF LINK-SLAB**

Submitted by: **Adel ElSafty**, Principal Investigator  
University of North Florida  
School of Engineering  
1 UNF Drive, Jacksonville, FL 32224-2645  
Email Address: [adel.el-safty@unf.edu](mailto:adel.el-safty@unf.edu)  
Phone Number: (904) 620-1398

**James Fletcher**, Co-Investigator  
University of North Florida  
School of Engineering  
1 UNF Drive, Jacksonville, FL 32224-2645  
Email Address: [jfletche@unf.edu](mailto:jfletche@unf.edu)  
Phone Number: (904) 620-1844

**Thomas Fowler**, Undergraduate  
University of North Florida  
School of Engineering  
1 UNF Drive, Jacksonville, FL 32224-2645  
Email Address: [n00880684@unf.edu](mailto:n00880684@unf.edu)

Submitted to: **Steven Nolan**, Project Manager  
The Florida Department of Transportation  
State Structures Design Office  
605 Suwannee Street, MS 33  
Tallahassee, FL 32399-0450  
Email Address: [Steven.Nolan@dot.state.fl.us](mailto:Steven.Nolan@dot.state.fl.us)  
Phone: (850) 414-4272

**Dr. Cheresa Y. Boston**, Director of Sponsored Research  
University of North Florida  
Office of Research and Sponsored Programs  
1 UNF Drive, Jacksonville, Florida 32224  
Email: [cheresa.boston@unf.edu](mailto:cheresa.boston@unf.edu)  
Phone: (904) 620-2455, Fax: (904) 620-2457

July 25, 2019

## **Deliverable 2 - TASK 2 – RECOMMENDATIONS FOR BRIDGE**

### **INSTRUMENTATIONS AND MONITORING OF LINK-SLAB**

#### **1. INTRODUCTION**

The aim of deliverable 2 of task 2 is to provide recommendations for the instrumentations of the link-slabs, a suggested monitoring plan, and instrumentation system to monitor the temperature, strain, rotation, and elongation of different link-slabs. The research team identified appropriate instrumentation for monitoring and locations for sensors and instrumentations for the BFRP-RC link-slab on Bridge No. 019003 over Morning Star Waterway. In this deliverable report, the team suggests a monitoring plan and an instrumentation system to monitor the temperature, strain, rotation, and elongation of link-slabs. During construction, the research team will inspect the instrument and sensor locations. The proposed link-slab is designed with enough BFRP reinforcement to withstand the loads placed on the bridge superstructure. Also, it is desired that the link-slab does not crack excessively under typical service loads. For the BFRP-RC link-slab, special measures should be considered to anchor the FRP reinforcement to the existing bridge deck during the installation of a link-slab in the existing deck. In general, the behavior and design of the link-slab are influenced by several variables such as span length and arrangement, bearing type, beam end rotation under load, bridge skew, and relative flexural stiffness of the beam and slab. For the investigated bridge link-slab in this study, it is required to measure and monitor the strains, deformations, and cracks in the link-slab, and rotation of beam ends. The monitoring of the tested bridge with the recorded data under long-term effects as well as live loads will investigate the link-slab behavior and the ability of the continuity detail to transfer forces from one girder to the adjacent girder across joint over the end bent.

#### **2. PROPOSED INSTRUMENTATION PLAN**

The research team identified appropriate instrumentation for monitoring and locations for sensors and instrumentations for the BFRP-RC link-slab on Bridge No. 019003 over Morning Star Waterway. The team also suggested a monitoring plan and instrumentation system to monitor the temperature, strain, rotation, and elongation of link-slabs. The bridge link-slab monitoring system will include three main components, (1) sensors, (2) data acquisition system, and (3) cabling and conduit. Sensor locations are shown on the figures. Details of the components of the monitoring system are also provided. The research team will inspect the instrumentations and sensor locations during construction.

#### **3. BRIDGE MONITORING SYSTEM INSTALLATION AND INSTRUMENTATION**

I. The system installation activities will be coordinated between involved parties (FDOT technical team, Contractor and other subcontractors, the project manager, and the research team) to establish the installation schedule of both the embedded and surface-mounted sensors. The monitoring system including sensors will be installed as construction on the bridge proceeds and the contractor shall provide a preliminary schedule for installation activities to FDOT. Once the preliminary schedule is approved, the contractor shall develop a detailed installation schedule that will be linked to the project schedule.

II. The following describes the phases required for complete installation of the monitoring system:

##### ***Phase 1. During Link-Slab Construction***

Investigated elements: Deck - Link-slab connecting spans 1 and 2.

Embedded sensors in the reinforced concrete deck shall be installed at the time of placing reinforcing bars of BFRP at the bridge site as per the plans. Initial readings shall be recorded at time of installation prior to, during, and after concrete casting. Parameters to be measured during this phase are:

- a) Strains in structural elements
- b) Temperatures at sensor locations
- c) Ambient temperature and relative humidity (To be determined from local weather forecasting reports).

**Phase 2. After Deck Pouring**

Investigated elements & spans: Bridge superstructure/beams and link-slab connecting spans 1 and 2. Once casting the concrete deck is complete, surface-mounted sensors shall be installed as shown in the figures. Initial readings shall be recorded. Parameters to be measured during this phase are:

- a) Strains and deformations in structural elements
- b) Crack propagation once developed in the link-slab
- c) Temperatures at sensor locations
- d) Relative movement between adjacent beams (using Vibrating Wire- Crackmeter Model 4420 for example) and beams’ rotation
- e) Ambient temperature and relative humidity (To be determined from local weather forecasting reports).

**Phase 3. Initial Bridge Condition upon Completion of Construction**

Once the bridge construction is completed, the contractor shall conduct a series of baseline tests so that the FDOT technical team can assess the performance of the monitoring system and quantify the initial condition of the link-slab and the bridge superstructure. The data collected during the baseline tests will represent the initial link-slab condition. A live load test with predetermined truck weight will be conducted by FDOT technical team or its representatives after completion of construction and prior to opening to traffic. The test load will be using an H10 design service vehicle with 20,000 lb.

Clear Deck Width	Design Vehicle
7 to 10 feet	H5
Over 10 feet	H10

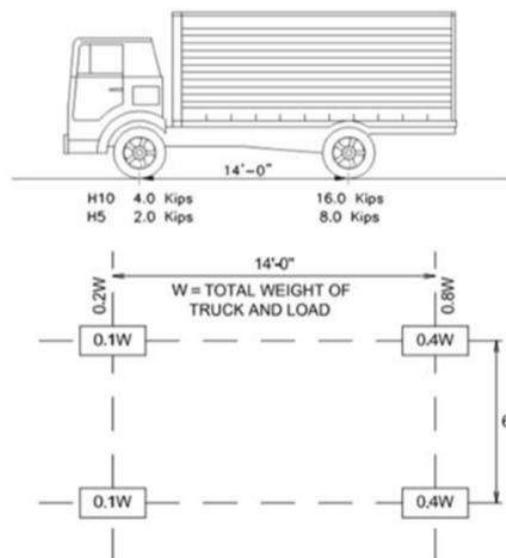


*Figure 1, Design Service Vehicle (H10)*

Parameters to be measured during this phase are:

- a) Strains and deformations in structural elements
- b) Crack propagation once developed in the link-slab
- c) Temperatures at sensor locations
- d) Relative movement between adjacent beams and beam end rotation
- e) Ambient temperature and relative humidity (To be determined from local weather forecasting reports).

III. The contractor shall document any early shrinkage cracking that may take place in the deck, link-slab, or the prestressed concrete girders.

IV. Extreme caution should be taken to protect all instrumentation during construction.

## 4. SYSTEM DETAILS

The link-slab monitoring system shall include three main components, (1) sensors, (2) data acquisition system, and (3) cabling and conduits. Sensor locations are shown on the change order plans. Details of each component of the system component are given next:

### 4.1 SENSORS

The bridge link-slab and exterior beams will be equipped with sensors designed to measure the following:

- a) Strains and deformations in the link-slab
- b) Crack propagation once developed in the link-slab
- c) Temperature at sensor locations
- d) Relative movement between adjacent beams ends and rotation of beams ends
- e) Ambient temperature and relative humidity will not be measured on location with sensors (to be determined from local weather reports).

The various types and quantity of each type are presented. Two types of sensors will be installed; an embedded type and a surface-mounted type. The embedded sensors are vibrating wire sisterbars and strandmeters. Surface mounted sensors are vibrating wire gapmeters and tiltmeters. All vibrating wire gages shall have an integral thermistor for determining temperature at the sensor location, at the time of measurement.

#### **EMBEDDED SENSORS:**

The embedded sensors are for measuring strains within and across the link-slab. This will be composed of a 3x3 array of sensor pairs, for a total of 18 (9 pairs) embedded sensors. Each pair consists of a sensor for measuring strain in the BFRP link-slab reinforcement (4410 or alternatively the 4151), and an adjacent "sisterbar" (4911) measuring strain in the link-slab concrete at approximately the same location. It is recommended by BDI that the sisterbar be tied off to its paired strandmeter via loose wire during installation.

The placement of the 3x3 array is with one longitudinal column at the centerline of the link-slab and two more columns approximately 48 inches to both sides of the centerline (the approximate center of outboard FSBs). The three transverse rows of these sensors should be spaced roughly 3 feet apart, with the middle row corresponding to the transverse midline of the link-slab/bridge. A cost-driven alternative

could be to use only the centerline column and one lateral column of sensors, for a total of 6 embedded locations (and 12 sensors).

**Strandmeter (4410, Geokon):** These strain sensors will be clamped to the link-slab reinforcement (BFRP bars/strands inside cast-in-place link-slab) at the specified locations. Special treatment per the product manual dictates surrounding sensor with grease prior to encasing inside concrete. BDI has expressed that the strandmeter sensor (4410) is preferable in this application because it is readily attached to a rounded surface (i.e. the reinforcement bars) and is more appropriate for embedment in concrete than the model 4151 alternative. **Number of sensors: 9**

**Miniature Strain Gauge (4151, Geokon):** A potential alternative to the 4410 strandmeters, should they be deemed non-applicable for the BFRP link-slab reinforcement. **Number of sensors: 9 (potentially)**

**Sisterbar (4911, Geokon):** These strain sensors are fabricated on a #4 steel reinforcing bar. The standard stock length is 36 inches, but can be ordered to custom lengths (down to 24 inches), or cut on-site. One sisterbar is paired with each strandmeter (BFRP gauge) and placed adjacent to it in order to measure strain in the concrete surrounding reinforcement bars. BDI suggests loosely tying each sisterbar to its accompanying strandmeter-mounted reinforcement bar with wire. Actual lengths of sisterbars will be customized to their location in the link-slab (see Appendix B). **Number of sensors: 9**

#### **SURFACE-MOUNTED SENSORS:**

**Micro Crackmeters (4422, Geokon):** Displacement gauges mounted on the top deck surface of the link-slab. Intended to measure crack growth in the link-slab; preemptively installed across the transverse midline. **Number of sensors: 3**

**Tiltmeters (6350, Geokon)-Optional:** These sensors will be installed to measure rotational deflection of FSB beam ends (within the vertical-longitudinal plane), at the bridge midline. They are to be located on the undersides of the two centerline FSB beams, 1 inch away from the bent cap (on either side of the bent cap). The sensors hang in a vertical orientation by a custom bracket connected to the FSB undersides by a groutable anchor bolt. The tiltmeter opposite of the transverse conduit will route its cable alongside the Convergence Meter (4425, Geokon, see Group#4).

Alternatively, the tiltmeters may be mounted on the outboard flanges of the FSB beams, on the lateral (side) face of the bridge. This position may provide less accurate measurements as the use of shims would be required to provide a true vertical surface against the angled FSB flange, and the additional rigidity of the concrete parapets above could reduce rotational deflection in this region. However, this outboard placement of the tiltmeters could be a more convenient location for installation and subsequent access. A cost-driven alternative would be to dismiss the use of tiltmeters altogether.

**Number of sensors: 2**

**Crackmeters (4420, Geokon):** Used for measuring displacement along the outboard sides of the link-slab (at top) and FSB beam flange (at bottom). These sensors are located to measure longitudinal displacement across the transverse midline (changes in gap width between the two sections of the bridge at the continuity). Sensors monitoring these external displacements are here forth referred to as “External Displacement Transducers” or “EDTs”. The pair of upper EDTs are located 3 inches from the top surface of the 6 inch thick link-slab, straddled across the midline. The pair of lower outboard EDTs are located on the outer flange of the lateral FSBs, 2 inches from the bottom surface of the 4 inch thick flanges, also straddling the midline.

The lower outboard EDTs necessitate a cutout modification on the shear key of the bent cap. This cutout was requested to be no longer than 12 inches, however, the shortest custom Crackmeter for this application is 10.35 inches in overall length, and therefore a 14 inch long cutout is suggested to provide enough clearance for installation. An alternative solution would be to replace the lower outboard EDTs with the arrangement used for the lower centerline EDT (Convergence Meter, 4425 Geokon) described below. This would use a passage placed through the bed of the bent cap instead of a cutout in the shear key. **Number of sensors: 4**

**Convergence Meter (4425, Geokon):** Used to gain a lower, centerline measurement to compliment the external displacement profile generated from the EDTs (See previous sensor definition; 4420 Crackmeters). Mounting anchor points are located on underside of centerline FSBs, on either side of the bent cap. A 2 inch PVC pipe inlaid across the bent cap (at centerline and approximately 1.5 inch from top of cap) provides a path for the instrument to span between each FSB. This sensor will require 1 to 2 feet of stainless steel extension rod, provided by the manufacturer. **Number of sensors: 1**

**Total number of sensors to be deployed: 28**

All sensors are of commercial-grade quality vibrating wire devices and shall be installed in accordance with manufacturers' recommendations. Sensor specifications are shown in Table 1 below. Manufacturer's data sheets along with images/illustrations is provided within Appendix-A.

Group #	Sensor Objective	Gauge Type/Model & Source	Sensor Resolution	Sensor Accuracy	Sensor Measuring Range	Sensor Dimensions
1	Strain in BFRP	Strandmeter (4410, Geokon)	<5 $\mu\epsilon$	(+/-) 0.003 mm	3 mm (15000 $\mu\epsilon$ )	8" Long x 1.77" Wide Clamps
2	Strain in Concrete Link-Slab	Sisterbar (4911, Geokon)	0.4 $\mu\epsilon$	(+/-) 7.5 $\mu\epsilon$	3000 $\mu\epsilon$	36" Stock Length, Actual Length custom cut. #4 Size Rebar (0.5" Dia)
3	Crack Width in Link-Slab	Micro Crackmeter (4422, Geokon)	.001 mm	(+/-) 0.004 mm	4 mm	4.725" Long x 0.315" Diameter
4	Lower centerline EDT, (Collinear middle FSBs)	Convergence Meter (4425, Geokon)	.000625 mm	(+/-) 0.025 mm	25 mm	1" Dia., Combined Length between 42"-48"
5	External Displacement Gauges (EDTs)	Crackmeter (4420, Geokon)	.00625 mm	(+/-) 0.025 mm	25 mm	Length: 12.5"(standard) or 10.35"(custom), Dia:1"
6	Rotation of Beam Ends	Tiltmeter (6350, Geokon)	8 Arc Seconds	(+/-) 0.01 Degree	(+/-) 10 Degrees	7.638" Long x 1.26" Diameter
7	Datalogging	Datalogger (8600-1, Geokon)	.001Hz RMS	(+/-) .0013% of VW Reading, (+/-) .25% of Thermistor Reading	100 - 6000 Hz	LWH: 15.43"x13.86"x6.34"
8	Signal Gathering/Splitting	Multiplexer/MUX (8032, Geokon)	N/A	N/A (.1 Ohm Contact Resistance)		LWH: 12.52"x10.91"x6.26"
18	Alternative to Strandmeters	Miniature Strain Gauge (4151, Geokon)	0.4 $\mu\epsilon$	15 $\mu\epsilon$ , (50 $\mu\epsilon$ for larger range model)	3000 $\mu\epsilon$ , (10,000 $\mu\epsilon$ Available)	2.25" Length x 0.25" Dia

*Table 1, Sensor Models and Specs*

## 4.2 Sensor Wiring:

### Sensor Cables

Connections between the sensors and data acquisition system is accomplished via a “5-wire” cable that has 2 twisted pairs (red/black & white/green), foil shielded, 22AWG stranded copper wire, 0.0625 inch PVC jacketed). An estimated total of 971 feet of cable will be used in routing between sensors and the data acquisition system. See Table 2 below for breakdown of cable length estimate.

All cabling running from the sensors to the data acquisition system will be either embedded in concrete and/or routed through conduits. Embedded sensor cables shall be routed transversely across concrete reinforcement to the nearest 3 inch or 4 inch conduit and shall be secured to reinforcements with zip-ties. After exiting through the side of the link-slab, embedded sensor cables will be collected into the conduit through the nearest PVC tee opening. For the midline row of embedded sensors, care should be taken when routing the cable inside the link-slab, so that cables are not located where anchors shall be installed for the upper, outboard EDTs (upper 4420 Crackmeters).

Embedded sensors shall be delivered with pre-attached heavy grade insulation cables to survive the thermal and chemical environment of the concrete during curing. Special care shall be taken to protect the cables, especially at exit points for embedded sensors’ cables and around sharp edges. This may include embedding small conduit couplings into concrete at the exit of each individual cable. Protective containers should be provided at exit points with enough room to store cable ends for protection against damage and accidental cutting during concrete casting, curing, transportation and erection. High quality cable tags shall be used at multiple points along each cable in order to positively identify each cable and its associated sensor. This is especially important for embedded sensors/cables.

Cabling running from the surface mounted Micro Crackmeters (Group #3) will be protected with heavy duty cable runners. These will be laid transversely across the midline and lead the cables through the bottom of the concrete parapet, toward the main conduit line where the cables will be collected.

Cable Requirements		
Group #	Sensor Group	Cable Length for Group (feet)
1 & 2	3x3 Array of embedded sensors (Strandmeters/Sisterbars)	543
3	Link-Slab Crack Growth	90.5
4	Lower Centerline EDT	30.25
5	Outboard EDTs	120
6	Tiltmeters	60.5
	<b>Total (ft):</b>	844.25
	<b>Plus 15%, Total (ft):</b>	971

*Table 2, Total Estimated Cable Length for Sensors*

### Conduit Housing

In order to try and reduce overall cost of the package, the conduits housing the cables are designed with regular schedule 40 PVC fittings at junctions and elbows, rather than electrical junction boxes which are significantly more expensive for the given size of conduits. The spans of straight conduit use gray, electrical grade PVC conduit and consists of 4 inch, 3 inch, and 1.5 inch diameters.

The conduit is laid out to minimize overall length of piping. The widest section is 4 inch diameter pipe, housing a max of 28 Vibrating Wire cables. This steps down to a 3 inch section that houses between 5 and 13 cables, the smallest section of piping is 1.5 inches which houses 2 cables. 30 to 45 degree elbows are on all horizontal terminal ends, to help prevent water/debris intrusion. The only vertical terminal ends are downward facing. All terminal ends are to be fitted with a flexible rubber cap to be punctured/cut with openings for cables; the intent of which is to prevent infiltration of conduit by wildlife.

At three points flexible rubber couplings are installed in the conduit line to allow for expansion/contraction/translational movement of the system. Two of these are at points crossing the midline, and one that leads a 3 dimensional turn in the conduit. Additionally, it is recommended to drill a few strategically located small holes (maximum .25 inch diameter) along the bottom facing portion of the bottom most conduit line. This is to allow drainage of water that may intrude by vapor condensation.

### 4.3 DATA ACQUISITION:

Data Acquisition will be accomplished by one datalogger module (8600-1, Geokon) to record measurements, and two multiplexers (8032 MUX, Geokon) for connecting the 28 sensors to the datalogger. With the one datalogger and two multiplexer arrangement, up to 32 Vibrating Wire sensors could be deployed, providing an excess of 4 sensors.

Datalogger internal power is supplied by a 12 volt, 7 amp-hour gel cell, maintained by an external, AC regulated waterproof charger. The external power source is yet to be determined; an off-grid solar power system is expected to be beyond the budgetary scope for this project.

Recorded sensor data shall be accessed by direct retrieval through a USB port using a Windows based computer system. Standard memory capacity for the 8600-1 datalogger is 128 MB of battery-backed SRAM, which can be expanded with an SD card. According to Geokon, the data storage capacity is far more than what will be required for this project. Assuming a measurement frequency of 1 data point per hour, per sensor over a one month period, only a fraction of the total data capacity will be used. Remote access to the data is not planned for this project as of now.

Datalogger and multiplexer units come housed in weather proof boxes, which will be securely mounted at location(s) approved by the FDOT. Suggested mounting location is on the outboard side of the cement parapet at a terminal end of the bridge, to allow unencumbered access. Additional secure enclosure for data acquisition system may be requested at the discretion of FDOT. Budgeting for lightening protection of data acquisition and sensor systems is at the discretion of FDOT. The datalogger and multiplexer units do come standard with an integrated surge protection system. Table 3 below shows specifications of data acquisition components.

Component	Model	Resolution	Accuracy	Range	Dimensions
Datalogging	<i>Datalogger (8600-1, Geokon)</i>	.001Hz RMS	(+/-) .0013% of VW Reading, (+/-) .25% of Thermistor Reading	100 - 6000 Hz	LWH: 15.43"x13.86"x6.34"
Signal Gathering/Splitting	<i>Multiplexer/MUX (8032, Geokon)</i>	N/A	N/A (.1 Ohm Contact Resistance)		LWH: 12.52"x10.91"x6.26"

**Table 3, Datalogger and Multiplexer Specs**

## 5. INSTRUMENTATION SETUP

**It is worth highlighting some points on the proposed instrumentation setup:**

**1)** Installing the EDTs on the outside of the bridge is acceptable; however, having the 27 inch-concrete parapet (barrier wall) right on top of these locations could provide additional stiffness that affects the readings in these locations. That behavior of the exterior beams (stiffened with the parapet) may be different than the behavior of the middle beam. Upper outboard EDTs are to be located 3 inch from top of link-slab deck (middle of 6 inch link-slab). This consideration reinforces the suggestion of including a lower centerline EDT measurement, as is the purpose of the Convergence Meter (4425, Geokon) that is included in Group #4 of the sensor list (also, see paragraphs 3 and 6 below).

**2)** In order to provide clearance for installation of and access to the lower outboard EDTs, it is proposed to modify the bent cap shear key with a rectangular cutout in the top surface of the shear key, against the inboard edge, centered with the midline. FDOT previously recommended the length of this cutout be no greater than 12 inches, however, the gauges recommended for this application (4420 Crackmeter) have a standard overall length of 12.5 inches, and a minimum length of 10.35 inches for custom Crackmeter gauges. Thus, the cutout dimensions are proposed to be 14 inches long, 6 inches wide, and 8 inches deep with a bottom sloping upward to the outboard (2/3 slope), as this should provide ample clearance for installation of the custom Crackmeters. Lower outboard EDTs are to be located at a height of 2 inch measured from the bottom of the FSB beam (mid height of the 4 inch bottom flange thickness).

An alternative to modifying the shear key to accommodate outboard mounted lower EDTs would be to mount longer sensors on the underside of the lateral FSB beams. This would require the same modification as described in paragraph 3, below, whereby a 2 inch PVC pipe is inlaid the bent cap. This pipe would provide a pathway for a Convergence Meter (model 4425, Geokon) to pass through and mount to anchors set into the ends of the lateral FSB beams.

**3)** There are no risers in the investigated bridge, which prevents measurement of external displacement at the bottom-side centerline with the same instruments used for the outboard EDTs (4420 Crackmeters). Further modification of the bent cap is proposed to accommodate a lower centerline EDT measurement by placing a 2 inch PVC pipe inside the bent cap. This “through pipe” is along the centerline; with 1.5 inches between the top of the pipe and the top surface of the bent cap bed (depth may be changed to accommodate bent cap reinforcement). This would provide a pathway for a 52 inch long Convergence Meter (28 inch long instrument, with 24 inches of extension rod – model 4425, Geokon) to mount onto anchors set in the underside of the FSB beams on opposing sides of the bent cap. This would provide a more complete picture of the external displacement profile.

**4)** To accurately detect and measure the force in the link-slab, the strandmeter (4410, Geokon) is recommended to be clamped onto the reinforcement bars (BFRP). Geokon (the manufacturer) recommends these gauges be encased with grease after mounting to reinforcement, before pouring of surrounding concrete. Various size strandmeter clamps are available from Geokon; the BFRP reinforcement bars used in the link slab have a diameter of approximately 0.625 inches and clamps will be sized accordingly. Gauges that are clamped to reinforcement bars are needed since the gauges embedded in concrete will be greatly affected by concrete cracking that could result in wrong readings or no reading at all. Those gauges on BFRP reinforcement are in addition to the embedded gauges in concrete.

5) The locations of paired strain gauges embedded in the link-slab should be a 3-row x 3-column array with one longitudinal column at the centerline of the link-slab and two more columns 47.625 inches either side of the centerline (the approximate center of outboard FSBs). The three transverse rows of these sensors should be spaced 3 feet apart, with the middle row corresponding to the transverse midline of the link-slab/bridge. A cost-driven alternative could be to use only the centerline column and one lateral column of sensors, for a total of 6 embedded locations (and 12 sensors).

6) It is recommended to install two Tiltmeter gauges to measure angular deflection (in the vertical-longitudinal plane) of FSB beam ends at the midline junction. They are to be located on the undersides of both the centerline FSB beams, 1 inch away from the bent cap, on the centerline. The mounting brackets provided with the sensors will need two additional holes drilled to allow vertical hanging of the sensors from a horizontal surface. It is suggested these sensors are located on the centerline FSBs since deflection of the lateral beams may be suppressed by the added rigidity of the concrete parapets (see paragraph 1, above).

Alternatively, the tiltmeters could be mounted on the outboard flanges of the FSB beams, on the lateral (side) face of the bridge. This position may provide less accurate measurements as the use of shims would be required to provide a true vertical surface against the angled FSB flange and the additional rigidity of the concrete parapets above could reduce rotational deflection in this region. However, this outboard placement of the tiltmeters could be a more convenient location for installation and subsequent access. A cost-driven alternative would be to dismiss the use of tiltmeters altogether.

## 6. Estimated Cost

### 6.1 Preferred Sensor Package

Currently, the total estimated cost of the sensor package is \$20,756.50 before taxes or potential shipping costs. This estimate only includes the required sensors; data acquisition system; cabling between the sensors and data acquisition system; conduit to house and protect cabling; and some various installation hardware. The selected sensors and hardware are shown in the charts below along with their prospective application, technical specifications, and costs.

Group #	Sensor Objective	Gauge Type/Model & Source	# of Units	Unit Price (USD)	Part Total (USD)	Note
1	Strain in BFRP	<i>Strandmeter (4410, Geokon)</i>	9	345.00	3105.00	
2	Strain in Concrete Link-Slab	<i>Sisterbar (4911, Geokon)</i>	9	345.00	3105.00	
3	Crack Width in Link-Slab	<i>Micro Crackmeter (4422, Geokon)</i>	3	445.00	1335.00	
4	Lower centerline EDT, Collinear middle FSBs	<i>Convergence Meter (4425, Geokon)</i>	1	620.00	620.00	
5	External Displacement Gauges (EDTs)	<i>Crackmeter (4420, Geokon)</i>	4	335.00	1340.00	
6	Rotation of Beam Ends	<i>Tiltmeter (6350, Geokon)</i>	2	530.00	1060.00	
7	Datalogging	<i>Datalogger (8600-1, Geokon)</i>	1	4135.00	4135.00	
8	Signal Gathering/Splitting	<i>Multiplexer/MUX (8032, Geokon)</i>	2	905.00	1810.00	

9	Multiplexer Cable Connectors	<i>Pin connection between MUX and Datalogger, Geokon</i>	2	180.00	360.00	
10	Model4420 Groutable Anchors	<i>Anchors Sold as Set of Two (MNT 4420-02, Geokon)</i>	4	46.00	184.00	
11	Convergence Meter(4425) Groutable Anchors	<i>Individual Eyebolt anchors for 4425, Geokon</i>	2	26.00	52.00	
12	Convergence Meter(4425) rod extensions	<i>stainless steel rod for 4425, sold by the foot, Geokon</i>	2	3.95	7.90	price/ft
13	Protective Tube for Micro Crackmeter	<i>4422 AI Housing (SPC-4422-01, Geokon)</i>	3	75.00	225.00	
14	Micro Crackmeter Groutable Anchors.	<i>Micro Crackmeter Anchors (MNT-4420-02, Geokon)</i>	3	48.00	144.00	Sold as pair
15	Uni-Axial Mounting Bracket	<i>Tiltmeter Bracket (MNT-6350-01 , Geokon)</i>	2	95.00	190.00	
16	Tiltmeter Aluminum Protective Cover	<i>Tiltmeter Cover (SPC-6350-01, Geokon)</i>	2	145.00	290.00	
17	Conduit to House Cables and Hardware	<b>See Conduit Costs Below</b>	/	/	703.67	
18	Cable	<i>VW cable(IC-02-250, Geokon), unit price/ft.</i>	971	0.92	893.32	
19	Various Hardware	<b>See Miscellaneous Costs Below</b>	/	/	1850.38	
20	Micro SD Card		1	50.00	50.00	Est. price
		<b>Package Pre-Tax &amp; Shipping Total (USD):</b>		<b>\$20,756.50</b>	<b>Plus Tax (7%) Total:</b>	<b>\$22,209.46</b> (Does Not Include Shipping )

*Table 4, Estimated Total Cost of Preferred Sensor Plan*

*Miscellaneous and Conduit Costs Continued on Next Page*

Miscellaneous Items	Price per Unit	# of Units	Cost (USD)	Source
2" x 10' PVC Pipe/Conduit (for Bent Cap Thru Hole, Group #4)	8.31	1	8.31	HDX/Lowes
15' of rubber HD cord cover/runner (for containing microcrackmeter cables)	100.00	1	100.00	Cabletiesandmore.com
Various Concrete Anchors	50.00	1	50.00	(estimated quantity/cost)
Estimate Flex Factor (5% of SubTotal) <i>for Preferred Sensor Package</i>	988.40	1	988.40	
Estimate Flex Factor (5% of SubTotal) <i>for Cost Driven Sensor Package</i>	763.30	1	763.30	
Conduit Parts and Hardware:	Price per Unit	# of Units	Cost (USD)	Source
3 in. Hinged Split Ring Pipe Hanger in Galvanized Malleable Iron (5-Pack)	63.99	1	63.99	HDX/Lowes
Wedge-All 7/8 in. x 6 in. Zinc-Plated Expansion Anchor (5-Pack), for 4" and 3" Pipe Hangers	34.99	2	69.98	HDX/Lowes
1-1/2 in. 2-Piece Copper Epoxy Coated Iron, Split Ring Pipe Hanger (5-Pack)	15.49	1	15.49	HDX/Lowes
4 in. Hinged Split Ring Pipe Hanger in Galvanized Malleable Iron (5-Pack)	82.29	1	82.29	HDX/Lowes
Wedge-All 3/8 in. x 7 in. Zinc-Plated Expansion Anchor (50-Pack), for 1.5" Pipe Hangers	47.87	1	47.87	HDX/Lowes
Schedule 40 PVC Conduit with Bell End, Trade Size: 4", Nominal Length: 10 ft.	57.82	3	173.46	Grainger (grainger.com)
Schedule 40 PVC Conduit with Bell End, Trade Size: 3", Nominal Length: 10 ft.	43.73	2	87.46	Grainger (grainger.com)
Schedule 40 PVC Conduit with Bell End, Trade Size: 1-1/2", Nominal Length: 10 ft.	16.16	2	32.32	Grainger (grainger.com)
4 in. x 4 in. PVC Mechanical Flexible Expansion Coupling	12.83	1	12.83	HDX/Lowes
3 in. x 3 in. PVC Mechanical Flexible Expansion Coupling	9.25	1	9.25	HDX/Lowes
1-1/2 in. x 1-1/2 in. DWV Flexible PVC Expansion Coupling	9.41	1	9.41	HDX/Lowes
4" Schedule 40 PVC 45 Elbow Socket, 417-040 (white)	9.29	1	9.29	pvcpipesupplies.com
3" Schedule 40 PVC 45 Elbow Socket, 417-030 (white)	5.19	1	5.19	pvcpipesupplies.com
1 1/2" Schedule 40 PVC 45 Elbow Socket, 417-015 (white)	0.99	1	0.99	pvcpipesupplies.com
4" x 2" Schedule 40 PVC Tee Socket, 401-420 (white)	10.59	2	21.18	pvcpipesupplies.com
3" x 2" Schedule 40 PVC Tee Socket, 401-338 (white)	6.29	2	12.58	pvcpipesupplies.com
3" Schedule 40 PVC 90 Elbow Socket, 406-030 (white)	3.99	2	7.98	pvcpipesupplies.com
1 1/2" Schedule 40 PVC 90 Elbow Socket, 406-015 (white)	0.69	2	1.38	pvcpipesupplies.com
4 in. Plastic DWV Flexible Cap	4.65	1	4.65	HDX/Lowes
2 in. PVC DWV Flexible Cap	3.47	4	13.88	HDX/Lowes
1-1/2 in. PVC DWV Flexible Cap	3.13	1	3.13	HDX/Lowes
4" x 3" Schedule 40 PVC Coupling Socket, 429-422 (white)	9.79	1	9.79	pvcpipesupplies.com
3" x 2" Schedule 40 PVC Coupling Socket, 429-338 (white)	7.79	1	7.79	pvcpipesupplies.com
2" x 1 1/2" Schedule 40 PVC Coupling Socket, 429-251 (white)	1.49	1	1.49	pvcpipesupplies.com
<b>Total Misc. and Conduit Cost for Preferred Package</b>	<b>\$</b>		<b>1,850.38</b>	
<b>Total Misc. and Conduit Cost for Cost Driven Package</b>	<b>\$</b>		<b>1,616.97</b>	

Table 5, Conduit Components and Miscellaneous Hardware Costs

## 6.2 Cost Driven Sensor Package

An alternative arrangement from the above proposed sensor package deducts some instrumentation and hardware to achieve a lower cost. The 3x3 array of embedded strandmeter (4410, Geokon) and sisterbar (4911, Geokon) pairs is reduced to a 3x2 array, thus accounting for a decrease in 6 sensors and approximately \$2178.<sup>00</sup> in total cost (before tax). This 3x2 array would be arranged such that a centerline column of 3 sensor pairs (oriented longitudinally) is flanked on one side by another column of 3 sensor pairs set 47.625 inches from the centerline. Each column would be centered on the midline with two pairs of sensors 3 feet away from both sides of the midline.

Additionally, the lower centerline EDT (the Convergence Meter sensor, model 4425, Geokon, aka Group #4 sensors) could be altogether dismissed. This would further reduce the cost by approximately \$720.<sup>00</sup>. The tiltmeters could also be subtracted from the sensor plan, which would save another \$1604.<sup>00</sup>. It should be noted, however, that each of these modifications to the sensor plan would reduce the reliability, accuracy, and overall fidelity of the strain model developed from this study's data. A table of the alternative sensor package is shown below. The estimated total for this arrangement is \$16,029.25 before taxes.

Group #	Sensor Objective	Gauge Type/Model & Source	Number of Units	Unit Price (USD)	Part Total (USD)
1	Strain in BFRP	Strandmeter (4410, Geokon)	6	345.00	2070.00

2	Strain in Concrete Link Slab	<i>Sisterbar (4911, Geokon)</i>	6	345.00	2070.00
3	Crack Width in Link Slab	<i>Micro Crackmeter (4422, Geokon)</i>	3	445.00	1335.00
4	none	<i>none</i>	none	none	none
5	External Displacement Gauges	<i>Crackmeter (4420, Geokon)</i>	4	335.00	1340.00
6	none	<i>none</i>	none	none	none
7	Datalogging	<i>Datalogger (8600-1, Geokon)</i>	1	4135.00	4135.00
8	Signal Gathering/Splitting	<i>Multiplexer/MUX (8032 , Geokon)</i>	2	905.00	1810.00
9	Multiplexer Cable Connectors	<i>Pin connection between MUX and Datalogger</i>	2	180.00	360.00
10	Model4420 Groutable Anchors	<i>Anchors Sold as Set of Two (MNT 4420-02, Geokon)</i>	4	46.00	184.00
11	Protective Tube for Micro Crackmeter	<i>4422 AI Housing (SPC-4422-01, Geokon)</i>	3	75.00	225.00
12	Conduit to House Cables and Hardware	<b><i>See Conduit Costs in previous section</i></b>	/	703.67	703.67
13	Cable	<i>VW cable(IC-02-250, Geokon), unit price/ft.</i>	819	0.92	753.48
14	Micro Crackmeter Groutable Anchors	<i>Micro Crackmeter Anchors (MNT-4420-02, Geokon), Sold as Pair</i>	3	48.00	144.00
15	Various Hardware	<b><i>See Miscellaneous Costs in previous section</i></b>	/	913.30	913.30
16	Micro SD Card		1	50.00	50.00
		<b>Package Pre-Tax &amp; Shipping Total (USD):</b>		<b>\$16,029.25</b>	
				<b>Plus Tax (7%) Total:</b>	<b>\$17,151.30</b>

*Figure 2, Estimated Total Cost of Cost Driven Sensor Plan*

Note: The cost of retaining the Lower Centerline EDT (model 4425 Convergence Meter) with the Cost Driven Sensor Plan would be an additional \$712.<sup>00</sup>. It is recommended to retain this sensor, even if the low cost sensor plan is selected.

**7. Illustrations**  
**(Dimensioned Drawings are in Appendix B)**  
*Images of Bridge Sensor Setup*  
*All bridge components are partially translucent in illustrations*

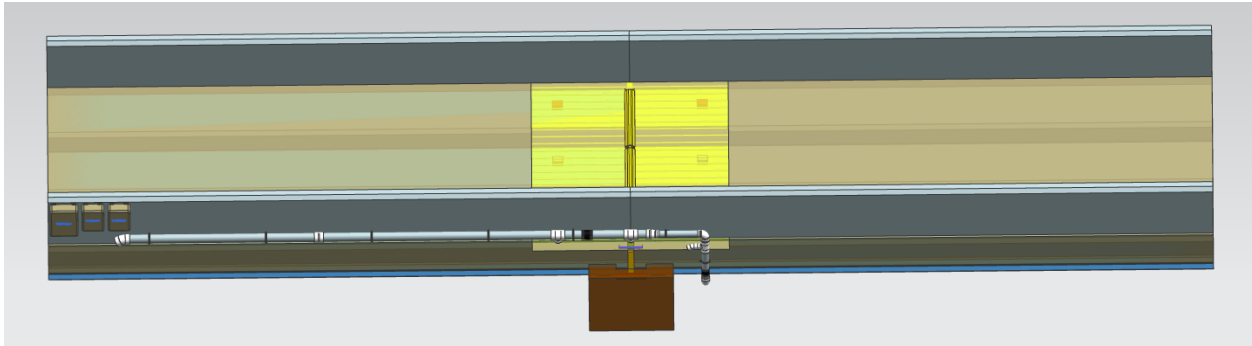


Figure 3, Side Pan View

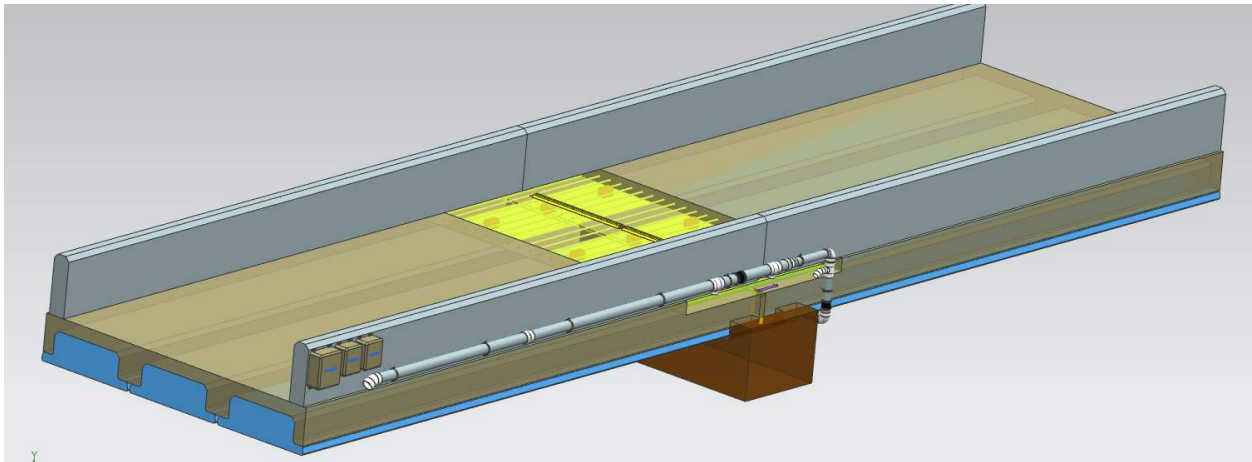


Figure 4, Long View

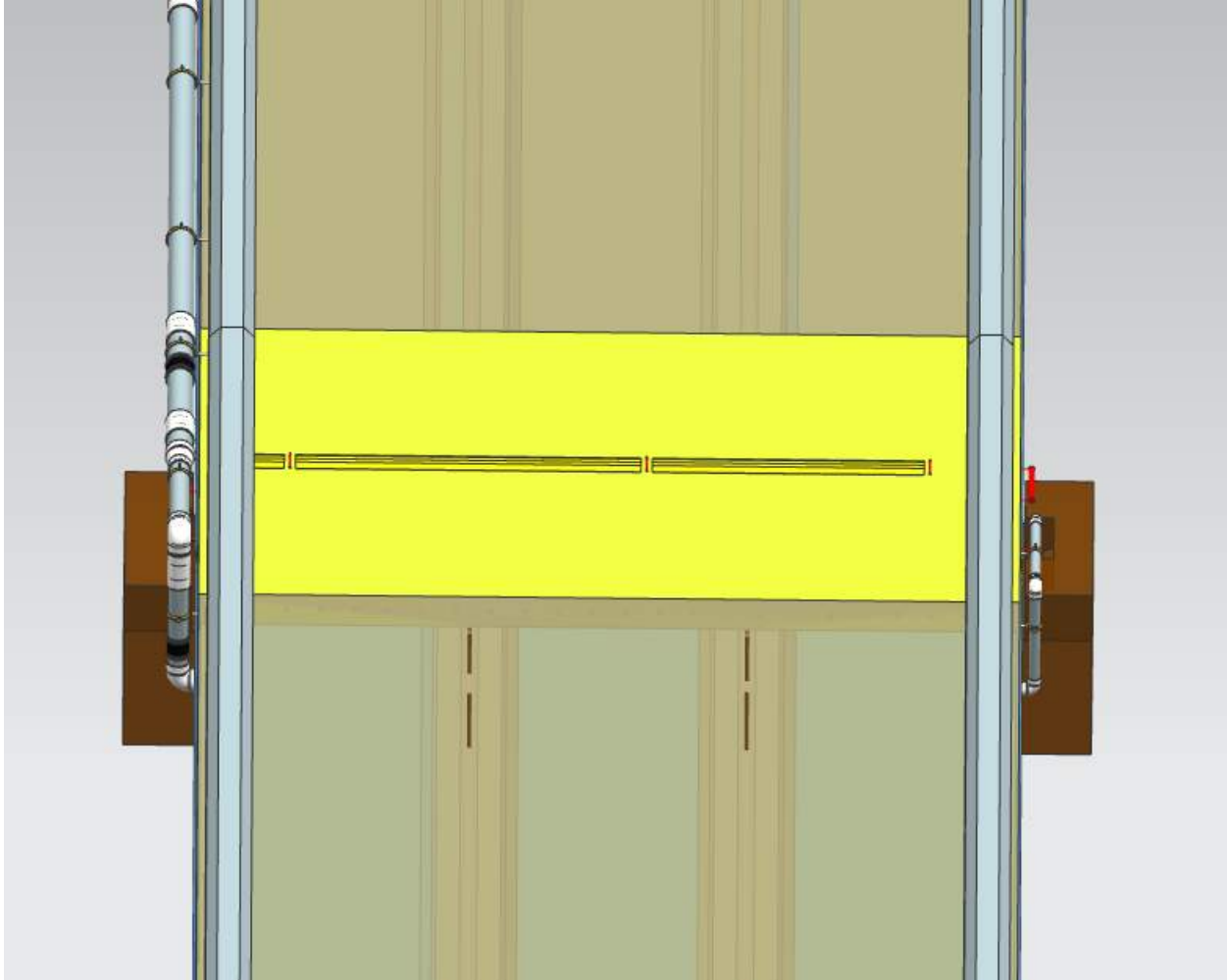


Figure 5, Top View

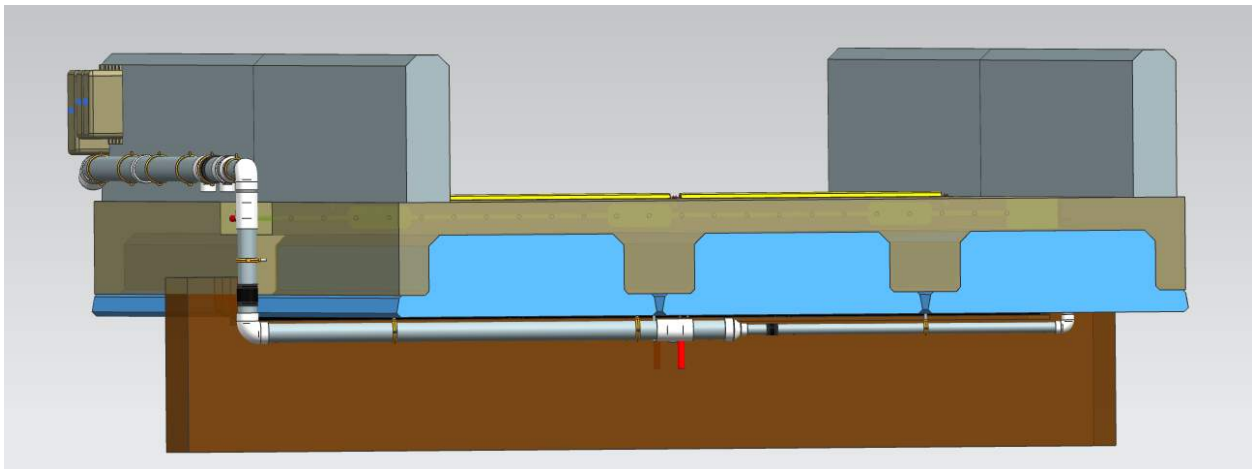


Figure 6, End View

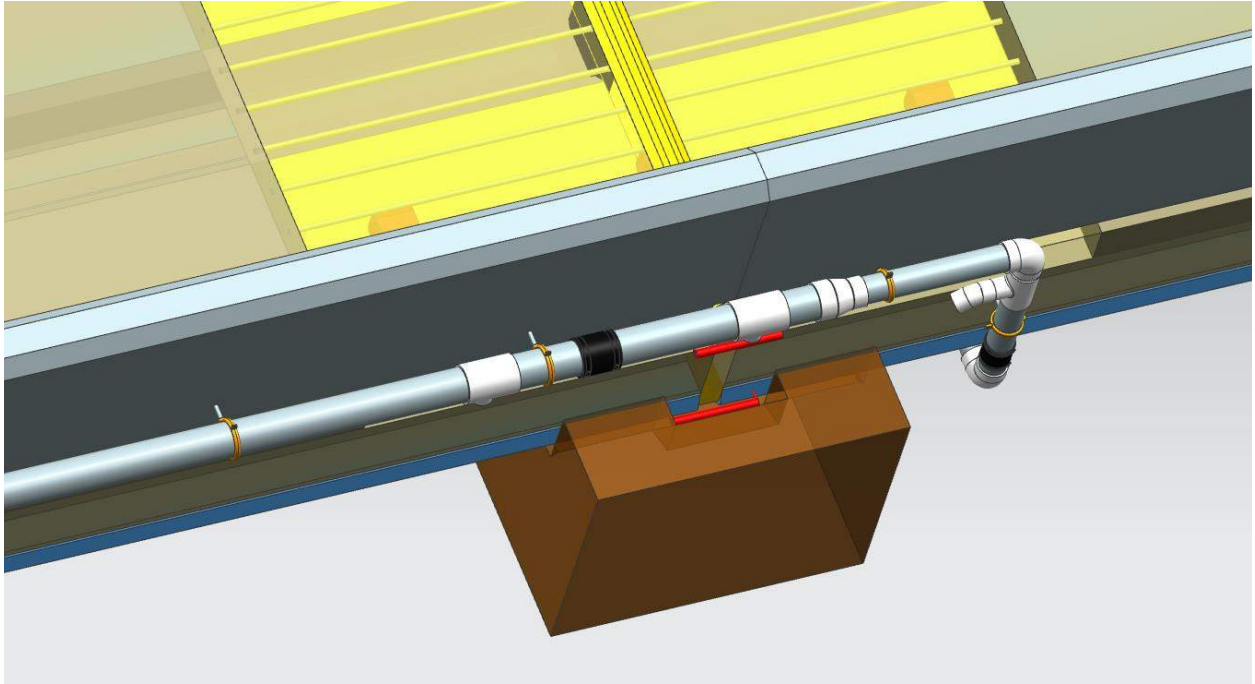


Figure 7, Top View of Shear Key

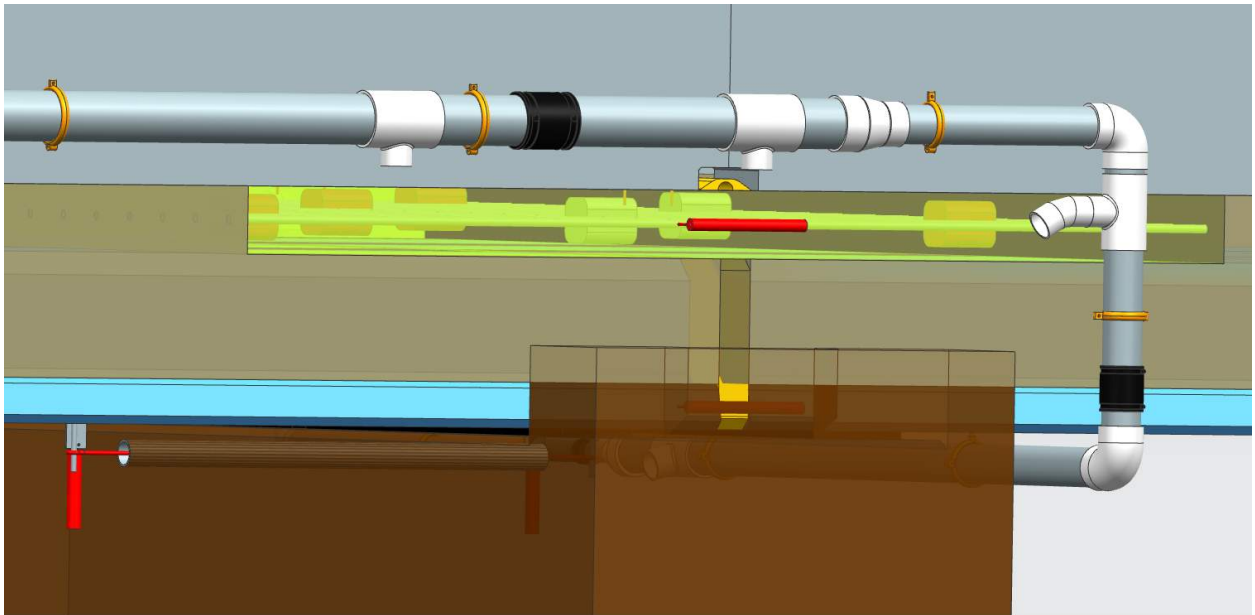


Figure 8, Side View of Shear Key

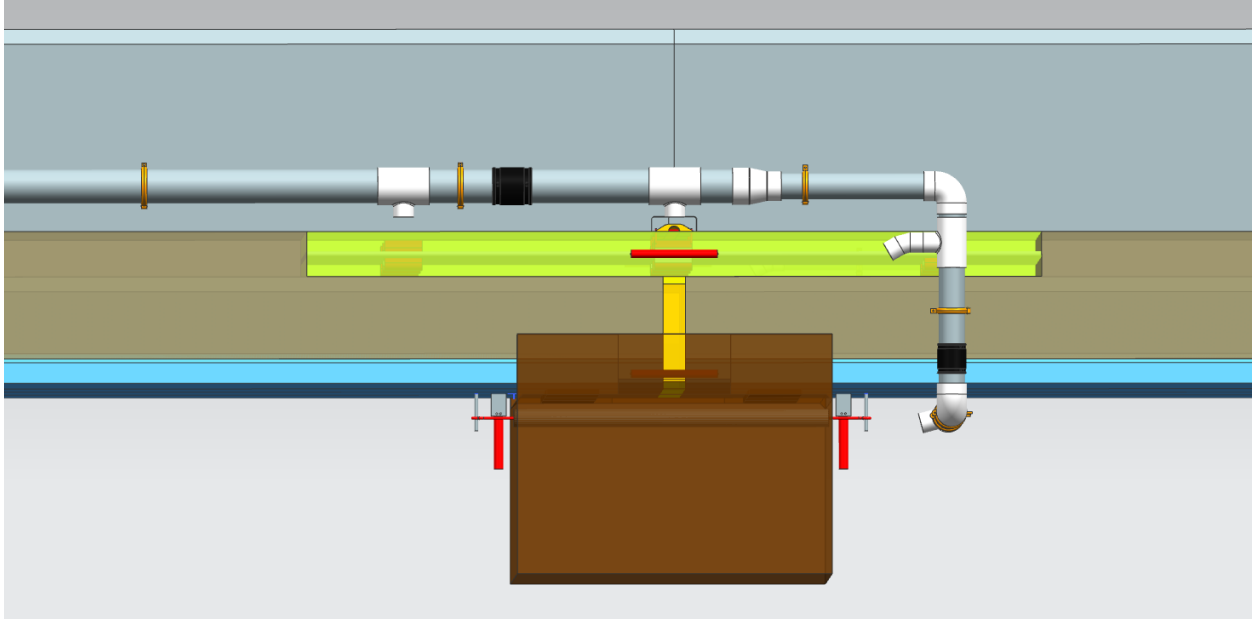


Figure 9, Side View Detail

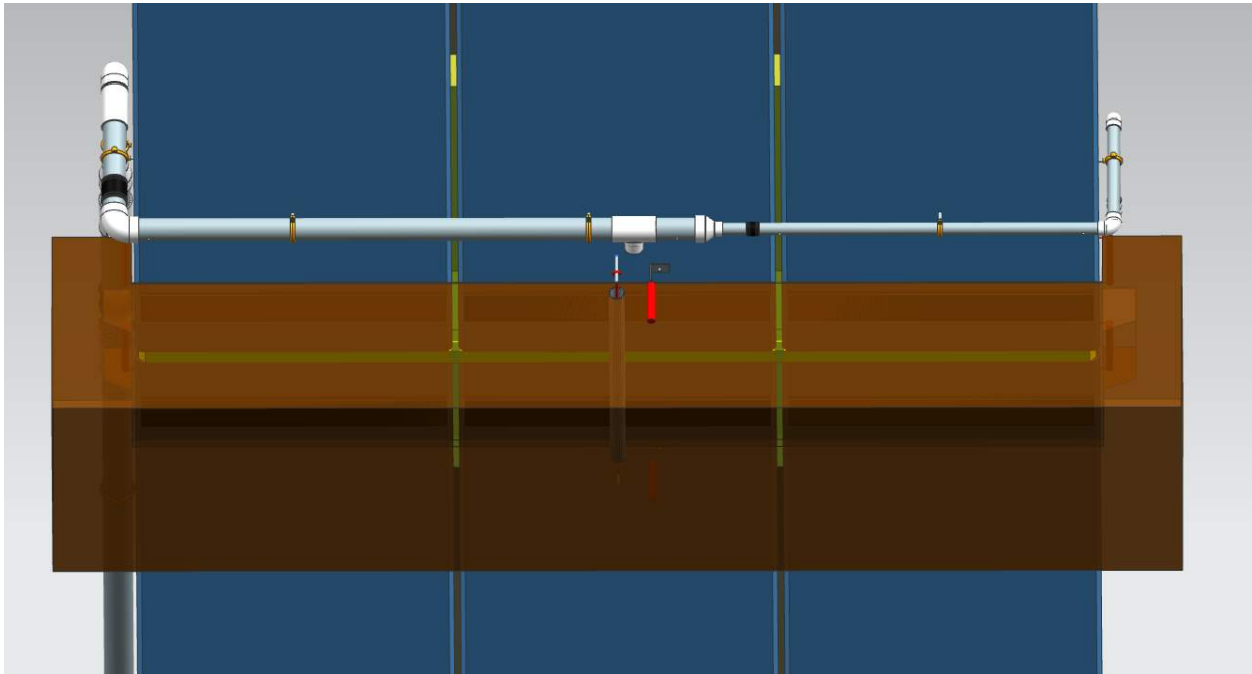


Figure 10, Bottom View of Side with Conduit

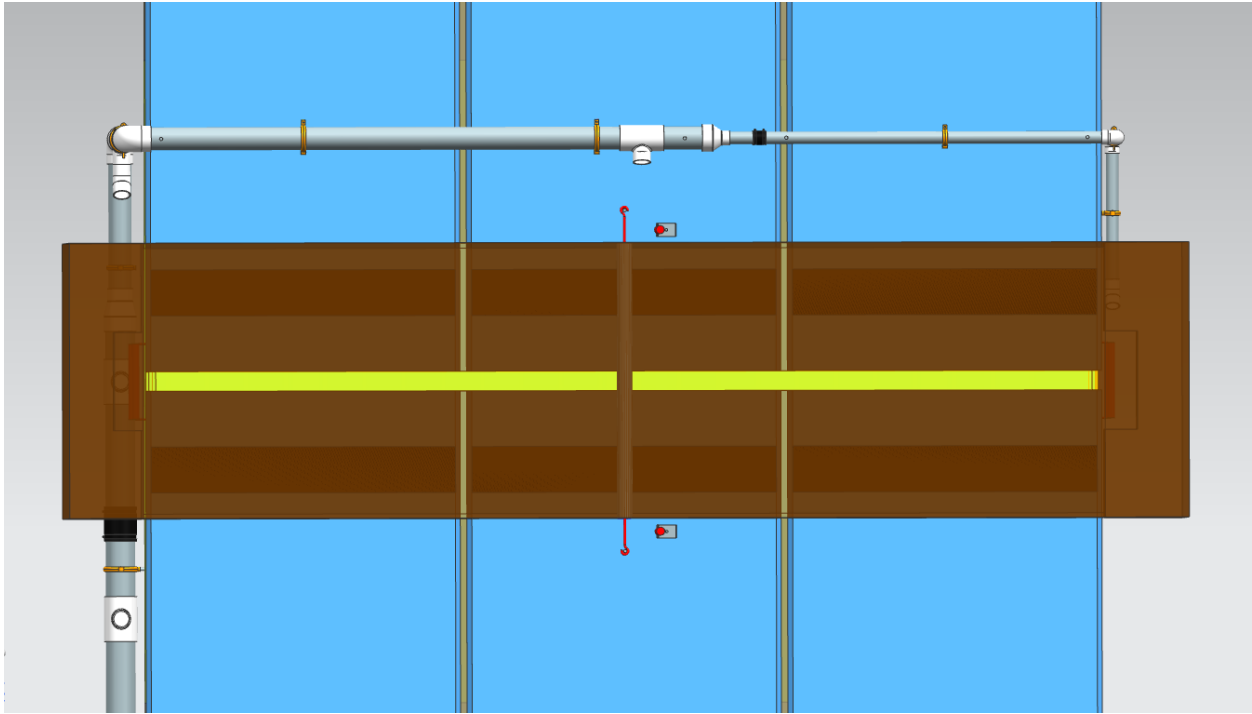


Figure 11, Bottom View

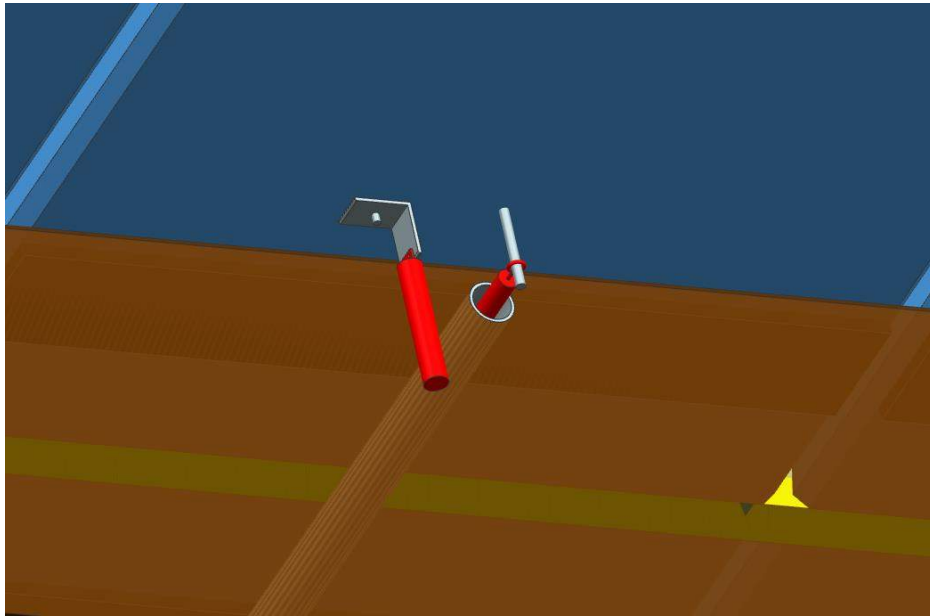


Figure 12, Detail of Suggested Tiltmeter Location and Convergence Meter (Bottom View, Side without Conduit)

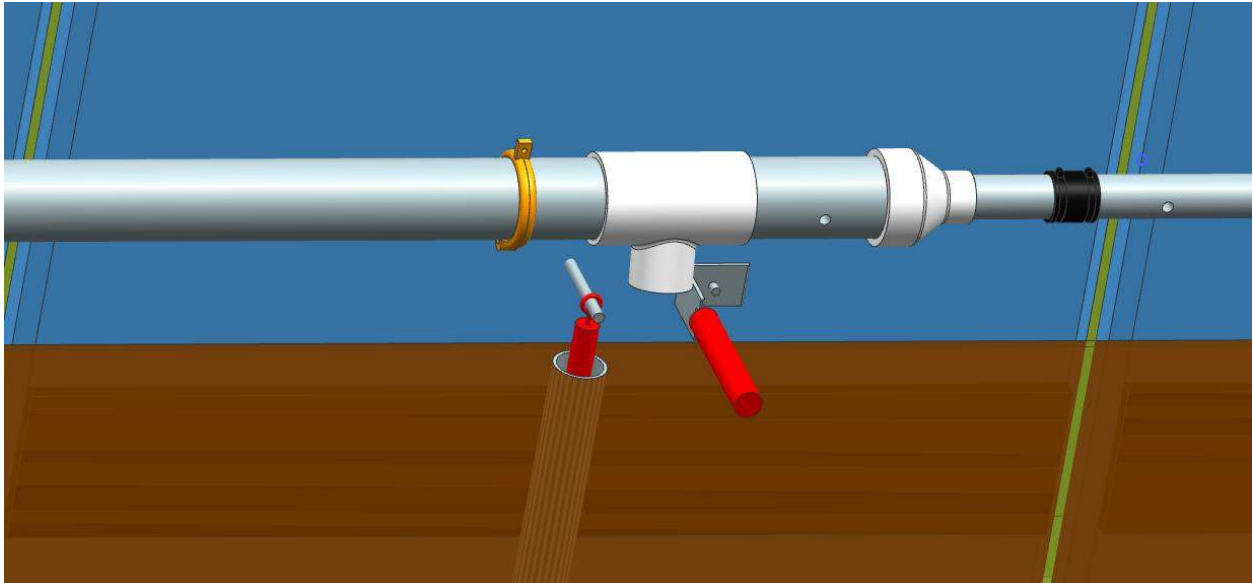


Figure 13, Detail of Suggested Tiltmeter Location and Convergence Meter (Bottom View, Side with Conduit)

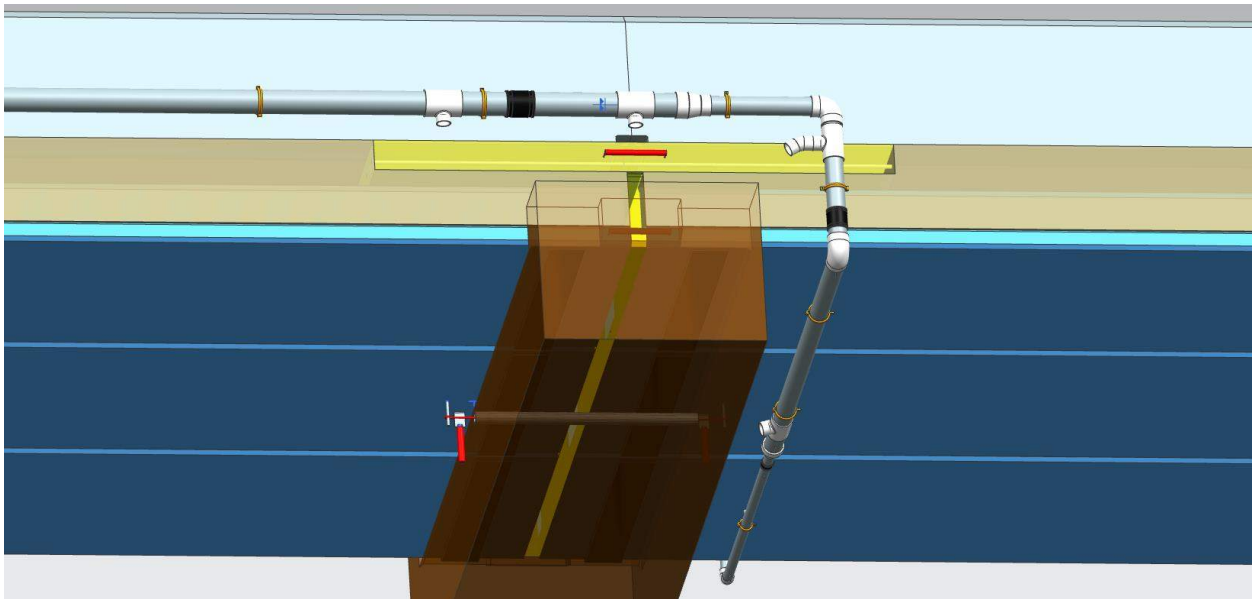


Figure 14, Bottom View Bent Cap

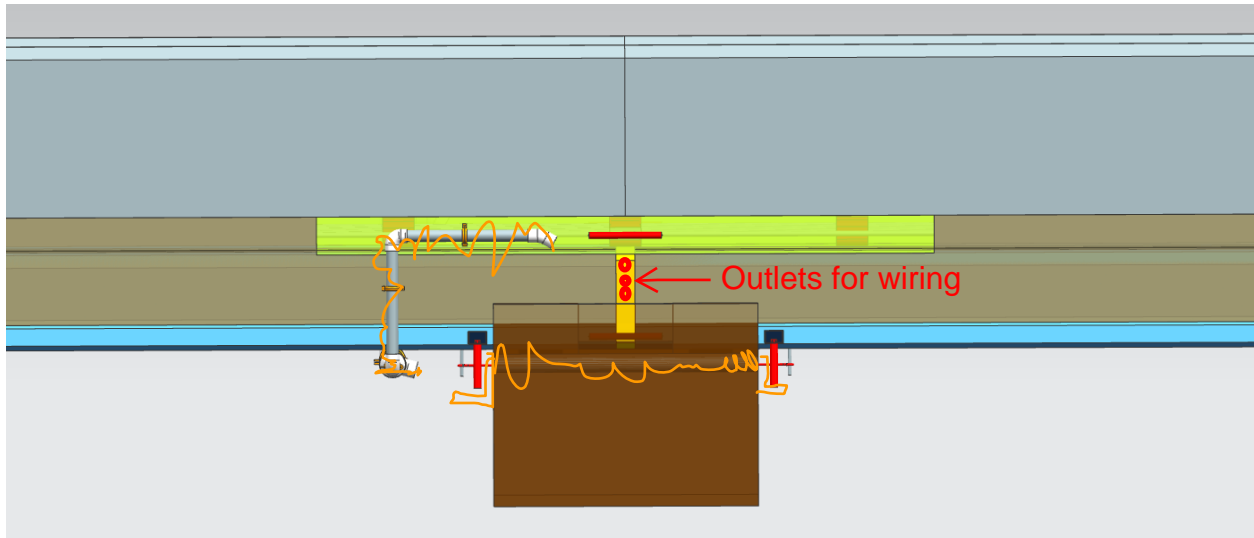


Figure 15, Side Opposite of Data Acquisition and Main Conduit.

Displaying Alternative Outboard Mounted Tiltmeters.

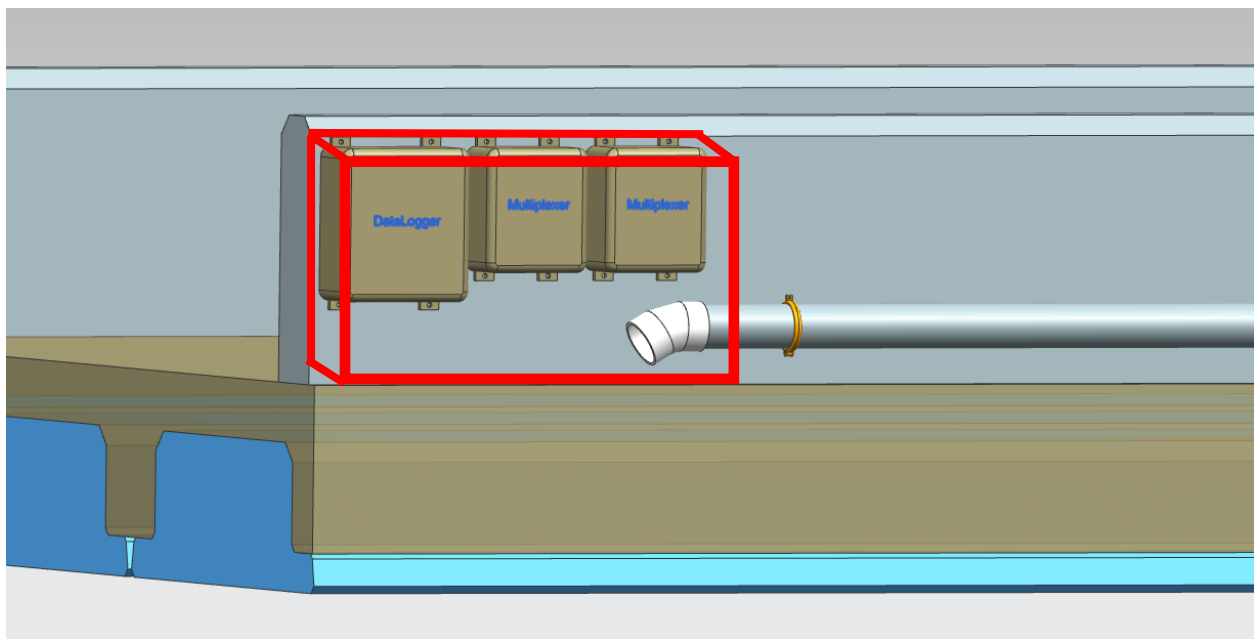


Figure 16, Detail Data Acquisition

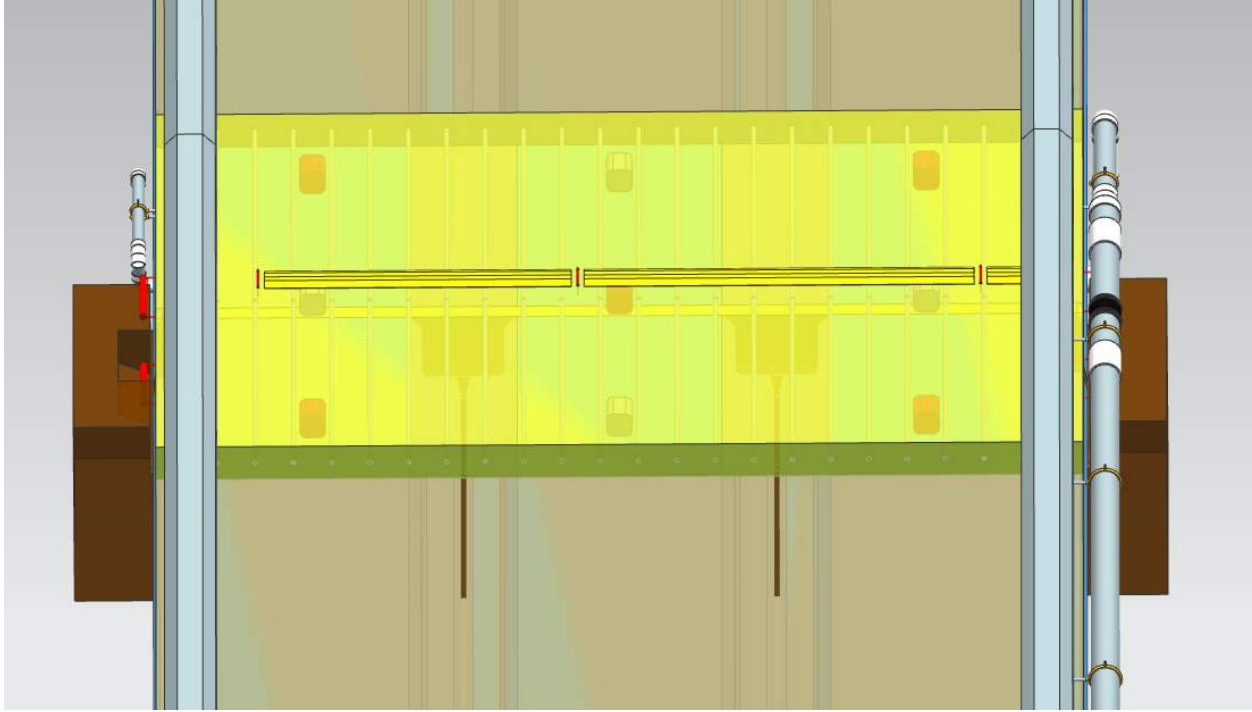


Figure 17, Detail Link-Slab (top view)

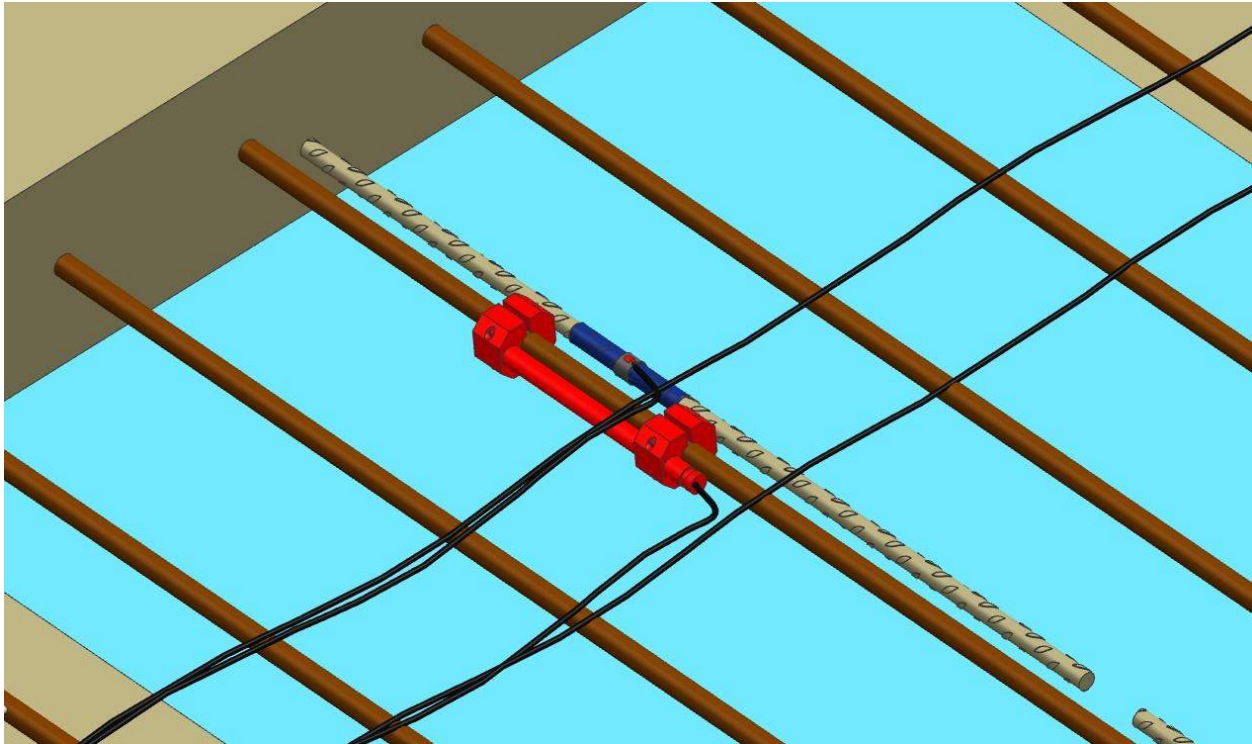


Figure 18, Example of an Embedded Pair (Sisterbar and Strandmeter)

## Summary

The team will investigate the concrete simple-span beams that are made continuous by pouring a continuity link-slab between the beam ends. The bridge will be instrumented with embedded and surface-mounted sensors and will be monitored for over 2 years to evaluate the performance of the new continuity detail.

Several types of sensors will be used and a data acquisition system will record strain/loads a regular time interval. The preferred sensor types for this application are vibrating wire sensors with integrated thermistors (per FDOT request). The sensors are strategically located on both sides of the midline to capture the important measures that are most influenced by continuity, such as strains in BFRP bars, strains in concrete, and the gap between adjacent beams' ends. The relative movement between the bottom flanges at the ends of the adjacent beams on both sides of the continuity (at the joint over the end bent) will be investigated using the Crackmeters installed on the outboard sides of beams. Rotations on both sides of the continuity link-slab will be recorded.

All measurements should be corrected for temperature changes per recommendations of the gauge manufacturer. Data can be collected during field tests and service. The data acquisition system should be able to keep record when certain strains are reached in the FRP reinforcement.

A live load test on the monitored link-slab will be conducted to assess the performance of the link-slab continuity under truck loads. The truck's weight will be determined later and used to load the bridge in nine static loading cases.

## APPENDIX A

### Manufacturer Data Sheets of Sensors (Credit: Geokon)

Figure 19, Model 4420 Data Sheet



• Model 4420 Crackmeter.

The Model 4420 Crackmeters are designed to measure movement across joints such as construction joints in buildings, bridges, pipelines, dams, etc.; tension cracks and joints in rock and concrete.

The ends of the sensor are attached to anchors (with ball joints) that have been grouted, bolted, welded or bonded on opposite sides of the crack or fissure to be monitored. 3-D mounting brackets, which allow measurement of displacements in three orthogonal directions, and special clamps for attachment to a variety of earth reinforcements and geogrids, are also available.

Special versions are offered for underwater use, where water pressures exceed 1.7 MPa, and for use in cryogenic or elevated temperature regimes.

Figure 20, Model 4410 Data Sheet

### Model 4410 Strandmeter



• Model 4410 Strandmeter.

The Model 4410 Strandmeter is designed to measure strains in tendons and steel cables, including bridge tendons, cable stays, ground anchors, tiebacks, etc. Two clamps at each end of the strandmeter hold it firmly onto the cable. Various size clamps are available.

Figure 21, Model 4422 Data Sheet

### Model 4422 Micro Crackmeter



• Model 4422 Micro Crackmeter.

The Model 4422 is a miniature crackmeter intended to measure displacements across surface cracks and joints. It has been specially designed for applications where access is limited and/or where monitoring instrumentation is to be as unobtrusive as possible (e.g. on historical structures or buildings).

Figure 22, Model 4425 Data Sheet

**Model 4425 Convergence Meter**



● Model 4425 Convergence Meter.

The Model 4425 Convergence Meter is designed to detect deformation in tunnels and underground caverns by measuring the contraction (or elongation) between 2 anchor points fixed in the walls of the tunnel or cavern.

The Model 4425 consists of a spring-tensioned vibrating wire transducer assembly, turnbuckle, 6 mm diameter connecting rods (stainless steel, fiberglass or graphite), rod clamp, and a pair of anchor points. Changes in distance between the 2 anchors are conveyed by the connecting rods and measured by the transducer.

The Model 4425 can operate in horizontal, inclined or vertical orientations. In areas where construction traffic is expected or where the instrument may be left in an exposed location, some form of protective housing should be considered.

**Technical Specifications**

Model	Standard Ranges <sup>1</sup>	Resolution	Accuracy	Nonlinearity	Temperature Range <sup>1</sup>	Dimensions
4400 Embedment Jointmeter	12.5, 25, 50, 100 mm	0.025% F.S.	±0.1% F.S.	< 0.5% F.S.	-20°C to +80°C	Length: 406 mm Flange Diameter: 51 mm
4410 Strandmeter	20,000 µε	< 5 µε	±0.1% F.S.	< 0.5% F.S.	-20°C to +80°C	Length: 203 mm Clamp Width: 45 mm
4420 Crackmeter	12.5, 25, 50, 100, 150 mm	0.025% F.S.	±0.1% F.S.	< 0.5% F.S.	-20°C to +80°C	Lengths: 318, 362, 527 mm Coil Diameter: 25 mm
4422 Micro Crackmeter	3 mm (±1.5 mm)	0.001 mm	±0.1% F.S.	< 0.5% F.S.	-20°C to +80°C	Length: 120 mm Diameter: 7.9 mm
4425 Convergence Meter	25, 50, 100, 150 mm	0.025% F.S.	±0.1% F.S.	< 0.5% F.S.	-20°C to +80°C	Transducer Lengths: 356, 508, 838 mm Transducer Diameter: 25 mm
4427 Long-Range Displacement Meter	1, 2 m (without resetting)	0.025% F.S.	±1.0% F.S.	—	-30°C to +60°C	Enclosure (L × W × H): 610 × 152 × 152 mm
4430 Deformation Meter	25, 50, 100 mm	0.02% F.S.	±0.1% F.S.	< 0.5% F.S.	-20°C to +80°C	Length: varies Flange Diameter: 50 mm
4450 Displacement Transducer	12.5, 50, 100, 150, 300 mm	0.02% F.S.	±0.1% F.S.	< 0.5% F.S.	-20°C to +80°C	Lengths: 210, 212, 270, 410 mm Coil Diameter: 19 mm

Figure 23, Sensor Technical Specs

Figure 24, Model 6350 Data Sheet

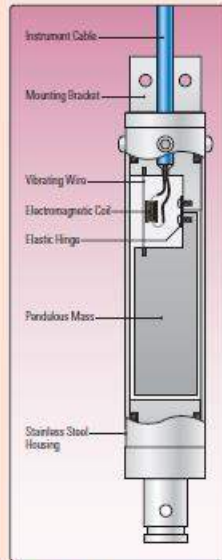
**Model 6350**

## Vibrating Wire Tiltmeter

**Applications**

The Model 6350 Vibrating Wire Tiltmeter is designed to measure tilt in structures including...

- Buildings
- Dams
- Embankments
- Slopes
- Excavation walls
- Open pits



• Vibrating wire tilt sensor construction



• Model 6350 Vibrating Wire Tiltmeter shown with mounting bracket assembly.

**Operating Principle**

The Model 6350 Tiltmeter is designed for attachment to structures, on either a vertical or horizontal surface by means of an adjustable bracket, and for the subsequent measurement of any tilting that may occur.

When at rest, in a vertical configuration, a pendulous mass inside the sensor, under the force of gravity, attempts to swing beneath the elastic hinge on which it is supported but is restrained by the vibrating wire. As the tilt increases or decreases the mass attempts to rotate beneath the hinge point and the tension in the vibrating wire changes, altering its vibrational frequency. This frequency is measured using the Geokon Model GK-401, GK-403 or GK-404 Readout Box, or the Model 8020 Micro-10 Datalogger, and is then converted into an angular displacement by means of calibration constants supplied with the sensor.

**Advantages and Limitations**

Vibrating wire tiltmeters combine a high range with high sensitivity, and very high calibration accuracy. They have excellent long-term stability and their temperature dependence is close to zero.

The sensor output is a frequency, which can be transmitted over long cables, and renders the sensors less susceptible to the effects of moisture intrusion.

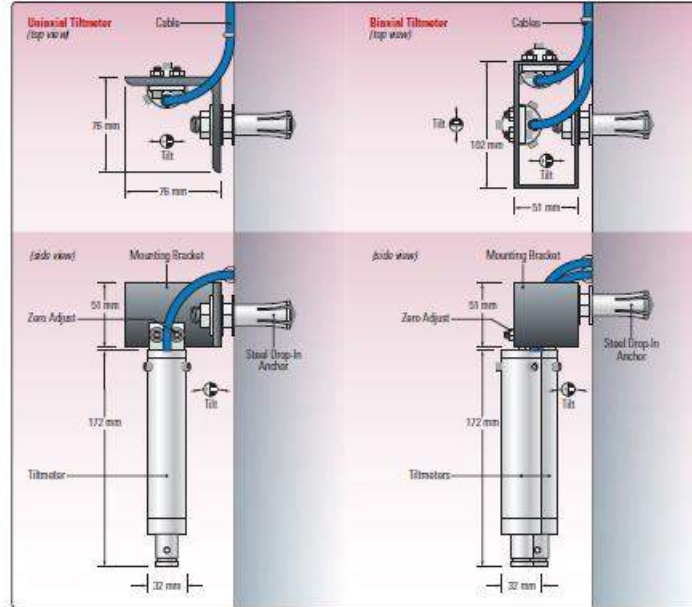
Biaxial measurements can be achieved by mounting the sensors in pairs, each member oriented at 90 degrees to the other.

Damping fluid may be added to the sensor to counteract the effect of any vibrations of the structure.

In-built shock absorbers protect the sensor from shock loading.



• Model G350 installation using a custom mounting bracket designed for concrete face rock fill dam applications (shown with protective cover removed)



• Installation details and dimensions for the Model G350 Uniaxial (left) and Biaxial versions (right).

#### System Components

The basic transducer is mounted inside a stainless steel housing equipped with a lug for mounting the sensor to an adjustable bracket. The bracket is bolted to the structure using hardware supplied with the sensor, which includes a 3/8-inch drop-in anchor. Special biaxial mounting brackets and protective enclosures are also available.

A thermistor mounted inside the sensor housing permits the measurement of temperatures.

Readout is accomplished using a Geokon Model GK-401, GK-403 or GK-404 Readout Box.

#### Technical Specifications

Standard Range <sup>1</sup>	±10°
Resolution	±10 arc seconds (±0.05 mm/m)
Accuracy <sup>2</sup>	±0.1% F.S.
Temperature Range	-20°C to +50°C
Shock Survival	50 g
Length x Diameter <sup>3</sup>	128 x 32 mm

<sup>1</sup>Other ranges available on request.  
<sup>2</sup>Established under laboratory conditions.  
<sup>3</sup>Transducer only.

**Model 4100**

## Spot-Weldable Strain Gauges

### Applications

The 4100 Series Vibrating Wire Strain gauges are designed to measure strains in or on...

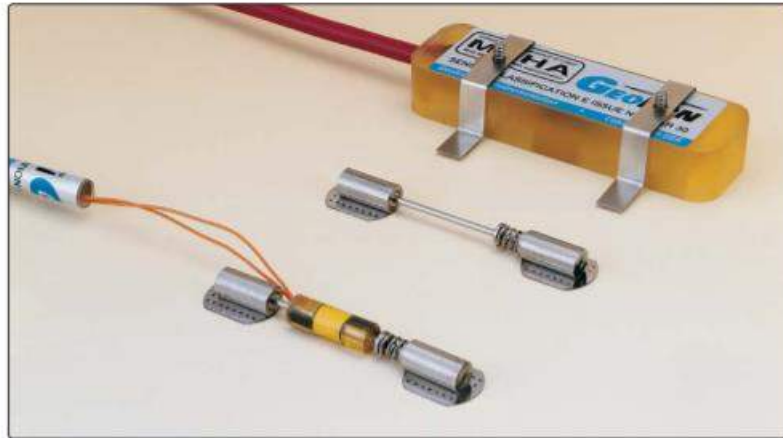
- Pipelines
- Bridges
- Buildings
- Tunnel linings
- Piles
- Reinforcement bars



• Model 4150 shown with optional arc-weldable mounting blocks.



• Model 4151 Strain Gauge mounted to a fiberglass rebar.



• Model 4150 (front) and Model 4100 Spot-Weldable Strain Gauges.

### Operating Principle

The Model 4100 and 4150 Vibrating Wire Strain Gauges are designed primarily to measure strains on the surface of steel structures, although they may also be used to measure strains in other materials. Essentially, the gauges consist of a steel wire tensioned between two mounting blocks. These blocks are attached to stainless steel shim-stock tabs, which can be either spot-welded or epoxy bonded to the surface in question. Also available is the Model 4151 Strain Gauge with groutable pins welded to the end-blocks.

Deformation of the structure under load causes the end blocks to move relative to one another resulting in a change in the wire tension and a corresponding change in the fundamental, resonant frequency of vibration of the wire.

The wire is plucked by means of an electronic coil and permanent magnet connected by a signal cable to a readout, which sends voltage pulses to the coil. The vibration of the wire so produced induces an alternating current in the coil—the frequency of which is the same as the vibrational frequency of the wire and is measured using the same electronic coil and a readout. The frequency value is squared and multiplied by a constant so that the values displayed by the readout are directly in microstrain.

### Advantages and Limitations

The Model 4100 and 4150 strain gauges are small so that they can be used in confined spaces. They are particularly useful for spot-welding to steel reinforcement bars and rock bolts and for spot welding to pipelines and other sensitive structures where arc welding is prohibited, or where the services of an arc welder are unavailable.

All components are made from stainless steel for corrosion protection and the gauges are waterproof.

The Model 4100 and 4150 enjoy all the advantages of vibrating wire sensors: i.e., excellent long term stability, maximum resistance to the effects of water and a frequency output suitable for transmission over very long cables.

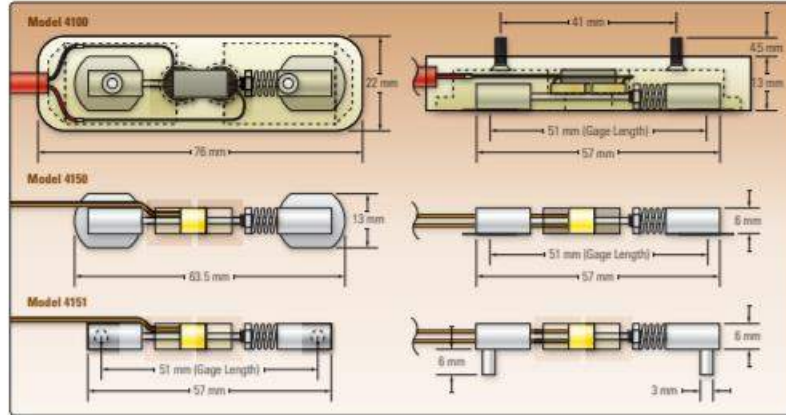
Each gauge also incorporates a thermistor so that the temperature can be read and displayed by the readout.

An external spring holds the wire in initial tension thus greatly simplifying the installation procedure.

Gauges are certified by MSHA for use in explosive atmospheres when used with certified readouts.



• Model 4150 under the Model 4150-1 protective cover plate, with dimensions.



• Dimensions of the Models 4100, 4150 and 4151 strain gauges.

### System Components

The Model 4100 consists of two main components: the gauge itself and a separate plucking coil housing. The stainless steel tube around the wire is O-ring sealed so that the gauges are waterproof. This tube floats free and thus does not impede the free movement of the end blocks. The coil housing contains a thermistor and fits loosely over the gauge. It is secured in place by means of stainless steel straps. It also serves as a measure of protection from mechanical damage.

The model 4150 consists of only one component since the coil housing is encapsulated around the stainless steel tube that protects the wire. The instrument cable is connected to the coil housing through small diameter lead wires. A thermistor, contained in a small encapsulation, is provided at the end of the cable. A

separate cover plate protects the gauge from mechanical damage. Stainless steel straps hold the cable and cover plate firmly to the structure.

The model 4151 is a modification of the 4150 strain gauge in which the spot-weldable tabs have been replaced by pins welded to the end blocks and designed to be grouted into two short holes drilled into the material under test. Special versions of the 4151 are available with extended ranges: 5,000  $\mu\epsilon$  (4151-1) and 10,000  $\mu\epsilon$  (4151-2). These gauges are particularly useful for measurements in high strain regimes such as on plastic pipes or piles and on fiberglass structural members and rebars.

Accessories include setting tools, capacitive discharge welder (for spot welding) and epoxy kits (for bonded applications).

### Technical Specifications

	4100	4150	4151	4151-1	4151-2
Standard Range	3000 $\mu\epsilon$	3000 $\mu\epsilon$	3000 $\mu\epsilon$	5,000 $\mu\epsilon$	10,000 $\mu\epsilon$
Resolution	0.4 $\mu\epsilon$	0.4 $\mu\epsilon$	0.4 $\mu\epsilon$	1.0 $\mu\epsilon$	2.0 $\mu\epsilon$
Accuracy <sup>1</sup>	$\pm 0.5\%$ F.S.	$\pm 0.5\%$ F.S.	$\pm 0.5\%$ F.S.	$\pm 0.5\%$ F.S.	$\pm 0.5\%$ F.S.
Nonlinearity	< 0.5% F.S.	< 0.5% F.S.	< 0.5% F.S.	< 0.5% F.S.	< 0.5% F.S.
Temperature Range <sup>2</sup>	-20 °C to +80 °C	-20 °C to +80 °C			
Active Gauge Length	51 mm	51 mm	51 mm	51 mm	51 mm

<sup>1</sup> $\pm 0.5\%$  F.S. with standard batch calibration.  $\pm 0.1\%$  F.S. with individual calibration. Accuracy established under laboratory conditions.  
<sup>2</sup>Other ranges available on request.

**Model 4911, 4911A**

# Rebar Strainmeters and "Sister Bars"

## Applications

Rebar Strainmeters are commonly used for measuring strains in...

- Concrete piles & caissons
- Slurry walls
- Cast-in-place concrete piles
- Concrete foundation slabs and footings
- Osterberg pile tests
- All concrete structures



• Close-up of Model 4911 shown as installed in concrete pile reinforcing cage.



• Model 4911A Rebar Strainmeter (front) and the Model 4911 "Sister Bar" (rear).

## Operating Principle

Rebar Strainmeters and "Sister Bars" are designed to be embedded in concrete for the purpose of measuring concrete strains due to imposed loads. The Rebar Strainmeter is designed to be welded into, and become an integral part of, the existing rebar cage, while the "Sister Bar" is installed by tying it alongside an existing length of rebar in the rebar cage.

The rebar extensions on either side of the central strain-gauged area are long enough to ensure adequate contact with the surrounding concrete so that the measured strains inside the steel are equal to the strains in the surrounding concrete.

In use, Rebar Strainmeters and "Sister Bars" are usually installed in pairs on either side of the neutral axis of the structural member being investigated. This is done so that bending moments may be analyzed in addition to axial loads.

A built-in thermistor enables the measurement of temperatures and aids in the evaluation of thermally induced strains.

## Advantages and Limitations

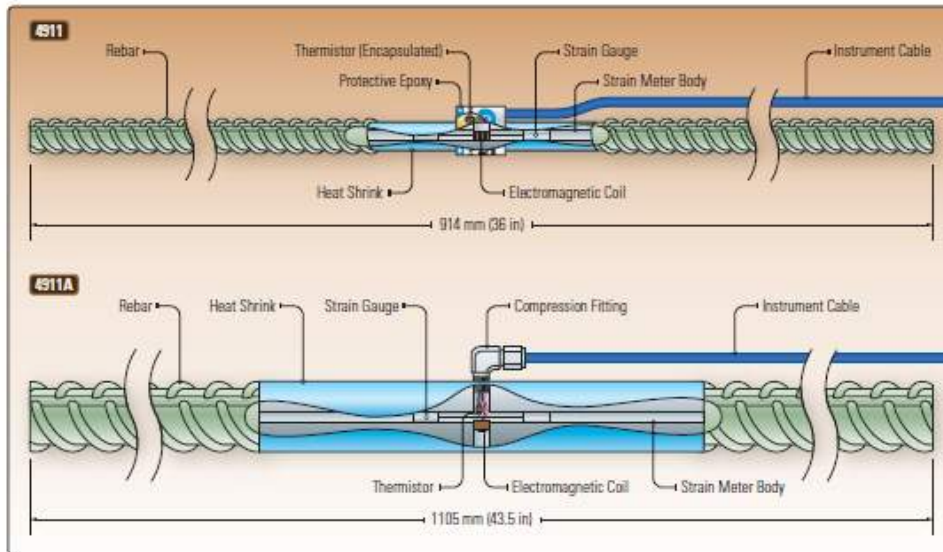
The main advantage of the Rebar Strainmeters and "Sister Bars" lies in their ruggedness. They are fully waterproof and virtually indestructible so that, if the cable is adequately protected, they are safe from damage during the concrete placement.

Each Rebar Strainmeter and "Sister Bar" is individually calibrated and tested for weld strength. The Rebar Strainmeter requires the services of an experienced welder who can guarantee full-strength welds, whereas the "Sister Bar" is very easy to install.

The single vibrating wire strain sensor, located along the axis of the strainmeter, is not affected by the bending of the strainmeter itself. It also has the advantage of all vibrating wire sensors, namely: long-term stability, it can be used with long cables and it's relatively unaffected by moisture intrusion into the cables.



● Installation of the Model 4911 in an Osterberg Cell pile test. (For more information regarding Osterberg Cell pile testing, please contact Inertec Inc. — [www.inertec.com](http://www.inertec.com))



● Illustration of the Model 4911 "Sister Bar" and Model 4911A Rebar Strainmeters and their various components.

### System Components

A vibrating wire strain gauge sensor is fixed axially inside a short, central length of round steel bar. This central section is de-bonded from the surrounding concrete by means of a plastic coating, and is extended by welding a length of rebar to each end. The Model 4911A Rebar Strainmeter is available in various sizes to match the size of the rebar cage into which it is to be welded, whereas the Model 4911 "Sister Bar" comes in one size only (#4 rebar, at approximately 12.7 mm in diameter).

A thermistor to measure temperature changes can be included in the 4911 and 4911A sensors.

### Readouts and Cables

The 4911 Series Rebar Strainmeters are read using the Model GK-404 or GK-405 Readouts. Alternatively, the LC-2 Series or 8600 Series Dataloggers can be used.

The 4911 Series Rebar Strainmeters use the Model 02-250V6 4 pair, 22 AWG cable.

### Technical Specifications

	4911	4911A
Standard Range	3000 $\mu\epsilon$	3000 $\mu\epsilon$
Resolution	0.4 $\mu\epsilon$	0.4 $\mu\epsilon$
Accuracy <sup>1</sup>	$\pm 0.25\%$ F.S.	$\pm 0.25\%$ F.S.
Nonlinearity	< 0.5% F.S.	< 0.5% F.S.
Temperature Range <sup>2</sup>	-20°C to +80°C	-20°C to +80°C
Rebar Sizes	#4 (Sister Bar)	#6, 7, 8, 9, 10, 11, 14
Length	914 mm	1105 mm

<sup>1</sup>Accuracy established under laboratory conditions.  
<sup>2</sup>Other ranges available on request.

## APPENDIX B

### Dimensioned Drafts of Preferable Sensor Plan (All Dimensions in Inches)

Group #	Sensor Objective	Gauge Type/Model & Source	Sensor Dimensions
1	Strain in BFRP	<i>Strandmeter (4410, Geokon)</i>	8" Long x 1.77" Wide Clamps
2	Strain in Concrete Link-Slab	<i>Sisterbar (4911, Geokon)</i>	36" Length, #4 Rebar (0.5" Diameter)
3	Crack Width in Link-Slab	<i>Micro Crackmeter (4422, Geokon)</i>	4.725" Long x 0.315" Diameter
4	Lower centerline EDT, Collinear middle FSBs	<i>Convergence Meter (4425, Geokon)</i>	1" Dia., Combined Length between 42"-48"
5	External Displacement Gauges (EDTs)	<i>Crackmeter (4420, Geokon)</i>	Length: 12.5"(standard) or 10.35"(custom), Dia:1"
6	Rotation of Beam Ends	<i>Tiltmeter (6350, Geokon)</i>	7.638" Long x 1.26" Diameter
7	Datalogging	<i>Datalogger (8600-1, Geokon)</i>	LWH: 15.43"x13.86"x6.34"
8	Signal Gathering/Splitting	<i>Multiplexer/MUX (8032, Geokon)</i>	LWH: 12.52"x10.91"x6.26"

#### [BRIDGE END VIEW]

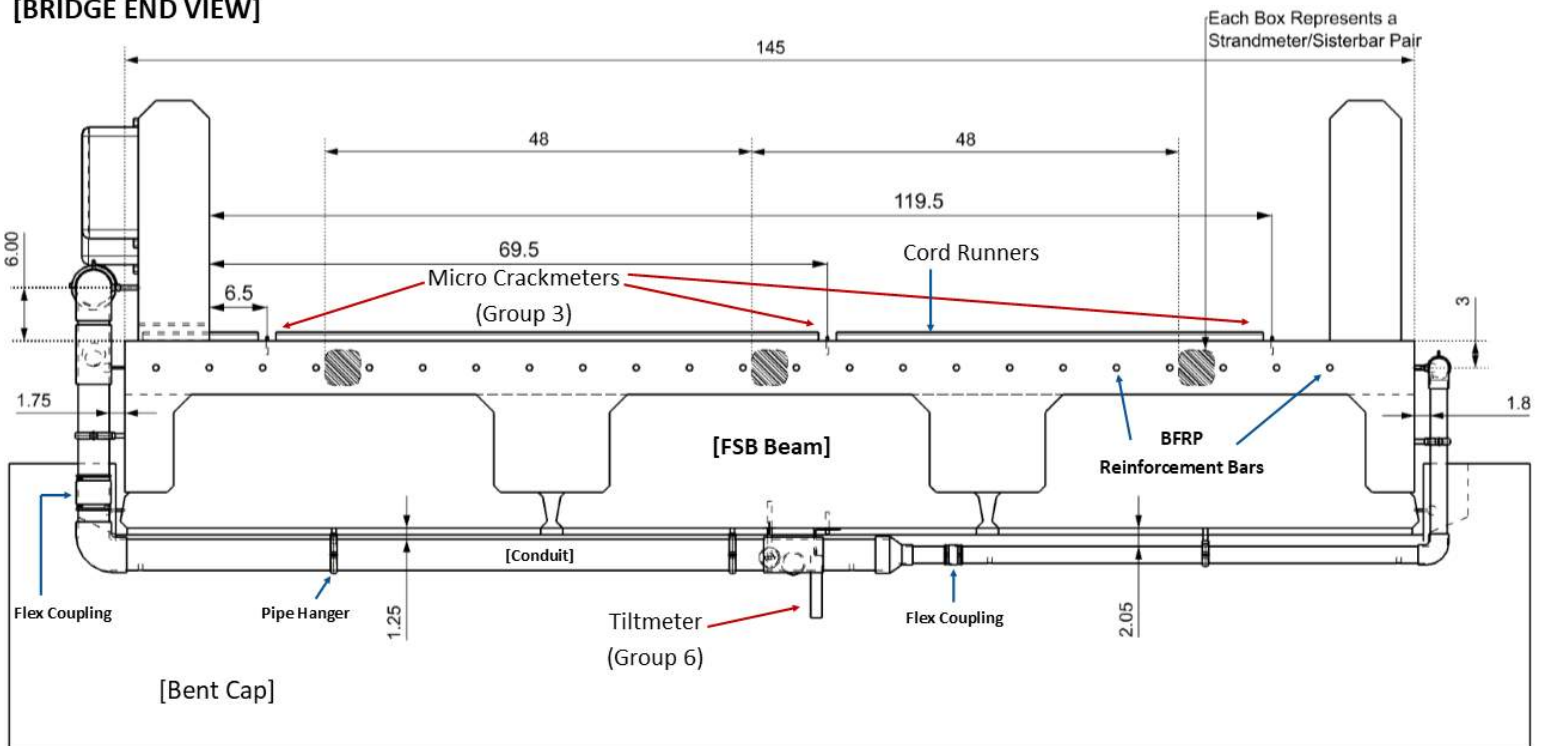


Figure 27, Dimensioned Bridge End View, 1

**[Bridge End View]**

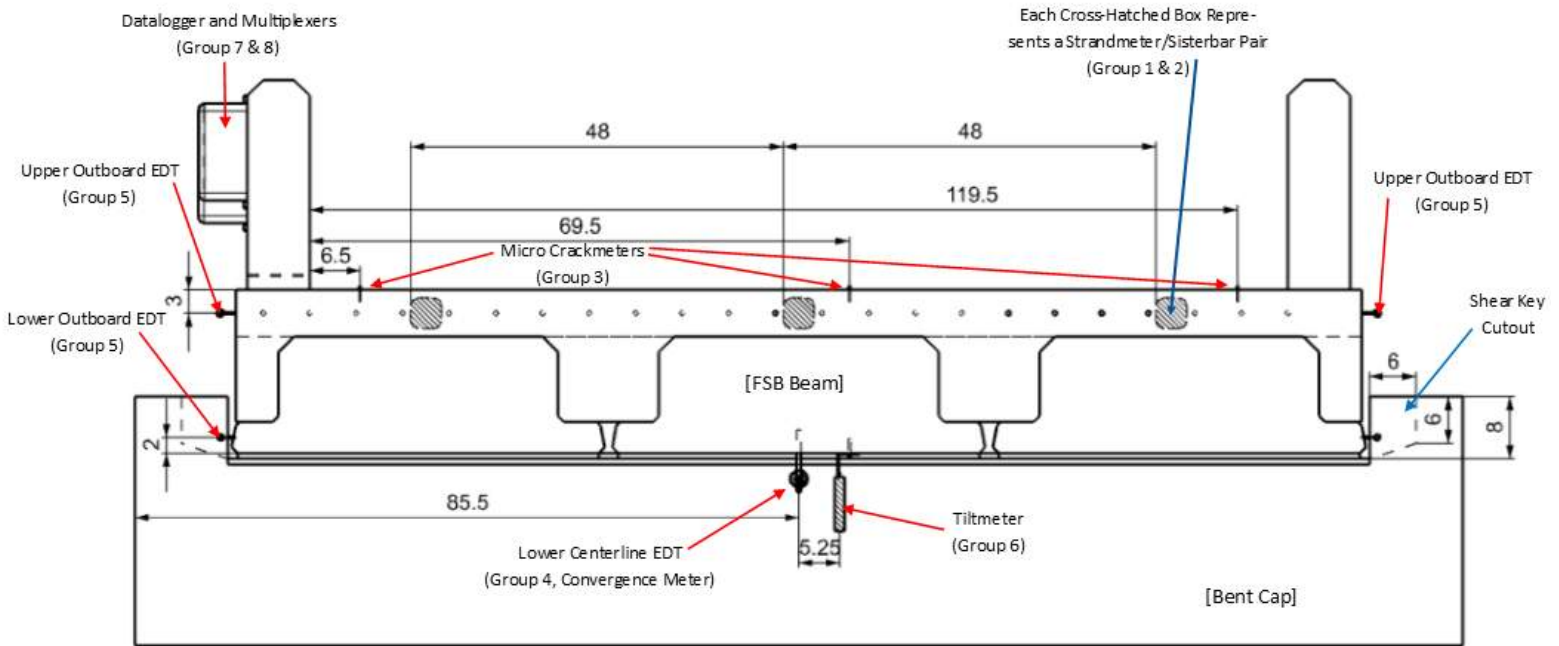
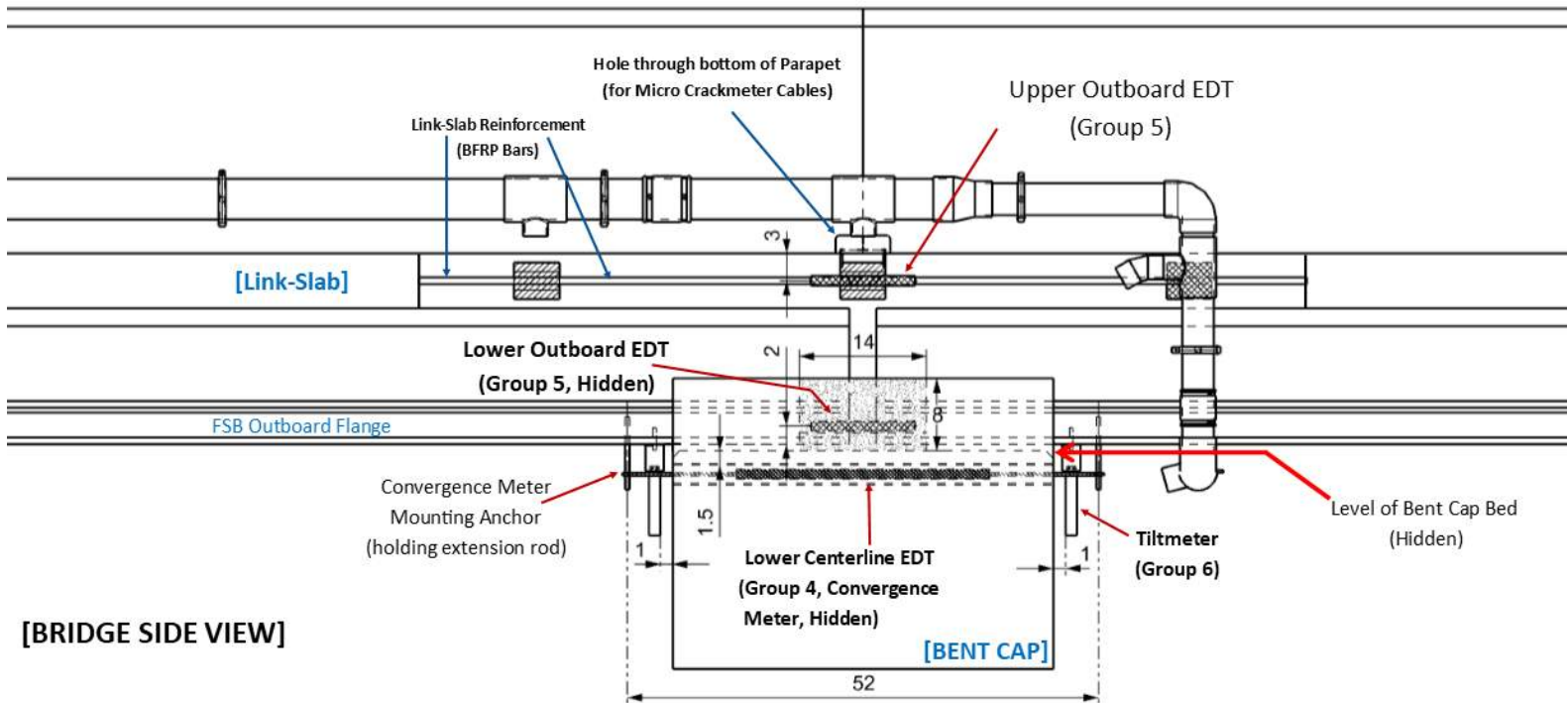


Figure 28, Dimensioned Bridge End View, 2 (Conduit and Cord Runners not Shown)



**[BRIDGE SIDE VIEW]**

Figure 29, Dimensioned Bridge Side View, 1

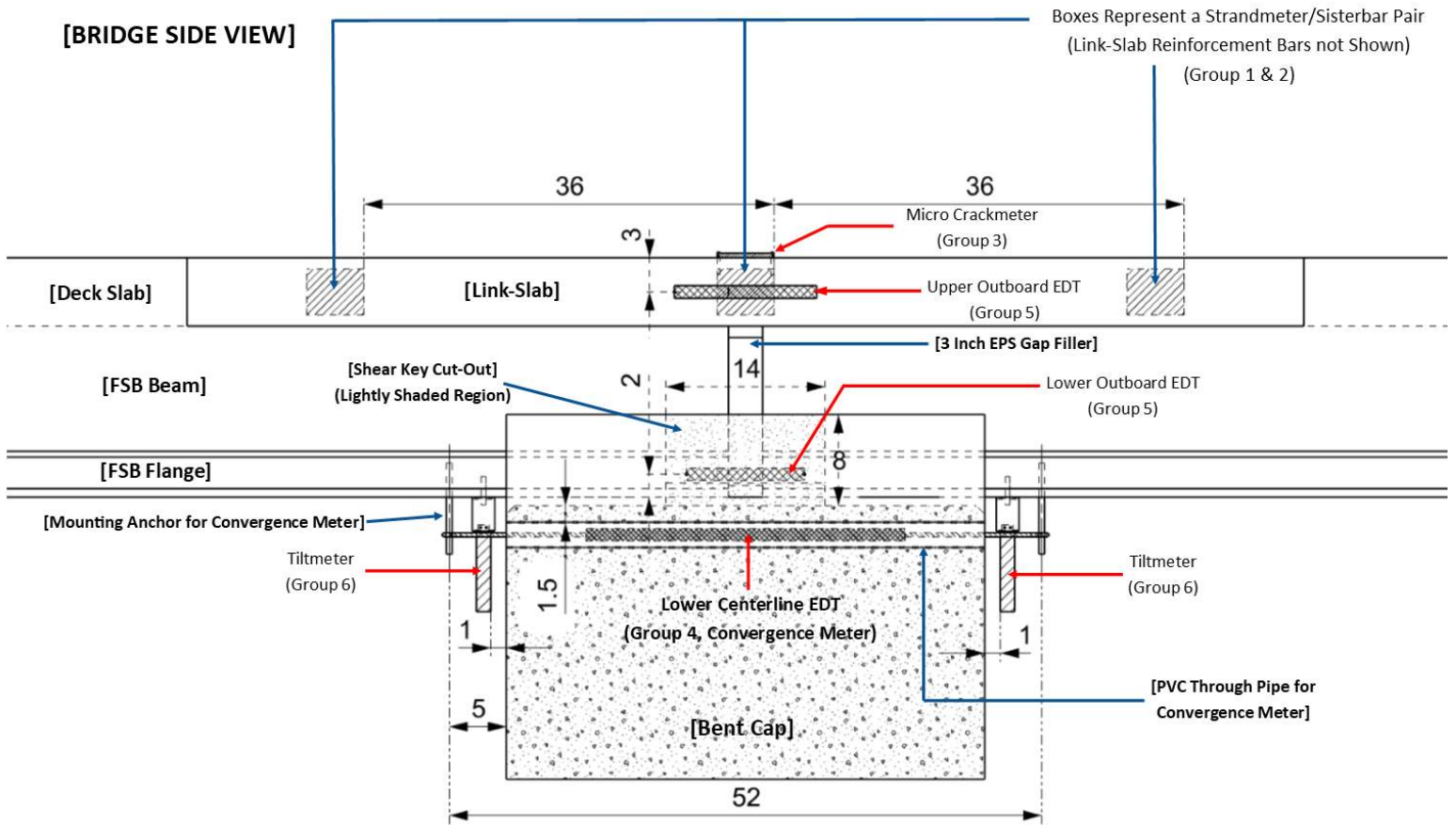


Figure 30, Dimensioned Bridge Side View, 2 (Parapet, Conduit, Link-Slab Reinforcement, and Cord Runners not Shown)



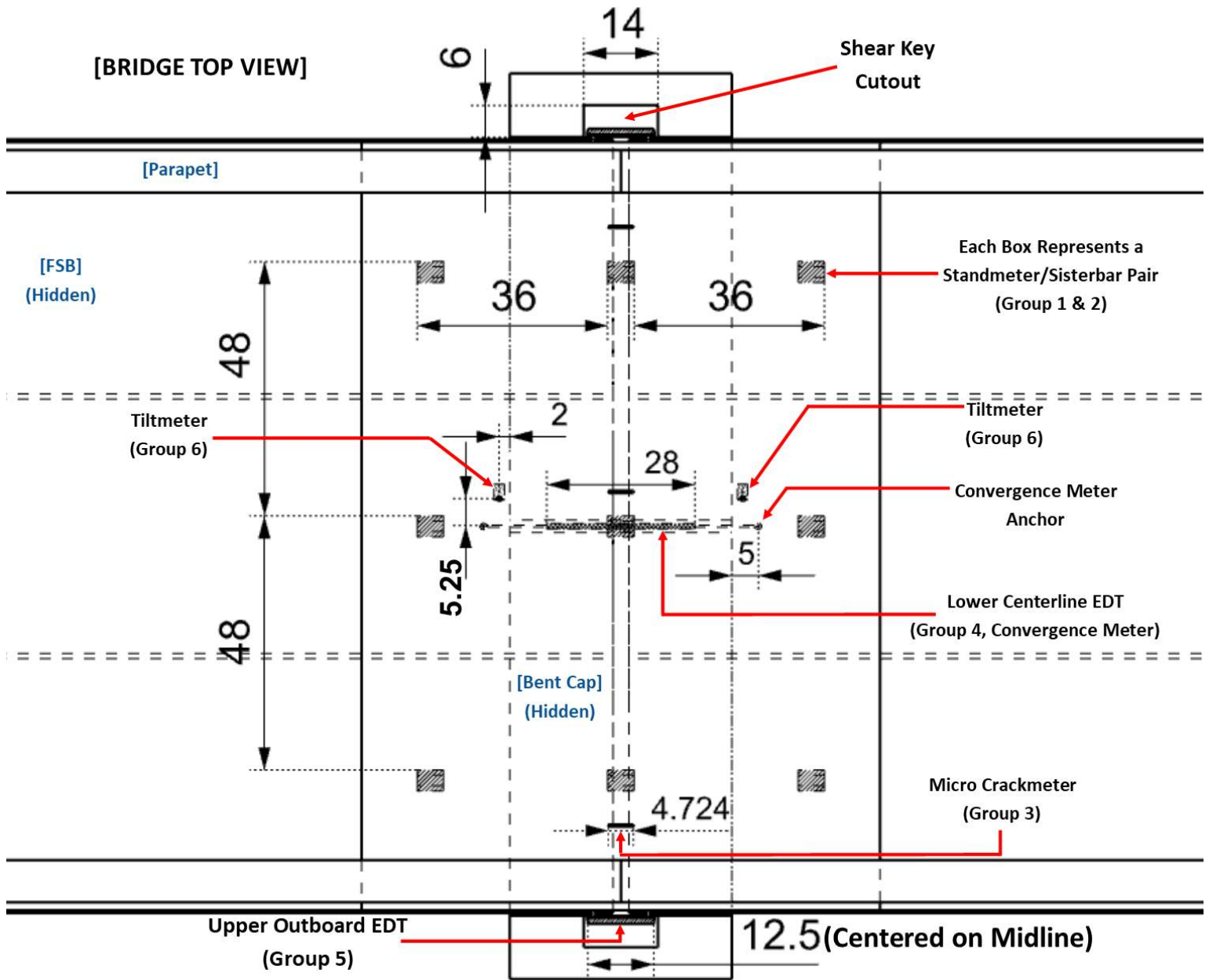


Figure 32, Dimensioned Bridge Top View, 2 (Conduit, Cord Runners, Lower Outboard EDTs, and BFRP Reinforcement not Shown)

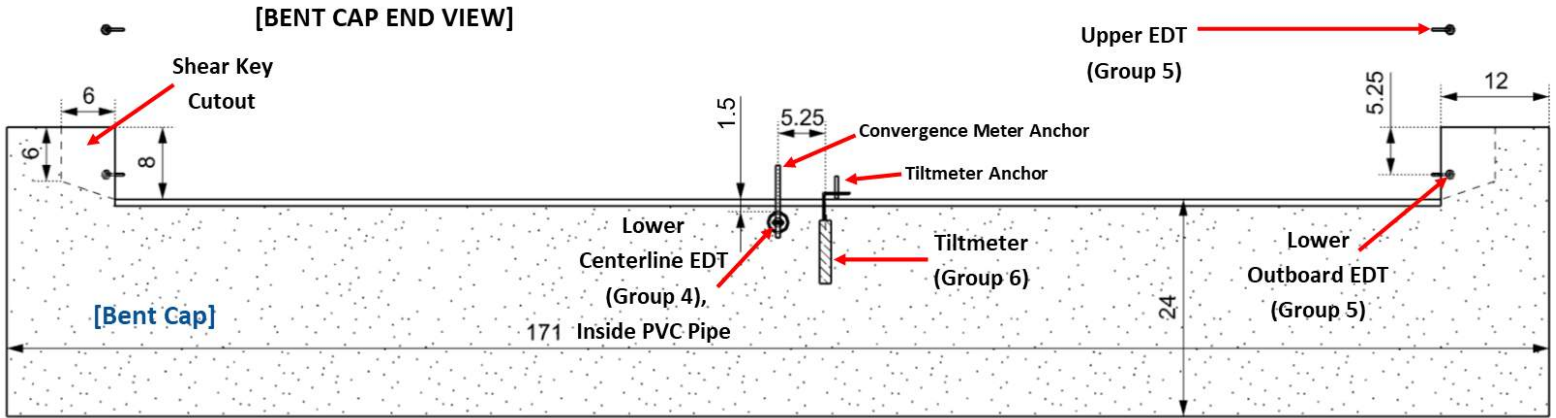


Figure 33, Dimensioned Bent Cap End View (Bridge Beams, Decks, Link-Slab, Conduit, and Parapets not Shown)

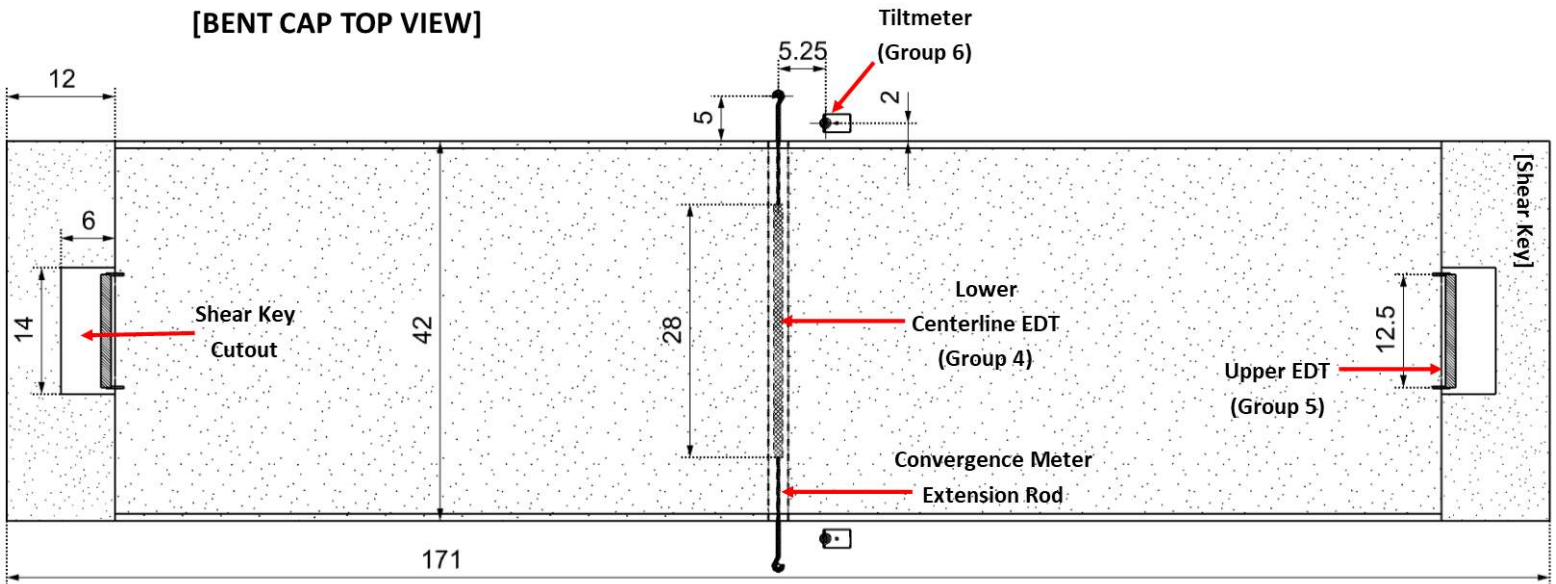


Figure 34, Dimensioned Bent Cap Top View (Bridge Beams, Decks, Link-Slab, Conduit, and Parapets not Shown)

[BENT CAP SIDE VIEW]

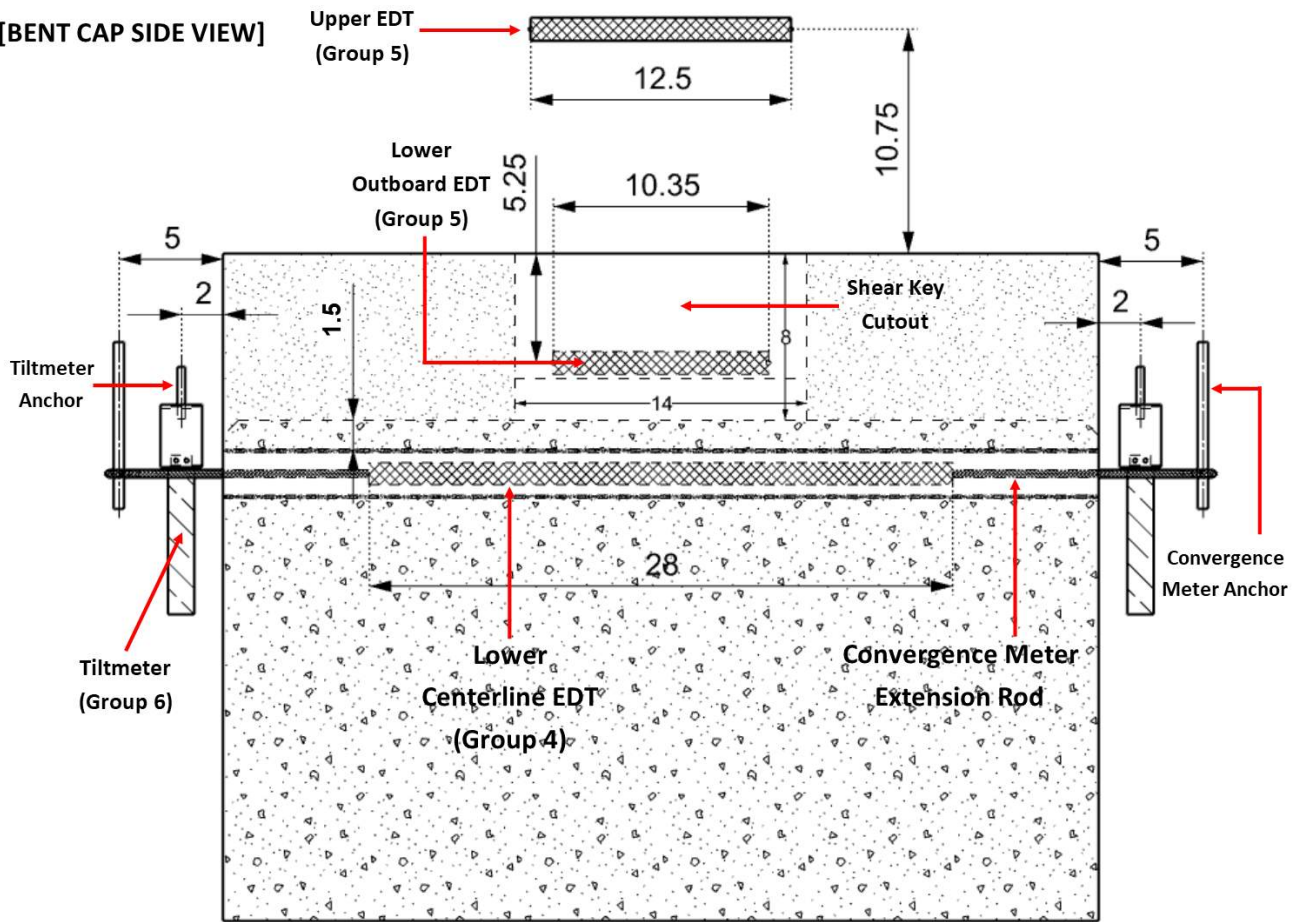


Figure 35, Dimensioned Bent Cap Side View (Bridge Beams, Decks, Link-Slab, Conduit, and Parapets not Shown)

[LINK-SLAB TOP VIEW]

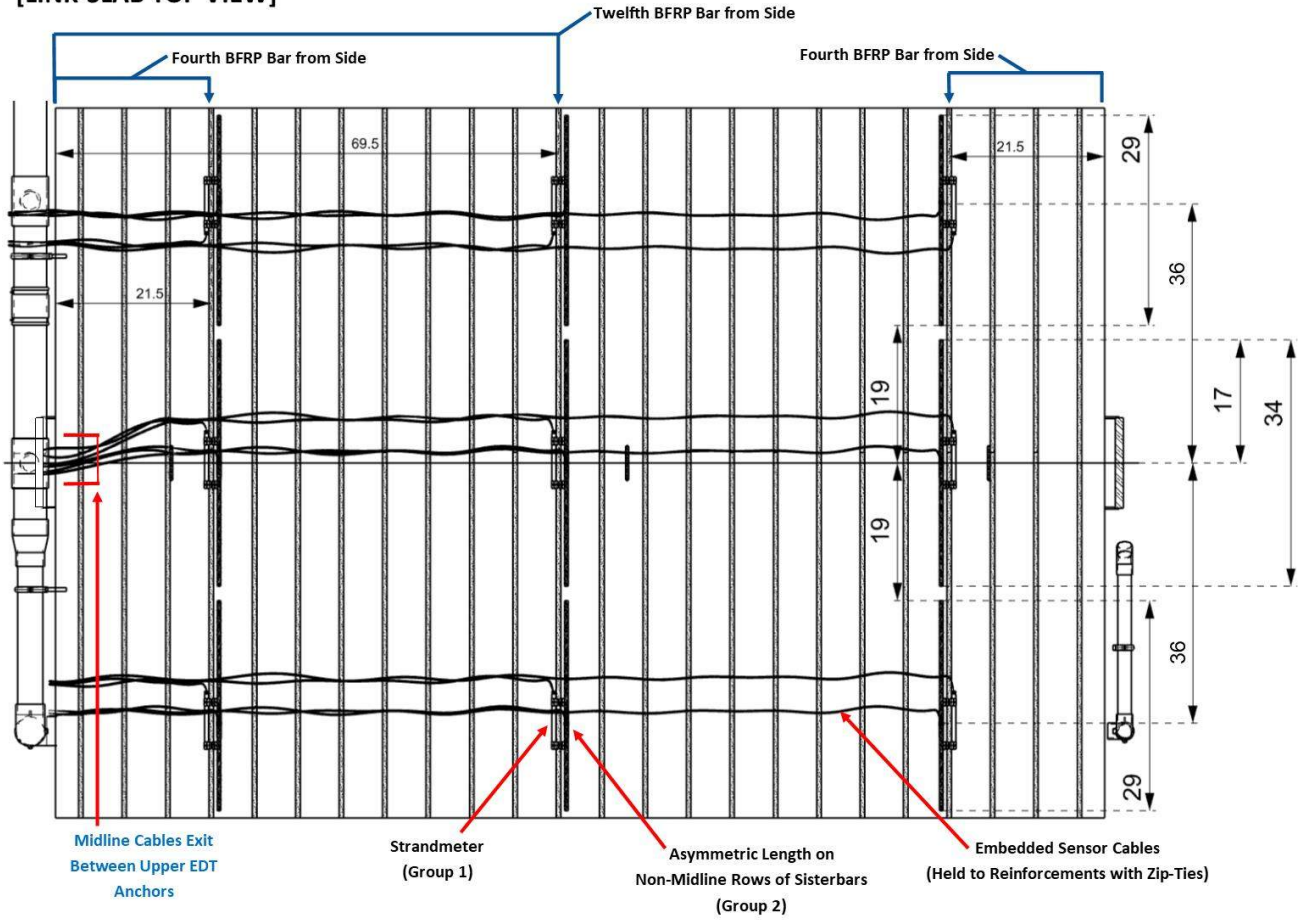


Figure 36, Dimensioned Link-Slab Top View, Layout of Embedded Sensors and Cables

[LINK-SLAB MIDLINE DETAIL]

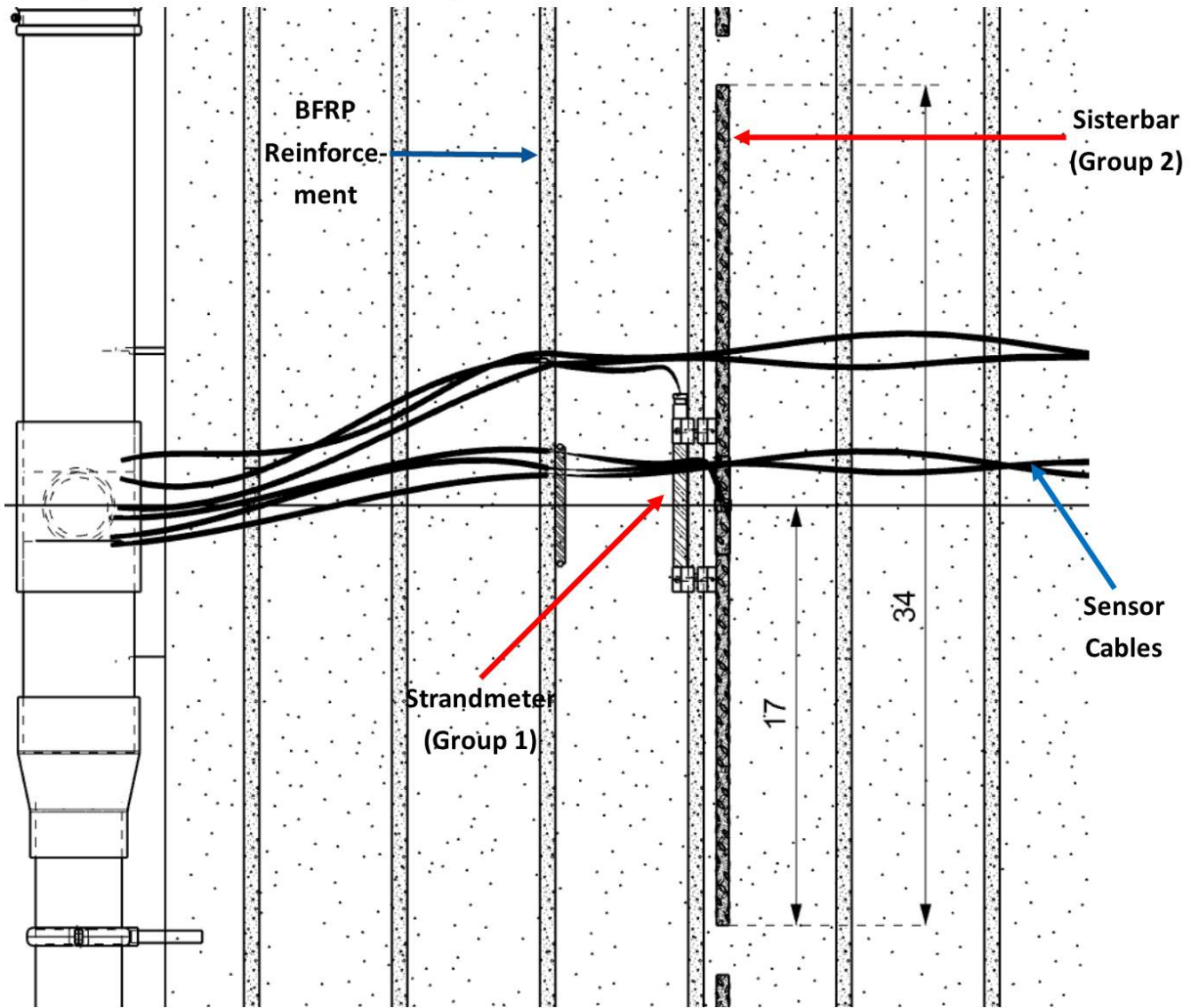


Figure 37, Detail of Midline Embedded Sensors (Strandmeter & Sisterbar)

[LINK-SLAB NON-MIDLINE ROW DETAIL]

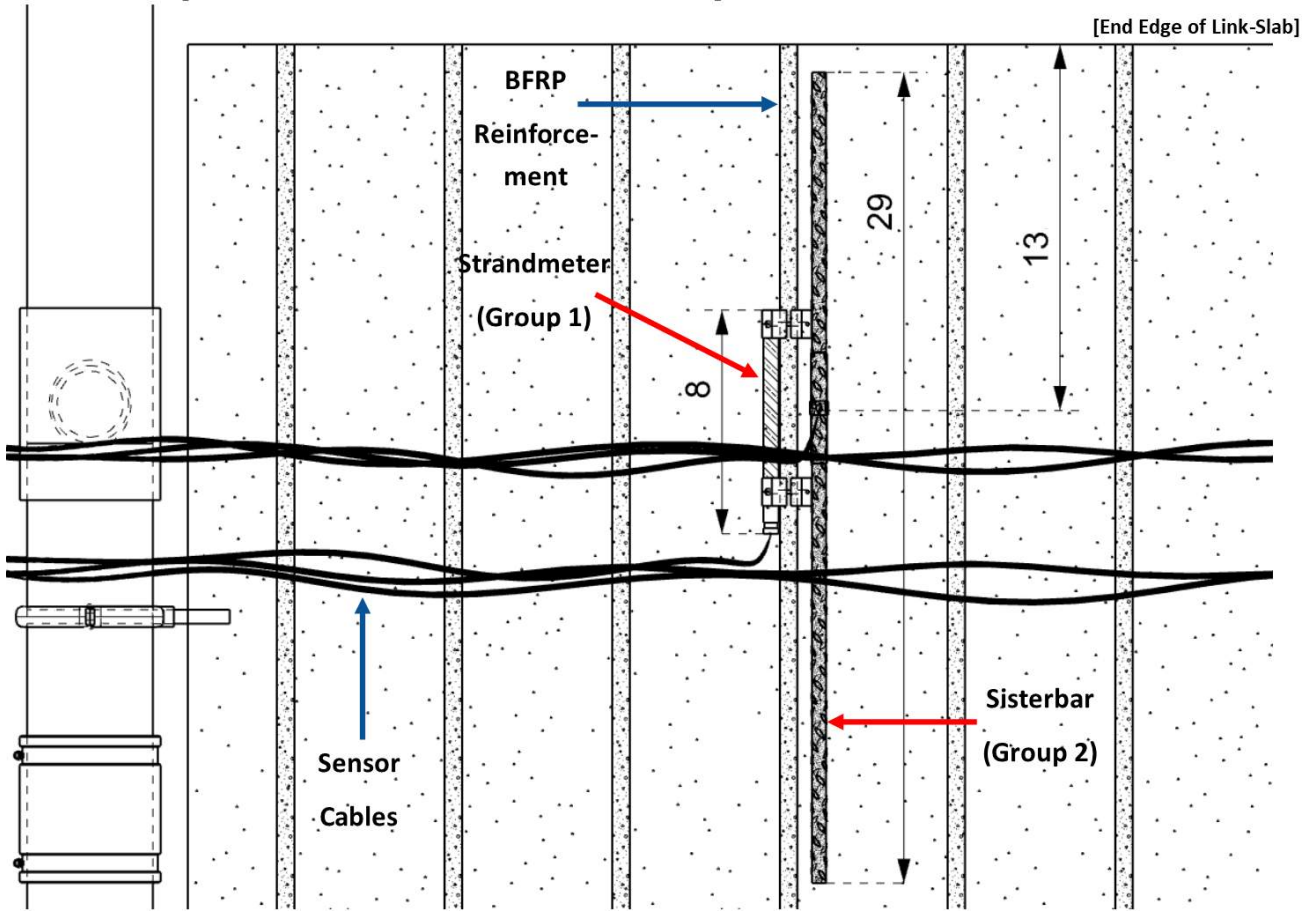


Figure 38, Detail of Non-Midline Embedded Sensors (Strandmeter & Sisterbar)

[CONDUIT TOP VIEW]

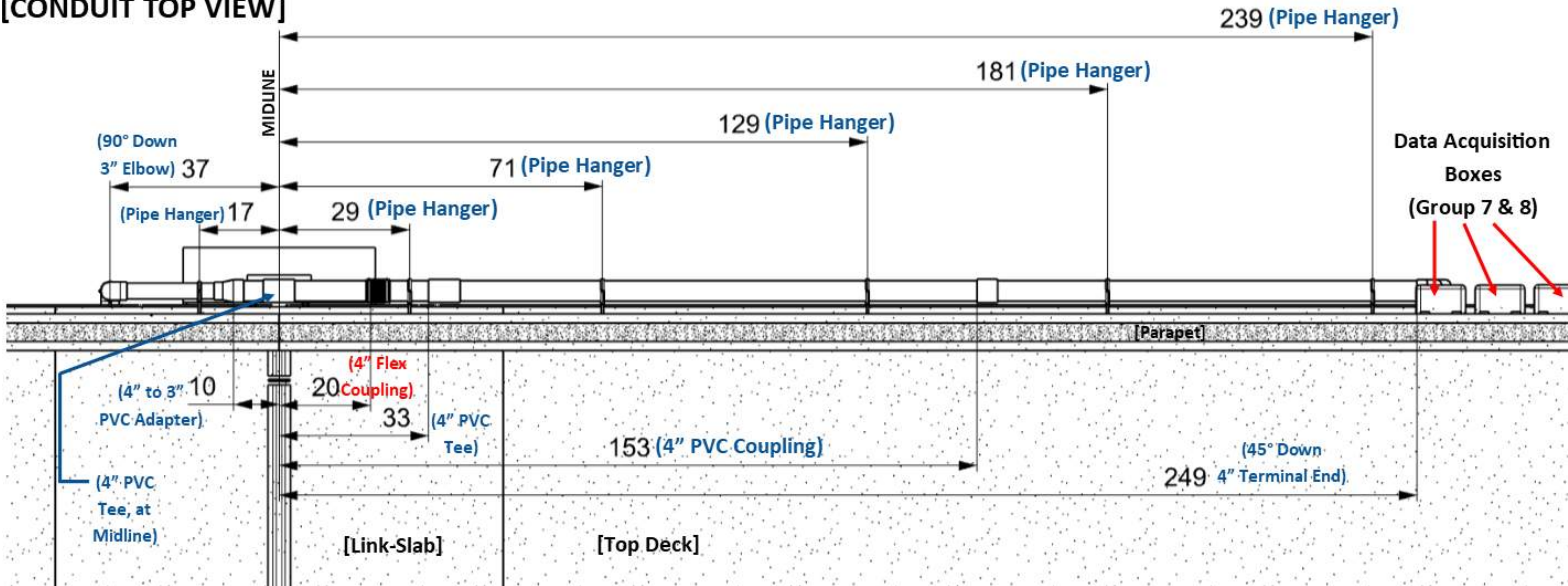


Figure 39, Layout of Conduit and Conduit Fittings

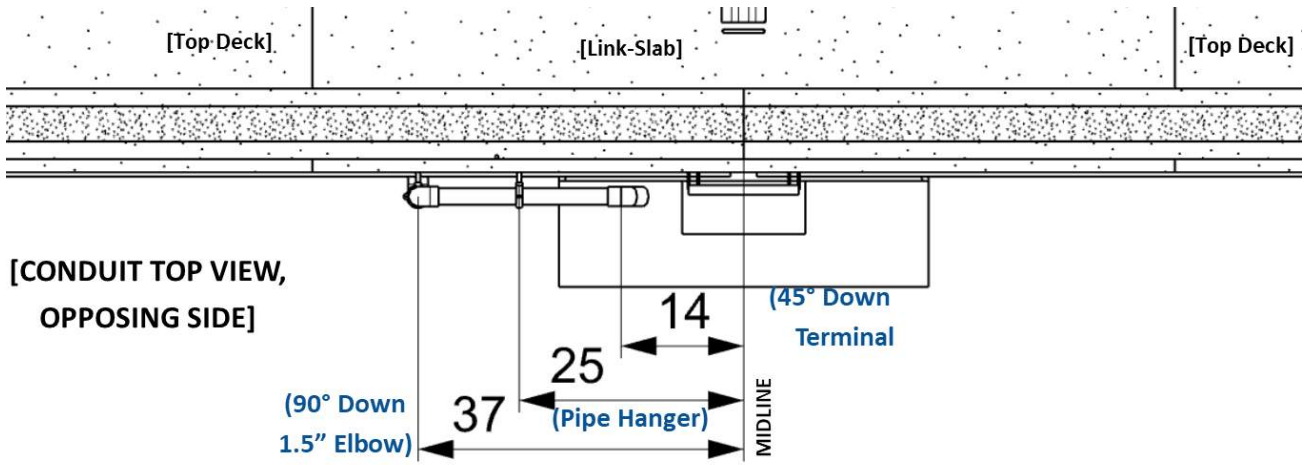


Figure 40, Layout of Conduit and Conduit Fittings, 2

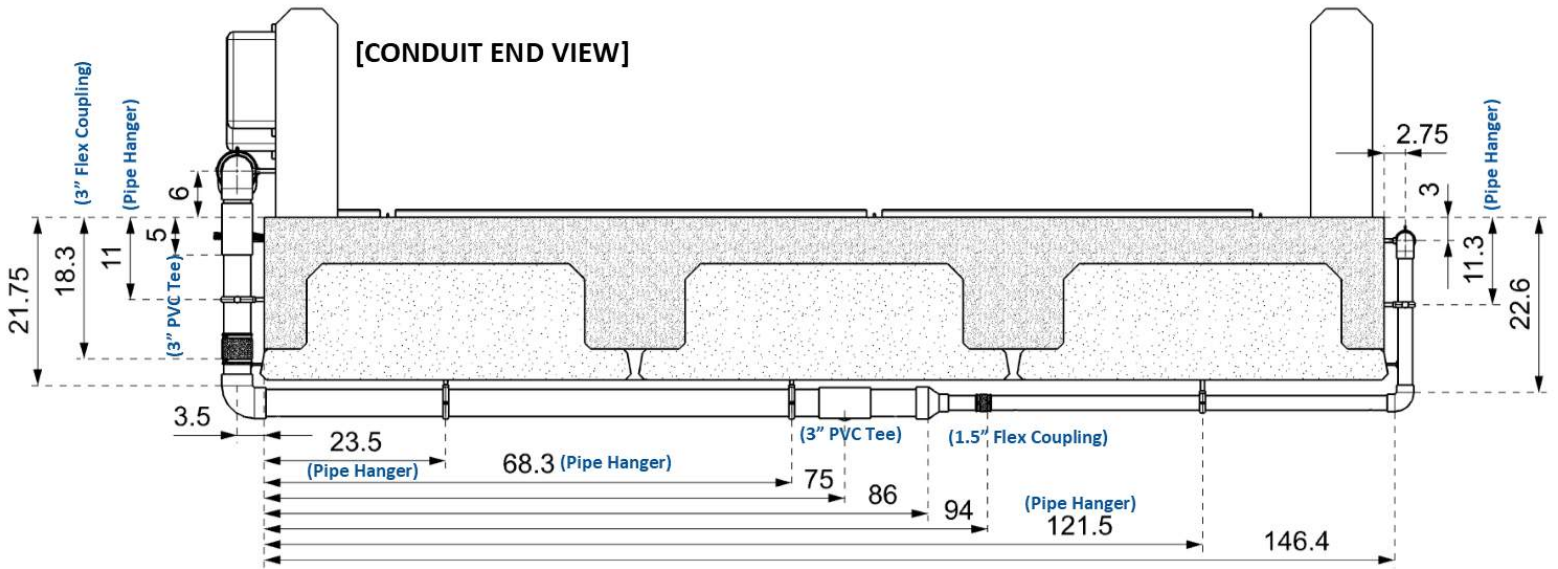


Figure 41, Layout of Conduit and Fittings, 3

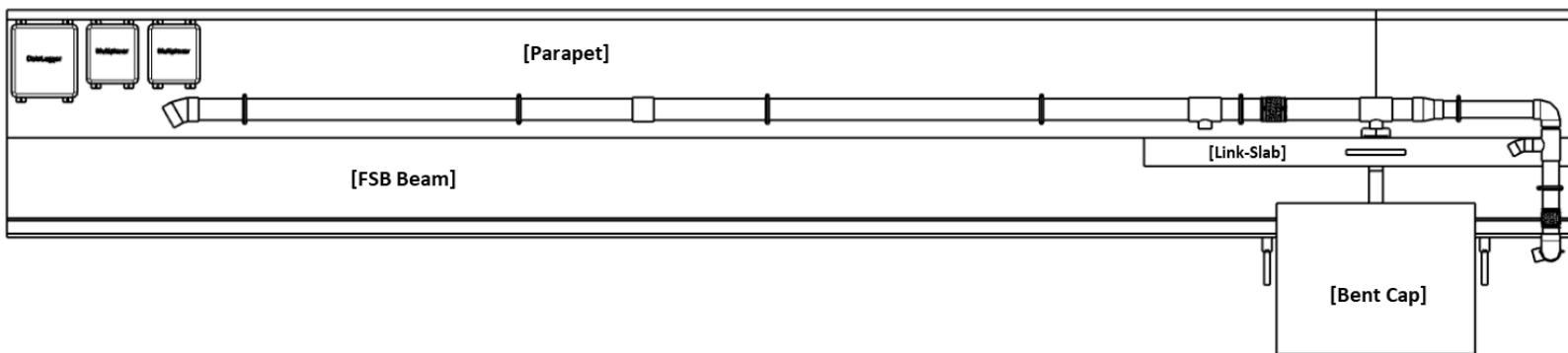


Figure 42, Layout of Conduit and Fittings, 4

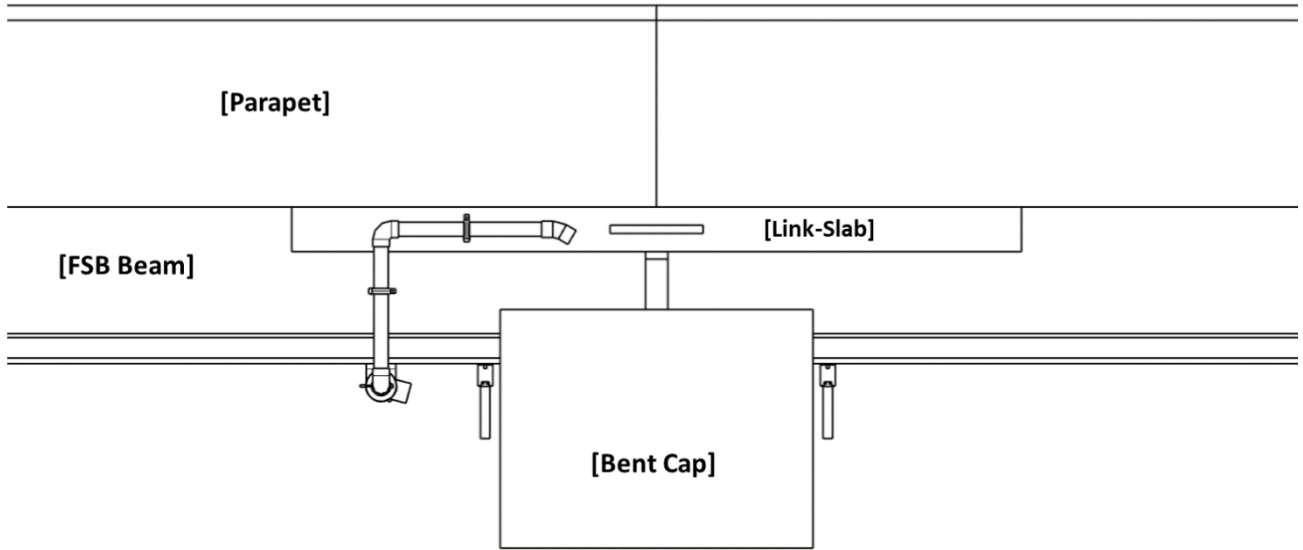


Figure 43, Layout of Conduit and Conduit Fittings, 5

## **Appendix F**

### **BDV30 986-02 Deliverable 6: Closeout Presentation**

(68 pages)



Florida A&M University-Florida State University  
**College of Engineering**

Department of Civil and Environmental Engineering

Performance Evaluation, Material and Specification Development for Basalt Fiber Reinforced Polymer(BFRP) Reinforcing Bars Embedded in Concrete.

Raphael Kampmann

# Welcome

## Overview

- Benefits to the state
- Implementation items
- Introduction
- Problem statement
- Experimental program
- Experimental results
- Closing Remarks
- Recommendations to the FDOT

Benefit to the State

# Project Benefits

- Qualitative:
  - Progress toward implementation of alternative reinforcements
  - Reduction in structural failure due to corrosion
  - Potential extension of structural service life
  
- Quantitative:
  - Characterization of new construction materials/products
  - Evaluation of specific materials/products
  - Product acceptance testing for use in Florida

Implimentation

# Implementation Items

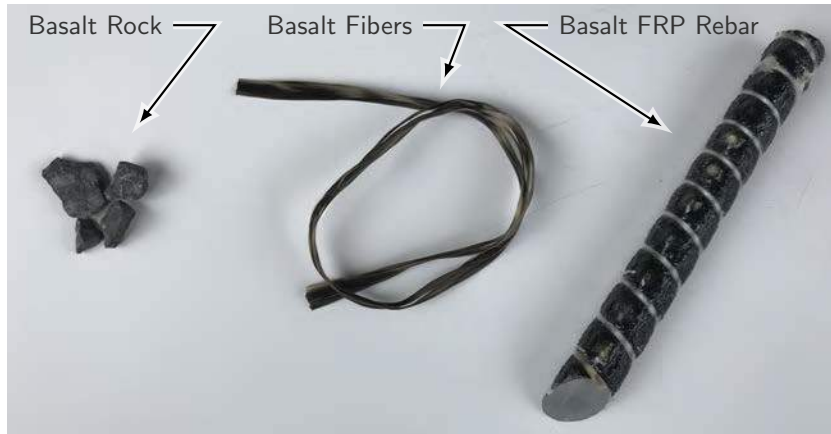
- Additional stakeholder include:
  - Other DOTs and regulating agencies
  - BFRP rebar manufacturer
  
- Additional steps the benefit the implementation progress:
  - Interaction with other agencies that regulate material implementations
  - Communication with BFRP rebar manufacturers
    - To provide suggestions for improved material quality

# Introduction

# Introduction

- FDOT project
- Advancing toward non-corrosive material technologies
- Transforming from Glass FRP rebar to Basalt FRP rebar

# Introduction



# Introduction

## Basalt rock

- Igneous rock
- Continuous fiber
- No need for additional ingredients

# Introduction

## Invention of basalt fiber

- 1923, Paul Dhe
- 1933, Games Slayter
- 1991, Soviet Union collapse

# Introduction

## Benefits of basalt fibers

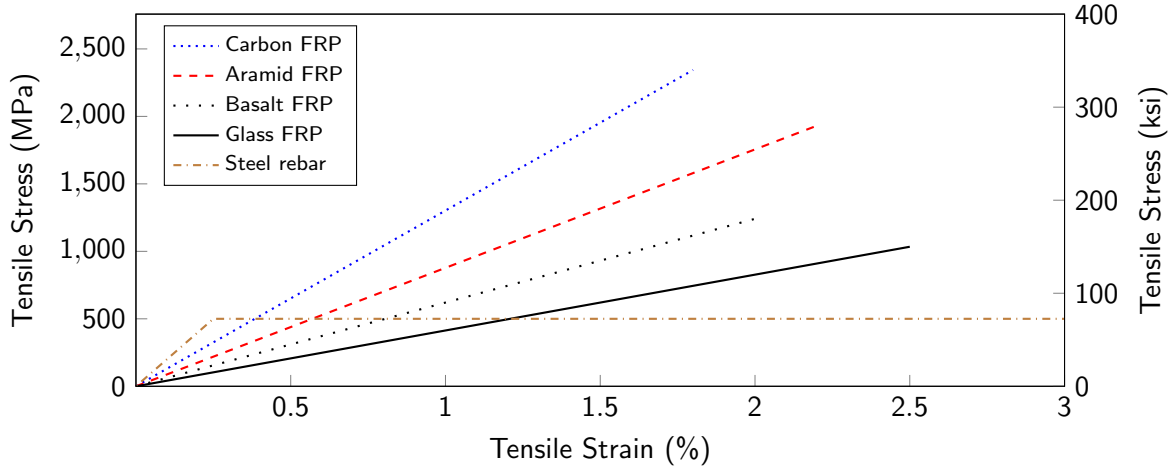
- Cost efficient
- Stronger than GFRP in tensile strength
- Thermally stable, works as a good insulating material

# Introduction

## Advantages in structural engineering

- Low weight
- High strength
- Three times the serviceability
- 35 % to 42 % more modulus of elasticity
- 20 % to 30 % high tensile strength
- 5 % to 10 % more damping capacity

# Introduction



# Introduction

## Other beneficial properties of basalt FRP's

- High impact resistance and high energy absorption capacity
- Magnetically transparent
- Corrosion resistant
- Better UV resistance

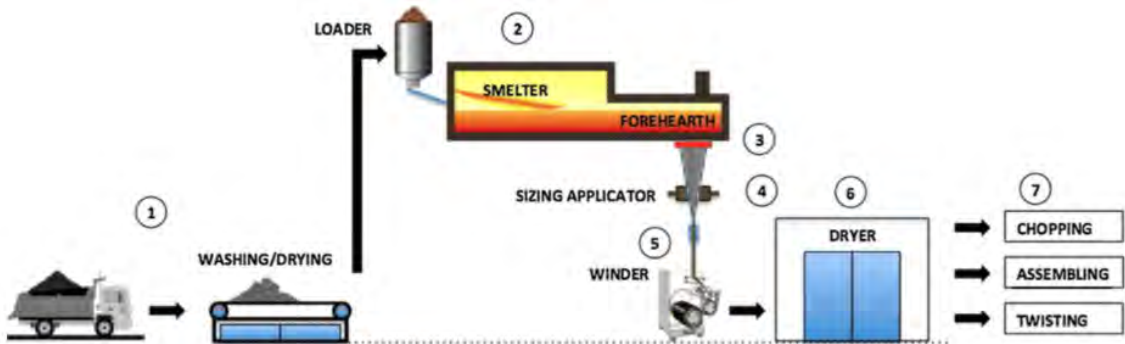
# Introduction

## Production of BFRP rebars

- Pultrusion or wet-laying
- Embedded in polymeric resin matrix
- Surface enhancement for increased friction (Sand coat, ribs, helical wrap, etc.)

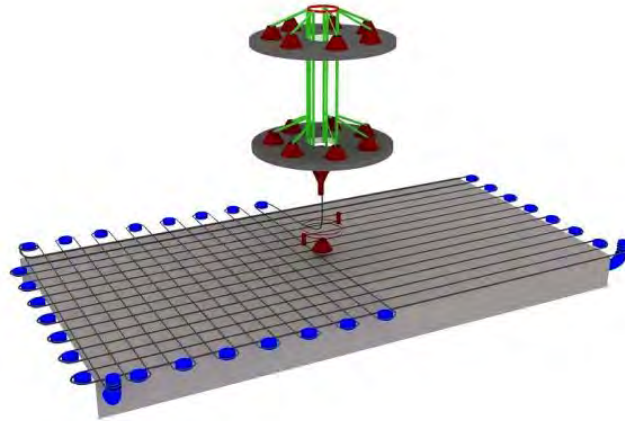
# Introduction

## Pultrusion



# Introduction

## Wet layup



# Introduction

## Epoxy resin



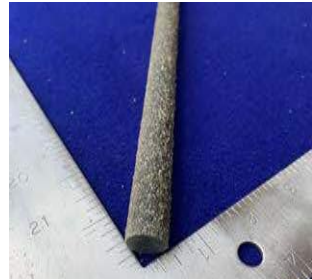
# Introduction

Tested BFRP rebar #3



# Introduction

Tested BFRP rebar # 5



# Problem Statement

# Problem Statement

- No ASTM standards for BFRP rebar
- A wide range of products available in market
  - Products not standardized
- International Code Council Evaluation Services (ICC-ES)
  - Accepted FRP for internal reinforcement of concrete

# Experimental Program

# Experimental Program

## Evaluation of material characteristics

- For three different rebar manufacturers
- Two most common rebar sizes
  - # 3 and # 5

# Experimental Program

## Physical properties

- Cross sectional properties
- Fiber content
- Moisture absorption property

# Experimental Program

## Strength characteristics

- Transverse shear strength test
- Apparent horizontal shear test
- Tensile strength test
- Bond to concrete strength

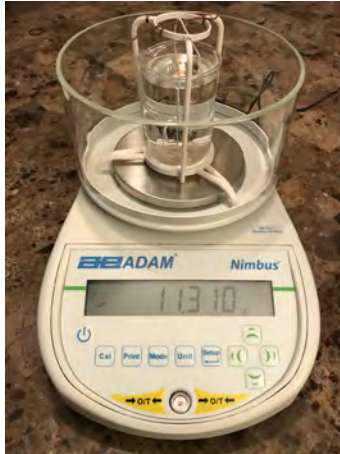
# Experimental Program

## Physical properties

- Cross-sectional properties
  - Cross-sectional area
  - Diameter
  - Density

# Experimental Program

Cross-sectional properties — Water displacement method



# Experimental Program

## Physical properties

- Fiber content
  - Burning rebar at 565 °C
  - Until no more weight change occurs

# Experimental Program

## Fiber content test — Specimen



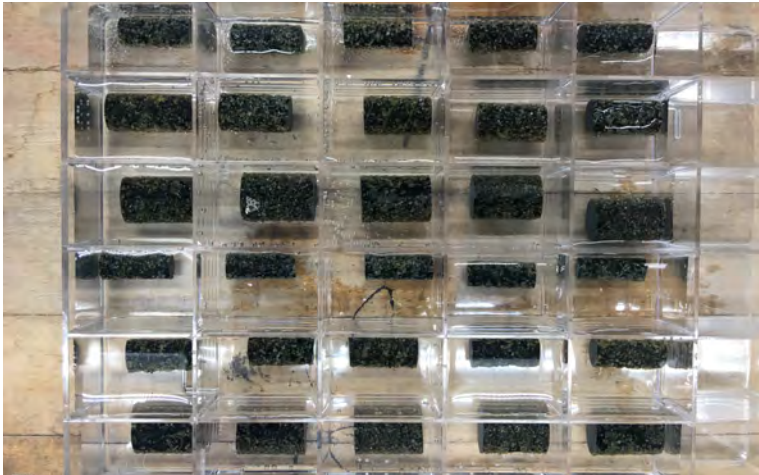
# Experimental Program

## Physical properties

- Moisture absorption property
  - Submerge in distilled water at 50 °C
  - Take measurements every two weeks
    - Until no more weight change occurs

# Experimental Program

## Conditioned BFRP rebar — Specimens



# Experimental Program

## Strength characteristics

- Transverse Shear

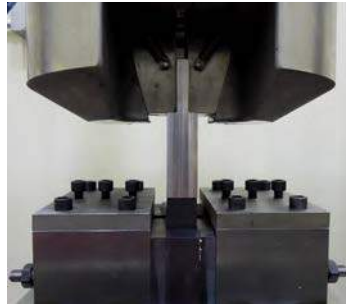
# Experimental Program

## Transverse shear test — Test fixture



# Experimental Program

## Transverse shear test — Test fixture



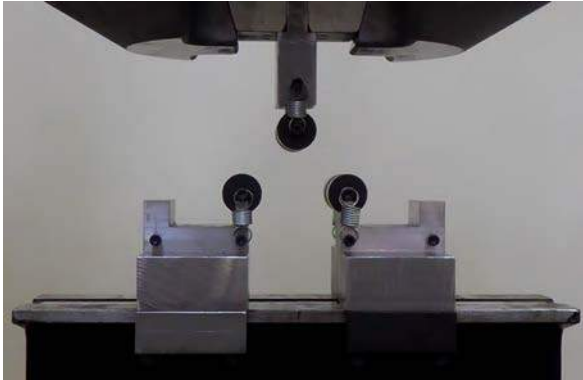
# Experimental Program

## Strength characteristics

- Apparent horizontal Shear

# Experimental Program

## Horizontal shear test — Test fixture



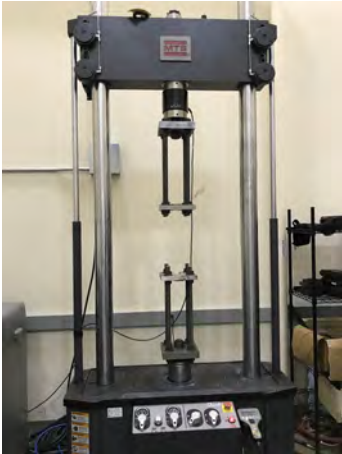
# Experimental Program

## Strength characteristics

- Tensile strength test

# Experimental Program

## Tensile strength test — Test fixture



# Experimental Program

## Tensile strength test — Specimen failure



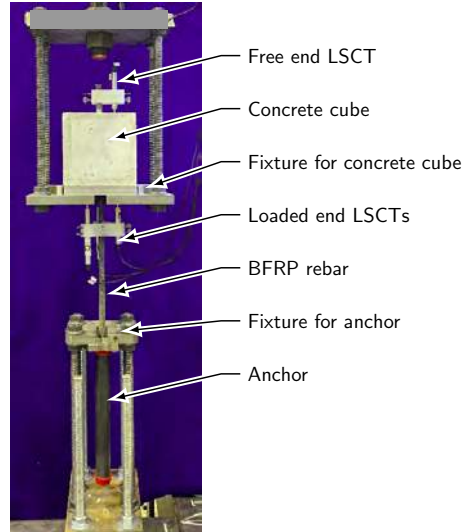
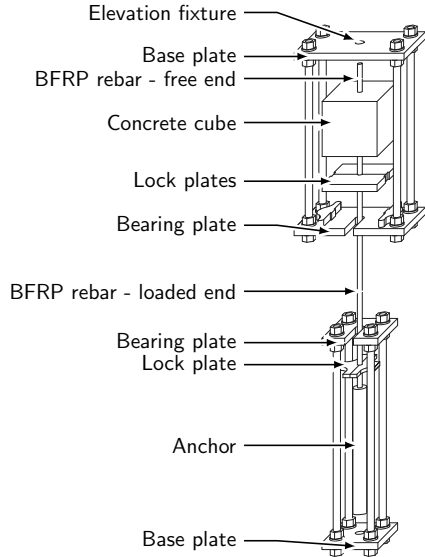
# Experimental Program

## Strength characteristics

- Bond-to-concrete
  - Pullout method
  - Rebars embedded in 8 in.-cubes

# Experimental Program

## Bond-to-concrete test — Test setup



# Experimental Program

## Bond to concrete test — Failure pattern



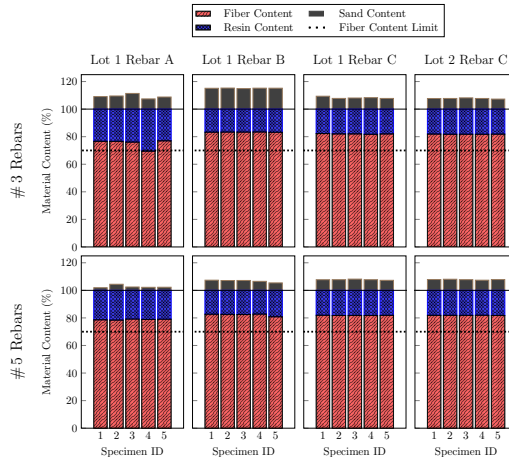
# Experimental Results

# Experimental Results

- Fiber content test
- Moisture absorption test
- Transverse shear
- Apparent horizontal shear
- Tensile strength test
- Bond to concrete

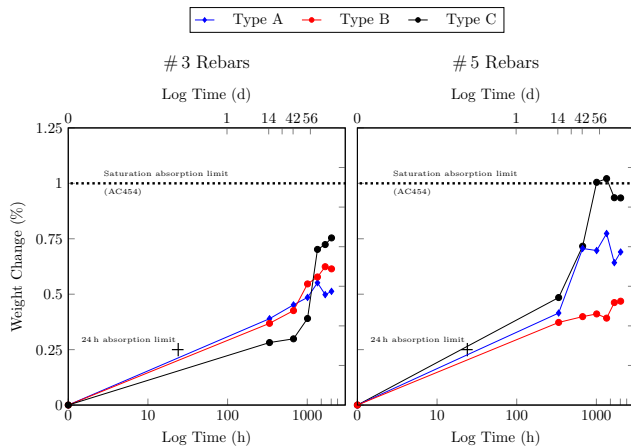
# Experimental Results

## Fiber Content test



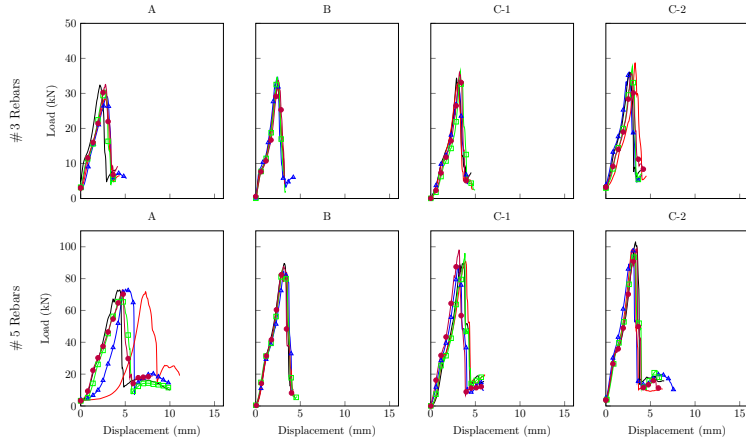
# Experimental Results

## Moisture absorption test



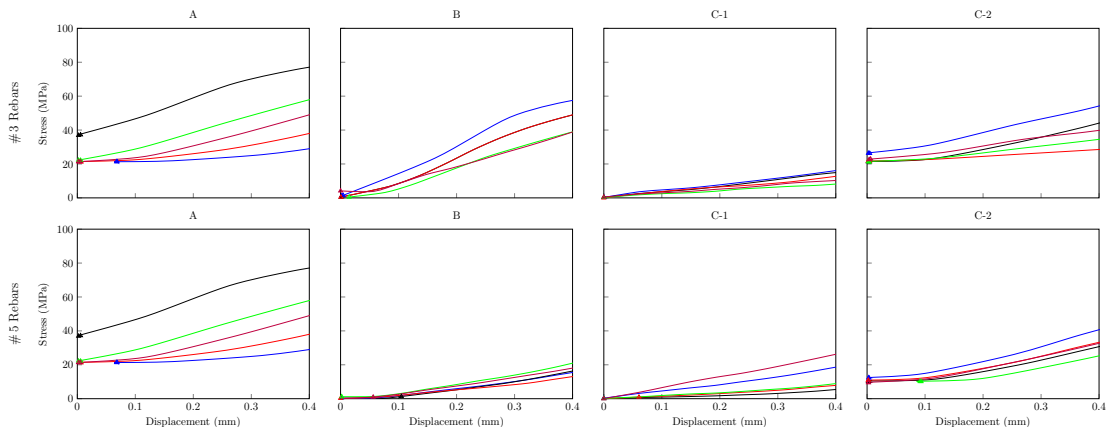
# Experimental Results

## Transverse shear test — Shear force vs displacement



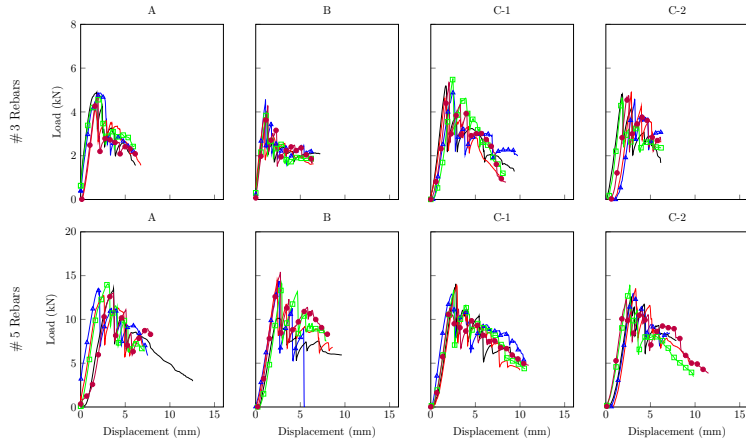
# Experimental Results

## Transverse shear test — Shear stress vs extension



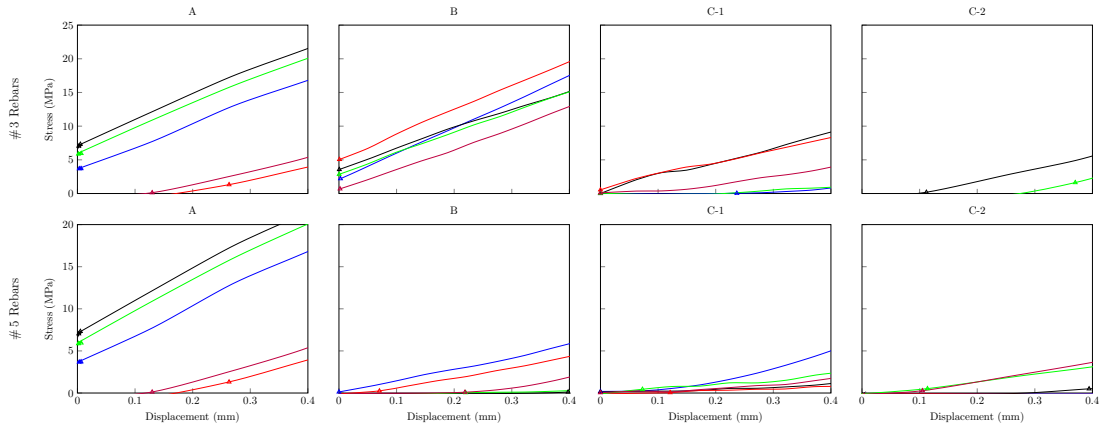
# Experimental Results

## Horizontal shear test — Shear force vs displacement



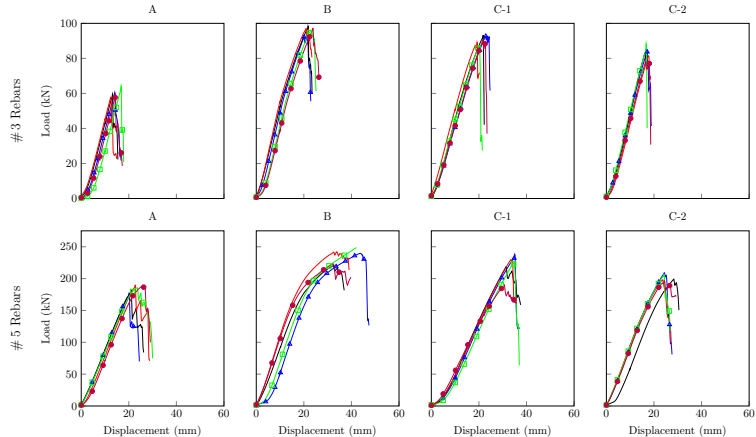
# Experimental Results

## Horizontal shear test — Shear stress vs extension



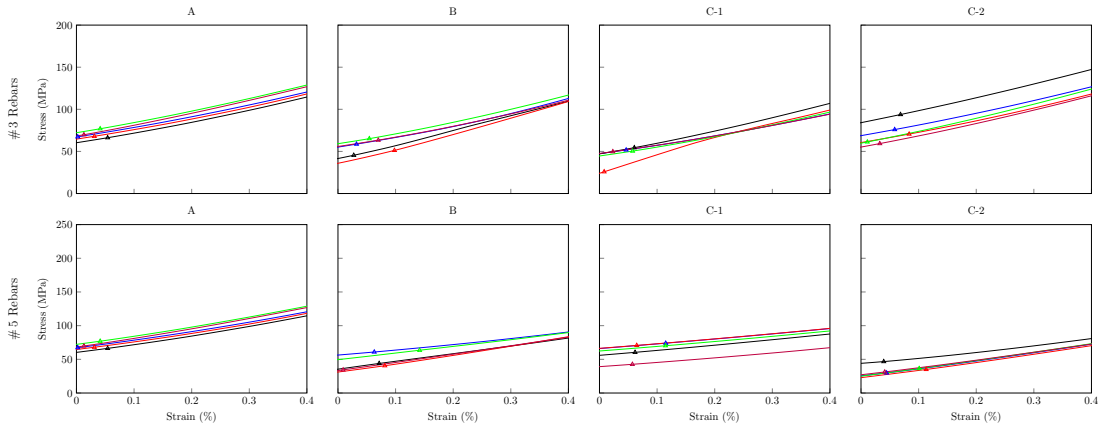
# Experimental Results

## Tensile strength test — Tensile force vs displacement



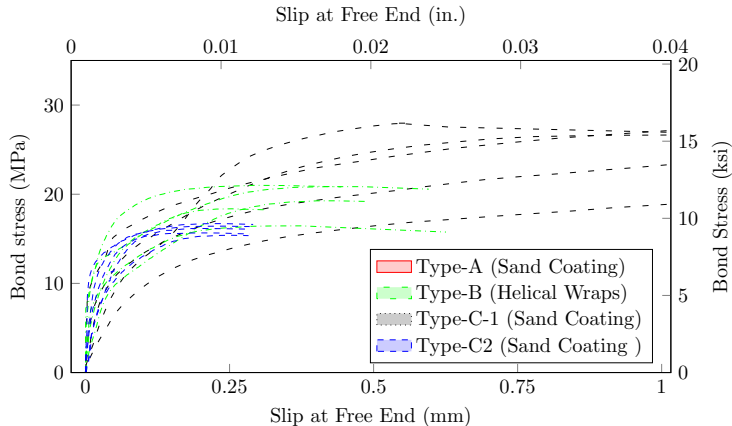
# Experimental Results

## Tensile strength test — Stress vs strain



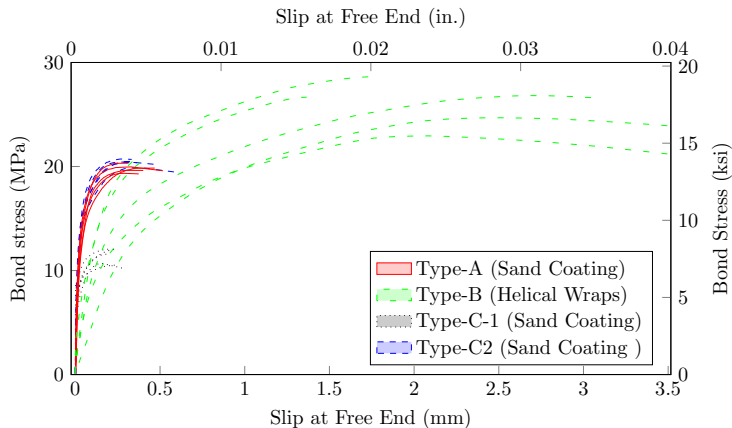
# Experimental Results

Bond to concrete test — # 3 rebars



# Experimental Results

Bond to concrete test — # 5 rebars



# Closing Remarks

# Closing Remarks

## Summary

- Performance evaluation of BFRP Rebars
- Three different rebar types were tested
  - From different manufacturers
- Two most common rebar sizes (# 3, # 5) were tested
- Seven different tests
  - Physio-mechanical characteristics were defined
- All products passed surpassed the minimum performance requirements for GFRP
  - Except for one product and one material characteristic

# Closing Remarks

## Conclusions

- Strength properties of different types of rebars vary vastly
  - Based on the manufacturer type, raw materials, and surface enhancement property
- BFRP rebars appear to be [notably] stronger than GFRP rebars
- The fiber content of BFRP rebars is consistent and similar
  - With minimal coefficients of variations, indicating high-quality products
- The rebar strength is inversely proportional to moisture absorption property
  - Because of the related porosity that potentially leads to material imperfections

# Closing Remarks

## Conclusions

- BFRP transverse shear strength  $\gg$  GFRP transverse shear strength
- Horizontal shear strength of BFRP rebars is similar to GFRP rebars
- The size effect (shear lag) also applies to BFRP rebars
- The bond-to-concrete property is highly dependent on the surface enhancement
  - Less dependent on the fiber type (Glass vs. Basalt)
  - Helical wrapping leads to better interlocking than sand coat
- The minimum bond criteria  $\geq 1.1$  ksi appears to be at the lower limit
  - All rebars outperformed the criteria by more than 200 %
  - Individual rebar types went beyond 300 %

## Recommendations

# Recommendations to FDOT

# Recommendations

## New Material Adoption

- Include BFRP materials in FDOT Section 932
  - To add alternative materials and promote competition
- Set benchmark values comparable to GFRP (For now)
- Without durability testing, do not allow material in submerged environments

# Recommendations

## New Test Standard

- Include horizontal shear test in FDOT Section 932
  - To increase reliability and quality control measures
  
- Consider flexural tests (three point bending)
  - For future replacement of tensile tests

# Recommendations

## Bond-to-Concrete

- Evaluate “bond stiffness” of various surface enhancement types
  - Maximum bond strength not fully reflective of material performance
  - Too high stiffness leads to unfavorable behavior and concrete split
- Determine upper limit for “bond stiffness”
- Evaluate bond durability of products for use in FDOT projects
  - Performance of surface deformation vs. sand coating only
    - Evaluate longevity of surface enhancements without deformations

# Recommendations

## Durability Testing

- Study combined effect of high pH and high salinity environments
  
- Iron in BFRP may react with combined environments

Recommendations

Thank you

# Recommendations

## Acknowledgements

- Chase Knight and Steven Nolan
- FDOT Research Center
- FDOT State Materials Office
- FDOT Structures Design
- Research Assistants: Srichand Telikapalli, Andre Schmidt, Tim Schneider

# Recommendations

Questions?

Raphael Kampmann  
kampmann@eng.fsu.edu

Michelle Roddenberry  
roddemi@eng.fsu.edu

Francisco De Caso  
f.decasoybasalo@miami.edu

Srichand Telikapalli  
st15d@my.fsu.edu